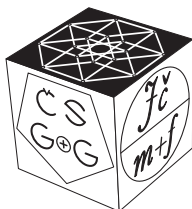


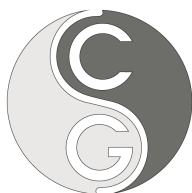
CZECH SOCIETY FOR GEOMETRY AND GRAPHICS
OF THE UNION OF CZECH MATHEMATICIANS AND PHYSICISTS

42nd Conference on
Geometry and Graphics



PROCEEDINGS OF THE
CZECH-SLOVAK CONFERENCE ON
GEOMETRY AND GRAPHICS 2022

Olomouc
September 12–15, 2022



31st Symposium on
Computer Geometry SCG'2022

SLOVAK SOCIETY FOR GEOMETRY AND GRAPHICS

Language correction of the publication was not performed, language accuracy is the sole responsibility of the contributing authors.

Contributions included in the proceedings were selected by the scientific committee members based on reviews.

All rights reserved. No part of this work may be used or reproduced in any manner whatsoever or transmitted in any form or by any means, electronic or mechanical, including photocopy, recording, or any information storage and retrieval system, without written permission from the publisher and copyright owner.

Vydavateľstvo SCHK
Slovak Chemistry Library
Faculty of Chemical and Food Technology STU
Radlinského 9, 812 37 Bratislava

Proceedings of the Czech-Slovak Conference on Geometry and Graphics 2022
First edition

© Miroslav Lávička, Daniela Velichová, Dagmar Szarková, 2022

© Vydavateľstvo SCHK, 2022

ISBN 978-80-8208-092-9

EAN 9788082080929

Czech-Slovak Conference on Geometry and Graphics 2022

Organized by:

Czech Society for Geometry and Graphics

in cooperation with

Department of Algebra and Geometry, Faculty of Science,
Palacký University in Olomouc

Union of Czech Mathematicians and Physicists,
Olomouc branch

Organizing Committee:

Radomír **Halaš** – Palacký University in Olomouc (CZ)

Marie **Chodorová** – Palacký University in Olomouc (CZ)

Jiří J. **Kratochvíl** – Palacký University in Olomouc (CZ)

Patrik **Peška** – Palacký University in Olomouc (CZ)

Lukáš **Rachůnek** – Palacký University in Olomouc (CZ)

Lenka **Rýparová** – Palacký University in Olomouc (CZ)

Scientific Committee:

Roman **Hašek** – Jihočeská univerzita v Českých Budějovicích (CZ)

Pavel **Chalmovianský** – Univerzita Komenského v Bratislave (SK)

Mária **Kmeťová** – Univerzita Konštantína Filozofa, Nitra (SK)

Miroslav **Lávička** – Západočeská univerzita v Plzni (CZ)

Pavel **Pech** – Jihočeská univerzita v Českých Budějovicích (CZ)

Hellmuth **Stachel** – Technische Universität Wien (AT)

Zbyněk **Šír** – Univerzita Karlova (CZ)

Daniela **Velichová** – Slovenská technická univerzita v Bratislave (SK)

Gunter **Weiss** – Technische Universität Wien (AT)

Table of Contents

FOREWORDS.	9
PLENARY TALKS	11
BARTOŇ MICHAEL <i>5-axis flank CNC machining of free-form surfaces using custom- shaped tools</i>	13
BRAJERČÍK JÁN <i>Problems of Global Variational Geometry.</i>	21
KOVÁCS ZOLTÁN <i>Stepwise discovery of geometrical knowledge in GeoGebra</i>	33
MIKEŠ JOSEF <i>190. výročí Jánose Bolyaie v Olomouci a neeuclidovská geometrie</i>	43
CONTRIBUTED TALKS.	49
BEGANOVÁ JULIANA <i>Vytváranie animácie v Geogebre</i>	51
BIZZARRI MICHAL, LÁVIČKA MIROSLAV, VRŠEK JAN <i>Exact and approximate symmetries of discrete curves in plane</i>	55
BLAŽEK JIŘÍ, PECH PAVEL <i>A spatial generalization of Wallace–Simson theorem on four lines parallel to a plane</i>	63
CIBULKA JAROSLAV <i>Parametrické modelování letadlových kompresorových lopatek</i>	69
FERDIÁNOVÁ VĚRA, PLINTA MARTIN, SOVÁKOVÁ BARBORA <i>Výuka geometrie ve Vietnamu.</i>	75
FERDIÁNOVÁ VĚRA, SOVÁKOVÁ BARBORA, PLINTA MARTIN <i>Architektonické prvky a jejich využití ve výuce geometrie</i>	81
HAMAJOVÁ KLAUDIA, CHALMOVIANSKÝ PAVEL <i>Nonlinear subdivision schemes using conic sections</i>	89

HASS JOEL, TRNKOVÁ MARIA <i>Aproximace izoploch pomocí trojúhelníkových sítí se zaručenou kvalitou</i>	95
HAŠEK ROMAN <i>Úvod do dynamického konstruování v prostředí programu GeoGebra</i>	99
HLAVOVÁ MARTA, LINKEOVÁ IVANA <i>Construction of interpolation B-spline curve for technical application</i>	103
HOLEŠOVÁ MICHAELA <i>Modern technologies in teaching geometry</i>	109
CHALMOVIANSKÝ PAVEL <i>Examples in multiplicity theory</i>	115
KOLÁŘOVÁ DANA, ČEČÁKOVÁ STANISLAVA <i>3D Modelling of Geometry Surfaces for the Education of Future Architects</i>	121
KRÁLOVÁ ALICE <i>Parametrizace parabolického konoidu a jeho zobrazení v programech GeoGebra a Maple</i>	127
LINKEOVÁ IVANA, HLAVOVÁ MARTA <i>CTU freeform standard Pharaoh</i>	135
MÜLLER JAKUB <i>Analýza odchylky bodu od plochy</i>	141
RÜCKSCHLOSSOVÁ TATIANA <i>Surfaces of technical practice – creating of printed 3D models</i>	147
ŠAFAŘÍK JAN <i>Počátky kartografie Od nejstarších památek po středověk</i>	155
ŠÍR ZBYNĚK <i>Non-generic curves of given direction</i>	163
TEREŇOVÁ ZUZANA <i>Geometria pre študijný program Matematicko-počítačové modelovanie na SvF STU v Bratislave</i>	171

VAJSÁBLOVÁ MARGITA	
<i>Vedutes and their geometric character</i>	177
VELICHOVÁ DANIELA	
<i>Pselical Surfaces.</i>	185
WEISS GUNTER	
<i>Symmetry – a natural phenomenon causing homo sapiens to become a homo mathematicus</i>	191
ZAMBOJ MICHAL	
<i>Higher-dimensional spaces arising from robot kinematics . . .</i>	201
LIST OF PARTICIPANTS	209

Forewords

The 8th CZECH-SLOVAK CONFERENCE ON GEOMETRY AND GRAPHICS took place in Olomouc, a wonderful historic city in Moravia and the capital of the region of the same name, on September 12–15, 2022. The conference was hosted by the Department of Algebra and Geometry, Faculty of Science, Palacký University in Olomouc in collaboration with the Union of Czech Mathematicians and Physicists, Olomouc branch. As has become a tradition in recent years, it was a joint event of two traditional conferences organized by national societies for geometry and graphics, 42nd CONFERENCE ON GEOMETRY AND GRAPHICS in the Czech Republic and the 31st SYMPOSIUM ON COMPUTER GEOMETRY SCG '2022 in Slovakia.

About 45 conference participants from 5 countries – Czech Republic, Slovakia, Austria, Hungary and Spain, enjoyed the rich conference programme from various disciplines of geometry and graphics. In addition to 29 contributed talks (most of which are presented in the form of an article in these proceedings) from applied and pure geometry, graphics and education of geometry, participants enjoyed four interesting invited plenary lectures on various topics.

JOSEF MIKEŠ from Palacký University in Olomouc (Czechia) gave a presentation on *The 190th anniversary of János Bolyai in Olomouc and non-Euclidean geometry*. As the title suggests, the lecture recalled János Bolyai's stay in Olomouc in 1832–1833. Invited lecture *Problems of Global Variational Geometry* presented by JÁN BRAJERČÍK from University of Presov (Slovakia) was devoted to studying extremals of integral variational functionals for sections of fibered manifolds, corresponding differential equations, and objects invariant under transformations of underlying geometric structures. MICHAEL BARTOŇ from Basque Center for Applied Mathematics in Spain presented lecture entitled *5-axis flank CNC machining of free-form surfaces using custom-shaped tools* about recent advances in rationalization of free-form surfaces in the context of 5-axis flank CNC machining. In particular, he discussed initialization strategies for flank milling of free-form surface using curved tools and on an example of spiral bevel gears he demonstrated a more efficient variant of flank machining called double-flank. Invited speaker ZOLTÁN KOVÁCS from the Johannes Kepler University Linz, Austria, showed in his talk recent improvements in the well-known dynamic geometry software tool GeoGebra. The presentation explained how stepwise discovery mode could be helpful in teaching planar geometry at secondary level, or in the researcher's work. This plenary lecture was simultaneously the opening of the GeoGebra Workshop, which is a traditional part of the conference.

The conference participants enjoyed the sights of the historical city of Olomouc, whose well-preserved old town is one of the most beautiful in the Czech Republic and a UNESCO World Heritage Site. Additional social programme included the tour to the nearby classicist chateau Čechy pod Kosířem, a place closely connected with a famous Czech painter Josef Mánes who regularly visited it and worked here from 1849 to 1870. The participants also greatly enjoyed a visit to the magical museum of historical coaches in the same town. The conference dinner was held in Fort Science (Olomouc), the architecturally exceptional building that served as an artillery depot in the 19th century and nowadays functioning as the progressive Palacký University interactive science centre.

We would like to invite you to attend the next joint event of the 32nd SYMPOSIUM ON COMPUTER GEOMETRY SCG '2023 and the 43rd CONFERENCE ON GEOMETRY AND GRAPHICS that will be held again together by representatives of both societies for geometry and graphics as the 9th *Slovak–Czech Conference on Geometry and Graphics* in September 2023, in the historic Central Slovakian town Kremnica, with a thousand-year tradition of gold mining and a seven-hundred-year-old functional mint.

Let us keep the good tradition of our common meetings deeply rooted in the history.

October 25, 2022

Miroslav Lávička
chair of CSG

Daniela Velichová
chair of SSG

PLENARY TALKS

5-axis flank CNC machining of free-form surfaces using custom-shaped tools

Michael Bartoň

*Basque Center for Applied Mathematics (BCAM)
Alameda de Mazarredo 14, 48009 Bilbao, Basque Country, Spain*

*Ikerbasque – Basque Foundation for Sciences
Maria Diaz de Haro 3, 48013 Bilbao, Basque Country, Spain*

email: mbarton@bcamath.org

Abstract. Computer numerically controlled (CNC) machining is the leading subtractive manufacturing technology and even though it is in use since decades, it is far from being fully solved and still offers a rich source of challenging problems in geometric computing and motion planning. While geometric modeling of free-form surfaces is a relatively easy task for a moderately experienced modeler, manufacturing (aka rationalization) and the related problems such as optimal tool selection and its motion planning are very difficult due to very complex nature of a general free-form surface. This paper discusses some recent advances in rationalization of free-form surfaces in the context of 5-axis flank CNC machining. In particular, initialization strategies for flank milling of free-form surface using curved tools are discussed [1, 2], and on an example of spiral bevel gears is demonstrated a more efficient variant of flank machining called double-flank [3, 4].

Keywords: 5-axis CNC machining, custom-shaped tool, finishing operations, tangential movability, free-form shape manufacturing, tool path-planning

1 Introduction

Highly-accurate manufacturing of general free-form surfaces is a fundamental part of production pipelines in many industrial sectors, automotive or aeronautical to name a few. Components like turbine blades, rotors, impellers, or gears are smooth, yet curvature-varying objects and their efficient manufacturing introduces several challenging problems in geometric modeling and computing because the very complex shape of these objects prevents them to be manufactured using simple straight cutting tools [6].

5-axis Computer Numerically Controlled (CNC) machining is the leading subtractive technology where the milling tool, navigated by a path-planning software, moves in 3D space and removes extra material from a material block. Even though additive technologies like 3D printing are becoming more and more popular [5], there are workpieces that, e.g. for stiffness reasons, have to be manufactured from a single material block using traditional subtractive methodologies.

The presented research belongs to the category of 5-axis *flank* milling where the tool touches tangentially the designed surface Φ , theoretically at

infinitely many points. At each time instant, the tool touches its envelope along a curve called *characteristic* (aka grazing curve in the engineering literature) which shall approximate Φ within fine machining accuracy. However, this curve, changes its shape over time depending on the instantaneous motion, which makes the problem difficult. For milling tools with linear profiles (conical or cylindrical), the characteristic can be, for some special motions, a straight line (lying on the cone or cylinder), however, for a general instantaneous motion, it is not a straight line anymore, but an algebraic curve of degree four, the intersection of the cone (cylinder) with its derivative w.r.t. time [13].

1.1 Related Work

Since the inception of computer-aided design in the late 60's, geometric modeling of 3- and 5-axis CNC machining processes has become a vivid research area and has attracted attention of many researchers in the past several decades [6, 7, 8, 9, 10, 11, 32, 33].

The tool can be a general surface of revolution [6, 14, 15], but traditionally the tools for flank milling are conical or cylindrical [16, 17, 18, 19, 20, 10, 8]. Rigid body motions of a cylindrical tool are studied in [20]. The motion of the cutting tool is controlled via two rail curves and the characteristic is approximated in each time instant. In the case of cylindrical tools, a lot of research has been devoted to approximation of offset surfaces by ruled surfaces, the offsetting distance being the radius of the cylindrical tool [16, 21, 22]. This simplification applies only to cylinders, but already for conical tools such an approach is not feasible and one has to look for 3D directions for which the point-surface distance changes linearly to find good positions of a conical tool [19].

Flank milling using conical and barrel tools is studied in [6]. Flank-millable surfaces, i.e., exact envelopes of rigid tools, are approximated by NURBS surfaces. Recently, multipass flank milling method has been introduced [23]. A free-form surface is partitioned using a tangent vector field that gives good directions for a given conical tool to move. Other relevant works on 5-axis flank milling can be found in the survey paper [24].

There are other physical entities that affect the quality of the machining process, e.g. the cutting speed and cutting force. As the cutting speed is correlated with the tool vibration, there is a broad literature that studies how to set the feedrate to minimize the machining error and to optimize the surface finish [25, 26, 27]. A trade-off between geometric accuracy and surface smoothness is discussed in [28]. An approach that updates milling paths to compensate the error caused by the tool deflections is presented in [29]. For other physical issues related to 5-axis machining, we refer the reader to [30].

2 Flank CNC machining with custom-shaped tools

Traditionally, curved surfaces such as blisk or impellers are machined with tools that are conical, however, one can achieve higher approximation quality when using curved tools. With new technologies at hand, such as 3D printing, it is feasible can manufacture curved tools for a reasonable cost.



Fig. 1: A curved tool for 5-axis flank CNC machining.

2.1 Initialization strategies for curved tools [1]

Curved tools exist on the market already, see Fig. 2. There are several manufacturers that can provide such tools, however, there is very little knowledge about path-planning of curved tools, and commercial software typically does not have modules to support flank milling using these tools.

A step towards flank milling with curved tools has been done in [1]. Given a free-form surface and a curved tool as an input, one can look at directions \mathbf{v} , in which the distance function d to the surface behaves equally, up to second order, as a radial function r that describes the shape of the tool. This second order distance matching is expressed as

$$\begin{aligned} \nabla_{\mathbf{v}} d &= r'(s) \\ \nabla_{\mathbf{v}}(\nabla_{\mathbf{v}} d) = \nabla_{\mathbf{v}}^2 d &= r''(s), \end{aligned} \quad (1)$$

which, after incorporating the approximation of the distance function and applying an assumption that $\|\mathbf{v}\| = 1$ leads to

$$\begin{aligned} v_1^2 + v_2^2 &= 1 - r'(s)^2, \\ \frac{v_1^2}{r(s) - \rho_1} + \frac{v_2^2}{r(s) - \rho_2} &= r''(s), \end{aligned} \quad (2)$$

where v_1 and v_2 are the first two coordinates of \mathbf{v} and $-\rho_{1,2}$ are the principal curvature radii of the reference surface Φ at the contact point between the tool and Φ .

More details on the actual path-planning algorithm as well as the results can be found in [1].

2.2 Curve-guided 5-axis CNC flank milling of free-form surfaces using custom-shaped tools [2]

The second project discussed in the lecture was on a path-planning algorithm that considers the shape of the tool as a variable [2]. Given a free-form reference surface and a guiding path that roughly indicates the motion of the milling tool, tangential movability of quadruplets of spheres centered along a straight line is analyzed to indicate possible shapes and their motions. This results in G^1 Hermite data in the space of rigid body motions that are interpolated and further optimized, both in terms of the motion and the shape of the milling tool itself.

A quadruplet on non-congruent spheres centered along a line (the tool's axis) is shown in Fig. 2. At each time instant, one needs to compute the instantaneous vector field that moves the line. This is encoded in two vectors \mathbf{v}_a , \mathbf{v}_b associated at the endpoints of the axis. The axis, however, is a rigid line, so these two vectors have to satisfy a constraint

$$\langle \mathbf{b} - \mathbf{a}, \mathbf{v}_a \rangle = \langle \mathbf{b} - \mathbf{a}, \mathbf{v}_b \rangle. \quad (3)$$

which is known as the *projection rule*, see Fig. 2.

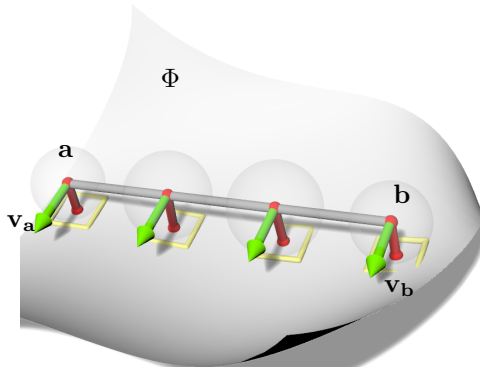


Fig. 2: Tangential movability. Four spheres (transparent) centered along a line \mathbf{ab} are required to move tangentially along a free-form surface Φ .

Except the tangentiality to Φ , there are other objectives on the motion namely that the instantaneous motion moves the line in a direction (almost) perpendicular to the direction $\mathbf{b} - \mathbf{a}$ and/or that the end velocity vectors \mathbf{v}_a and \mathbf{v}_b point a similar direction to prevent a “back-and-forth” motion of the tool, see Section 3.1 in [2] for more details.

To incorporate the projection rule (3) directly into our formulation, we eliminate one variable from the six-tuple $(\mathbf{v}_a, \mathbf{v}_b) = (v_a^1, v_a^2, v_a^3, v_b^1, v_b^2, v_b^3)$.

Due to the linearity, one controls the instantaneous motion using 5 parameters $\mathbf{h} := (h_1, h_2, h_3, h_4, h_5)$. The other constraints are also linear and the therefore the search for the instantaneous motion leads to

$$\min_{\mathbf{h}} \|\mathbf{A}\mathbf{h}\|, \quad \|\mathbf{h}\| = 1, \quad (4)$$

which is a generalized eigenvalue problem and the solution is provided by the eigenvector \mathbf{h}_1 of $\mathbf{A}^\top \mathbf{A}$ corresponding to the smallest eigenvalue λ_1 , and this value is also the actual error. The solution determines the instantaneous motion up to a scaling factor, see [2] for more details and also for the results of the path-planning algorithm based on the above-described tangential movability analysis.

2.3 5-axis double-flank CNC machining of spiral bevel gears via custom-shaped milling tools [3, 4]

Finally, in the last part of the lecture a new variant of flank CNC machining, called *double-flank*, was discussed. It was shown that for some specific geometries, demonstrated on the test case on spiral bevel gears, one can aim at tangential contact on both sides of the reference surface, yielding in a more efficient variant of traditional flank machining.

Similarly to [2], one has to consider the shape of the tool as a variable. The initial trajectory of the milling tool is estimated by fitting a ruled surface to the self-bisector of the two reference flanks. The shape of the tool and its motion then both undergo global optimization that seeks high approximation quality between the input free-form surface and its envelope approximation, fairness of the motion and the tool, and prevents overcutting.

The modeling part of the algorithm can be found in [3], while the physical experiments using a metallic abrasive tool have been presented in [4]. The illustration in Fig. 3 shows a 3D printed prototype and the final metal workpiece, where the custom-shaped tool was used in the semi-finishing stage [4].

3 Conclusion

Three recent advances on 5-axis flank CNC machining of free-form surfaces have been discussed. It was demonstrated on benchmark industrial free-form geometries that using curved tools, either given or specifically designed, offers better approximation quality than using the traditional straight (conical or cylindrical) tools.

Acknowledgements

This work was supported by the Spanish Ministry of Science, Innovation and Universities, grant No PID2019-104488RB-I00, the Ramón y Cajal

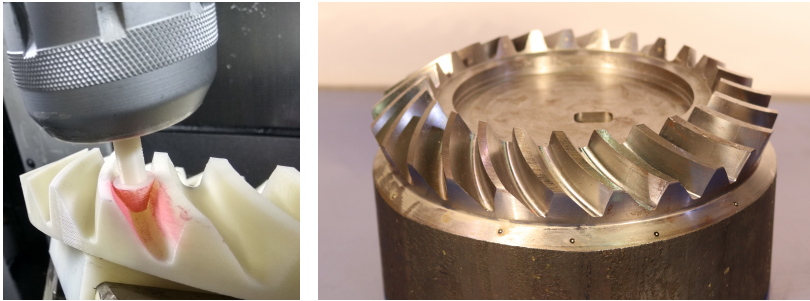


Fig. 3: Double-flank CNC machining of spiral bevel gears. Left: a 3D printed prototype is used to validate the double-flank property [3]. Right: A final gear geometry manufactured with an abrasive metallic tool [4].

fellowship RYC-2017-22649, BCAM Severo Ochoa accreditation (SEV-2017-0718), and by the European Unions Horizon 2020 program under grant agreement No 862025.

References

- [1] P. Bo, M. Bartoñ: *On initialization of milling paths for 5-axis flank CNC machining of free-form surfaces with general milling tools*, Computer Aided Geometric Design 71, 2019, pp. 30–42
- [2] K. Rajain, O. Sliusarenko, M. Bizzarri, M. Bartoñ: *Curve-guided 5-axis CNC flank milling of free-form surfaces using custom-shaped tools*, Computer Aided Geometric Design 94, 2022, 102082 p.
- [3] P. Bo, H. Gonzalez, A. Calleja, N. Lopez de Lacalle, M. Bartoñ: *5-axis double-flank CNC machining of spiral bevel gears via custom-shaped milling tools – Part I: Modeling and simulation*, Precision Engineering 40, Volume 62, 2020, pp. 204-212
- [4] G. Escudero, P. Bo, H. Gonzalez, A. Calleja, M. Bartoñ, N. Lopez de Lacalle: *5-axis double-flank CNC machining of spiral bevel gears via custom-shaped milling tools – Part II: Physical validations and experiments*, International Journal of Advanced Manufacturing Technology 119, 2022, pp. 1647-1658
- [5] W. Gao, Y. Zhang, D. Ramanujan, K. Ramani, Y. Chen, C. B. Williams, C. C. Wang, Y. C. Shin, S. Zhang, P. D. Zavattieri: *The status, challenges, and future of additive manufacturing in engineering*, Computer-Aided Design 69, 2015, pp. 65–89
- [6] C. Li, S. Bedi, S. Mann: *Flank millable surface design with conical and barrel tools*, Computer- Aided Design and Applications 5, 2008, pp. 461–470

- [7] D. Roth, S. Bedi, F. Ismail, S. Mann: *Surface swept by a toroidal cutter during 5-axis machining*, Computer-Aided Design 33 (1), 2001, pp. 57–63
- [8] G. Elber, R. Fish: *5-axis freeform surface milling using piecewise rule surface approximation*, ASME Journal of Manufacturing Science and Engineering 119 (3), 1997, pp. 383–387
- [9] G. Zheng, Q.-Z. Bi, L.-M. Zhu: *Smooth tool path generation for five-axis flank milling using multi-objective programming*, in: Proceedings of the Institution of Mechanical Engineers, Part B: Journal of Engineering Manufacture, Vol. 226, 2012, pp. 247–254
- [10] C. Wang, G. Elber: *Multi-dimensional dynamic programming in ruled surface fitting*, Computer-Aided Design 51, 2014, pp. 39–49
- [11] M. Bartoň, M. Bizzarri, F. Rist, O. Sliusarenko, H. Pottmann: *Geometry and tool motion planning for curvature adapted cnc machining*, ACM Trans. Graph. 40 (4), 2021, pp. 1–16
- [12] P. Bo, M. Bartoň, D. Plakhotnik, H. Pottmann: *Towards efficient 5-axis flank CNC machining of free-form surfaces via fitting envelopes of surfaces of revolution*, Computer-Aided Design 79, 2016, pp. 1–11
- [13] H. Pottmann, M. Peternell: *Envelopes-computational theory and applications*, in: Proceedings of Spring Conference on Computer Graphics, 2000, pp. 3–23
- [14] L. Zhu, Y. Lu: *Geometric conditions for tangent continuity of swept tool envelopes with application to multi-pass flank milling*, Computer-Aided Design 59, 2015, pp. 43–49
- [15] L. Zhu, H. Ding, Y. Xiong: *Simultaneous optimization of tool path and shape for five-axis flank milling*, Comput. Aided Des. 44, 2012, pp. 1229–1234
- [16] K. Sprott, B. Ravani: *Cylindrical milling of ruled surfaces*, Int. J. Adv. Manuf. Technol. 38, 2008, pp. 649–656
- [17] C. Li, S. Bedi, S. Mann: *Flank milling of a ruled surface with conical tools – an optimization approach*, Int. J. Adv. Manuf. Technol. 29, 2006, pp. 1115i–1124
- [18] L. Zhu, G. Zheng, H. Ding, Y. Xiong: *Global optimization of tool path for five-axis flank milling with a conical cutter*, Computer-Aided Design 42 (10), 2010, pp. 903–910
- [19] P. Bo, M. Bartoň, H. Pottmann: *Automatic fitting of conical envelopes to free-form surfaces for flank CNC machining*, Computer-Aided Design 91, 2017, 84–94
- [20] S. Bedi, S. Mann, C. Menzel: *Flank milling with flat end milling cutters*, CAD 35 (3), 2003, pp. 293–300
- [21] H. Gong, C. Li-Xin, L. Jian: *Improved positioning of cylindrical cutter for flank milling ruled surfaces*, Computer-Aided Design 37, 2005, pp. 1205–1213

- [22] J. Redonnet, W. Rubio, G. Dessein: *Side milling of ruled surfaces; optimum positioning of the milling cutter and calculation of interference*, The International Journal of Advanced Manufacturing Technology 14 (7), 1998, pp. 459–465
- [23] D. He, Z. Li, Y. Li, K. Tang: *Quasi-developable and signed multi-strip approximation of a freeform surface mesh for efficient flank milling*, Computer-Aided Design 140, 2021, 103083 p.
- [24] R. F. Harik, H. Gong, A. Bernard: *5-axis flank milling: A state-of-the-art review*, Computer-Aided Design 45 (3), 2013, 796–808.
- [25] Y. Sun, J. Sun, J. Li, W. Li, B. Feng: *Modeling of cutting force under the tool flank wear effect in end milling Ti6Al4V with solid carbide tool*, The International Journal of Advanced Manufacturing Technology 69 (9-12), 2013, pp. 2545–2553
- [26] A. Larue, Y. Altintas: *Simulation of flank milling processes*, International Journal of Machine Tools and Manufacture 45 (4), 2005, pp. 549–559
- [27] X. Beudaert, S. Lavernhe, C. Tournier: *Feedrate interpolation with axis jerk constraints on 5-axis NURBS and G1 tool path*, International Journal of Machine Tools and Manufacture 57, 2012, pp. 73–82
- [28] P. Y. Pechard, C. Tournier, C. Lartigue, J. P. Lugarini: *Geometrical deviations versus smoothness in 5-axis high-speed flank milling*, International Journal of Machine Tools and Manufacture 49, 2009, pp. 453–461
- [29] L. L. De Lacalle, A. Lamikiz, J. Sanchez, M. Salgado: *Toolpath selection based on the minimum deflection cutting forces in the programming of complex surfaces milling*, International Journal of Machine Tools and Manufacture 47 (2), 2007, pp. 388–400
- [30] Y. Altintas, P. Kersting, D. Biermann, E. Budak, B. Denkena, I. Lazoglu: *Virtual process systems for part machining operations*, CIRP Annals 63 (2), 2014, pp. 585–605
- [31] G. Zheng, L. Zhu, Q. Bi: *Cutter size optimisation and interference-free tool path generation for five-axis flank milling of centrifugal impellers*, International Journal of Production Research 50 (23), 2012, pp. 6667–6678
- [32] M. Bizzarri, M. Bartoň: *Manufacturing of screw rotors via 5-axis double-flank CNC machining*, Computer-Aided Design 132, 2021, 102960 p.
- [33] A. Calleja, P. Bo, H. González, M. Bartoň, L. N. López de Lacalle: *Highly accurate 5-axis flank CNC machining with conical tools*, The International Journal of Advanced Manufacturing Technology, 2018, pp. 1–11

Problems of Global Variational Geometry

Ján Brajerčík

University of Prešov

17. novembra 1, Prešov, Slovak Republic

email: jan.brajercik@unipo.sk

Abstract. We introduce the global variational geometry as a modern mathematical discipline integrating the knowledge of many areas of mathematics. It generalizes classical calculus of variations, and its subject is a geometric structure consisting of a smooth manifold endowed with a differential form. In this contribution, basic concepts of the global variational geometry are characterized. We also discuss some problems solved by methods of the global variational geometry.

Keywords: Global variational geometry, calculus of variations, fibered manifold, jet, Lagrangian, Euler-Lagrange equations.

1 Introduction

The *global variational geometry* is a branch of mathematics, devoted to extremal problems on the frontiers of differential geometry, topology, global analysis, algebra, the calculus of variations, and mathematical physics. It generalizes classical calculus of variations, where underlying Euclidean spaces are replaced by *smooth manifolds* and *fibered spaces*, and Lagrange functions are replaced by *Lagrange differential forms*. The subject of global variational geometry is to study extremals of *integral variational functionals* for sections of fibered manifolds, corresponding differential equations, and objects invariant under transformations of underlying geometric structures.

Basic geometric ideas allowing us to globalize the classical calculus of variations come from the concepts of E. Cartan [2] in the calculus of variations of simple integrals, and especially from the work of Lepage [12]. Main contributors to the global theory since its formation are Dedecker [3] (geometric approach to the calculus of variations), Garcia [5] (Poincaré-Cartan form, invariant geometric operations), Goldschmidt and Sternberg [7] (Cartan form, Hamilton theory) Krupka [10] (Lepage forms, higher order variational functionals), and Trautman [13] (invariance of Lagrange systems). For more comprehensive exposition of the global variational geometry we refer to Krupka [9].

In Section 2 we briefly recall basic concepts of the classical of the calculus of variations, illustrated by several simple variational problems and their solutions. Section 3 is devoted to description of topological, smooth and fibered manifolds. In Section 4 we introduce a concept of a jet applied to the construction of jet prolongations of fibered manifold as basic underlying structures of the global variational geometry. The structure of the integral variational functional is characterized in Section 5, including concepts of a Lagrangian, and the Euler-Lagrange equations.

2 Calculus of variations

Crucial role in the calculus of variations is played by variable quantities called functionals. By a *functional* we mean a correspondence which assigns a definite (real) number to each function (or curve) belonging to some class. *Calculus of variations* concerns with finding maxima and minima of functionals.

We now mention some typical examples of *variational problems*, i.e., problems involving the determination of extremal values of functionals.

1. Find the shortest plane curve joining two points A and B , i.e., find the curve $y = y(x)$ for which the functional

$$\int_a^b \sqrt{1 + (y')^2} dx$$

achieves its minimum. The curve in question turn out to be the straight line segment joining A and B .

2. Among all curves joining two fixed points $A = (x_A, y_A)$ and $B = (x_B, y_B)$, find the curve such that the particle takes the least time to go from A to B under the influence of gravity. We are searching the curve $y = y(x)$ for which the time functional

$$T = \int_A^B dt = \int_{x_A}^{x_B} \frac{ds}{v},$$

achieves its minimum. For simplicity let us assume that the original point A coincides with the origin of coordinates. Since

$$ds = \sqrt{1 + (y')^2} dx, \quad v = \sqrt{2gy},$$

then the transit time T is given by

$$T = \int_0^{x_B} \frac{\sqrt{1 + (y')^2}}{\sqrt{2gy}} dx.$$

The curve in question is called the *brachistochrone*. It turns out to be a part of cycloid, lying in the vertical plane and passing through A and B . It is given by the equations in parameter form

$$x = r(\theta - \sin \theta), \quad y = r(1 - \cos \theta),$$

where r is determined by initial conditions. The brachistochrone problem was posed by Johann Bernoulli in 1696, and played an important role in the development of the calculus of variations. The problem was solved, except Johann Bernoulli, by Jacob Bernoulli, Newton and L'Hospital.

3. Among all the curves joining two given points A and B , find the curve which generates the surface of minimum area when rotated about the x -axis. As it is well known, the area of the surface of revolution generated by rotating the curve $y = y(x)$ about the x -axis is

$$2\pi \int_{x_A}^{x_B} y \sqrt{1 + (y')^2} dx.$$

The required curve is a *catenary* passing through A and B , expressed by

$$y = C \cosh \frac{x + C_1}{C},$$

for the constants C, C_1 corresponding to the initial conditions represented by position of A and B (under some position of A and B , the solution may degenerate; for more details see Gelfand and Fomin [6]). The surface generated by rotation of the catenary is called a *catenoid*. The problem is also known as the *surface of a minimum area*, and was solved by Leibniz, Huygens and Johann Bernoulli in 1691.

All of the above problems involve integrals which can be written in the form

$$\int_a^b L(x, y, y') dx,$$

where $L : V \rightarrow \mathbf{R}$, $V \subset \mathbf{R} \times \mathbf{R} \times \mathbf{R}$, is called the *Lagrange function* (or *Lagrangian*). The Lagrange function L defines on the set of all admissible mappings $y = \gamma(x)$ the *action function of the Lagrangian* L on the interval $[a, b]$ by

$$S : \gamma \mapsto \int_a^b (L \circ \gamma)(x) dx \in \mathbf{R}. \quad (1)$$

A mapping γ for which the functional S gives maximum or minimum is called an *extremal* of S . An extremal of (1) is given as a solution of the *Euler-Lagrange equation*

$$\left(\frac{\partial L}{\partial y} - \frac{d}{dx} \frac{\partial L}{\partial y'} \right) \circ \gamma = 0. \quad (2)$$

As an example, let us consider the Lagrange function $L : \mathbf{R}^3 \rightarrow \mathbf{R}$, given by

$$L(t, q, \dot{q}) = \frac{1}{2} m \dot{q}^2 - mgq, \quad (3)$$

for some positive constants m, g . The corresponding Euler-Lagrange equation is $\ddot{q} = -g$, and its solution is expressed as

$$q(t) = -\frac{1}{2} gt^2 + c_1 t + c_2 \quad (4)$$

for the constants c_1, c_2 given by initial conditions. Lagrangian L (3) represents the difference of kinetic and potential energies of a particle of a mass m in the gravitational field with the acceleration due to gravity g . The solution (4) represents a free fall of a particle in the gravitational field.

More generally, if we consider a mechanical system with the kinetic energy T and the potential energy V , then extremal of the variational functional defined by Lagrangian $L = T - V$ determines the motion of a mechanical system.

3 Manifolds

This section is devoted to present one of the basic underlying structure of the global variational geometry, a *fibered manifold*. First, we describe the concepts of a *topological* and a *smooth manifolds*.

Let X be a topological space. We say that X is a *topological manifold* of dimension n if it has the following properties:

- X is a *Hausdorff space*, i.e., each two points of X can be separated by open sets on X ,
- X is *second countable*, i.e., the topology of X has a countable basis,
- X is *locally Euclidean* of dimension n , i.e., to each $x \in X$ there exist neighborhood U of x , and a homeomorphism $\varphi : U \rightarrow \tilde{U}$ from U to $\tilde{U} = \varphi(U) \subset \mathbf{R}^n$.

A trivial example of a topological manifold of dimension n is \mathbf{R}^n with standard topology of open balls. A set $S^1 = \{(x, y) \in \mathbf{R}^2 \mid x^2 + y^2 = 1\}$ considered with the topology induced by standard topology on \mathbf{R}^2 is a non-trivial example of a topological manifold of dimension 1.

Let X be a topological n -manifold. A *coordinate chart* on X is a pair (U, φ) , where U is an open subset of X and $\varphi : U \rightarrow \tilde{U}$ is a homeomorphism from U to $\tilde{U} = \varphi(U) \subset \mathbf{R}^n$. Directly from the definition of a topological manifold we have that to each point there is some coordinate chart. So, a topological manifold can be covered by charts allowing us to describe somehow a manifold. For example, as a coordinate chart for any $x \in \mathbf{R}^n$ we can take *global* coordinate chart $(\mathbf{R}^n, \text{id}_{\mathbf{R}^n})$. In generally, on a topological manifold there is not the global coordinate chart.

To ensure smooth transition from one coordinate chart to another we define the notion of smoothness of a function. If U and V are open subsets of Euclidean spaces \mathbf{R}^n and \mathbf{R}^m , respectively, a function $F : U \rightarrow V$ is said to be *smooth* if each of its component functions has continuous partial derivatives of all orders. If in addition F is bijective and has a smooth inverse map, it is called a *diffeomorphism*. Of course, F is a diffeomorphism implies $n = m$.

Let X be a topological n -manifold. Two charts (U, φ) , (V, ψ) are said to be *smoothly compatible* if either $U \cap V = \emptyset$, or the composition $\psi \circ \varphi^{-1} : \varphi(U \cap V) \rightarrow \psi(U \cap V)$ is a diffeomorphism.

In analogy with an effort to describe the Earth surface through particular charts we define a notion of an atlas. A *smooth atlas* for a topological manifold X is a collection of smoothly compatible charts whose domains cover X . To the given atlas on X we can add smoothly compatible charts until we obtain a maximal smooth atlas on X . Then a *smooth* (or *differentiable*, or C^∞) *structure* on a topological n -manifold X is a maximal smooth atlas on X . A *smooth manifold* is a pair (X, \mathcal{A}) , where X is a topological manifold and \mathcal{A} is a smooth structure on X .

In generally, on a X we can choose more smooth atlases representing the same smooth structure. For example, on S^1 we have the smooth atlas consisting of two charts determined by stereographic projections on the corresponding sets, or we can take the smooth atlas consisting of four charts with half circles as sets, and projections along coordinate axes of \mathbf{R}^2 as homeomorphisms to $(-1, 1) \subset \mathbf{R}$.

There are examples of topological spaces allowing to define more non-compatible smooth structures, even in \mathbf{R} considered with standard topology. On the other hand, there are topological spaces which do not admit a smooth structure (see, e.g. [11]).

Now we extend the definition of a smooth mapping between open subsets of Euclidean spaces to definition of a *smooth function* on a smooth manifold, and *smooth mapping* between two smooth manifolds. If X is a smooth manifold, a function $f : X \rightarrow \mathbf{R}$ is said to be *smooth* if for every $x \in X$ there exists a chart (U, φ) , on X , such that $x \in U$, and $f \circ \varphi^{-1}$ is smooth. Let X, Y be smooth manifolds, and let $F : X \rightarrow Y$ be any map. We say that F is *smooth map* if for every $x \in X$ there exist a chart (U, φ) containing x and a chart (V, ψ) containing $F(x)$ such that $F(U) \subset V$ and the composition $\psi \circ F \circ \varphi^{-1} : \varphi(U) \rightarrow \psi(V)$ is smooth.

By a *fibred manifold structure* on a smooth manifold Y we mean a smooth manifold X with a smooth surjective submersion $\pi : Y \rightarrow X$. A manifold Y endowed with a fibred manifold structure is called a (*smooth*) *fibred manifold*. X is the *base*, and π is the *projection* of the fibred manifold Y . The set $\pi^{-1}(x)$ is called the *fiber* over x .

Trivial example of a fibred manifold is $\pi_1 : \mathbf{R} \times \mathbf{R}^n \rightarrow \mathbf{R}$, and more generally, also each manifold Y in the form of Cartesian product of a base manifold X and other smooth manifold is a fibred manifold. On the other hand, non-trivial examples are $\pi_2 : M \rightarrow S^1$, where M is the *Möbius strip* (Fig. 1), and $\pi_3 : S^3 \rightarrow S^2$, also called the *Hopf fibration*, where S^n denotes n -dimensional sphere (a generalization of S^1 ; see Section 3). For a visualization of the Hopf fibration see, e.g., Zamboj [14].



Fig. 1: Möbius strip

Let $\pi : Y \rightarrow X$ be a fibered manifold, let us denote $\dim X = n$, $\dim Y = n + m$. Directly from the definition of a fibered manifold we have that to each point $y \in Y$ there exists a chart (V, ψ) , $\psi = (u^i, y^\sigma)$, at y , where $1 \leq i \leq n$, $1 \leq \sigma \leq m$, with the following properties:

- (a) There exists a chart (U, φ) , $\varphi = (x^i)$, at $x = \pi(y)$, where $1 \leq i \leq n$, in which the projection π is expressed by the equation $x^i \circ \pi = u^i$,
- (b) $U = \pi(V)$.

The chart (V, ψ) with these properties is called a *fibered chart* on Y . The chart (U, φ) is defined uniquely and is said to be *associated* with (V, ψ) . We usually write (V, ψ) , $\psi = (x^i, y^\sigma)$, i.e., x^i instead of u^i .

A *section* of a fibered manifold $\pi : Y \rightarrow X$ is a mapping $\gamma : U \rightarrow Y$, where $U \subset X$ is an open set, such that $\pi \circ \gamma = \text{id}_U$. In a fibered chart (V, ψ) , $\psi = (x^i, y^\sigma)$, on Y ,

$$x^i \circ \gamma = x^i, \quad y^\sigma \circ \gamma = f^\sigma(x^i).$$

To illustrate a fibered manifold, the example $\pi_1 : \mathbf{R} \times \mathbf{R}^n \rightarrow \mathbf{R}$ for $n = 1$ is often used (Fig. 2).

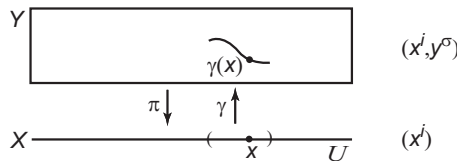


Fig. 2: Fibered manifold and its section

4 Jets

Our aim in this section is to introduce the concept of *jet prolongation of a fibered manifold*. To this purpose we first describe the concept of a *jet of a mapping*.

First, consider the following example. Let $f : \mathbf{R} \rightarrow \mathbf{R}$ be a mapping defined by $f(x) = \sin x$, and let $x_0 = \frac{\pi}{2}$. Then the ordered quadruple of real numbers

$$(x_0, f(x_0), Df(x_0), D^2f(x_0))$$

is called the *2-jet of the mapping f at x_0* , and is denoted $J_{x_0}^2 f$. Thus, $J_{x_0}^2 f = (\frac{\pi}{2}, 1, 0, -1)$. We are able to find other mapping $g : \mathbf{R} \rightarrow \mathbf{R}$ such that $J_{x_0}^2 f = J_{x_0}^2 g$. It is sufficient to take a part of the Taylor series with the corresponding coefficients, e.g., $g(x) = 1 - \frac{1}{2}(x - \frac{\pi}{2})^2$.

Let $\pi : Y \rightarrow X$ be a fibered manifold, let $y \in Y$ be a point, $x = \pi(y)$. Let r be positive integer. Denote $\Gamma_{x,y}^r$ the set of all C^r sections γ of Y defined in x such that $\gamma(x) = y$. Let us consider the binary relation \sim on $\Gamma_{x,y}^r$: $\gamma_1 \sim \gamma_2$ if and only if there exist a fibered chart (V, ψ) , $\psi = (x^i, y^\sigma)$, on Y such that

$$D_{i_1} D_{i_2} \dots D_{i_k} (y^\sigma \gamma_1 \varphi^{-1})(\varphi(x)) = D_{i_1} D_{i_2} \dots D_{i_k} (y^\sigma \gamma_2 \varphi^{-1})(\varphi(x))$$

for all $k = 1, 2, \dots, r$, and all $1 \leq i_1 \leq i_2 \leq \dots \leq i_k \leq n$.

The relation \sim is an equivalence relation on $\Gamma_{x,y}^r$, independent of the choice of a fibered chart. Equivalence classes of \sim whose representative is $\gamma \in \Gamma_{x,y}^r$ is called *r -jet of γ with source at x and target at y* , and is denoted $J_x^r \gamma$.

$J^r Y$ denotes the set of all r -jets with source in x and target in Y . Fibered manifold structure on Y induces the smooth structure on $J^r Y$, and $\pi^r : J^r Y \rightarrow X$ is a fibered manifold. $J^r Y$ with this structure is called the *r -jet prolongation of Y* .

If γ is a smooth section of Y , then the smooth mapping

$$J^r \gamma : x \mapsto J^r \gamma(x) = J_x^r \gamma$$

is called the *r -jet prolongation of γ* (a section of $\pi^r : J^r Y \rightarrow X$).

5 Variational structures on fibered manifolds

A concept to replace the Lagrange function in the functional (1) is a *differential form*. Let X be an n -dimensional smooth manifold, and $T_x X$ denote the *tangent space* of X at $x \in X$. Consider a vector space $\Lambda^k T_x X$ of k -forms, i.e., tensors of type $(0, k)$, at the vector space $T_x X$, and denote by

$$\Lambda^k T X = \bigcup_{x \in X} \Lambda^k T_x X$$

the *bundle of k -forms* on X . A *differential k -form* on $U \subset X$ is a smooth mapping

$$\eta : U \rightarrow \Lambda^k T X.$$

A *Lagrangian* (of order r) for a fibered manifold $\pi : Y \rightarrow X$, $\dim X = n$, is a π^r -horizontal n -form on the open subset of $J^r Y$. The requirement of horizontality with respect to the projection $\pi^r : J^r Y \rightarrow X$ means that in a fibered chart (V, ψ) , $\psi = (x^i, y^\sigma)$, on Y ,

$$\lambda = \mathcal{L} \omega_0, \quad \omega_0 = dx^1 \wedge dx^2 \wedge \dots \wedge dx^n,$$

where \mathcal{L} is the *Lagrange function* associated with (V, ψ) . By a *variational structure* we mean a pair (Y, λ) , where Y is a fibered manifold over an n -dimensional manifold X with projection π and λ is a Lagrangian for Y .

Suppose we have a variational structure (Y, λ) . Let Ω be a compact n -dimensional submanifold of X with boundary (a *piece* of X). Denote by $\Gamma_\Omega(\pi)$ the set of smooth sections of π over Ω . We get a function $\Gamma_\Omega(\pi) \ni \gamma \mapsto \lambda_\Omega(\gamma) \in \mathbf{R}$, defined by

$$\lambda_\Omega(\gamma) = \int_\Omega J^r \gamma^* \lambda.$$

λ_Ω is called the *variational functional*, associated with (Y, λ) (over Ω).

One of the tasks of the global variational geometry is to study extremal values, *extremals*, of given variational functional. A section $\gamma : U \rightarrow J^r Y$ of a fibered manifold Y is an extremal of the variational functional defined by Lagrangian λ over Ω if and only if for every fibered chart (V, ψ) , $\psi = (x^i, y^\sigma)$, such that $\pi(V) = U$, γ satisfies the system of partial differential equations

$$E_\sigma(\mathcal{L}) \circ J^{2r} \gamma = 0, \quad 1 \leq \sigma \leq m. \quad (5)$$

Equations (5) are called the *Euler-Lagrange equations*. The functions $E_\sigma(\mathcal{L})$ are the *Euler-Lagrange expressions*. $E_\sigma(\mathcal{L})$ are the components of the *Euler-Lagrange form* E_λ associated with Lagrangian λ ; E_λ is $(n+1)$ -form of order $2r$.

For example, if we consider a variational problem defined by first-order Lagrangian

$$\lambda = \mathcal{L} \omega_0, \quad \mathcal{L} = \mathcal{L}(x^i, y^\sigma, y_j^\sigma)$$

the Euler-Lagrange equations are in the form

$$\left(\frac{\partial \mathcal{L}}{\partial y^\sigma} - \frac{\partial^2 \mathcal{L}}{\partial x^i \partial y_i^\sigma} - \frac{\partial^2 \mathcal{L}}{\partial y^\nu \partial y_i^\sigma} y_i^\nu - \frac{\partial^2 \mathcal{L}}{\partial y_j^\nu \partial y_i^\sigma} y_{ji}^\nu \right) \circ J^2 \gamma = 0, \quad (6)$$

where $1 \leq \sigma \leq m$, and m is the dimension of each fiber of Y . Taking $n = m = 1$, the equation (6) corresponds with (2).

6 Selected problems

In this Section we mention some problems where methods and concepts of the global variational geometry are applied. First of them is a complete characteristic of extremals of the *Hilbert variational functional*. Formulated by Hilbert (1915) in [8], it is a variational functional for metric fields on a general n -dimensional manifold X . For $n = 4$, its Euler-Lagrange equations are the *Einstein vacuum equations* in the general relativity theory.

Let X be an n -dimensional smooth manifold, $T_2^0 X$ the vector bundle of tensors of type $(0, 2)$ over X . Consider $\text{Met } X$ as an open subset of $T_2^0 X$ of *symmetric, regular bilinear forms* on $T_x X$, $x \in X$. Sections of $\tau : \text{Met } X \rightarrow X$ are *metric fields* on X . Integral variational functionals for the metric fields are defined by n -forms on $J^r \text{Met } X$.

Any chart (U, φ) , $\varphi = (x^i)$, on X , induces a chart (V, ψ) , $\psi = (x^i, g_{ij})$, on $\text{Met } X$, where $V = \tau^{-1}(U)$, and g_{ij} are the functions on V defined by

$$g = g_{ij} dx^i \otimes dx^j, \quad g_{ij} = g_{ji}, \quad \det(g_{ij}) \neq 0.$$

The functions

$$\Gamma_{ij}^k = \frac{1}{2} g^{kl} \left(\frac{\partial g_{il}}{\partial x^j} + \frac{\partial g_{jl}}{\partial x^i} - \frac{\partial g_{ij}}{\partial x^l} \right),$$

where g^{kl} are elements of the inverse matrix of the matrix g_{ij} , are called *Christoffel symbols*. The expressions

$$R_{ik} = \frac{\partial \Gamma_{ik}^l}{\partial x^l} - \frac{\partial \Gamma_{il}^l}{\partial x^k} + \Gamma_{ik}^l \Gamma_{lm}^m - \Gamma_{km}^l \Gamma_{il}^m, \quad R = g^{ik} R_{ik},$$

define the *Ricci tensor* with components R_{ik} , and a function $R : J^2 \text{Met } X \rightarrow \mathbf{R}$, called the *scalar curvature*, respectively. The *Hilbert Lagrangian* is given by the formula

$$\lambda = R \sqrt{|\det(g_{ij})|} \cdot \omega_0,$$

and the variational functional

$$\Gamma_\Omega(\tau) \ni g \mapsto \lambda_\Omega(g) = \int_\Omega J^2 g^* \lambda \in \mathbf{R}.$$

is the *Hilbert variational functional* for the metric fields on X . The corresponding Euler-Lagrange equations are *Einstein vacuum equations*

$$\left(R_{ij} - \frac{1}{2} R g_{ij} \right) \circ J^2 g = 0. \tag{7}$$

The well known solution of (7) is the *Schwarzschild metric* (1916), in spherical coordinates $(t, r, \varphi, \vartheta)$, on $\mathbf{R} \times \mathbf{R}^3 \setminus \{(0, 0, 0)\}$ given by

$$g = - \left(1 - \frac{C}{r}\right) dt \otimes dt + \left(1 - \frac{C}{r}\right)^{-1} dr \otimes dr + r^2 (\sin^2 \vartheta d\varphi \otimes d\varphi + d\vartheta \otimes d\vartheta).$$

A complete characteristic of the solutions of (7), independent of a metric *signature*, a choice of a base manifold X of the given variational problem, and searching for solutions of generalized versions of the equations (7) belong among open questions in general relativity theory.

Other famous problem of the global variational geometry is the *inverse problem of calculus of the variations*. Roughly speaking, it consists in finding *conditions* under which there exists a Lagrangian whose Euler-Lagrange equations coincide with a given system of differential equations. If such conditions are satisfied, then the problem is to find *all* Lagrangians for the system of equations.

Consider a system of m ordinary second-order differential equations in an implicit form,

$$\varepsilon_i(x^j, \dot{x}^j, \ddot{x}^j) = 0, \quad i, j = 1, 2, \dots, m,$$

for m functions of one real variable $t \mapsto x^j(t)$. We say that a system of functions $\varepsilon = \{\varepsilon_i(x^j, \dot{x}^j, \ddot{x}^j)\}$ is *variational* if there exists a function $\mathcal{L} = \mathcal{L}(x^j, \dot{x}^j)$ such that

$$\varepsilon_i = \frac{\partial \mathcal{L}}{\partial x^i} - \frac{d}{dt} \frac{\partial \mathcal{L}}{\partial \dot{x}^i}, \quad i = 1, 2, \dots, m.$$

The following two conditions are equivalent.

- (a) The system $\varepsilon = \{\varepsilon_i(x^j, \dot{x}^j, \ddot{x}^j)\}$ is variational.
- (b) The functions ε_i satisfy

$$\begin{aligned} \frac{\partial \varepsilon_i}{\partial \ddot{x}^l} - \frac{\partial \varepsilon_l}{\partial \ddot{x}^i} &= 0, \\ \frac{\partial \varepsilon_i}{\partial \dot{x}^l} + \frac{\partial \varepsilon_l}{\partial \dot{x}^i} - \frac{d}{dt} \left(\frac{\partial \varepsilon_i}{\partial \ddot{x}^l} + \frac{\partial \varepsilon_l}{\partial \ddot{x}^i} \right) &= 0, \\ \frac{\partial \varepsilon_i}{\partial x^l} - \frac{\partial \varepsilon_l}{\partial x^i} - \frac{1}{2} \frac{d}{dt} \left(\frac{\partial \varepsilon_i}{\partial \dot{x}^l} - \frac{\partial \varepsilon_l}{\partial \dot{x}^i} \right) &= 0. \end{aligned} \tag{8}$$

The system (8) is called the *Helmholtz conditions* (Helmholtz, 1887). If this system is satisfied then for a Lagrangian in question we can take the *Vainberg-Tonti Lagrangian* (see, e.g., [15]).

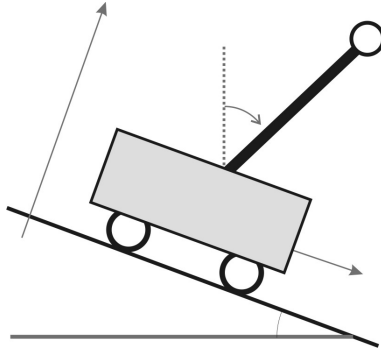


Fig. 3: Inverted pendulum on a cart

The theory is applicable in many variational problems. As an example we can introduce well known mechanical system, the *inverted pendulum on a cart* (IPC) (Fig. 3). The system consists of a pendulum of length l and a bob mass m_2 . The pendulum is attached to the top of a cart of mass m_1 . The configuration manifold of the system is $Q = \mathbf{R} \times S^1$, with coordinates x denoting the position of the cart, and φ denoting the angle of the pendulum with the upright vertical.

The Lagrange function for the system moving on horizontal x -axis is

$$\mathcal{L} = \frac{1}{2}(m_1 + m_2)\dot{x}^2 + m_2l \cos \varphi \dot{x}\dot{\varphi} + \frac{1}{2}m_2l^2\dot{\varphi}^2 - m_2gl \cos \varphi.$$

The Euler-Lagrange equations for the free motion of IPC are given by

$$\begin{aligned} m_2l\dot{\varphi}^2 \sin \varphi - (m_1 + m_2)\ddot{x} - m_2l\ddot{\varphi} \cos \varphi &= 0, \\ m_2l(g \sin \varphi - \ddot{x} \cos \varphi - l\ddot{\varphi}) &= 0. \end{aligned}$$

Of course, without any external intervention, the pendulum falls down. Our aim is to control the system stabilizing the pendulum in upright position through the *variational forces*. In generally, we search for ϕ_1, ϕ_2 , depending on $x, \varphi, \dot{x}, \dot{\varphi}$, such that the system

$$\begin{aligned} m_2l\dot{\varphi}^2 \sin \varphi - (m_1 + m_2)\ddot{x} - m_2l\ddot{\varphi} \cos \varphi &= \phi_1, \\ m_2l(g \sin \varphi - \ddot{x} \cos \varphi - l\ddot{\varphi}) &= \phi_2 \end{aligned}$$

is variational, and stabilizes the pendulum in upright position. Some results of the problem can be found, e.g., in [1], and [4]. The study of possible variational forces to stabilize the system is an object of current research.

Acknowledgements

The author would like to thank the organizers for the invitation to give a lecture at the conference, and for their kind hospitality during the event.

References

- [1] A. M. Bloch, N. E. Leonard, J. E. Marsden: *Controlled Lagrangians and the stabilization of mechanical systems. I. The first matching theorem*. IEEE Trans. Automat. Control 45 (2000), pp. 2253–2270
- [2] E. Cartan: *Lecons sur les Invariants Intégraux*. Hermann, Paris, 1922
- [3] P. Dedecker: *On the generalization of symplectic geometry to multiple integrals in the calculus of variations*, in: Lecture Notes in Math. 570. Springer, Berlin, 1977, pp. 395–456
- [4] M. Farré Puiggalí, T. Mestdag: *The Inverse Problem of the Calculus of Variations and the Stabilization of Controlled Lagrangian Systems*. SIAM J. Control Optim., 54 (6) (2016), pp. 3297–3318
- [5] P. L. Garcia: *The Poincare-Cartan invariant in the calculus of variations*. Symposia Mathematica 14 (1974), pp. 219–246
- [6] I. M. Gelfand, S. V. Fomin: *Calculus of Variations*. Prentice-Hall, Inc., Englewood Cliffs, New Jersey, 1963
- [7] H. Goldschmidt, S. Sternberg: *The Hamilton-Cartan formalism in the calculus of variations*. Ann. Inst. H. Poincaré 23 (1973) 203–267
- [8] D. Hilbert: *Die Grundlagen der Physik*. Nachrichten von der Gesellschaft der Wissenschaften zu Göttingen, Mathematisch-Physikalische Klasse (1915), pp. 325–407
- [9] D. Krupka: *Introduction to Global Variational Geometry*. Atlantis Studies in Variational Geometry, D. Krupka, H. Sun (Eds.), Atlantis Press, 2015
- [10] D. Krupka: *Some Geometric Aspects of Variational Problems in Fibered Manifolds*. Folia Fac. Sci. Nat. UJEP Brunensis, Physica 14, Brno, Czech Republic, 1973, 65 pp.
- [11] J. M. Lee: *Introduction to Smooth Manifolds*. Graduate Texts in Math. 218, Springer, 2006
- [12] Th. H. J. Lepage: *Sur les champs géodésics du calcul des variations, I, II*. Bull. Acad. Roy. Belg. 22 (1936) 716–729, pp. 1036–1046
- [13] A. Trautman: *Invariance of Lagrangian systems*, in: General Relativity, *Papers in Honour of J. L. Synge*. Oxford, Clarendon Press, 1972, pp. 85–99
- [14] M. Zamboj: *Synthetic construction of the Hopf fibration in a double orthogonal projection of 4-space*. Journal of Computational Design and Engineering 8 (3) (2021), pp. 836–854
- [15] D. Zenkov (Ed.): *The inverse problem of the calculus of variations*, Atlantis Studies in Variational Geometry, D. Krupka, H. Sun (Eds.). Atlantis Press, 2015

Stepwise discovery of geometrical knowledge in GeoGebra

Zoltán Kovács, Jonathan H. Yu

*The Private University College of Education of the Diocese of Linz
Salesianumweg 3, 4020 Linz, Austria
email: zoltan@geogebra.org*

*Gilman School
5407 Roland Avenue, Baltimore, Maryland 21210, USA
email: jonathanhy314@gmail.com*

Abstract. We describe an enhancement to GeoGebra, a well-known dynamic geometry software tool that calculates the significant geometric properties of a planar construction. In a previous experimental version of GeoGebra, “GeoGebra Discovery,” the Discover command determined geometric properties such as parallelism or perpendicularity of lines, equality of segment lengths, and collinearity or concyclicity of points. This work introduces a further improvement of the Discover command, the “stepwise discovery” mode, which supports real time, dynamic identification of true statements and geometric properties as each new point is added to the construction. Our contribution explains how the stepwise discovery mode can be helpful in teaching planar geometry at the secondary level or in the researcher’s work.

Keywords: GeoGebra, discovery, automated reasoning, plane geometry.

1 Introduction

Proving plane geometry theorems mechanically has roots in algebraic geometry and logic. For example, Chou [1] proved 512 theorems in the plane geometry mechanically through algebraic means, *i.e.*, by using coordinates and systems of equations. Chou used two different approaches in manipulating these equation systems: the Wu-Ritt characteristic sets (a reasonably fast approach), and elimination via Grbner bases (somewhat slower but more complete).

Algebraic methods, however, cannot handle certain situations, such as restricting points on segments or half-planes, so a more complete study of plane geometry problems usually requires additional methods like *real geometry*, via cylindrical algebraic decomposition or regular chains, or *synthetic methods* via axioms, with both methods being complete but computationally intensive.

In this work we focus on the *presentation* of mechanically proven results. This can be helpful in classroom use and also for some research questions. Given a planar geometry figure, the GeoGebra program determines and reports salient patterns, properties, and theorems. Our work extends GeoGebra’s Automated Reasoning Toolset by introducing *stepwise discovery* which detects these patterns dynamically, in real time, for a GeoGebra user.

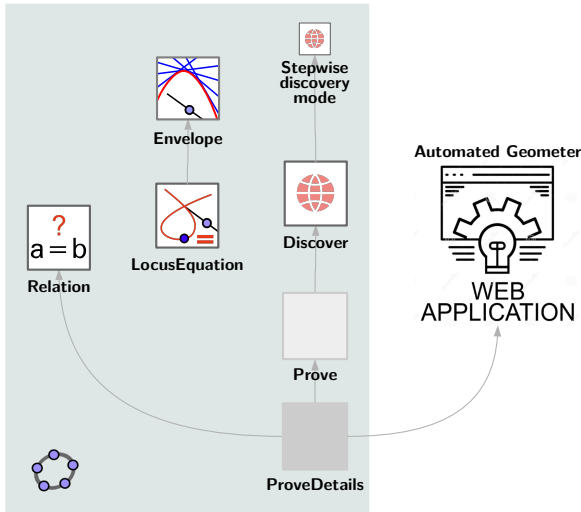


Fig. 1: Available tools and commands in GeoGebra and GeoGebra Discovery

2 GeoGebra Automated Reasoning Tools

GeoGebra comes with a set of automated tools (Figure 1) to symbolically check and discover geometric properties of a given planar construction:

- The **ProveDetails** command uses Gröbner bases to prove or disprove its input statement and determine any non-degeneracy conditions if they exist for the given input.
- The **Prove** command returns a yes/no answer if its input statement is true or false, based on the background analysis provided by the **ProveDetails** command.
- The **Relation** tool and command decides if two or more selected objects has a certain property, based on the background analysis from the **ProveDetails** command.
- The **LocusEquation** command and tool finds geometric loci for the given input.
- The **Envelope** command and tool determines the envelope equation of the input parameters.
- The **Discover** command and tool systematically detects all possible patterns of a given input point after an automated background analysis, based on the **Prove** command. The results are communicated both graphically and in list form.

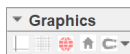


Fig. 2: Toolbar in the Graphics View in GeoGebra Discovery version 5

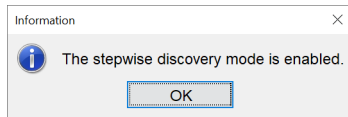


Fig. 3: Stepwise discovery is enabled in GeoGebra Discovery version 5

- *Automated Geometer*, a web based application discovers relevant patterns for the entire figure. Based on GeoGebra's JavaScript API, it performs the background analysis via the `ProveDetails` command and a programmatic JavaScript connection.

While some of these features are available only in an experimental version of GeoGebra, *GeoGebra Discovery*, our contribution adds a new tool: the *stepwise discovery mode* in GeoGebra Discovery [2].

3 Stepwise discovery

The stepwise discovery mode can be enabled either in the Graphics View Toolbar (Fig. 2), or with the command `StepwiseDiscovery` with a Boolean parameter that switches this mode on or off. Once enabled, a popup window informs the user of the change (in version 5, see Figure 3) or the Toolbar icon gets a blue frame (in version 6).

At that point, the stepwise discovery mode starts the `Discover` command [3] automatically for each newly added point. The software displays all of its relevant calculations graphically and in real time. The list of results in text format is not shown to avoid an overly cluttered output.

3.1 An example

We now demonstrate stepwise discovery with the Euler line of a triangle: *In each non-degenerate, non-regular triangle the circumcenter, the orthocenter and the barycenter are collinear.*

1. In Figure 4 an arbitrary non-degenerate triangle is drawn. (It is important to draw a non-regular triangle to make sure that the three investigated points do not coincide.)
2. In Figure 5 we create the midpoint D of segment a . The program determines that the midpoint designates two congruent segments, f and g , which are colored green.

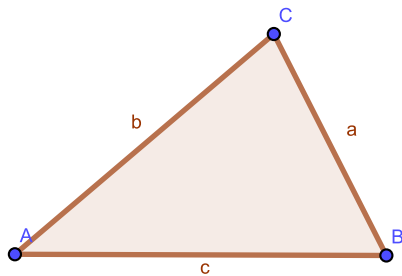


Fig. 4: An arbitrary triangle ABC is drawn

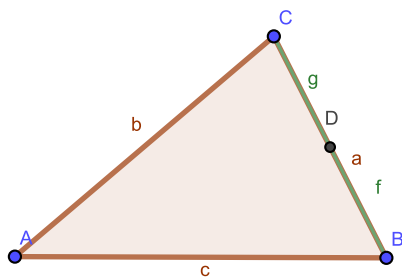


Fig. 5: First step of discovery by designating midpoint D of a

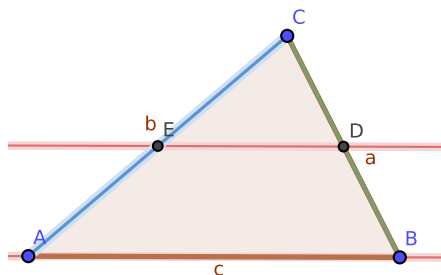


Fig. 6: Second step of discovery by designating the midpoint E of b

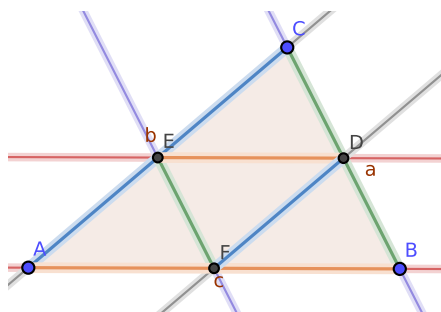


Fig. 7: Third step of discovery by designating the midpoint F of c

3. Two discoveries are found with the midpoint E of b . First, the midpoint creates two congruent segments, as occurred in the section above. Also, two parallel lines are identified: AB and DE .
4. After creating the midpoint F of c , the software determines the following:
 - $AF = BF = DE$,
 - $AE = CE = DF$,
 - $BD = CD = EF$,
 - $BC \parallel EF$,
 - $AC \parallel DF$,

and the formerly identified $AB \parallel DE$ is also highlighted because the newly added point F is related to AB .

5. Now two medians AD and BE are constructed, along with their intersection G . Here the program detects numerically and proves symbolically that G lies on CF , that is, the medians of a triangle

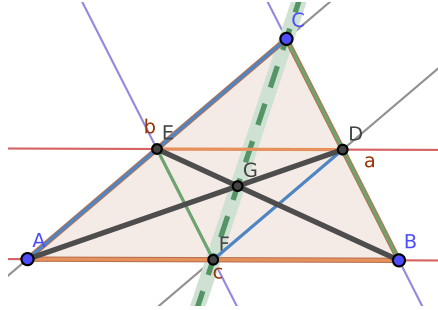


Fig. 8: Fourth step of discovery by intersecting two medians

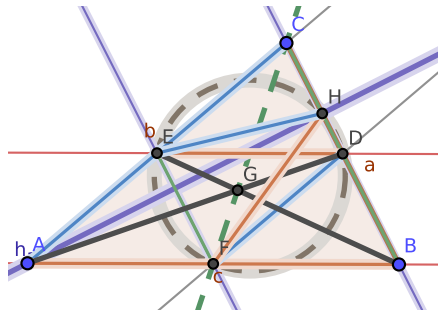


Fig. 9: Fifth step of discovery: creating a foot point of an altitude

are concurrent (Fig. 8). The previously discovered properties do not play a direct role related to G , so they are not highlighted at this step.

6. Next, we construct the height for side a and its intersection H with side a (Fig. 9). New discoveries are made: lines BC , EF and AH build a set of parallel and orthogonal lines, so they are colored uniformly. In addition, EH has the same length as AE , CE and DF . Similarly, FH has the same length as AF , BF and DE , so they are colored with the same color. Also, D , E , F and H are found to be concyclic, as illustrated by the circle on each of these points.
7. In Figure 10 we show the height for side b and its intersection I with side b . Importantly, I is identified as a circumpoint of circles $AIHB$ and $EIHDF$, the latter of which has been found to have five remarkable points. If we continue our experiment by choosing the third foot point (which belongs to c), we can find the sixth point of the well-known 9-point circle. (Note that the figure was

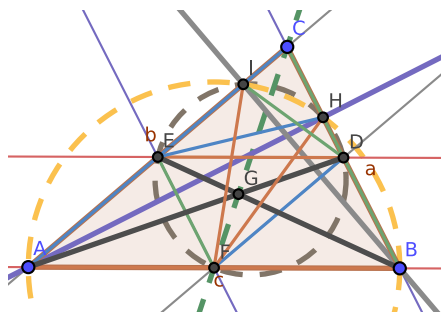


Fig. 10: Sixth step of discovery: creating a foot point of another altitude

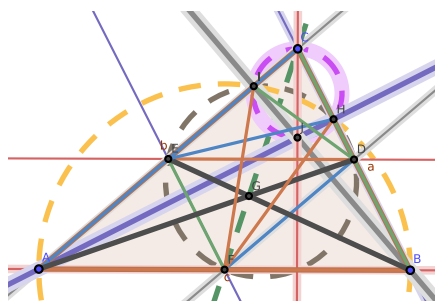


Fig. 11: Seventh step of discovery: creating the orthocenter

created after selecting all objects by using the shortcut Ctrl-A, and then de-selecting all of them by clicking to on an empty part of the screen.)

8. As our figure starts to be a bit complicated, we now zoom in to view more detail before performing the next step. By intersecting AH and BI , we obtain point J (the orthocenter), and we learn that $CJ \perp AB$ (they are shown in the same color to emphasize their perpendicularity), and also that $CIJH$ is a cyclic quadrangle (Fig. 11).
9. Finally, we generate the perpendicular bisectors for a and b , and their intersection K . The program then detects these noteworthy properties:
 - $AH \parallel DK$ and $BI \parallel EK$ (these are direct consequences of their definition),
 - $AK = BK = CK$ (indeed, K is the circumcenter of the triangle),

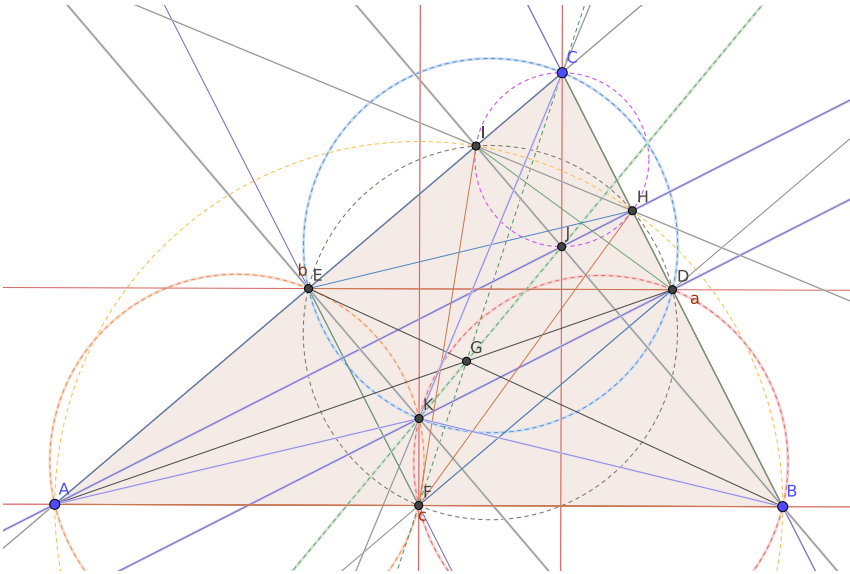


Fig. 12: Eighth step of discovery: identifying the Euler line

- circles AEF , BDF and CDE include K (this is quite clear because all of them are Thales circles of the diameters AK , BK and CK),
- G , J and K are collinear.

This final item clearly expresses the existence of the Euler line.

4 Conclusion

We have shown an introductory example of stepwise discovery in GeoGebra Discovery, available at <https://github.com/kovzol/geogebra/releases/tag/v5.0.641.0-2022Nov03>. Other software systems like *OK Geometry* (<https://www.ok-geometry.com/>) 19.1.1, the *Java Geometry Expert* (<https://github.com/yezheng1981/Java-Geometry-Expert>) 0.80, *Géométrie* (<http://geometrix.free.fr/site/logiciels.php>) 4.3, and others also support certain features of geometric discovery. However, GeoGebra Discovery has the advantages of a straightforward graphical user interface, as well as wide availability in multiple languages at no cost at <https://autgeo.online>

While it is useful to discover relationships or hidden features of a planar figure, there are several limitations in the latest public version of GeoGebra Discovery.

Stepwise discovery seems to be most effective in studying relationships when the number of discovered objects is not too high. Above a certain threshold, it is difficult to visually separate objects, even with different colors and notations. In addition, detecting congruent angles and investigating new segments, lines, or circles are not yet implemented. Not reporting trivial properties is a difficult task because of the challenge of objective and user-defined criteria to determine whether a feature is trivial.

Speed remains a major issue in the web version. The web implementation is based on a WebAssembly compilation of the underlying computer algebra system Giac, which is approximately 3 times slower than the native desktop version on the same hardware. (We used recent versions of Google Chrome and Firefox in our benchmarks.) In addition, one should avoid creating figures with an excessive number of points to avoid combinatorial explosion, as the computation of Grbner bases is computationally intensive.

In conclusion, we have described a new enhancement of stepwise discovery to GeoGebra, with real time, dynamic identification of geometric properties with each additional user input. This stepwise discovery mode has applications in teaching planar geometry or in research.

Acknowledgements

The authors are grateful to Xenia Burgholzer for her advice on some graphical preparations for this paper.

The first author was partially supported by a grant PID2020-113192GB-I00 (Mathematical Visualization: Foundations, Algorithms and Applications) from the Spanish MICINN.

References

- [1] S.-C. Chou: *Mechanical Theorem Proving*, D. Reidel Publishing Company, Dordrecht, Holland, 1988
- [2] Z. Kovács, T. Recio, M. P. Vélez: *GeoGebra Discovery in Context*. In Proceedings of the 13th International Conference on Automated Deduction in Geometry, Electronic Proceedings in Theoretical Computer Science 352, 2021, pp. 141-147
- [3] Z. Kovács, J. H. Yu: *Automated Discovery of Geometrical Theorems in GeoGebra*. In Proceedings 10th International Workshop on Theorem Proving Components for Educational Software, Electronic Proceedings in Theoretical Computer Science 354, 2022, pp. 1-12

190. výročí Jánose Bolyaie v Olomouci a neeuclidovská geometrie

The 190th anniversary of János Bolyai in Olomouc and non-Euclidean geometry

Josef Mikeš

*Přirodovědecká Fakulta, Univerzita Palackého v Olomouci
tř. 17. listopadu 12, 779 00 Olomouc
email: josef.mikes@upol.cz*

Abstract. This year, we celebrate the 190th anniversary of János Bolyai's presence in Olomouc. He stayed in Olomouc for a short period (1832-1833) during his military service. His studies brought a complete concept of non-Euclidean and hyperbolic geometry (whose origin is also attributed to Lobachevski and Gauss) that had, and still have, an impact on mathematics in general and various physics processes. The generalization of his studies also leads to the development of the theory of relativity.

Keywords: János Bolyai, non-Euclidean geometry, Hyperbolic geometry.

Klíčová slova: János Bolyai, neeuclidovská geometrie, hyperbolická geometrie.

1 Úvod

János Bolyai (Obr. 1) byl maďarský matematik a zakladatel nauky o neeuclidovské geometrii. Bolyai se narodil 15. prosince 1802 v Koloszáru (nyní je to Cluj-Napoca v Rumunsku) a zemřel 27. ledna 1860. Takže nyní je 220. výročí jeho narození.

Jeho otec Farkas Bolyai (1775-1856) pocházel ze zchudlého maďarského rodu, narodil se na zámku Bolyai. Byl prvním významnějším maďarským matematikem, který učil matematiku, fyziku a chemii na gymnáziu. János díky svému otci již ve třinácti letech zvládl kalkulus a analytickou mechaniku. V letech 1818–1823 studoval vojenskou inženýrskou akademii ve Vídni. Sedmileté studium zvládl za 4 roky. V armádě sloužil 11 let, byl dobrým důstojníkem a výtečným tanečníkem, nepil a nekouřil. Ovládal 9 jazyků. Ženíl se v 1834 s Rozálií Orbánovou, se kterou měl dvě děti. Rozvedli se v 1852 roce.

I když se celý život matematikou zabýval, nestal se profesionálním matematikem. Jeho práce nebyly druhými pochopeny či ohodnoceny, jak by očekával, a to ho uvrhovalo do mnoha psychických problémů, s kterými se potýkal do konce života. Své práce se později již bál publikovat. V 1860 roce zemřel sám a v nouzi ve věku 57 let, jeho otec o 4 roky dříve.



Obr. 1: János Bolyai

2 Život a dílo Jánose Bolyaie

Faktem je, že jedinou publikovanou prací při jeho životě je latinsky napsaný Apendix jako příloha středoškolské učebnice jeho otce Farkase v roce 1832. Rozšířený název této práce je *Appendix scientiam spatii absolute veram exhibens*, tj. *Přídavek předvádějící absolutně pravdivou vědu o prostoru*, viz Obr. 2.

Zde je v kompaktní formě na 26 stránkách rozpracována neeuklidovská geometrie, která je v současnosti nazývána buď geometrií Lobačevského, nebo hyperbolickou, tento název jí dal Felix Klein.

Tuto geometrii nezávisle na Jánoši Bolyai také objevili německý matematik Karl Gauss a ruský matematik Nikolaj Lobačevský. Gauss zřejmě jako první, nejspíše mnohem dříve než Bolyai i Lobačevský, ale jeho práce v tomto směru našli až po jeho smrti – nikdy je nepublikoval. Král matematiků nechtěl zůstat nepochopen. V 1831 roce, kdy mu poslali Apendix na posouzení, napsal příteli: Ten mladý geometr Bolyai je genius první třídy. Ale otci Farkasovi však napsal: Ocenit to, je to samé jako ocenit sebe. Protože vše co je tam napsané, je stejné s mými výsledky posledních 30-35 let na toto téma.

Lobačevský se touto tematikou zabýval ve dvacátých letech 19. století. 23. února 1826 na vědeckém semináři v Kazaňské univerzitě přednesl přednášku *Stručný výklad základů geometrie s přísným důkazem teoremy o paralelách*. Tento moment se počítá za úřední počátek neeuklidovských geometrií. Tyto výsledky publikoval poprvé na přelomu let 1829 a 1830 v časopise *Věstník Kazaňské univerzity*. A později 1837 i ve Francii.

A P P E N D I X.

SCIENTIAM SPATII absolute veram exhibens:
 a veritate aut falsitate Axiomatis XI Euclidis
 (a priori haud unquam decidenda) in-
 dependentem: adjecta ad casum fal-
 sitatis, quadratura circuli
 geometrica.

Auctore JOHANNE BOLYAI de eadem, Geometrarum
 in Exercitu Caesareo Regio Austriaco Ca-
 strensium Capitaneo

Obr. 2: Appendix

Géométrie imaginaire, J. Reine Angew. Math. 17, 295-320 (1837). Zdánlivá (imaginární) geometrie.

Význam Lobačevského práce byl plně doceněn až několik desítek let po jeho smrti – v podstatě až tehdy, když Albert Einstein použil zobecnění jeho myšlenek k matematické formulaci svojí obecné teorie relativity.

Jak známo, geometrie byla již ve starověku Euklidem uspořádaná do axiomatického systému, který se dle Začátků Euklida učil více než 2000 let. S některými metodickými modifikacemi se učí do dnes.

Protože popisuje mnohé mechanicko-fyzikální jevy, je nejvíce používanou geometrií vůbec. Její samozřejmost se proto střetávala s filosofickými názory na svět, např. Kantova teorie v 19. stol. tvrdila, že Euklidova geometrie je živým tvorům vrozená. Tento paradox vznikl proto, že bylo špatně pochopeno, že Euklidova geometrie je pouze aproximací fyzikálních a zvláště mechanických jevů. Toto bylo explicitně vyjádřeno ve 20. stol. v pracích Alberta Einsteina.

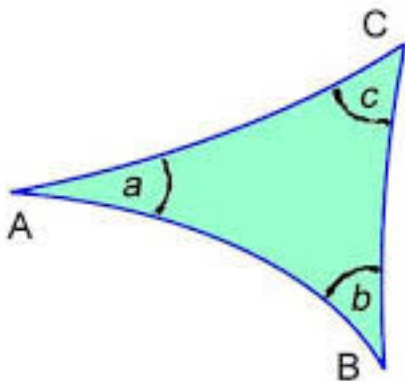
Po dobu 2000 let se precizovala axiomatika Euklidovy geometrie. Ještě ve starověku Archimédes přidal nový axiom a poslední byl přidán koncem 19. stol. Paschem.

Celou tuto dobu byl trnem v oku tzv. 5. axiom o rovnoběžkách. Ten se dá v zjednodušeném tvaru pro Euklidovskou rovinu formulovat takto: Buď dána přímka a bod, který na ní neleží. Pak existuje jediná přímka

procházející tímto bodem, se kterou nemá společný bod (rovnoběžka). Tento axiom se zdál být důsledkem ostatních axiomů. O důkaz tohoto faktu se pokoušeli mnozí matematikové (mnohdy se jim to bohužel podařilo).

V 19. století bylo této otázce věnováno mnoho energie. Již dříve mnozí autoři zaměnili 5. axiomu za její protiklad a snažili se najít spor. Karl Gauss, Nikolaj Lobačevský a János Bolyai explicitně rozvinuli geometrickou teorii, ve které v Euklidově axiomatice zaměnili axiom o rovnoběžkách takto: Existují aspoň dvě rovnoběžky k dané přímce. Tato geometrie měla samozřejmě podstatné odlišnosti od Euklidovy.

V jejím studiu nejdále zřejmě dospěl Lobačevský, který kompletně sestrojil trigonometrii v rámci této geometrie. Zajímavostí je např. to, že trojúhelník v Lobačevské geometrii má součet úhlů menší než π a objem celého prostoru je konečný, viz Obr. 3.



Obr. 3: Trojúhelník v Lobačevské geometrii

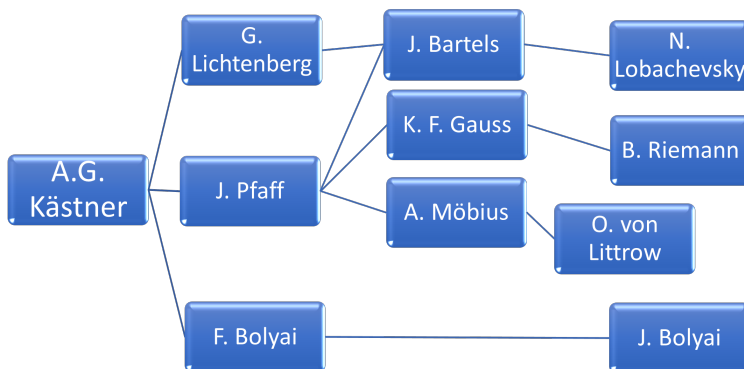
Při životě Gausse, Lobačevského a Bolyaie se tato teorie nesetkala s pochopením. Lobačevsky byl anonymně (Ostrogradským aj.) šikanován a posléze i úředně degradován. Po obdržení posmrtné bronzové Gaussovy medaile, mu byly vráceny všechny pocty, kterých si ale užil pouze dva poslední týdny svého života.

Bolyai byl profesionální voják. Konec jeho vojenské kariéry byl dovršen v Olomouci v roce 1833, kdy byl penzionován bez důchodu. Navíc se zřejmě jeho psychický stav natolik zhoršil, že byl nakonec odkázán na peněžní výpomoc svého otce.

Gaussovy výsledky v této oblasti se našly v trezoru až po jeho smrti.

3 Genealogie neeuclidovských geometrií

Co spojuje tyto tři osobnosti? Na grafu (viz Obr. 4) je znázorněna matematická genealogie, ze které vyplývá, že společným jmenovatelem by mohli být němečtí matematici Kazner, Lichtenberg a Pfaff, který se intenzivně zabýval euklidovskou axiomatikou, a také možná nejvíce Martin Bartels.



Obr. 4: Matematická genealogie

Martin Bartels byl školním učitelem Gausse. Společně pak byli aspiranty Pfaffa a jejich spolužákem byl i Farkas Bolyai – otec Jánose Bolyaie. Po zakončení těchto studií Bartels přenechal katedru matematiky Göttingenské univerzity talentovanějšímu Gaussovi a sám dostal místo v nově založené Kazaňské univerzitě v Rusku na Volze. Tam se od roku 1808 jeho žákem stal Lobačevský. Jeho učitelem byl i astronom Josef von Littrow, který se narodil v Čechách, byl absolventem UK a také šéfem observatoře v Krakově, Kazani a Vídni. Byly to zřejmě boží cesty zakladatelů neeuclidovské geometrie. Gauss zemřel v roce 1855, Lobačevský pak v roce následujícím a J. Bolyai v roce 1860.

Rehabilitace jejich výsledků se uskutečnila o osm let později. Italský matematik Eugenio Beltrami dokázal, že mezi prostory s konstantní Gaussovou křivostí lze vždy ustanovit geodetické zobrazení. Z toho mimo jiné vyplývalo, že přímky roviny se zobrazí na geodetické křivky prostoru s nenulovou konstantní křivostí. Mimo jiné na sféru a pseudosféru. Z toho vyplynulo, že na pseudosféře se splňují všechny axiomy Euklida kromě jednoho o rovnoběžnosti, tedy na pseudosféře se splňuje hyperbolická geometrie. Korektněji pseudosféra je částí Lobačevského roviny. V návaznosti na Beltrami vytvořili Klein a Poincaré několik dalších modelů hyperbolické geometrie.

V případě sféry se také narušuje pátý axiom (vůbec neexistují rovnoběžky) a vede k eliptické geometrii, kterou popsal Bernhard Riemann v roce 1854. V tomto případě je však narušen ještě jeden Euklidův axiom (nejednoznačnost přímky procházející dvěma body). Riemann tehdy založil ještě obecnější geometrii intenzivně využívanou v moderní geometrii a teoretické fyzice. Je to Riemannova a pseudo-Riemannova geometrie.

Poděkování

Článek vznikl za podpory grantu IGA Přf 2022017.

Literatura

- [1] J. Bolyai: *Non-Euclidean Geometry*, thesis, Royal Engineering College from Vienna, 1822 (supervisor F. Bolyai)
- [2] C. F. Gauss: *Demonstration nova theorematis omnem functionem algebraicam rationalem integram unius variabilis in factores reales primi vel secundi gradus resolvi posse*, Ph.D. thesis, Univ. Helmstedt, 1799 (supervisor J. F. Pfaff)
- [3] N. I. Lobachevsky: *Geometry*, thesis, Kazan State University, 1814 (supervisor J. M. Ch. Bartels)
- [4] J. Mikeš, et al: *Differential Geometry of Special Mappings*, Palacký University Press, Olomouc, 2019
- [5] B. Riemann: *Grundlagen für eine allgemeine Theorie der Funktionen einer veränderlichen complexen Grösse*, Ph.D. thesis, Göttingen Univ., 1851 (supervisor C. F. Gauss)

CONTRIBUTED TALKS

Vytváranie animácie v Geogebre

Creating an animation in Geogebra

Juliana Beganová

*Department of Mathematics and Descriptive Geometry, Faculty of Civil Engineering,
Slovak University of Technology in Bratislava
Radlinského 11, 810 05 Bratislava, Slovak Republic
email: juliana.beganova@stuba.sk*

Abstract. Animated videos support the visualization of objects in space and thus help students better understand the details of constructions. Different drawings in descriptive geometry challenge students' spatial imagination. The graphic program Geogebra helps us to better explain individual views. The entire object is drawn in the 3D space of the Geogebra program, where the animation itself is defined. The video is then created and edited using other programs and inserted into presentations.

Keywords: Video, animation, Geogebra

Kľúčové slová: Video, animácia, Geogebra

1 Motivácia

Vo výuke predmetu deskriptívna geometria sa stále častejšie stretávame s problémom študentov zobraziť objekt, ktorý je v priestore, na rovinu alebo naopak, objekt zobrazený v rovine predstaviť si v priestore. Hľadali sme preto spôsob ako im tento problém uľahčiť. Riešením sa ukázal grafický program Geogebra, ktorý je vhodný na kreslenie 3D objektov, prípadne vytvorenie pohybu rôznych objektov.

V príspevku je popísaný postup vytvorenia videa, ktoré zobrazuje sklopenie premietajúcej roviny osi z v kolmej axonometrii. Objekt je nakreslený v programe Geogebra, tu je zadefinovaný pohyb roviny. Celý pohyb je nasnímaný pomocou programu oCam na snímanie obrazovky a upravený v programe Video Editor. Takto pripravené video je vložené v prezentácii PowerPoint.

2 Vytvorenie animácie v Geogebre

Skôr než začneme kresliť všetky objekty, je potrebné si premyslieť postupnosť krokov vytvorenia celého pohybu nejakého objektu.

Prečo?

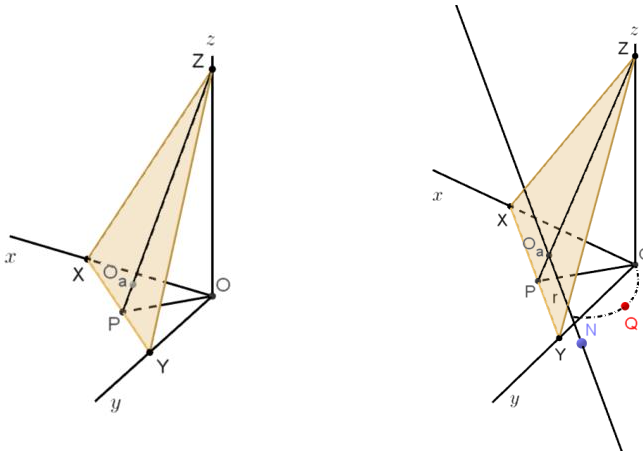
Pri vytváraní pohybu sa vždy pohybuje bod po nejakom útvere, napr. po priamke, po kružnici. Najskôr nakreslíme všetky statické objekty, ktoré nie sú súčasťou pohybujúcich sa objektov. Potom nakreslíme dráhu, po ktorej sa bude pohybovať bod, ktorým bude zadefinovaná animácia. Bod na útvere zobrazíme

pomocou príkazu **Point on Object**. Týmto bodom zadefinujeme objekty, ktoré sú súčasťou pohybu.

2.1 Podrobný postup konštrukcie

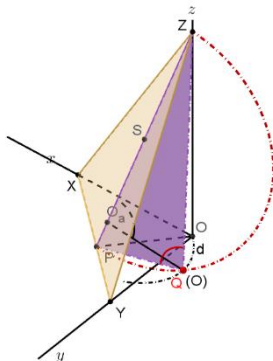
Nakreslíme všetky statické čiary a plochy.

1. Bod $O(0,0,0)$.
2. Oxi x, y, z ako úsečky ležiace na súradnicových osiach.
3. Body $X, Y, Z, X \in x, Y \in y, Z \in z$.
4. ΔXYZ – príkazom **Polygon**.
5. Rovina ρ kolmá na hranu XY , prechádzajúca bodom O .
6. Priesečnica roviny ρ s $\Delta XYZ = PZ$, obr. 1 vľavo.
7. $k, O \in k, k \perp \Delta XYZ$.
8. $O_a = k \cap \Delta XYZ$.
9. S – stred úsečky PZ .



Obr. 1: Zobrazenie statických prvkov kolmej axonometrie

10. $r, r \parallel XY, O_a \in r$, obr. 1 vpravo.
11. $N, N \in r$ – ľub.
12. Kružnicový oblúk d so stredom v bode O_a a prechádzajúci bodmi O, N .
13. Bod Q - **Point on Object** – bod na kružnicovom oblúku d . On sa bude potom pohybovať po oblúku.
14. Pomocou textu ho premenujeme na (O) , názov bodu Q vypneme.
15. Všetky objekty, ktoré chceme aby sa pohybovali spolu s bodom Q musíme zadefinovať bodom Q , obr. 2.
16. Polygon ZPQ .
17. Úsečka QO_a , oblúky pri bodoch O a O_a .

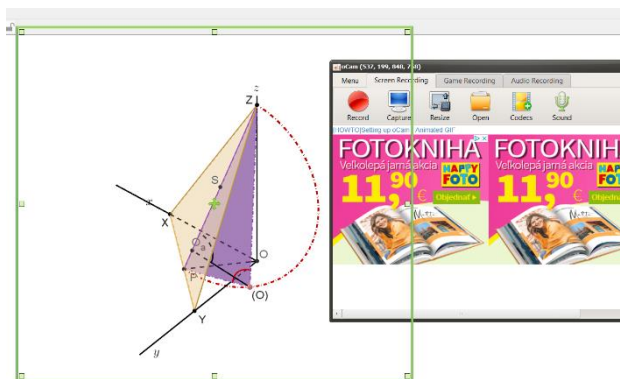


Obr. 2: Zobrazenie prvkov kolmej axonometrie

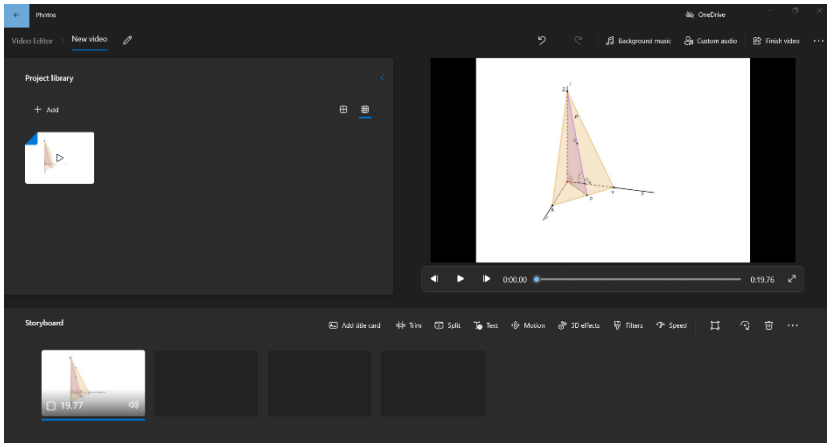
Samotná animácia sa spustí tak, že sa nastavíme myšou na názov bodu v algebraickom okne, klikneme pravým tlačidlom myši a v miestnej ponuke klikneme na **Animation on**.

3 Zaznamenanie pohybu

Celý pohyb zaznamenáme pomocou programu na snímanie obrazovky. Ja som použila program **oCam**. Zelené výberové okno umiestnime tak, aby v ňom bolo zobrazené všetko, čo chceme nasnímať. Skontrolujeme celú animáciu a pomocou **Record** spustíme nahrávanie, obr. 3. Nahratý súbor uložíme.

Obr. 3: Nasnímanie obrazovky pomocou programu **oCam**.

Video zostriháme pomocou programu **Video Editor**. Použijeme príkazy **Trim** a **Split**.



Obr. 4: Úprava videa pomocou programu Video Editor.

Väčšinou je video zostrihané na viac krokov. Výsledné video uložíme a vložíme do **PowerPoint** prezentácie. V prezentácii je potom možné upraviť zobrazenie videa.

4 Záver

Použitie videa na prednáškach deskriptívnej geometrie sa javí ako dobrá cesta podpory vizualizácie a uľahčenie štúdia pre študentov odborov stavebnej fakulty a fakulty architektúry.

Pod'akovanie

Tento článok vznikol za podpory projektu KEGA 008STU-4/2020.

Literatúra

Softvéry: Geogebra softvér 5.0, oCam. Ink, Video Editor 2022

- [1] M. Vajsáblová: *Deskriptívna geometria pre GaK*. Vydavateľstvo STU, Bratislava, 2009. 97 s. Dostupné online: http://www.svf.stuba.sk/docs//dokumenty/skripta/deskriptivna_gak/index.html

Exact and approximate symmetries of discrete curves in plane

Michal Bizzarri, Miroslav Lávička and Jan Vršek

*Department of Mathematics & NTIS, Faculty of Applied Sciences,
University of West Bohemia, Univerzitní 8, 301 00 Plzeň, Czech Republic*

email: bizzarri@kma.zcu.cz, lavicka@kma.zcu.cz, vrsekjan@kma.zcu.cz

Abstract. Recently, a new algorithm to decide whether a discrete curve is symmetric or not was presented in [4]. The basic strategy is to decompose a given curve into a family of suitable components (simpler discrete curves) whose symmetries can be found more easily. Using the designed method all existing rotational and reflectional symmetries can be determined. The formulated approach can be easily modified for perturbed discrete curves for which approximate symmetries are to be computed. In this contribution we shortly recall main steps of the algorithm from [4].

Keywords: Discrete curves, decomposition, exact and approximate symmetries

1 Introduction

Symmetries in the natural world are considered as an aspect of perfection, balance and harmony. They have served for people as inspiration to incorporate them when producing tools, buildings or artwork. From the point of view of geometry we must not forget Klein’s Erlangen Program and its basic concept for the characterization of geometries based on the symmetry groups, [8].

Symmetry is called global when it concerns the whole object, or local when only part of the object has this property. According to the type of transformation we can distinguish e.g. reflectional, rotational, central symmetries, etc. Symmetry can be exact or approximate with a tolerance. Symmetry detection belongs among classical problems in geometry, computer graphics, computer vision, geometric modelling, pattern recognition, etc. Mathematicians investigate predominantly global exact symmetries of objects given implicitly or by their rational parametrizations, see e.g. [5, 9, 1, 2, 3, 7].

This contribution is devoted to exact and approximate symmetries of planar discrete curves. It’s good to remember that the worlds of smooth and discrete shapes are inseparable. We often start with sets of points and work towards constructing smooth curves/surfaces. In other cases we begin with a smooth shape and by discretization we obtain a discrete version from it (e.g. for computational reasons), [6, 10]. And this is also closely connected to studying symmetries, let us recall e.g. symmetries of Bézier and B-spline shapes and relation to symmetries of their control polygons, see [11]. In this article we would like to briefly present the main procedures that were recently published in [4].

2 Preliminaries

An *isometry* in \mathbb{R}^2 is a mapping $\phi : \mathbb{R}^2 \rightarrow \mathbb{R}^2$ preserving distances, i.e.,

$$\mathbf{x} \mapsto \mathbf{A} \cdot \mathbf{x} + \mathbf{b}, \quad \text{where } \mathbf{A} \in \mathbf{O}(\mathbb{R}, 2) \text{ and } \mathbf{b} \in \mathbb{R}^2. \quad (1)$$

For $\det(\mathbf{A}) = 1$, or $\det(\mathbf{A}) = -1$ we speak about *direct*, or *indirect* isometries, respectively. A point set X has a *symmetry* if there exists a non-identical isometry ϕ such that $X = \phi(X)$. The *group of symmetries* of X will be denoted by $\mathbf{Sym}(X)$. Especially, we are interested in finite groups which are, in fact, the symmetries of regular m -gons (*cyclic groups* C_m and *dihedral groups* D_m).

By a *discrete curve* C we mean a finite set of vertices in \mathbb{R}^2 that are connected by line segments such that each vertex has exactly two neighbours. Let us emphasize that we consider only discrete curves which are closed, each three consecutive vertices are not collinear and all vertices are traced only once, on the other hand self intersections are allowed.

Let C be a discrete curve with n vertices $\mathbf{v}_0, \mathbf{v}_1, \dots, \mathbf{v}_{n-1}, \mathbf{v}_n = \mathbf{v}_0$. The vertices can be identified with the $n \times 2$ matrix (called a *parametrization* of C)

$$\mathbf{v} = \begin{pmatrix} x_0 & x_1 & \cdots & x_{n-1} \\ y_0 & y_1 & \cdots & y_{n-1} \end{pmatrix}^\top. \quad (2)$$

We will also work with two elementary reparametrizations $\mathbf{v}_i^{\beta\sharp} = \mathbf{v}_{i+\beta}$ for $\beta \in \mathbb{Z}_n$ (β -fold circular shift), and $\mathbf{v}_i^- = \mathbf{v}_{-i}$ (orientation reverse).

3 Main idea – decomposition

Consider a discrete curve C with a parametrization \mathbf{v} . Our plan is to find a decomposition of C such that

- (i) $\mathbf{v} = \sum_{\ell} \mathbf{v}^{(\ell)}$,
- (ii) $\mathbf{Sym}(C) \subset \mathbf{Sym}(C^{(\ell)})$.

Subsequently, the symmetries of C will be studied via the symmetries of the individual components $C^{(\ell)}$, see Fig. 1. Of course, the essential requirement is that the symmetries of $C^{(\ell)}$ must be easily identifiable.

For this purpose, let's move on to a new basis given by the orthogonal basis vectors

- $\mathbf{e}_0 = (1, 1, \dots, 1)^\top$,
- $\mathbf{e}_{2\ell-1} = \sqrt{2} \left(0, \sin \frac{2\pi\ell}{n}, \dots, \sin \frac{2(n-1)\pi\ell}{n} \right)^\top$ for $\ell = 1, \dots, \lceil \frac{n}{2} \rceil - 1$,
- $\mathbf{e}_{2\ell} = \sqrt{2} \left(1, \cos \frac{2\pi\ell}{n}, \dots, \cos \frac{2(n-1)\pi\ell}{n} \right)^\top$ for $\ell = 1, \dots, \lceil \frac{n}{2} \rceil - 1$,
- $\mathbf{e}_{n-1} = (1, -1, 1, -1, \dots, 1, -1)^\top$ only if n is even.

Then we arrive at

$$\mathbf{v} = \sum_{i=0}^{n-1} \mathbf{e}_i \cdot \hat{\mathbf{v}}_i, \text{ with } \hat{\mathbf{v}}_i = \frac{\mathbf{e}_i^\top \cdot \mathbf{v}}{n}, \quad (3)$$

which gives us the sought *components* in the form

$$\begin{aligned} \mathbf{v}^{(0)} &= \mathbf{e}_0 \cdot \hat{\mathbf{v}}_0 \quad (\hat{\mathbf{v}}_0 \text{ is the barycentrum of } C) \\ \mathbf{v}^{(\ell)} &= \mathbf{e}_{2\ell-1} \cdot \hat{\mathbf{v}}_{2\ell-1} \mathbf{e}_{2\ell} \cdot \hat{\mathbf{v}}_{2\ell}, \text{ where } \ell = 1, \dots, \lceil \frac{n}{2} \rceil - 1, \\ \mathbf{v}^{(\frac{n}{2})} &= \mathbf{e}_{n-1} \cdot \hat{\mathbf{v}}_{n-1} \quad (\text{only if } n \text{ is even}). \end{aligned} \quad (4)$$

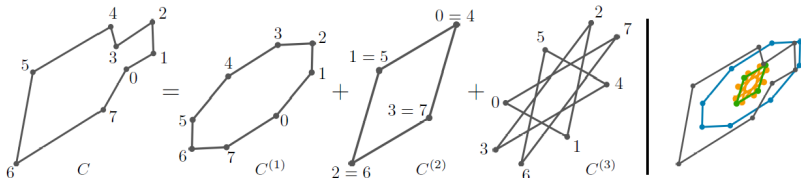


Fig. 1: Decomposition of the discrete curve C into components $C^{(\ell)}$, $\ell = 1, 2, 3$. This figure was taken from [4], originally Fig. 3.

For the sake of simplicity, we introduce the notation $\mathbf{E}_\ell = (\mathbf{e}_{2\ell-1} | \mathbf{e}_{2\ell})$ and $\mathbf{M}_\ell = \frac{1}{n} \mathbf{E}_\ell^\top \cdot \mathbf{v} = (\hat{\mathbf{v}}_{2\ell-1}, \hat{\mathbf{v}}_{2\ell})^\top$ and thus we can shortly write

$$\mathbf{v}^{(\ell)} = \mathbf{E}_\ell \mathbf{M}_\ell. \quad (5)$$

Main properties of this decomposition can be summarized as follows:

- the curve $C^{(\ell)}$ does not depend on the parametrization of C ,
- $\mathbf{Sym}(C) \subset \mathbf{Sym}(C^{(\ell)})$ for each $\ell = 1, \dots, \lceil \frac{n}{2} \rceil - 1$ and C having its barycenter in the origin,

see Corollary 11 and Theorem 12 in [4].

4 Exact symmetries of $C^{(\ell)}$ and C

In what follows we will presume that the barycenter of the vertices of C (possibly after translation) is at the origin. Next we assume that we have the decomposition of C into components $C^{(\ell)}$. Recall the property $\mathbf{Sym}(C) \subset \mathbf{Sym}(C^{(\ell)})$ from which it directly follows

$$\mathbf{Sym}(C) \subset \bigcap_{\ell \in I} \mathbf{Sym}(C^{(\ell)}). \quad (6)$$

This suggests to determine symmetries of all (or selected) individual components $C^{(\ell)}$ and next to find the intersection of all the obtained symmetry groups. It should be always verified whether the obtained candidate symmetries are also symmetries of the whole discrete curve C .

Hence, we have to start with formulating procedures how to find the reflectional and rotational symmetries of particular $C^{(\ell)}$. For the sake of brevity we recall without proofs the results from [4] (see Section 3.1).

Reflectional symmetries. If $\hat{\mathbf{v}}_{2\ell-1}$ and $\hat{\mathbf{v}}_{2\ell}$ are orthogonal and of the same length (we call such components *circular*) then it can be shown that $C^{(\ell)}$ is rotationally symmetric with the symmetry of m -gon, where

$$m = \frac{n}{\gcd(\ell, n)} > 2. \quad (7)$$

Remark 4.1 It can be easily shown that the points of $C^{(\ell)}$ given by

$$\mathbf{v}^{(\ell)} = \mathbf{E}_\ell \mathbf{M}_\ell$$

lie on the *associated ellipse*

$$\mathbf{p}_\ell(t) = \mathbf{a}_\ell \sin(\ell t) + \mathbf{b}_\ell \cos(\ell t) \quad (8)$$

with the conjugate half-diameters

$$\mathbf{a}_\ell = \sqrt{2} \hat{\mathbf{v}}_{2\ell-1}, \quad \mathbf{b}_\ell = \sqrt{2} \hat{\mathbf{v}}_{2\ell}. \quad (9)$$

It is well-known that the directions of the *axes* of \mathbf{p}_ℓ determined by \mathbf{a}_ℓ , \mathbf{b}_ℓ can be immediately computed as the eigenvectors of the symmetric matrix

$$\mathbf{Q} = \mathbf{M}_\ell^T \cdot \mathbf{M}_\ell. \quad (10)$$

However, it is necessary to confirm that the axis of symmetry of \mathbf{p}_ℓ obtained via this computation is also the reflection axis of $C^{(\ell)}$ as, in general, $\mathbf{Sym}(\mathbf{p}_\ell)$ can be bigger than $\mathbf{Sym}(C^{(\ell)})$.

Rotational symmetries. In this case we have to find reparametrization(s) $\mathbf{v}_i \mapsto \mathbf{v}_{\beta-i}$ relating symmetric vertices. One can identify two situations:

1. if $C^{(\ell)}$ is circular then β can be chosen arbitrarily;
2. if $C^{(\ell)}$ is non-circular then β (s) is(are) obtained as integer solutions of

$$\beta = \frac{n}{2\pi\ell} \left(\arctan \left(\frac{2\hat{\mathbf{v}}_{2\ell-1} \hat{\mathbf{v}}_{2\ell}}{\|\hat{\mathbf{v}}_{2\ell}\|^2 - \|\hat{\mathbf{v}}_{2\ell-1}\|^2} \right) + j\pi \right), \quad j = 0, \dots, n-1.$$

For each β the corresponding *reflection axis* r_β is found as the axis of the two non-identical reflectionally symmetric vertices \mathbf{v}_i and $\mathbf{v}_{\beta-i}$. We associate to each ℓ the *set of all pairs* $\mathcal{S}_\ell = \{(\beta, r_\beta)\}$.

The previous procedures bring us to formulation of two theorems dealing with exact reflectional and rotational symmetries of the whole curve C , for more details see again [4].

Theorem 4.2 C possesses the reflectional symmetry iff the intersection of all sets \mathcal{S}_ℓ is nonempty.

Theorem 4.3 *C possesses the rotational symmetry of m-gon ($m > 2$) if and only if*

- (i) *all the matrices \mathbf{M}_ℓ are scalar multiples of orthogonal matrices (which is equivalent to the circularity of all components), and*
- (ii) *$m = \gcd(n, \{\sigma_\ell \ell - \sigma_k k\}_{k,\ell})$ for all pairs k, ℓ , where $\sigma_k = \det \mathbf{M}_k \neq 0$, $\sigma_\ell = \det \mathbf{M}_\ell \neq 0$ (i.e., $\sigma_k, \sigma_\ell \in \{-1, 1\}$).*

We would like to emphasize that it follows from (ii) that for a certain m -gon only some particular components are allowed.

5 Approximate symmetries of perturbed discrete curves

One of the main advantages of the formulated approach lies in the fact that it can be, after a suitable modification, easily adapted also for detecting approximate symmetries of perturbed discrete curves. The readers more interested in all the details are kindly referred to [4, Section 4].

Now, the input is a curve \tilde{C} which is a perturbation of some unknown (perfectly) symmetric discrete curve C . Thus, we consider n vertices $\mathbf{v}_i = (x_i, y_i)$, $i = 0, \dots, n-1$, and their perturbed versions $\tilde{\mathbf{v}}_i = (\tilde{x}_i, \tilde{y}_i)$ such that

$$\tilde{x}_i = x_i + \varrho_i^x \varepsilon, \quad \tilde{y}_i = y_i + \varrho_i^y \varepsilon, \quad (11)$$

where $(x_i, y_i) \in [-h, h] \times [-h, h]$ (i.e., h describes the range of the input points), $0 < \varepsilon \ll h$ and $\rho_i^x, \rho_i^y \in \mathbb{R}$ are real numbers such that $|\rho_i^x| \leq 1$, $|\rho_i^y| \leq 1$. To obtain a better estimation reflecting the number of points, the probabilistic approach was used in [4], i.e., it was assumed that the errors $\varepsilon \varrho_i^x, \varepsilon \varrho_i^y$ (or only ϱ_i^x, ϱ_i^y) are random numbers with Gaussian distribution $N(\mu, \sigma^2)$.

Following the ideas from the previous section devoted to exact symmetries, also in this part we will work with the decomposition of \tilde{C} into components $\tilde{C}^{(\ell)}$. Nonetheless, we emphasize necessity of the verification step confirming that the found approximate symmetry ϕ from $\bigcap_{\ell \in I} \mathbf{Sym}(\tilde{C}^{(\ell)})$ is also an approximate symmetry of \tilde{C} . Next, we adopt the following two conventions, see Fig. 2:

- (i) $\tilde{C}^{(\ell)}$ in the decomposition of \tilde{C} is omitted if all its vertices $\mathbf{v}_j^{(\ell)}$ lie inside the circle with the radius ε – *approximately trivial/zero* component.
- (ii) $\tilde{C}^{(\ell)}$ in the decomposition of \tilde{C} is declared to be *approximately circular* if

$$\min \left\{ \|\tilde{\mathbf{b}}_\ell - (\tilde{\mathbf{a}}_\ell)^\perp\|, \|\tilde{\mathbf{b}}_\ell + (\tilde{\mathbf{a}}_\ell)^\perp\| \right\} < 2\varepsilon.$$

We must stress the necessity of verifying that the obtained map ϕ is indeed the approximate symmetry of \tilde{C} . So, we try to find $\tilde{\mathbf{v}}_j$ such that $\phi(\tilde{\mathbf{v}}_0) \approx \tilde{\mathbf{v}}_j$, which means that

$$\|\phi(\tilde{\mathbf{v}}_0) - \tilde{\mathbf{v}}_j\| < 2\sqrt{2}\varepsilon. \quad (12)$$

If such $\tilde{\mathbf{v}}_j$ does not exist then ϕ is not an approximate symmetry of \tilde{C} . In the affirmative case we continue to compare (via the approximate identity) the next

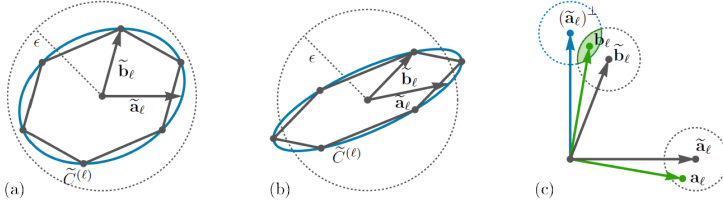


Fig. 2: Left: An approximately trivial component $\tilde{C}^{(\ell)}$ lying in the prescribed ϵ -neighbourhood. Middle: A component that cannot be considered as trivial although both half-diameters lie inside the ϵ -circle. Right: The component $\tilde{C}^{(\ell)}$ determined by the conjugate half-diameters $\tilde{a}_\ell, \tilde{b}_\ell$ which is approximately circular. *This figure was taken from [4], originally Fig. 12.*

vertices and their images as in the exact approach. All the corresponding vertices must be approximately identical and by the error of the approximate symmetry ϕ of \tilde{C} we understand the value

$$\delta_\phi = \frac{1}{n} \sum_{i=0}^{n-1} \left\| \phi(\tilde{\mathbf{v}}_i) - \tilde{\mathbf{v}}_{j \pm i} \right\| \quad (13)$$

for $\phi(\tilde{\mathbf{v}}_0) \approx \tilde{\mathbf{v}}_j$ and $+/-$ for rotations/reflections.

Rotational symmetries. First, we check if the decomposition of \tilde{C} consists of only approximately circular components $\tilde{C}^{(\ell)}$. If this is true then we proceed as in the exact case which helps us to determine whether $\tilde{C}^{(\ell)}$ exhibits some rotational symmetry of m -gon, $m > 2$, see Fig. 3.

Reflectional symmetries. We will distinguish between two situations. When the decomposition contains at least one elliptical component then we can determine the axes of the associate ellipse and then verify if these axes are reflection axes of \tilde{C} , see Fig. 4

If all components $\tilde{C}^{(\ell)}$ are only (approximately) circular then we construct the sets $\tilde{\mathcal{S}}_\ell = \{(\beta, \bowtie_{\beta, \ell})\}$, $\beta = 0, \dots, n-1$, where $\bowtie_{\beta, \ell}$ represents the set of all potential axes (which is caused by the input perturbation; see [4] for how to determine these double wedges). Then we find $\bigcap_\ell \bowtie_{\beta, \ell}$, see Fig. 5

6 Conclusion

In this contribution we shortly presented a recently proposed method for computing symmetries of planar discrete curves. The approach is based on the decomposition of a given curve into simpler discrete curves for which is much easier to find their symmetries. The value of this method lies mainly in the fact that it is also well capable of detecting symmetries of perturbed discrete curves, after a suitable modification. All details can be found in the original paper [4].

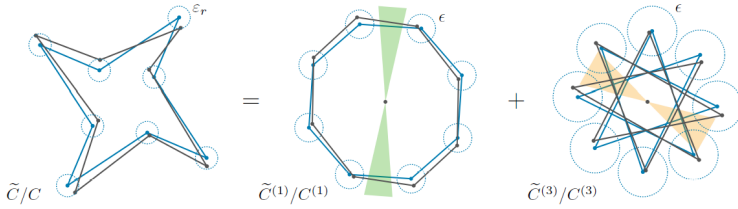


Fig. 3: Decomposition into approximately circular components. Curves $\tilde{C}^{(1)}/C^{(1)}$ and $\tilde{C}^{(3)}/C^{(3)}$ possess approximately/exactly rotational symmetries of 8-gon. However the approximate/exact rotational symmetries of \tilde{C}/C are only rotational symmetries of square. This figure was taken from [4], originally Fig. 13.

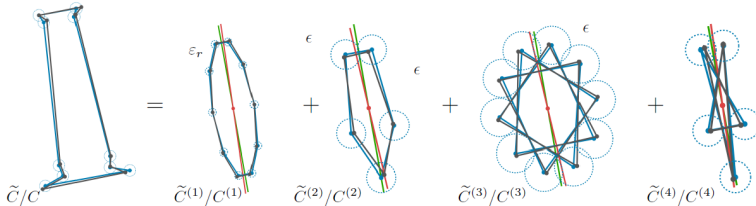


Fig. 4: Decomposition into components from which at least one is elliptical. This figure was taken from [4], originally Fig. 14.

Acknowledgments

The authors were supported by the grant 21-08009K *Generalized Symmetries and Equivalences of Geometric Data* of the Czech Science Foundation.

References

- [1] J. G. Alcázar: *Efficient detection of symmetries of polynomially parametrized curves*. Journal of Computational and Applied Mathematics 255 (2014), pp. 715 – 724
- [2] J. G. Alcázar, C. Hermoso, G. Muntingh: *Detecting symmetries of rational plane and space curves*. Computer Aided Geometric Design 31, 3 (2014), pp. 199 – 209
- [3] J. G. Alcázar, M. Lávička, J. Vršek: *Symmetries and similarities of planar algebraic curves using harmonic polynomials*. Journal of Computational and Applied Mathematics 357 (2019), pp. 302–318

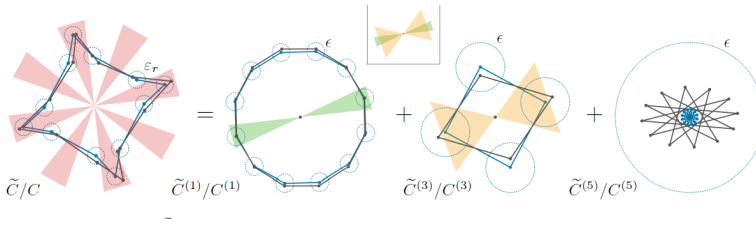


Fig. 5: Decomposition into only circular components. The green and orange double wedges indicate all possible axes of symmetry for $\beta = 2$ of $\tilde{C}^{(1)}$ and $\tilde{C}^{(3)}$, respectively. Intersecting these double wedges (framed) yields the double wedge (red) for \tilde{C} and $\beta = 2$. Analogously, we obtain non-empty intersections for $\beta = 5, 7, 11$ therefore we have four double wedges for possible reflection axes. The component $\tilde{C}^{(5)}$ is omitted because approximately trivial. *This figure was taken from [4], originally Fig. 17.*

- [4] M. Bizzarri, M. Lávička, J. Vršek: *Approximate symmetries of perturbed planar discrete curves*. Computer Aided Geometric Design 96 (2022), 102115
- [5] P. Brass, C. Knauer: *Testing congruence and symmetry for general 3-dimensional objects*. Computational Geometry 27, 1 (2004), pp. 3 – 11. Computational Geometry - EWCG'02
- [6] G. Farin: *Curves and Surfaces for Computer-Aided Geometric Design*. Academic Press, 1988
- [7] M. Hauer, B. Jüttler, J. Schicho: *Projective and affine symmetries and equivalences of rational and polynomial surfaces*. Journal of Computational and Applied Mathematics 349 (2019), 424–437
- [8] F. Klein: *Vergleichende betrachtungen ueber neuere geometrische forschungen*. Mathematische Annalen, 43 (1893), pp. 63–100
- [9] P. Leebmeir, J. Richter-Gebert: *Rotations, translations and symmetry detection for complexified curves*. Computer Aided Geometric Design 25, 9 (2008), pp. 707 – 719. Classical Techniques for Applied Geometry
- [10] D. Salomon *Curves and surfaces for computer graphics*. Springer, 2006
- [11] J. Sánchez-Reyes: *Detecting symmetries in polynomial Bézier curves*. Journal of Computational and Applied Mathematics 288 (2015), pp. 274–283

A spatial generalization of Wallace–Simson theorem on four lines parallel to a plane

Jiří Blažek, Pavel Pech

University of South Bohemia, Faculty of Education,
Jeronýmova 10, 371 15 České Budějovice, Czech Republic

email: jirablazek@seznam.cz, pech@pf.jcu.cz

Abstract. In the paper we explore 3D generalization of the well-known Wallace–Simson theorem: Given four straight lines which are *parallel* to a fixed plane. Determine the locus of the point P such that points which are symmetric with a point P with respect to these four lines are coplanar. The locus of P is a cylinder of revolution with the axis which is perpendicular to the fixed plane.

Keywords: Wallace–Simson theorem, locus in 3D, cubic surfaces, elimination.

1 Introduction

The well-known Wallace–Simson (W–S) theorem belongs to the most beautiful theorems of plane geometry. There exist several modifications and generalizations [6, 7, 8, 9, 10, 11, 12, 13]. We will explore 3D generalization of the following equivalent version of W–S theorem.

If P is a point in the circumcircle of a triangle ABC then points symmetric with P with respect to the sides of ABC are collinear.

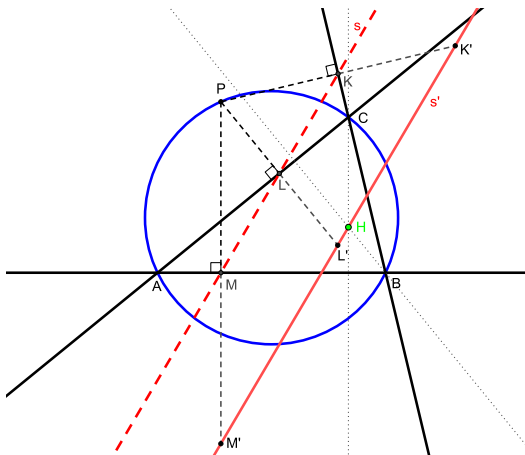


Fig. 1: Points K', L', M' are collinear

The line s' is parallel to the Simson line s and passes through the orthocenter H of $\triangle ABC$, Fig. 1.

2 Various generalizations

(Gergonne): *If P is a point of a circle which is concentric with the circumcircle of a triangle ABC then orthogonal projections K, L, M of P onto the sides of ABC form a triangle with constant area.*

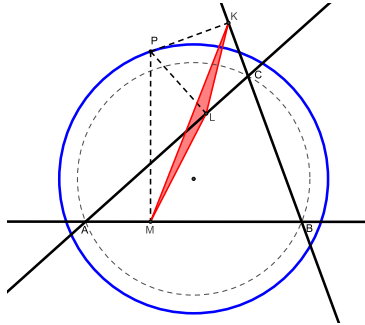


Fig. 2: Orthogonal projections K, L, M of P onto the sides of ABC form a triangle with constant area

If the area of $\triangle KLM$ equals zero we get W-S theorem, Fig. 2.

3D generalization of W-S theorem on a tetrahedron is following [9]:

Denote $A = (0, 0, 0)$, $B = (a, 0, 0)$, $C = (b, c, 0)$, $D = (d, e, f)$, $P = (p, q, r)$, Fig. 3.

Let K, L, M, N be orthogonal projections of a point P to faces BCD , ACD , ABD , ABC of a tetrahedron $ABCD$. Then the locus of P such that the tetrahedron $KLMN$ has constant volume s is the surface F

$$F := ac^2 f^3 G + sQ = 0,$$

where

$$G = c^2 f^2 p^2 q + cf(e^2 + f^2 - ce)p^2 r + cf^2(a - 2b)pq^2 + cf^2(a - 2d)pr^2 + 2cef(b - d)pqr + b(b - a)f^2 q^3 + f(be(a - b) + cd(d - a) + cf^2)q^2 r + f^2(b^2 - ab + c^2 - 2ce)qr^2 + (be(a - b) + cd(d - a) + ce(e - c))fr^3 - ac^2 f^2 pq + acf(ce - e^2 - f^2)pr + abc f^2 q^2 + (a(c^2 d - 2bce + be^2) - (cd - be)^2 + f^2(ab - b^2 - c^2))fqr + (ce^2(ab + ad - 2bd) + c^2 de(d - a) + be^3(b - a) + f^2(acd - be) + e(b^2 + c^2))r^2$$

and

$$Q = 6(e^2 + f^2)((cd - be)^2 + f^2(b^2 + c^2))((c(a - d) - e(a - b))^2 + f^2((a - b)^2 + c^2)).$$

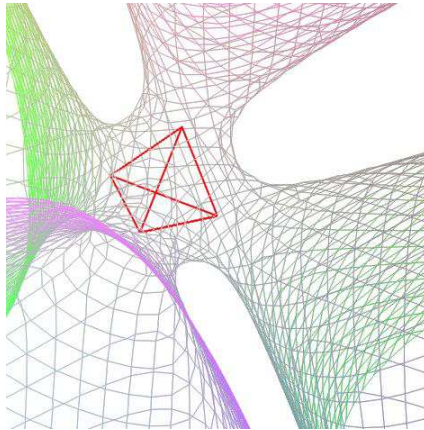


Fig. 3: For a regular tetrahedron and $s = -1/10$ we get a cubic surface

Another 3D generalization of the Wallace–Simson theorem might be as follows:

Determine the locus of the point P such that feet of perpendiculars from P to four arbitrary straight lines in three dimensional Euclidean space are coplanar.

It turns out that such a formulation leads to many complex cases. One might distinguish individual special positions of lines which lead to various types of cubics and quadrics.

In our opinion such a classification has not been done yet, it is a matter of further investigation.

3 Four lines parallel to a plane

In this section we will deal with a generalization of the W–S theorem in 3D when four straight which are parallel to a fixed plane are given.

Consider four straight lines k_1, k_2, k_3, k_4 which are parallel to a fixed plane. Let X_1, X_2, X_3, X_4 be points which are symmetric with the point P with respect to the lines k_1, k_2, k_3, k_4 . Then the locus of P is a cylinder of revolution.

Proof:

Adopt a rectangular coordinate system such that $a_1x + b_1y + c_1 = 0$, $a_2x + b_2y + c_2 = 0$, $a_3x + b_3y + c_3 = 0$, $a_4x + b_4y + c_4 = 0$ are equations of orthogonal projections of the lines k_1, k_2, k_3, k_4 in the fixed xy -plane.

Let $X_1 = (x_1, y_1, z_1)$, $X_2 = (x_2, y_2, z_2)$, $X_3 = (x_3, y_3, z_3)$, $X_4 = (x_4, y_4, z_4)$ be points symmetric with a point $P = (p, q, r)$ with respect to the lines k_1, k_2, k_3, k_4 , then:

X_1 is symmetric with P with respect to $k_1 \Rightarrow$

$$h_1 := a_1(p + x_1) + b_1(q + y_1) + 2c_1 = 0, \quad h_2 := b_1(p - x_1) - a_1(q - y_1) = 0,$$

X_2 is symmetric with P with respect to $k_2 \Rightarrow$

$$h_3 := a_2(p + x_2) + b_2(q + y_2) + 2c_2 = 0, \quad h_4 := b_2(p - x_2) - a_2(q - y_2) = 0,$$

X_3 is symmetric with P with respect to $k_3 \Rightarrow$

$$h_5 := a_3(p + x_3) + b_3(q + y_3) + 2c_3 = 0, \quad h_6 := b_3(p - x_3) - a_3(q - y_3) = 0,$$

X_4 is symmetric with P with respect to $k_4 \Rightarrow$

$$h_7 := a_4(p + x_4) + b_4(q + y_4) + 2c_4 = 0, \quad h_8 := b_4(p - x_4) - a_4(q - y_4) = 0,$$

X_1, X_2, X_3, X_4 are coplanar \Rightarrow

$$h_9 := \begin{vmatrix} x_1 & y_1 & z_1 & 1 \\ x_2 & y_2 & z_2 & 1 \\ x_3 & y_3 & z_3 & 1 \\ x_4 & y_4 & z_4 & 1 \end{vmatrix} = 0.$$

Elimination of 8 variables $x_1, y_1 \dots x_4, y_4$ in the ideal $J = (h_1, \dots, h_9)$ in CoCoA¹ which leads to the locus equation fails because of complexity.

To simplify the computation we use unit vectors (a_1, b_1) , (a_2, b_2) , (a_3, b_3) , (a_4, b_4) and put $a_1 = c_1 = 0, b_1 = 1, z_1 = 0$.

Now elimination of $x_1, y_1 \dots x_4, y_4$ in the ideal $J = (h_1, \dots, h_9)$ in CoCoA works. We get a locus equation

$$A(p^2 + q^2) + Bp + Cq + D = 0, \quad (1)$$

where

$$A = z_2 a_3 a_4 (a_3 b_4 - a_4 b_3) + z_3 a_2 a_4 (a_4 b_2 - a_2 b_4) + z_4 a_2 a_3 (a_2 b_3 - a_3 b_2),$$

$$B = z_2 (a_3 c_4 + a_4 c_3) (a_3 b_4 - a_4 b_3) + z_3 (a_2 c_4 + a_4 c_2) (a_4 b_2 - a_2 b_4) + z_4 (a_2 c_3 + a_3 c_2) (a_2 b_3 - a_3 b_2),$$

¹Software CoCoA is freely distributed at <http://cocoa.dima.unige.it>

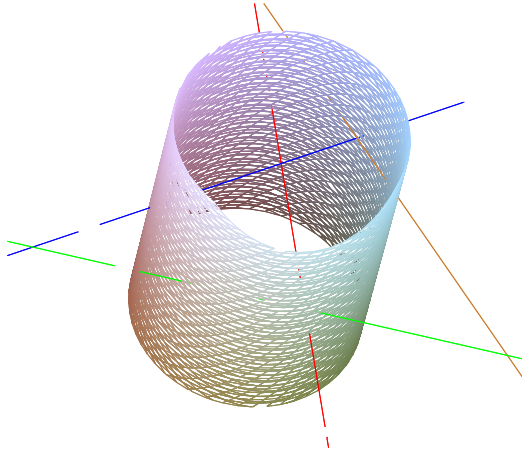


Fig. 4: The locus of P is a cylinder of revolution

$$C = z_2(a_3a_4 + b_3b_4)(a_3c_4 - a_4c_3) + z_3(a_2a_4 + b_2b_4)(a_4c_2 - a_2c_4) + z_4(a_2a_3 + b_2b_3)(a_2c_3 - a_3c_2),$$

$$D = z_2c_3c_4(a_3b_4 - a_4b_3) + z_3c_2c_4(a_4b_2 - a_2b_4) + z_4c_2c_3(a_2b_3 - a_3b_2).$$

We see that the locus is a cylinder of revolution whose axis is perpendicular to xy -plane, Fig. 4.

Realize that for any point P of the locus the whole line perpendicular to the fixed plane belongs to the locus.

Remarks:

1. Note that the coefficient A by $p^2 + q^2$ in (1) depends only on directions of the lines k_1, k_2, k_3, k_4 and their distances z_1, z_2, z_3, z_4 to the fixed xy -plane because of the absence of terms c_1, c_2, c_3, c_4 .
2. If all the lines k_1, k_2, k_3, k_4 intersect a line which is perpendicular to the fixed plane (axis z in our coordinate system) then the locus of P is this line instead of the cylinder of revolution. To see it realize that in this case all coefficients c_1, c_2, c_3 and c_4 vanish. This implies $B = C = D = 0$ in (1).

4 Conclusion

In the text a 3D version of W–S theorem when four given lines are parallel to a fixed plane is investigated. We explore points P such that points which are symmetric with P with respect to given four lines are coplanar. The locus of the point P is a cylinder of revolution with the axis which is

perpendicular to the fixed plane.

The authors are still working on this problem. In future we would like to analyze 3D version of W–S theorem with arbitrary positions of given four lines. Also generalization in n -dimensional Euclidean space seems to be possible.

References

- [1] J. Blažek, P. Pech: *A Spatial Generalization of Wallace-Simson Theorem on Four Lines*. Advances in Intelligent Systems and Computing, 2021, vol. 1296, pp. 103-114
- [2] A. Capani, G. Niesi and L. Robbiano: *CoCoA, a System for Doing Computations in Commutative Algebra*. 1995
- [3] D. Cox, J. Little and D. O’Shea: *Ideals, Varieties, and Algorithms*. Second Edition, Springer, New York, Berlin, Heidelberg 1997
- [4] H. S. M. Coxeter, S. L. Greitzer: *Geometry revisited*. Toronto, New York 1967
- [5] R. Johnson: *Advanced Euclidean Geometry*. Dover, New York 1960
- [6] M. Guzmán: *An Extension of the Wallace–Simson Theorem: Projecting in Arbitrary Directions*. Amer. Math. Monthly **106**, 1999, pp. 574–580
- [7] E. Molnár, P. Pech, J. Szirmai: *Simson–Wallace locus in d -dimensional projective-metric space*. Journal of Geometry **108**, 2017, pp. 393-409
- [8] B. Odehnal: *Degenerate Cubic Surfaces and the Wallace–Simson Theorem in Space*. Proceedings of 7th International Conference on Geometry and Graphics, Beijing 2016
- [9] P. Pech: *On Simson–Wallace Theorem and Its Generalizations*. J. Geometry and Graphics **9**, 2005, pp. 141–153
- [10] P. Pech: *On a 3D Extension of the Simson–Wallace theorem*. J. Geometry and Graphics **18**, 2014, pp. 205-215
- [11] P. Pech: *Extension of Simson–Wallace theorem on skew quadrilaterals and further properties*. In: Botana, F., Quaresma, P. (eds.) Automated Deduction in Geometry (ADG) 2014, LNAI vol. 9201, Springer, Berlin 2015, pp. 108-118
- [12] R. Riesinger: *On Wallace Loci from the Projective Point of View*. J. Geometry and Graphics **8**, 2004, pp. 201-213
- [13] E. Roanes–Lozano, E. Roanes–Macías: *Automatic Determination of Geometric Loci. 3D-Extension of Simson–Steiner Theorem*. In: AISC 2000, J. A. Campbell, E. Roanes–Lozano, (eds), LNAI vol. 1930, Springer, Berlin 2000, pp. 157-173

Parametrické modelování letadlových kompresorových lopatek

Parametrical modeling of aircraft compressor blades

Jaroslav Cibulka

FS ČVUT v Praze

Karlovo náměstí 13 Praha 2 Nové Město 121 35, Česká republika

email: jaroslav.cibulka@fs.cvut.cz

Abstract. NASA rotor 37 je letadlový transsonický axiální kompresor sestavený ze 36 lopatek vytvořený a testovaný ve výzkumném středisku NASA Lewis Research Center v 70. letech. Geometrie lopatek a experimentální měření aerodynamických vlastností provedené v NASA se později staly základem pro vytvoření testovací úlohy pro ověření vlastností numerických metod v aerodynamice. Matematická analýza geometrie lopatky a použití vhodného softwaru pro sestavení parametrického 3D modelu lopatky, včetně implementovaných geometrických modifikací 3D geometrie je vhodný postup pro vytvoření testovací geometrie pro numerické analýzy.

Keywords: NASA rotor 37, parametrical model, compressor blade, geometry analyses

Klíčová slova: NASA rotor 37, parametrický model, kompresorová lopatka, analýza geometrie

1 Úvod

Tvarová optimalizace geometrie lopatek turbokompresorových strojů je předmětem vědeckého výzkumu numerického modelování mechaniky tekutin a strukturálních analýz. Požadavek vysoké efektivity kompresorových strojů klade vysoké nároky na geometrii lopatek, numerické analýzy i fyzické testy ve zkušebních aerodynamických tunelech. Pro ověření vlastností numerických modelů i aerodynamických testů je vhodné použít referenční testovací geometrii s velkým množstvím ověřených výsledků. Ideálním kandidátem je NASA rotor 37. [1]

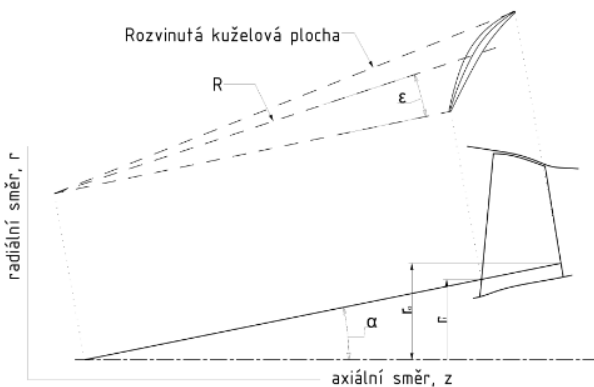
Pro vytvoření přesné geometrie je nutné podrobně odvodit matematickou parametrizaci jednotlivých profilů lopatky a následně jejich sestavení pro tvorbu 3D modelu. Vstupní geometrie numerických simulací vyžaduje formát .step. Tuto podmínku splňují konvenční softwary (např. BladeGenerator). Dalším požadavkem je parametrizace geometrie lopatky pro urychlení nebo úplnou automatizaci procesu numerické analýzy a následné geometrické optimalizace. Ideálním nástrojem je vytvoření matematického modelu geometrie lopatky ve volně dostupném programovacím jazyce (např. Python)

spolu se softwarem pro tvorbu CAD geometrie v požadovaném formátu (např. Salomé). [1]

Pro ověření vlastností vytvořené geometrie je vhodné použít kontrolní nástroje počítačové grafiky. Hlavními kontrolními nástroji je zobrazení pruhů zebry, pro kontrolu spojitosti ploch a jejich napojení a zobrazení grafu křivosti pro kontrolu spojitosti křivek a jejich napojení.

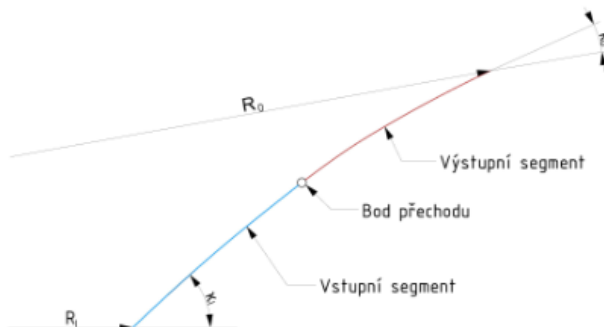
2 MCA profil

V této kapitole je uvedena metodika tvorby MCA lopatky podle [2]. Kuželová aproximace povrchu proudnic použitá při tvorbě lopatky je zobrazena pomocí schématu na obr. 1, kde α je poloviční vrcholový úhel kužele. Ilustrace umístění lopatky na kuželu je zobrazena na obr. 1 v souřadnicovém systému $O(R, \varepsilon)$. V tomto souřadnicovém systému je povrch kužele rozvinut do roviny pro následný popis profilů lopatek v rovinném souřadnicovém systému. V souřadnicovém systému $O(R, \varepsilon)$ představuje R délku spojnice vrcholu kužele s příslušným bodem (bod na vstupu, bod přechodu, bod maximální tloušťky profilu, bod na výstupu) na kružnicovém segmentu lopatky a ε je úhel mezi referenčním průvodičem a průvodičem k příslušnému bodu. Kuželová aproximace proudnicového povrchu je definována pomocí r_i , r_o a z . Jsou to poloměry vzdálenosti od osy ke středu náběžné hrany, odtokové hrany a axiální vzdálenost mezi těmito dvěma poloměry. Úhel lopatky κ je definován pomocí úhlu mezi průvodičem R a tečnou k povrchu lopatky nebo ke střednici profilu. Metodický postup vytvořený [2] je určený pro rozmístění profilů lopatky na kuželovém povrchu a nezahrnuje předešlé kroky konstrukčního procesu potřebného pro získání parametrů lopatky. Každý profil lopatky je charakterizován 11 parametry [3].



Obr. 1: Kuželová aproximace povrchu proudnic

Pro sestavení lopatky jsou profily a střednice profilů konstruovány ze dvou segmentů, vstupního a výstupního s konstantní křivostí $d\kappa/ds$, kde κ je lokální úhel lopatky a s je délka profilu.



Obr. 2: Popis profilu

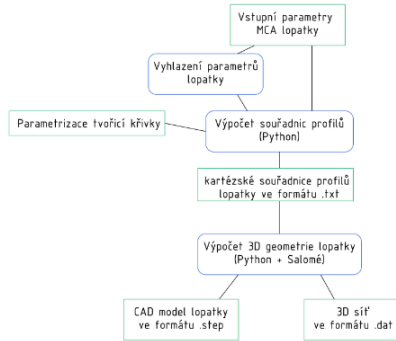
Bod, kde se tečně dotýkají vstupní a výstupní segment profilu, je definován jako bod přechodu.

3 3D model

Pro tvorbu CAD modelu byl použit volně dostupný software [4]. Tento software umožňuje tvorbu parametrického modelu MCA lopatky a je založený na NASA rotoru 37 a programu ve Fortran IV [2]. Profily zde mohou být sestaveny vertikálně podél přímky nebo se zahrnutím natočení tvořící křivky při sestavení lopatky. V takovém případě jsou profily při sestavení lopatky vzájemně posunuty nebo natočeny. Původní parametrizace podle [2] uvažuje pouze konstantní úhel natočení tvořící křivky, při její modifikaci lze konstruovat lopatku s komplexní geometrií.

Kód je strukturován do tří samostatných modulů, které lze spustit individuálně:

- Vyhazení parametrů: Vyhazení parametrů MCA lopatky podél rozpětí lopatky pro získání hladší geometrie.
- Souřadnice profilů: Výpočet kartézských souřadnic bodů každého profilu z parametrů profilů a axiální a tečná transformace tvořící křivky, tedy popis celé 3D geometrie jako množiny bodů.
- CAD model lopatky: Vytvoření CAD modelu a síť z bodů souřadnic pomocí softwarové platformy Salomé. [5]

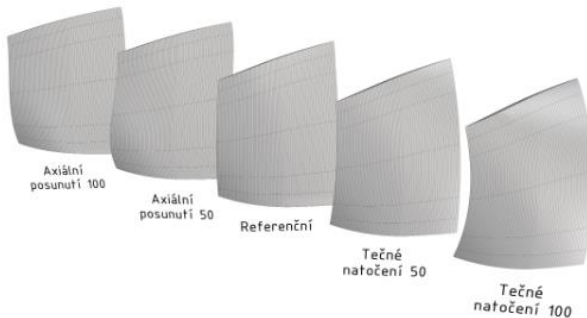


Obr. 3: Schéma programu

Výstupem jsou následující soubory v závislosti na vybrané možnosti exportu.

- CAD model lopatky reformátu .step.
- Síť bodů ve formátu .dat.

Na obr. 4 jsou zobrazeny všechny vytvořené lopatky rotoru 37 s modifikací geometrie tvořící křivky (axiální posunutí, radiální natočení) včetně referenčního rotoru 37.

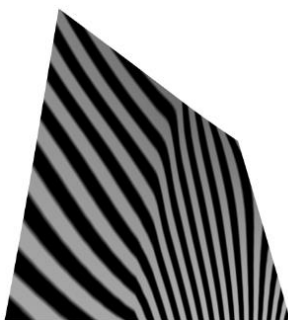


Obr. 4: Katalog CAD modelů lopatek rotoru 37 s modifikovanou geometrií tvořící křivky

4 Analýza geometrie

Pro analýzu vytvořené geometrie byla vybrána lopatka s referenčními vstupními parametry rotoru 37 bez modifikace natočení a posunutí tvořící křivky. Z grafické analýzy zobrazením pruhů zebry na tlakové, resp. sací straně lopatky na obr. 5, resp. 6 je patrné napojení vstupního a výstupního segmentu s minimální G1 spojitostí. Dále je ze spojitých pruhů patrná minimální G2 spojitost ploch jednotlivých segmentů. Při detailní analýze napojení vstupního

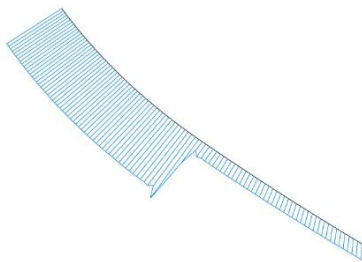
a výstupního segmentu tlakové strany profilu v 0.5 rozpětí lopatky na obr. 7 zobrazením grafu křivosti je patrný vyhlazený minimálně G2 spojitý přechod. Tento přechod je způsoben vyhlazením parametrů lopatky při tvorbě 3D geometrie. Dále je z obrázků patrná minimální G2 spojitost vstupního a výstupního segmentu lopatky.



Obr. 5: Tlaková strana lopatky



Obr. 6: Sací strana lopatky



Obr. 7: Graf spojitosti tlakové strany profilu v 0.5 rozpětí lopatky

5 Závěr

Předmětem výzkumu bylo vytvoření parametrického CAD modelu kompresorové lopatky vhodného jako testovací vstupní geometrie pro ověření numerických modelů. Vzhledem k množství dostupných dat z měření v aerodynamických tunelech a numerických simulací byl zvolen NASA rotor 37.

Pro tvorbu 3D CAD modelu ve formátu .step byl zvolen volně dostupný software [4]. Matematická definice geometrie lopatky včetně modifikace geometrie tvořící křivky je zde zpracována v programovacím jazyce Python. Tvorba 3D CAD modelu ve formátu .step byla provedena pomocí volně dostupné softwarové platformy Salomé. Celkem bylo vytvořeno 5 lopatek,

referenční NASA rotor 37, dvě lopatky s axiálním natočením tvořící křivky a dvě lopatky s tečným natočením tvořící křivky. Následně byla provedena analýza výsledné geometrie lopatky s parametrizací referenčního rotoru 37.

Z provedené analýzy geometrie lopatky pomocí zobrazení pruhů zebry vyplývá minimální G2 spojitost plátů lopatky na tlakové i sací straně a minimálně G1 spojitě napojení plátů vstupního a výstupního segmentu. Při detailní analýze napojení segmentů profilu lopatky na tlakové straně bylo zjištěno minimálně G2 spojitě napojení a to vlivem vyhlazení vstupních parametrů při tvorbě 3D modelu lopatky.

Použitý software vyhovuje požadavkům na vstupní geometrii pro numerické simulace a vzhledem k veřejně dostupnému kódu je vhodný pro implementaci například v softwaru pro numerické simulace OpenFoam nebo další modifikaci pro tvorbu lopatek definovaných pomocí funkce střednice profilu.

Poděkování

Tento článek vznikl za podpory projektu Studentské grantové soutěže ČVUT v Praze – Aplikace matematicko-geometrického modelování ve strojírenství SGS21/148/OHK2/3T/12

Literatura

- [1] J. Cibulka: *3D modelování kompresorových lopatek*, Praha, 2021, Diplomová práce, FS ČVUT V PRAZE, Vedoucí práce doc. Ing. Ivana Linkeová, Ph.D.
- [2] J. E. Crouse, D. C. Janetzke, R. E. Schwirian: *A computer program for composing compressor blading from simulated circular-arc elements on conical surfaces*, Tech. rep., NASA, 1969
- [3] M. Ringström, W. Björn: *Reduced order modelling of optimized transonic compressor rotor blades: Master's thesis in Mechanics and Maritime Sciences*. Gothenburg, Sweden, 2018. Master's thesis. Department of Mechanics and Maritime Sciences CHALMERS UNIVERSITY OF TECHNOLOGY. Vedoucí práce Gonzalo Montero Villar, Marcus Lejon
- [4] E. Piollet, A. Batailly: *A program to compute compressor blade geometries from multiple-circular-arc parameters with sweep and lean (v1.0)[source code]*, available at hal.archives-ouvertes.fr, 2019
- [5] A. Ribes, C. Caremoli: *Salome platform component model for numerical simulation*. In Computer Software and Applications Conference, 2007. COMPSAC 2007. 31st Annual International, Vol. 2, IEEE, 2007, pp. 553-564

Výuka geometrie ve Vietnamu

Teaching geometry in Vietnam

Věra Ferdiánová, Martin Plinta, Barbora Sováková

*Dept. of mathematics, Faculty of Science, University of Ostrava
30. dubna 22, 701 03 Ostrava, Czech Republic
email: vera.ferdianova@osu.cz, P21143@student.osu.cz, P21049@student.osu.cz*

Abstract. At first view, it may seem that mathematics teaching around the world must be similar. For some areas this is the case, but for example the teaching of geometry in Vietnam is very different. The aim of this paper is to present some interesting geometry problems and their solutions that are taught in this country.

Keywords: Book of geometry, educational system in Vietnam

Klíčová slova: Učebnice geometrie, vzdělávací systém ve Vietnamu.

1 Edukační systém ve Vietnamu

Vzdělávací systém a jednotlivé jeho úrovně jsou velmi podobné našemu českému systému (Obr. 1). Podle Vietnamského národního shromáždění (1998, kapitola 1, článek 6; 2005, kapitola 1, článek 4), národní vzdělávací systém zahrnuje předškolní vzdělávání, všeobecné vzdělávání, odborné vzdělávání a postgraduální vzdělávání. Žáci začínají povinnou školní docházku v 6 letech, přičemž většina dětí je zapojena i do předškolního vzdělávání v rámci různých předškolních zařízení. Kompletní vietnamský národní vzdělávací systém můžete dohledat v oficiálních dokumentech na webových stránkách Ministry of education and training (MoET). Během přechodu na další úroveň studenti skládají různé zkoušky a např. u matematiky na základní škole mají studenti test o časové dotaci 120 minut, jež se skládá z algebry a geometrie, obsahující teoretické a výpočtové úlohy. Z pohledu výuky geometrie se dlouhodobě razila striktní axiomatická výstavba, kdy si žáci vybudovali postupně celkový aparát s definicemi a větami. Po reformě se absolutní pohled založený na axiomech v geometrii nahradil alternativním vizuálním pohledem a uvažováním. Geometrie na střední škole není konstruována jako čistá dedukce, přesto ve srovnání s českým systémem obsahuje minimum konstrukčních úloh. Namísto striktních matematických důkazů v některých případech mohou studenti měřit, pozorovat, experimentovat a poté vyvozovat závěry (bez důkazů). V nižších ročnících je geometrických důkazů výrazně méně. Načrtáváním a pozorováním obrazců, měřením úseček a úhlů pomocí skládání a stříhání papíru mají žáci možnost komentovat události a předvídat vlastnosti dřívě, než jsou oficiálně představeny geometrické věty a jejich důkazy. Na základě rozhovorů s kolegy a studenty se na vysoké škole geometrie povětšinou vyučuje přes axiomatickou výstavbu a je spíše teoretického charakteru s minimem ilustračních úloh. Konstrukční

a deskriptivní geometrie je spíše doménou technických univerzit zaměřených na stavebnictví a strojírenství.

V rámci programu Erasmus byl u nás realizován předmět pro větší skupinku studentů z Vietnamu, ve kterém byla zahrnuta geometrie. Reakce studentů na výuku byly kladné, jelikož studenti měli kvalitní základy teoretické geometrie, které aplikovali na vybrané úlohy.

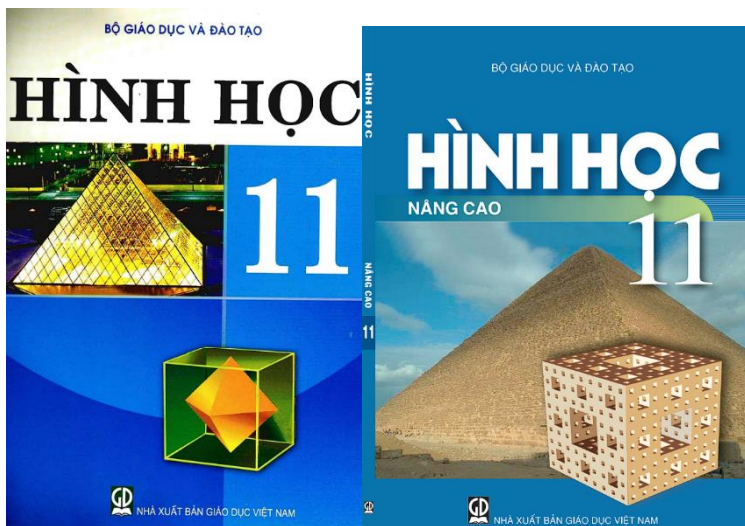
Age	Year		
22 +		} Colleges, Universities	
21 +			
20 +			
19 +			
18 +			
17 +	12	} Senior Secondary School	General Certificate of Secondary Education Examination (6 subjects taken)
16 +	11		
15 +	10		
14 +	9	} Junior Secondary School	Examination (6 subjects taken)
13 +	8		
12 +	7		
11 +	6		
10 +	5	} Primary School	Examination (Vietnamese, Mathematics)
9 +	4		
8 +	3		
7 +	2		
6 +	1		
5 +			'Young Shoot' education

Obr. 1: Struktura edukačního systému ve Vietnamu [1]

2 Učebnice

Ve Vietnamu obvykle po celou dobu studia existuje jedinečná celostátní řada učebních osnov a učebnic pro všechny úrovně škol. Výjimečně na počátku 90. let až do konce 90. let 20. stol. existovaly tři řady středoškolských učebnic (pro některé předměty), které napsaly tři různé autorky, skupiny autorů z hanojské Pedagogické univerzity, z univerzity v Ho Či Minově Městě a Národního institutu pro vzdělávací vědy (NIES). Nicméně v roce 2000 byly tyto řady opraveny, upraveny a sjednoceny, aby vytvořily jedinečnou řadu s názvem Základní vzdělávání (1. až 5. třída, věk 6 až 11 let), pokročilé základní vzdělávání (třídy 6 až 9, resp. 11 až 14 let) středoškolské vzdělávání (třídy 10 až 12 let, ve věku 15 až 17 let. Kromě toho MoET provedlo experiment, podle něhož byli středoškoláci rozděleni do tří skupin: Přírodní vědy (Skupina A), Technika (Skupina B) a Společenské vědy (Skupina C) od roku 1992 do roku 1997. Vietnamské národní matematické kurikulum je navrženo a určeno podle MoET. Vyskytují se i učebnice experimentální, jejichž autoři jsou většinou akademici z univerzit. Učebnice jsou testovány na některých školách (popřípadě klinických

školách u „pedagogických“ fakult) v různých oblastech v průběhu několika let a jsou aktualizovány, než se začnou oficiálně používat ve všech školách. Všechny schválené školní učebnice jsou vydávány speciálním nakladatelstvím Educational Publishing House. Učebnice matematiky jsou rozděleny do několika kapitol obsahujících lekce. Jednotlivé lekce obsahují motivační úlohy, formální matematické definice, věty. V závislosti na cílovou skupinu se v učebnicích vyskytují lehké modifikace. Jen na okraj – tím, že Vietnam se rozlohou řadí mezi větší země, tak se ve výuce vyskytují různé modifikace motivačních a praktických úloh vzhledem k regionu.



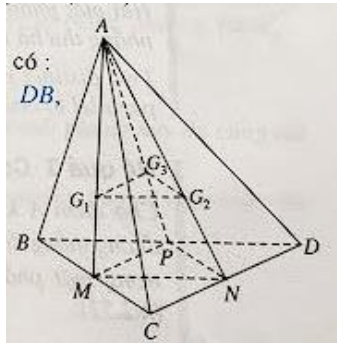
Obr. 2: Učebnice geometrie

2.1 Ukázky úloh z učebnice

Učebnice (Obr. 2 vlevo [2]), ze které budou představeny úlohy je v bilingvní verzi a uváděná řešení jsou přímo z učebnice, nejedná se o autorský počín, ale o překlad a značení převedeno dle našich konvencí.

Příklad 1. Mějme čtyřstěn $ABCD$. Necht' body G_1, G_2, G_3 jsou středy trojúhelníků ABC, ACD, ABD . Dokažte, že rovina $G_1G_2G_3$ je rovnoběžná s rovinou BCD .

Řešení: Mějme body M, N, P , jež jsou středy hran BC, CD a DB (Obr. 3).



Obr. 3: Ilustrace z učebnice str. 65

Mějme

$$M \in AG_1 \wedge \frac{AG_1}{AM} = \frac{2}{3};$$

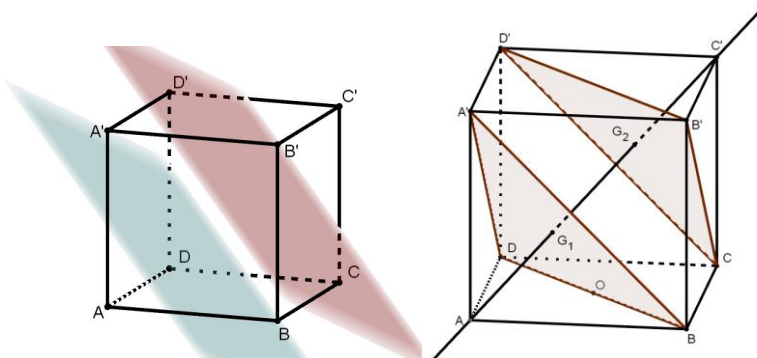
$$N \in AG_2 \wedge \frac{AG_2}{AN} = \frac{2}{3};$$

$$P \in AG_3 \wedge \frac{AG_3}{AP} = \frac{2}{3};$$

Tedy $\frac{AG_1}{AM} = \frac{AG_2}{AN}$, z toho usuzujeme $G_1G_2 \parallel MN$. Víme, že MN leží v rovině BCD, pak $G_1G_2 \parallel BCD$. Obdobně $\frac{AG_1}{AM} = \frac{AG_3}{AP}$, z toho usuzujeme $G_1G_3 \parallel MP$. Víme, že úsečka MP leží v rovině BCD, pak $G_1G_3 \parallel BCD$. Proto $G_1G_2G_3 \parallel BCD$.

Příklad 2. Mějme krychli $ABCA'B'C'D'$.

- Dokažte, že rovina BDA' je rovnoběžná s rovinou $B'D'C'$.
- Dokažte, že diagonála AC' prochází skrz středy G_1, G_2 dvou trojúhelníků BDA' a $B'D'C'$.



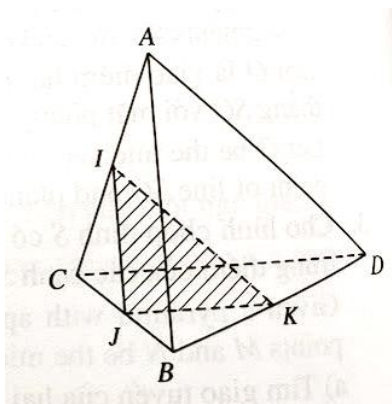
Obr. 4: Doprovodné ilustrace vytvořené v GeoGebře

Řešení: a) Využijte vlastnosti: „Pokud rovina obsahuje dvě různoběžky a, b , které jsou rovnoběžné s přímkami jiné roviny, pak dvě roviny jsou rovnoběžné.“

- b) Mějme bod O , který je středem rovnoběžníku $ABCD$ a $G_1 = AC' \cap A'O$. Dokažte $\frac{A'G_1}{A'O} = \frac{2}{3}$. Následně stejně aplikujte na G_2 .

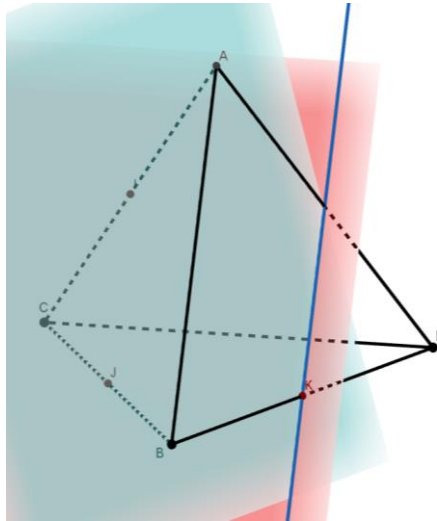
Příklad 3. Mějme čtyřstěn $ABCD$. Mějme body I, J, K , jež jsou středy hran AB, BC, BD . Průsečnice dvou rovin ABD a IJK je

- KD
- KI
- Přímka procházející bodem K a rovnoběžná s hranou AB
- Neexistuje



Obr. 5: Doprovodný obrázek v učebnici k zadání na str. 78

Všechny tři úlohy byly vybrány z druhé kapitoly Rovnoběžné roviny, přičemž Příklad 1. můžeme v rámci našich učebnic označit jako vzorový, Příklad 2. jako úloha k procvičení a poslední byl vybrán ze závěrečného testu s uzavřenými odpověďmi. V učebnici autoři nerozlišují úlohu a příklad, ale vše je označeno jako příklad, proto bylo zanecháno původní označení. Taktéž autoři podstavu tělesa oddělují tečkou, pokud se jedná o čtyřstěn, pak vždy prvním písmenem označují vrchol, který nenáleží podstavě čtyřstěnu (Obr.5).



Obr. 6: Výsledné řešení v GeoGebře

3 Závěr

Cílem příspěvku bylo seznámit s formou zadání úloh, jež se vyskytují v učebnici geometrie ve Vietnamu. Jedná se o malý exkurz do výuky geometrie v jiných zemích, kde se na konstrukční úlohy neklade takový důraz. Vzhledem k tomu, že většina vysokých škol v České republice nabízí anglické studium, mohou se na ně přihlásit studenti z Vietnamu. Je to ukázka toho, že je dobré být seznámen i s jinou formou, jelikož studenti mohou řešit zadané úlohy s největší pravděpodobností jinými postupy než studenti z českých středních škol. Celkově problematiku výuky matematiky ve Vietnamu a zejména geometrie shrnuje disertační práce od dr. Tuan Anh Le, viz [3].

Poděkování

Tento článek vznikl za podpory SGS03/PřF/2022 – Matematická fyzika, geometrie a teorie čísel.

Literatura

- [1] D. Do: *Mathematics Teaching and Learning in Vietnam*, Centre for Curriculum Development and Teaching Methodology, NIES, 2000
- [2] T. Van Hao: *Hình Học (Geometry) 11*. Vietnam Education Publishing House. 2015
- [3] T. Anh Le: *Applying Realistic Mathematics Education in Vietnam: Teaching middle school geometry*. University of Postdam, 2006

Architektonické prvky a jejich využití ve výuce geometrie

Architectural design elements and their use in teaching geometry

Věra Ferdiánová, Barbora Sováková, Martin Plinta

*Dept. of mathematics, Faculty of Science, University of Ostrava
30. dubna 22, 701 03 Ostrava, Czech Republic
email: vera.ferdianova@osu.cz, P21049@student.osu.cz, P21143@student.osu.cz*

Abstract. Already in the 1934 textbook of drawing by Božena Ritschlová-Vanečková there is a special chapter of ornamental examples. The paper will focus on the elements found in the architecture of Socialist Realism, which is very typical for the city of Havířov and the Poruba part of Ostrava. Using GeoGebra software we will present examples suitable for teaching geometry.

Keywords: GeoGebra, SORELA,

Klíčová slova: GeoGebra, SORELA

1 Dobový kontext a SORELA

Po skončení druhé světové války nastala potřeba opravit zničená města po bombardování. Například Ostrava zažila masivní bombardování 29. srpna 1944, kdy se spojenecká vojska zaměřila na těžký průmysl v Ostravě. Značná poškození vznikla v městských částech Zábřeh, Vítkovice, Slezská Ostrava či v centru Ostravy. Tento nálet si vyžádal přes 500 obětí na životech z řad civilního obyvatelstva. Budovy, které nešly zrekonstruovat, tak byly určeny k demolici, což přispělo ke vzniku proluk. Samozřejmě i během druhé světové války docházelo k cílenému poškozování budov a historických staveb okupanty. Během osvobození byla poškozena infrastruktura a další budovy nejen spojené s ní, což se na výsledné architektonické podobě měst projevilo. V poválečné době docházelo ke snahám obnovit rozvíjející se stavitelství první republiky – poválečné Československo mělo vynikající předpoklady k rychlé obnově a vybudování pozice silného průmyslového státu s vyspělou architekturou. Pováleční architekti mají také do značné míry společné hledání socialismu (sovětského, skandinávského, anglického atd.) Zlom nastává po „vítězném únoru“ v roce 1948, kdy se naše země dostává prioritně pod sféru vlivu Sovětského svazu a je nucena se podřídit stalinistickému neoklasicismu, též zvaného socialistický realismus neboli zkráceně SORELA. V té době probíhá zestátnění stavebního průmyslu a vzniku Stavoprojektu. Řízením těchto gigantických podniků byli pověřeni bývalí levicoví avantgardisti Karel Janů

a Jiří Voženílek, přičemž podniky charakterizují do podoby průmyslového závodu, kde tvorba ustupuje ekonomické výhodnosti a kvantitě.[1]

Základní znaky socialistického realismu v architektuře:

- Typické pro stavby socialistického realismu byla především monumentalita, a především reprezentace moci vzrůstajícího Sovětského svazu
- Zásady staveb vycházely z klasické architektury (v podstatě renesanční) s hojným využitím výzdobných technik – nástěnné malby, sgrafita, figurální plastika, reliéfy, ozdobné mříže, zábradlí balkónů.
- Přísné ideologický program malířské a sochařské výzdoby.
- Urbanismus SORELY:
 - Obnova tradičních urbanistických bloků s náměstími s výškovými či jinými dominantními budovami v osách a průhledech.
 - Důležitost symetrie a pravidelnosti městského půdorysu
 - Široké hlavní bulváry, vedle nich uzavřené a klidné dvory
 - Zeleň
- Přírodní, historický a budovatelský dekor
- Inspirace lidovou (jihočeskou) architekturou
- Barevnost – písková, okrová v kombinaci s červenohnědou a bílou.[1][6]

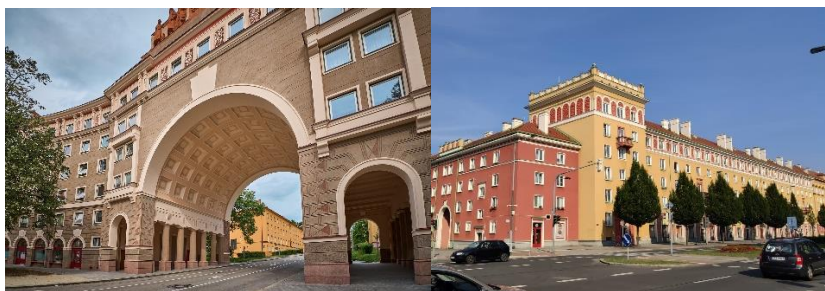
Městskou část Poruba (1951 – 1955) navrhoval Vladimír Meduna. Ve stejné době se započal návrh nového nejmladšího města republiky Havířova. Mělo to být město reprezentující socialistický rozkvět pro jeho mladé obyvatele, kteří se prioritně měli zapojit do práce v těžkém průmyslu a v nedalekých dolech. Původně se počítalo s výstavbou města na „zelené louce“, což nebyla zcela pravda, jelikož vesnice Šumbark a Bludovice byly přičleněny do nového územního plánu města. To mělo za následek, že některé z původních domů byly „vykoupeny“ a následně ustoupily nové výstavbě. V první fázi výstavby byly vystavěny obytné domy pro dělníky tzv. „brigoš baráky“, jež měly být po výstavbě města upraveny a popřípadě zbourány. Zajímavostí je, že předesílaný osud těchto domů se naplnil až v letošním roce. Taktéž noví obyvatelé města Havířova o pracovních sobotách vypomáhali s výstavbou některých budov, např. budova ZŠ Školní (původně Pionýrů). Hlavním projektantem města byl opět architekt Zdeněk Meduna, jenž si do týmu přivedl Zdeňka Špačka, Rudolfa Spáčila a Drahomíra Macháta. V dnešní době je územní část města Havířova chráněnou památkovou zónou, jež je z jedné strany ohraničena lesoparkem, na druhé straně meandry řeky Lučiny, na jihovýchodě je zóna zakončena u kina Centrum. Směrem od Ostravy zahrnuje i zámek a kostel sv. Anny, což nejsou stavby v Sorela stylu. Dominantou u domu Labužník, v němž sídlila jedna z prvních velkých samoobsluh u nás s bistrem v 1. patře, je obří neonový nápis.

Zajímavostí je, že nápis navrhl (nakreslil) samotný architekt Bronisław Firla, jenž za něj dostal honorář v podobě jedné láhve vína.[4]



Obr. 1: Zrekonstruovaný nápis Labužník na základě originálu od B. Firla

Typickým znakem města je široký bulvár, uzavřené dvory, důraz na symetrii, hojná výzdoba a zeleň. Dokonce byl i začleněn potenciální obchvat centra po ul. Na Nábřeží, jenž se v praxi projevil jako nedostatečný, jelikož součástí je i prudká zatáčka, kde by kamionová doprava měla problém.



Obr. 2: Porubské podlouhí (vlevo) a Hl. třída v Havířově (vpravo)

Od tradičního pojetí stalinské architektury se ustupuje až v polovině 50. let, zejména v souvislosti se smrtí J. V. Stalina (1953) a kritikou kultu osobnosti.

2 Využití architektonických prvků ve výuce

Již v učebnici Užitého rýsování z roku 1931 od Boženy Ritschlové-Vanečkové se vyskytuje praktická kapitola O užitných vzorech. Vzhledem k tomu, že na naší univerzitě připravujeme budoucí učitele a napomáháme jim i s přípravou a tvorbou různých projektů, vznikla myšlenka již v době pandemie jak žáky a studenty dostat ven. V rámci různých projektových dní jsme navrhli projekt Poznávám své město z pohledu geometrie a výběr pro ilustrační zadání jednoznačně padlo na město Havířov. Důvody byly hned dva, jelikož studenti mají vnímat svět kolem sebe a měli by aplikovat své získané znalosti na reálné situace a druhý důvod je nepopulární oblast geometrie. S využitím moderních i

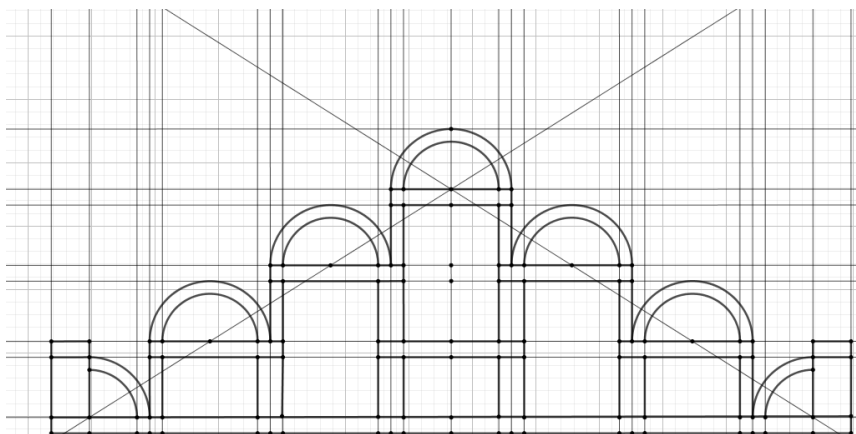
klasických rýsovacích pomůček jsme se rozhodli žákům přiblížit zajímavosti jejich města. Tuto koncepci lze samozřejmě aplikovat na libovolný styl. Úlohy můžeme pojmut nejen z pohledu konstrukčního, ale i z pohledu procvičování odhadů. Další z možností je, že učitel si připraví pracovní listy a žáci následně dorýsují dané objekty.

Úloha 1. Na základě přiložené fotografie vytvoř konstrukci obloukového štítu.



Obr. 3: Příloha k zadání

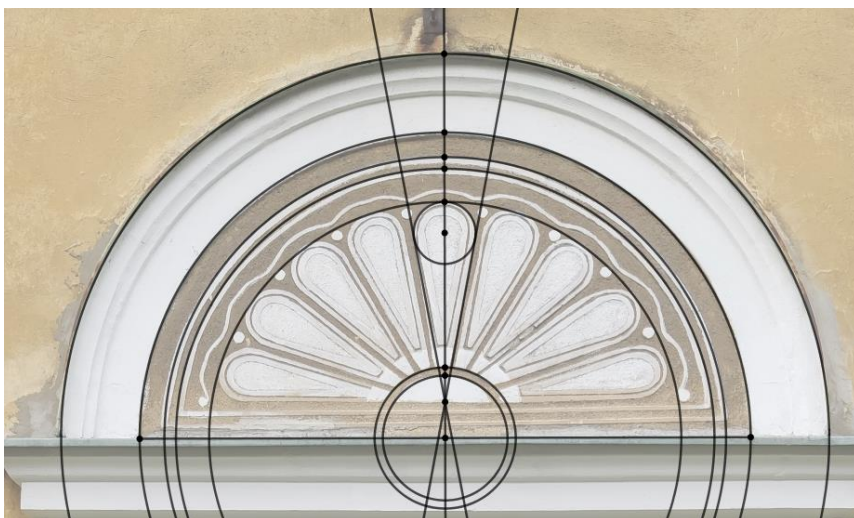
Úlohu lze již začlenit do oblasti M-5-3-01 (narýsování a znázornění základních rovinných útvarů) až po oblasti M-9-3-06 a M-9-3-08, pod které jsou začleněny konstrukce rovinných útvarů a zobrazení souměrných útvarů. Žák si při návrhu konstrukčního řešení uvědomí spojitost mezi jednotlivými geometrickými útvary a symetrií. Učitel může danou úlohu využít jako motivační úlohu a vysvětlit žákům princip a využití štítů. Úskalí materiálů se vyskytuje ve faktu, že fotografie jsou získávány pod daným úhlem a dochází k deformacím, což může vést u mladších žáků k mystifikaci.



Obr. 4: Ukázka možného řešení dané úlohy

Úloha 2. Nalezni ve svém okolí tympanon, zrekonstruuj a popiš polohy jednotlivých útvarů, které se v něm vyskytují.

„Tympanon označujeme výzdobu v ploše štítového nástavce. Trojúhelníková, polokruhová nebo segmentem (obloukem) vymezená plocha štítu nad průčelím, portálem nebo oknem. Architektonická část nástavce různé velikosti se nazývá fronton, zatímco tympanonem rozumíme především reliéfní výzdobu plochy vymezené zpravidla profilovanou římsou a štítovými rameny. V lidové architektuře bývá také u zděných vjezdů do dvora.“ [3]



Obr. 5: Ilustrace vzájemné polohy kružnic a přímek v tympanonu

Úlohu je možné začlenit do vyšších ročníků a propojit mezipředmětově s výtvarnou výchovou, popřípadě i začlenit jako výstup v rámci očekávaných výstupů z oblasti VV-9-1-03 (užívání prostředků pro zachycování jevů). Žák si uvědomí spojitosti mezi soustřednými kružnicemi a tečnami ke kružnici. Žák může využít softwaru GeoGebra, nahrát jeho získanou fotografii na pozadí a následně zrekonstruovat tympanon. Úlohu lze také využít způsobem, kdy konstrukce je prvně navržena a následně pomocí rozšířené reality v terénu přiřazena k danému tympanonu.

Úloha 3. Vytvoř trojrozměrný model části Lunetové římsy u společenského domu Radost.

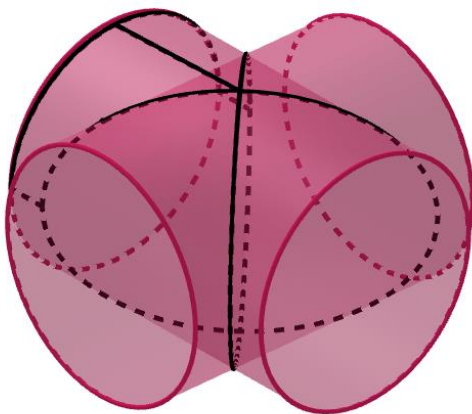
Lunetovou římsou nazveme podstřešní římsu podporovanou částmi křížové klenby ve tvaru lunet nebo polovinou valené klenby s drobnými lunetovými kápěmi.[2] Kulturní dům Radost je z architektonického pohledu jedna

z významných budov, ve které původně sídlilo i kino, v divokých dobách porevolučních kasino a následně bylo zpět vráceno ke svému původnímu účelu.



Obr. 6: Kulturní dům Radost (vlevo)
a detailní fotografie lunetové římsy (vpravo)

Úloha je určena pro studenty středních škol a může být využita i v rámci deskriptivní geometrie, kde studenti nebudou tvořit 3D model, ale zadání může být upraveno pro Mongeovo promítání. V rámci řešení úlohy byla využita GeoGebra 3D, ve které byl vytvořen dynamický trojrozměrný model (Obr. 7)



Obr. 7: Model části lunetové římsy s využití křížové klenby

Fotografii lze využít i z pohledu zobrazení kružnice ve středové kolíneaci, jelikož kruh nebo část kruhového oblouku se zobrazí jako regulární kuželosečka nebo její část. Regulární kuželosečky se liší podle počtu nevlastních bodů. Ve středové kolíneaci jim říkáme úběžníky a leží na úběžnici. Díky tomu platí, že:

- Nemá-li kružnice s úběžnicí žádný společný bod, pak je obrazem kružnice elipsa.
- Má-li kružnice s úběžnicí právě jeden společný bod, pak je obrazem kružnice parabola.
- Má-li kružnice s úběžnicí dva různé průsečíky, pak je obrazem kružnice hyperbola. [5]

Popřípadě lze demonstrovat, že v osové afinitě bude obrazem elipsa.

Další úlohy mohou být zaměřeny na popisy křivek, které byly využity na ozdobných mřížích či fasádních výzdobách domů.



Obr. 8: Ozdobná mříž v průjezdu domu (vlevo)
a ukázka fasádní výmalby (vpravo)

3 Závěr

Celkově se jedná o velmi zajímavou problematiku, kdy fantazii učitelů i žáků se meze nekladou. Úlohy lze různě modifikovat a divergovat na požadovanou úroveň. Využití architektonických prvků ve výuce geometrie na všech stupních škol může vést k odstranění neoblíbenosti geometrie u některých žáků a poukázání na využití jejich znalostí a dovedností v praxi. Taktéž je velmi užitečné se spojit v rámci mezipředmětové spolupráce a částečně práci začlenit do výtvarné výchovy, kterou žáci nevnímají za stresovou, ale spíše za předmět relaxačního typu. Podobné projekty ocení rodiče i žáci, kteří se mohou vydat do terénu a za pomoci základní techniky, kterou mají k dispozici, pořídí požadované fotografie, se kterými následně mohou pracovat v digitální nebo tištěné podobě.

V letošním akademickém roce byl v rámci výuky Konstruktivní geometrie zadán výstup na téma Architektonické prvky a jejich začlenění do výuky geometrie. Prvotní nadšení nebylo velké, ale při upřesnění zadání bylo akceptovatelné a motivační pro studenty učitelství.

Poděkování

Tento článek vznikl za podpory SGS03/PrF/2022 – Matematická fyzika, geometrie a teorie čísel.

Literatura

- [1] R. Biegel: *Přehled dějin českého umění (Architektura 1945-1989)*. Praha, 2012
- [2] O. Blažiček: *Slovník pojmů z dějin umění; Názvosloví a tvarosloví architektury, sochařství, malby a užitého umění*; Odeon 1991; s. 122-123
- [3] V. Frolec, J., Vařeka: *Lidová architektura (Encyklopedie)*. SNTL a ALFA, L 17-U3-VI-31f/2145 1. vydání, Praha 1983
- [4] D. Macháček: *Sorela lahůdkám nepřála přesto stvořil Labužník (rozhovor s architektem B. Firlou)* [online] [4.9.2022] 17.05.2014 <https://davidmachacek.wordpress.com/2014/05/17/sorela-lahudkam-neprala-presto-stvoril-labuznika/>
- [5] Katedra didaktiky matematiky, MFF, KU: *Portál deskriptivní geometrie. 2010-2022* [online] [5.9.2022] <https://www2.karlin.mff.cuni.cz/~jole/plichtova/Diplomka/AfinitaAKoloneace/?page=SKKruznice>
- [6] O. Šefců: *Lexikon architektonických prvků a stavebního řemesla*. Grada 2012

Nonlinear subdivision schemes using conic sections

Klaudia Hamajová, Pavel Chalmovianský

Department of algebra and geometry

Mlynská dolina, 842 48 Bratislava, Slovak Republic

email: klaudia.hamajova@fmph.uniba.sk, pavel.chalmoviansky@fmph.uniba.sk

Abstract. Subdivision is a well-known and established method for generating smooth curves and surfaces from discrete data by repeated refinements. We describe modifications of a nonlinear method for constructing a sequence of refined polygons, which starts with a sequence of points and associated normals. The newly generated points are sampled from conics which approximate the given points and the corresponding normals according to the proposed refinement rules.

Keywords: nonlinear subdivision, conic sections, approximation, ellipse.

1 Introduction

Subdivision has been one of the most efficient ways for curve and surface design in computer graphics, with successful applications in computer animation (e.g., film production) and the video game industry in particular. Refinement is a method for generating smooth curves and surfaces from discrete data by repeated refinements.

Subdivision schemes are divided according to the way of obtaining refined data into linear and nonlinear. The most common and oldest subdivision schemes are based on linear refinement rules, which are applied separately to each coordinate of the control points, and the analysis of these schemes is well understood. Since the resulting limit curves are not sufficiently sensitive to the geometry of the control polygons, there is a need for subdivision schemes. Such schemes take the geometry of the control polygons into account by using nonlinear refinement rules and are known to generate better limit curves. The author Marcel Makovník deals with nonlinear schemes of surfaces in the article [2]. Nonlinear methods offer enough problems to solve. The case of curves is covered by the results of U. Reif, E. Lipovetsky, N. Dyn, J. Wallner and others. Results in the field of nonlinear schemes are offered by the authors P. Chalmovianský and B. Jüttler [1], Jian-ao Lian [3], E. Lipovetsky and N. Dyn [4].

In our work, we study nonlinear subdivision methods curves using conic sections. We present a new nonlinear method. In the beginning, we are given discrete data forming a curve (a piecewise polygonal line in parts). Subsequently, the curve is refined either by adding new points or by modifying the original points of the curve. The goal of refinement is to obtain a curve with the desired properties in the limit and its approximation after a sufficiently large number of refinements. The resulting

curve can either interpolate or approximate the original data according to the choice of calculation of the new conic section or according to the application of the input data.

2 Steps of the proposed new nonlinear subdivision scheme

We describe a new method for constructing a sequence of refined polygonal lines.

1. In the beginning, we have a sequence of points and normals $\{(p_i, \vec{n}_{p_i})\}$.
2. We look for the conic section for every three consecutive points and two corresponding normals to the points.
3. The newly generated points are sampled from the conics which approximate the given points and the corresponding normals according to the proposed refinement rules.
4. In each iteration, the total number of points is (roughly) doubled.
5. It is an approximation method.

3 Fundamental step of the proposed construction

Consider three different points $p_{i-1}, p_i, p_{i+1} \in \mathbb{R}^2$ with associated normals $\vec{n}_{p_{i-1}}, \vec{n}_{p_{i+1}} \in \mathbb{S}^1$ associated to the points p_{i-1} and p_{i+1} , respectively. We construct a conic

$$g_i(x, y) = 0,$$

where

$$g_i(x, y) = a_i x^2 + 2b_i xy + c_i y^2 + 2d_i x + 2e_i y + f_i, \quad a_i, b_i, c_i, d_i, e_i, f_i \in \mathbb{R},$$

which minimizes the objective function

$$F_i(a_i, b_i, c_i, d_i, e_i, f_i) = g_i(p_{i-1})^2 + g_i(p_i)^2 + g_i(p_{i+1})^2 + \|\nabla g_i(p_{i-1}) - \vec{n}_{p_{i-1}}\|^2 + \|\nabla g_i(p_{i+1}) - \vec{n}_{p_{i+1}}\|^2. \quad (1)$$

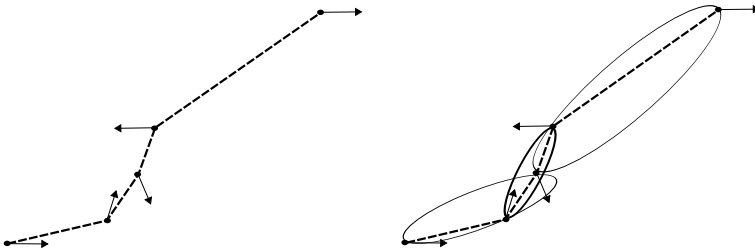


Fig. 1: First and second step of a new nonlinear subdivision scheme.

The task is to find

$$\arg \min_{a_i, b_i, c_i, d_i, e_i, f_i \in \mathbb{R}} F_i(a_i, b_i, c_i, d_i, e_i, f_i),$$

hence, to solve a system of linear equations with unknowns a, b, c, d, e, f

$$\frac{\partial F_i}{\partial a_i} = 0, \frac{\partial F_i}{\partial b_i} = 0, \frac{\partial F_i}{\partial c_i} = 0, \frac{\partial F_i}{\partial d_i} = 0, \frac{\partial F_i}{\partial e_i} = 0, \frac{\partial F_i}{\partial f_i} = 0. \quad (2)$$

The solution of (2) is invariant with respect to Euclidean transformations. Therefore, we suppose the following choice of the coordinate system

$$p_{i-1} = (-r, 0), \quad p_i = (r, 0), \quad p_{i+1} = (m, n) \quad (3)$$

where $n > 0, r > 0$ and

$$\vec{n}_{i-1} = (\cos \eta, \sin \eta), \quad \vec{n}_{i+1} = (\cos \phi, \sin \phi) \quad (4)$$

for $\eta, \phi \in \mathbb{R}$. Any three non-identical points with given associated normals can be mapped to this situation using a Euclidean transformation, see the figure 2. The problem (2) has a unique solution and that

$$a_i = \frac{-(\cos(\eta) - \cos(\phi))}{4r}, \quad b_i = \frac{-(\sin(\eta) - \sin(\phi))}{4r},$$

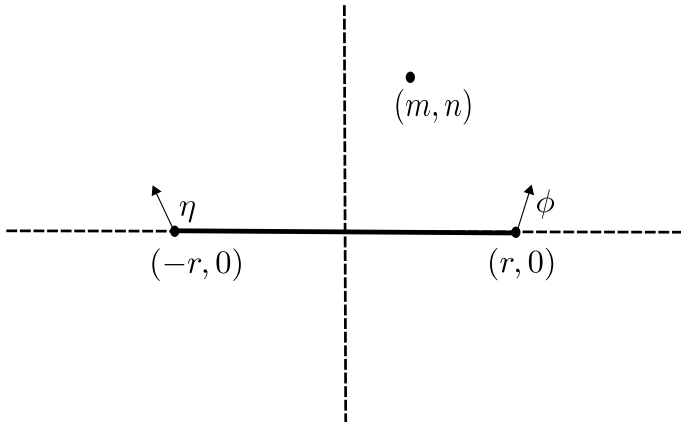


Fig. 2: Local coordinates for analyzing the conic fit.

$$\begin{aligned}
c_i = & \\
& - \frac{(m^2 \cos(\phi) - m^2 \cos(\eta) + r^2 \cos(\eta) + r^4 \cos(\eta) - r^2 \cos(\phi) - r^4 \cos(\phi) + 2mr \cos(\eta))}{4n^2 r(r^2 + 1)} \\
& - \frac{(2mr \cos(\phi) - 2mn \sin(\eta) + 2mn \sin(\phi) + 2nr \sin(\eta) + 2nr \sin(\phi) + 2nr^3 \sin(\eta))}{4n^2 r(r^2 + 1)} \\
& - \frac{(2nr^3 \sin(\phi) - m^2 r^2 \cos(\eta) + m^2 r^2 \cos(\phi) - 2mnr^2 \sin(\eta) + 2mnr^2 \sin(\phi))}{4n^2 r(r^2 + 1)},
\end{aligned}$$

$$d_i = \frac{\cos(\eta) + \cos(\phi)}{4(r^2 + 1)}, \quad e_i = \frac{\sin(\eta) + \sin(\phi)}{4}, \quad f_i = \frac{r \cos(\eta) - r \cos(\phi)}{4}.$$

If

$$\begin{aligned}
a_i c_i - b_i^2 = 0 & \Rightarrow g_i \text{ is a parabola,} \\
a_i c_i - b_i^2 > 0 & \Rightarrow g_i \text{ is an ellipse,} \\
a_i c_i - b_i^2 < 0 & \Rightarrow g_i \text{ is a hyperbole.}
\end{aligned}$$

Let

$$\alpha = \frac{\eta - \phi}{2}, \quad \beta = \frac{\eta + \phi}{2}. \quad (5)$$

After substituting into equation (3) we get

$$\begin{aligned}
a_i c_i - b_i^2 = & - \frac{(2 \sin \alpha \cos \beta)^2}{16r^2} + \\
& (-2 \sin \alpha \sin \beta) \frac{4r \cos \alpha (m \cos \beta - n(r^2 - 1) \sin \beta) + 2 \sin \alpha ((r^2 + 1) \sin \beta (m^2 - r^2) - 2mn \cos \beta)}{16n^2 r^2 (r^2 + 1)}.
\end{aligned}$$

By analyzing this expression, we will know what kind of conic we get during refining.

4 Refining process – the newly generated point

Let us focus on the case when we get an ellipse during refinement. A new point is obtained from the intersection of the line l and the ellipse, where the line l is the axis of the line segment of two different adjacent points

$$l : x = \frac{1}{2}p_i + \frac{1}{2}p_{i+1} + t(p_{i+1} - p_i)^\perp, t \in \mathbb{R}. \quad (6)$$

This step is shown in figure 3. Through this intersection, we get two new points, we choose the one that is closer to the given points, see the figure 4 on the left. Then the new normal is determined by the normal of the conic, see the figure 4 on the right.

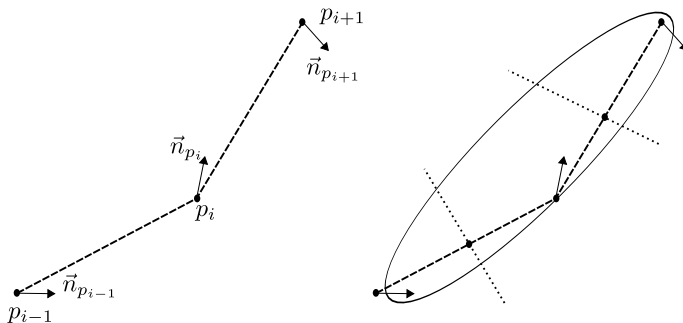


Fig. 3: Input data on the left and a process of generating a new point on the right.

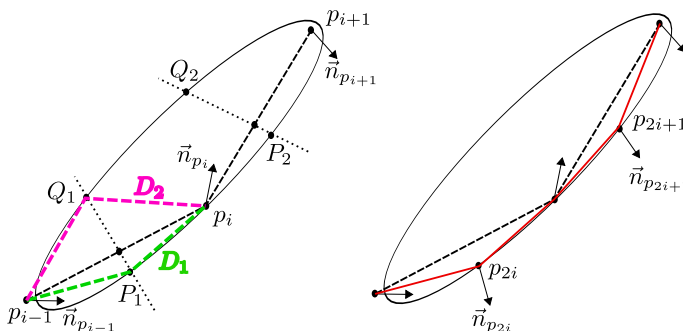


Fig. 4: Selecting a new point during refining and determining the corresponding normal.

5 Example on given random input data

Consider five consecutive points with their corresponding normal vectors. Let us choose these points and the normals from the set of points and normals when we get an ellipse during refinement. It is obvious that during refinement there may be a case when we obtain a different type of conic section, for example, a hyperbola or a parabola. If such a case occurs, we adjust the input data in the next iteration so that we get an ellipse. Several other iterations are shown in figure 5.

6 Conclusion

This paper presents a new nonlinear refinement method using conic sections. We have described the individual steps of the refinement algorithm using conic sections. And we have shown how to find a solution to a system of linear equations (2), with the help of which we can determine the

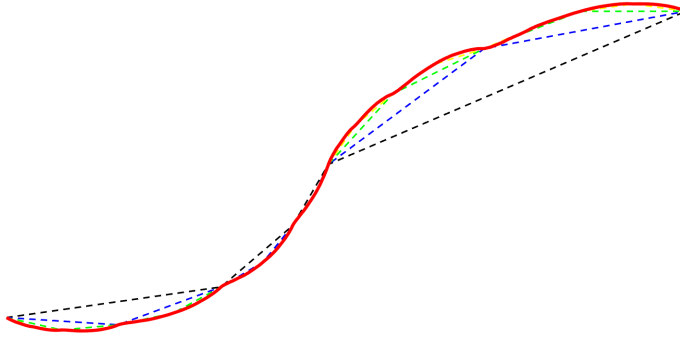


Fig. 5: Iterations using ellipse

prescription of a given conic section during refining. We visualized several iterations on random input data.

In future work, we want to expand the proposed method using all types of conic sections and look at the smoothing of the limit curve. We will try to design an efficient way of selecting a new point and we will extend the scheme to include weights of points and normal vectors.

Acknowledgements

This work was supported by the grant VEGA 1/0596/21 and by Grant of Comenius University No. UK/313/2022.

References

- [1] P. Chalmovianský, B. Jüttler: *A Non-linear Circle-preserving Subdivision Scheme*, Advances in Computational Mathematics, pp. 375-400, 2007
- [2] M. Makovník, P. Chalmovianský: *Point Cloud Upsampling via Quadric Fitting*, International Conference on Geometry and Graph-ics, Springer, p. 263–275, 2022
- [3] L., Jian-ao: *A New Four Point Circular-Invariant Corner-Cutting Subdivision for Curve Design*, Applications and Applied Mathematics: An International Journal (AAM), Vol. 7, Iss. 1, Article 30
- [4] E. Lipovetsky, N. Dyn: *Extending editing capabilities of subdivision schemes by refinement of point-normal pairs*, Computer-Aided De-sign, 2020

Aproximace izoploch pomocí trojúhelníkových sítí se zaručenou kvalitou

Approximating isosurfaces by guaranteed-quality triangular meshes

Joel Hass, Maria Trnková

*Department of Mathematics, University of California, Davis,
One Shields Ave, Davis, CA USA*

email: hass@math.ucdavis.edu, mtrnkova@math.ucdavis.edu

Abstract. We describe a new method for approximating an implicit surface F by a piecewise-flat triangulated surface whose triangles are as close as possible to equilateral. The main advantage is improved mesh quality which is guaranteed for smooth surfaces. The GradNormal algorithm generates a triangular mesh that gives a piecewise-differentiable approximation of F , with angles between 35.2 and 101.5 degrees. As the mesh size approaches 0, the mesh converges to F through surfaces that are isotopic to F . The complete version of the paper is available at [1].

Keywords: surface, mesh, triangulation and object representations

Klíčová slova: plocha, síť, triangulace a reprezentace objektů.

1 Úvod

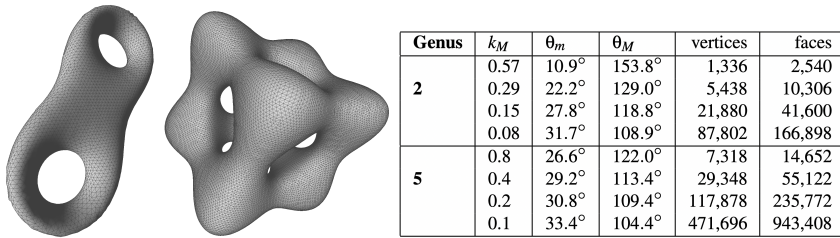
V tomto příspěvku chceme seznámit s novou metodou aproximace implicitní plochy F pomocí po částech rovinných trojúhelníkových ploch tak, aby tyto trojúhelníky byly co nejbližší rovnostranným. Hlavní výhodou je lepší kvalita sítě, která je zaručena pro hladké povrchy. Algoritmus GradNormal generuje trojúhelníkovou síť, která poskytuje po částech diferencovatelnou aproximaci F . Jak se velikost sítě blíží k nule, konverguje síť k F prostřednictvím ploch, které jsou izotopické s F . Tečné roviny GradNormal sítě konvergují k tečným rovinám diferencovatelné implicitně zadané plochy $F \subset R^3$, přičemž vnitřní úhly trojúhelníků GradNormal sítě jsou z intervalu $[35.2^\circ, 101.5^\circ]$. Tyto úhlové meze byly důsledně stanoveny. Kompletní verze článku je k dispozici na [1].

2 GradNormalová síť

Studujeme problém aproximace plochy v R^3 pomocí sítě, která má optimální úhlové vlastnosti. Při výpočtech vycházejících z ploch zadaných pomocí jejich sítě je často nezbytné, ale obtížné se vyhnout tzv. "třískám", neboli trojúhelníkům s úhly blízkými nule. Špatně tvarované trojúhelníky mohou z numerických důvodů způsobit selhání algoritmů na takto zadaných plochách.

Hledání pravidelné sítě, jejíž trojúhelníky se blíží tečným prostorům daného povrchu, vede ke dvěma protichůdným cílům. Jedním cílem je, aby se trojúhelníky co nejvíce blížily rovnostranným, a druhým cílem je, aby se síť diferencovatelně přizpůsobovala ploše tak, aby se její tečné roviny blížily tečným rovinám plochy.

Příklady sítí vytvořených algoritmem GradNormal pro implicitně zadané plochy definované jako množiny explicitně zadaných matematických funkcí v jednotlivých úrovních jsou uvedeny na obrázku 1. Jsou získány dlaždicováním jednotkové krychle pomocí 869 652 čtyřřetěňů a zobrazeny pomocí programu MeshLab. Údaje o tom, jak se tyto úhly zlepšují s tím, jak je dlaždicování jemnější, najdete na obrázku 1.



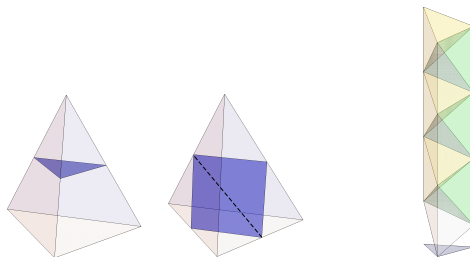
Obr. 1: Tyto sítě mají 10 346 (pro genus 2) a 55 122 (pro genus 5) trojúhelníkových ploch. Mají úhly v intervalech $[22.1^\circ; 129.0^\circ]$ (genus 2) a $[29.2^\circ; 113.4^\circ]$ (genus 5).

2.1 Kroky algoritmu GradNormal

Algoritmus GradNormal probíhá ve třech krocích.

1. V prvním kroku se vytvoří síť s ostrými trojúhelníky, kterou nazýváme MidNormal síť. Tento krok je podobný algoritmu Marching Tetrahedra, ale s důležitými rozdíly. Základní myšlenka obou algoritmů se objevuje v teorii normálových ploch, což je mocný nástroj používaný ke studiu ploch na trojrozměrných varietách. Algoritmus začíná dlaždicováním prostoru R^3 čtyřřetěňů pevného tvaru. Používá dlaždice čtyřřetěňů vybrané tak, aby optimalizovaly úhly vyskytující se v konečné síti. Průsečík povrchu F s těmito dlaždicemi čtyřřetěňů vytvoří aproximaci F pomocí trojúhelníků a čtyřúhelníků, jak je znázorněno na obrázku 2. Ačkoli má velmi dobré úhlové vlastnosti a poskytuje síť z dvourozměrných mnohoúhelníků, která leží blízko implicitně zadané plochy, její normálové vektory nesplývají s normálovými vektory F .

2. Druhý krok zahrnuje projekci vrcholů MidNormal sítě na implicitně zadanou plochu, takže normálové vektory splynou s normálovými vektory dané plochy. Takto vytvořená trojúhelníková síť má požadované vlastnosti



Obr. 2: (Vlevo) Elementární disky čtyřstěnu: trojúhelníky a čtyřúhelníky - tvoří část normálové plochy pro algoritmus MidNormal. (Vpravo) Čtyřstěny se skládají na sebe a vyplní se prostor.

s výjimkou bodů valence čtyři.

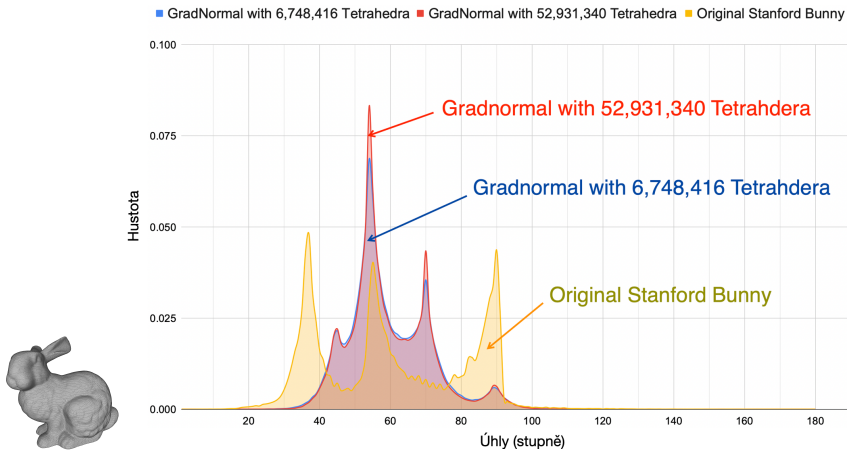
3. Poté následuje jediný krok opětovného síťování (nezahrnuje vrcholy valence čtyři). Pečlivou analýzou zkreslení úhlů v rámci tohoto kroku se stanoví vlastnosti deklarované pro GradNormal síť.

2.2 Další deskriptory povrchu

Algoritmus GradNormal přijímá jako vstup implicitní plochu zadanou jako množinu explicitních funkcí v R^3 v jednotlivých úrovních, ale i jiné formy vstupního zadání ploch.

Pokud je například vstupem triangulovaná plocha (tedy nehladký povrch popsáný jako sjednocení polygonálních ploch) s nízkou kvalitou sítě, pak existují postupy pro vytvoření funkce na R^3 , která počítá vzdálenost bodu od povrchu. Pokud vstupem popisujícím plochu je Point Cloud, metody jako Moving Least Squares a Adaptive Moving Least Squares vytvářejí funkci poskytující popis dané izoplochy. Tuto funkci pak lze použít jako vstup pro algoritmus GradNormal. To nám umožňuje použít tento algoritmus ke zlepšení sítě s nízkou kvalitou úhlů.

Jako příklad jsme zkonstruovali síť Stanford Bunny pomocí algoritmu GradNormal z původní Stanford Bunny sítě. Na obrázku 3 vidíme rozsah úhlů sítě vytvořených algoritmem GradNormal při dvou rozlišeních a úhly v původní síti Stanford Bunny. Při použití na nehladký povrch, který má ve vrcholech ostré rohy a na hranách záhyby, neplatí omezení úhlů, které zaručuje GradNormal pro hladké povrchy, a to ani v limitě. Přesto je vidět, že úhly jsou více seskupeny kolem 60° než v původní síti. Abychom mohli porovnat rozložení úhlů v jednom grafu, byly počty normalizovány vydělením trojnásobkem počtu trojúhelníkových ploch, tedy 348 162 pro síť GradNormal s 6 748 416 čtyřstěny a 1 400 310 pro síť GradNormal s 52 931 340 čtyřstěny. Obě sítě GradNormal mají velmi podobné rozložení, většina úhlů se pohybuje mezi 40° a 80° , zatímco původní Stanford síť



Obr. 3: Rozložení úhlů pro původní síť Stanford Bunny a pro GradNormal síť Stanford Bunny ve dvou rozlišeních.

měla mnoho úhlů blízko 30° a 90° . Kód použitý k vytvoření těchto obrázků je k dispozici na adrese na GitLabu [2].

3 Závěr

Představili jsme nový algoritmus pro aproximaci izoploch. Mezi hlavní výhody patří jednoduchost algoritmu, rychlý běh, malá spotřeba místa a zaručená vysoká kvalita trojúhelníků při aplikaci na hladký povrch. Experimenty s povrchy definovanými jednoduchými matematickými funkcemi ukazují, že výsledná síť má rozumné úhlové meze i při použití hrubé dlaždice čtyřstěnu a že zaručené úhlové meze $[35, 2^\circ; 101, 5^\circ]$ pro síť aproximující hladké povrchy jsou dosažitelné při použití dlaždice praktické velikosti. Nevýhodou algoritmu GradNormal je, stejně jako u jiných metod založených na pravidelných sítích, že není přizpůsoben lokálním vlastnostem povrchu. Zejména ostré rysy, úhly a rohy nemusí být tímto postupem zachyceny, a pokud je GradNormal aplikován na nehladké povrchy, požadované úhlové meze neplatí.

Literatura

- [1] J. Hass, M. Trnkova: *Approximating isosurfaces by guaranteed quality triangular meshes*, Computer Graphics Forum 39(5):29-40, August 2020
- [2] J. Hass, M. Trnkova: *Gradnormal source files*, git-lab.com/joelhass/midnormal, December 2019

Úvod do dynamického konstruování v prostředí programu GeoGebra

Introduction to dynamic construction in GeoGebra

Roman Hašek

*Jihočeská univerzita v Českých Budějovicích, Pedagogická fakulta
Jeronýmova 10, 371 15 České Budějovice, Česká republika
email: hasek@pf.jcu.cz*

Abstract. The paper deals with the basic principles of constructing planimetric geometric figures in the dynamic geometric environment of GeoGebra, with an emphasis on preparing students for their correct execution. It is primarily devoted to the use of the GeoGebra infrastructure for the realization of Euclidean constructions; the editing of the GeoGebra toolbar, the creation of online applets and their use in the GeoGebra Classroom environment.

Keywords: Dynamic geometry software, euclidean constructions, GeoGebra.

Klíčová slova: Dynamický geometrický software, eukleidovské konstrukce, GeoGebra.

1 Úvod

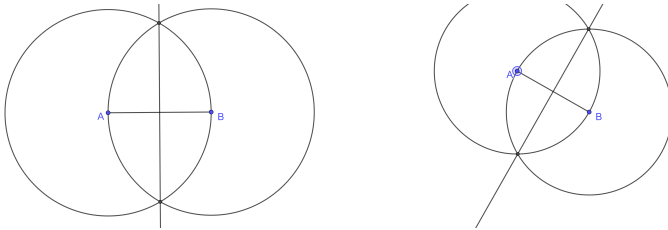
Článek se věnuje základním principům tvorby planimetrických dynamických konstrukcí v prostředí programu GeoGebra (geogebra.org). Důraz je kladen na nezbytnost přípravy žáků na specifika práce s dynamickým geometrickým programem (DGS). Jak ukazují osobní zkušenosti autora článku a jeho kolegů ze základních škol [3, 5], stejně jako poznatky zahraničních odborníků [7], přechod od klasického rýsování tužkou na papír k rýsování v programu dynamické geometrie přináší změnu paradigmatu, se kterou je třeba ve výuce počítat. Článek nabízí řešení ve formě jednoduchých adaptačních konstrukčních úloh, k jejichž zadání je použito prostředí *GeoGebra Classroom* (*GeoGebra Třída*) [2] umožňující učitelům poskytovat žákům okamžitou zpětnou vazbu.

2 Dynamická geometrická konstrukce

Klíčovou vlastností dynamické geometrické konstrukce, která má zjevný didaktický potenciál, je zachování vlastností daných zadáním úlohy při libovolné manipulaci s jejími nezávislými body. Hovoříme o tzv. *robustní konstrukci* [4, 7].

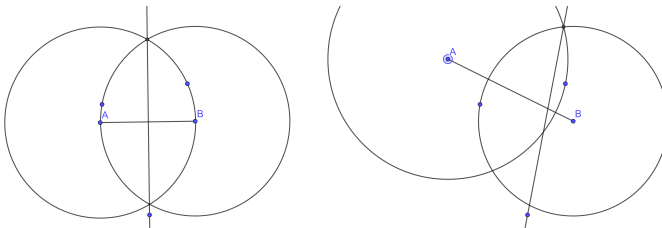
2.1 Robustnost konstrukce

Pojem *robustní konstrukce* (*robust construction*) pro konstrukci sestrojenou v programu dynamické geometrie, která zachovává své vlastnosti při tažení nezávislých bodů myší, používá Collete Laborde v článku [4]. Protikladem robustní konstrukce je v tomto článku *měkká konstrukce* (*soft construction*). Jedná se o pojem, který je chápán pozitivně, jako záměrně použitá konstrukce s daným vzdělávacím cílem. Pro potřeby našeho článku, který sleduje linii žákových miskoncepce vznikajících přenosem praktik ručního rýsování do programu dynamické geometrie, je výstižnějším protikladem pojmu robustní konstrukce pojem *konstrukce od oka*. Příklad robustní konstrukce v programu GeoGebra, konkrétně



Obr. 1: Robustní konstrukce

konstrukce osy dané úsečky AB , je představen na Obr. 1 (kliknutím na popis obrázku lze otevřít příslušný applet, platí i pro další obrázky). Konstrukce je provedena eukleidovskými, podle prvních tří Eukleidových postulátů, viz [1], nikoliv pomocí příslušného nástroje *Osa úsečky* nabízeného programem. Robustnost se projevuje zachováním sestrojené osy úsečky AB , bez ohledu na přemístění bodů A, B myší. Příklad konstrukce stejné



Obr. 2: Konstrukce od oka

úlohy od oka je zachycen na Obr. 2. Po přetažení bodů A, B myší se konstrukce „rozpadá“, původně osa úsečky již neplní tuto roli. Příčinou nedokonalosti této konstrukce je skutečnost, že její autor není obeznámen

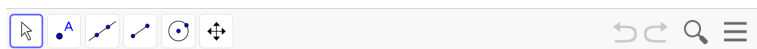
se specifiky konstrukce v prostředí DGS. Místo aby respektoval vztahy incidence a příslušné objekty spolu striktně provazoval tak, že by k definici nových používal průsečíky těch stávajících nebo volné body dané zadáním úlohy, nové objekty umísťuje do nákresny pouze od oka, jako více či méně nezávislé na zadání úlohy. Výsledný dynamický obrázek potom neodráží geometrické vztahy dané zadáním a konstrukcí úlohy, ale je tvořen souborem zcela nebo částečně nezávislých objektů. V případě konstrukce na Obr. 2 tak jsou obě kružnice pouze zdánlivě vedeny krajními body úsečky AB , a domnělá osa pouze zdánlivě prochází jedním z průsečíků těchto kružnic. Nedostatky konstrukce od oka se projeví po přemístění nezávislých bodů konstrukce (GeoGebra nezávislé body kreslí modře, závislé černě).

2.2 Adaptační úlohy

Praxe použití DGS s žáky základních a středních škol i se studenty učitelství matematiky ukazuje, že tvorba robustních konstrukcí pro řadu z nich není samozřejmá a je třeba je na ni připravit. Ačkoliv se jedná o generace, které vyrůstaly obklopeny digitálními technologiemi, přechod z papíru do prostředí DGS pro ně není automatický. Potvrzují se tak slova D. Willingham *“Technology changes everything ... but not the way you think.”* [8] Jako vhodný prostředek adaptace žáků na konstrukce v digitálním prostředí se osvědčily eukleidovské konstrukce, ideálně zadávané v prostředí GeoGebra Classroom [3].

2.3 Příprava prostředí GeoGebry

Eukleidovskými konstrukcemi rozumíme konstrukce prováděné podle prvních tří Eukleidových postulátů, viz [1]. Je proto vhodné, připravit si prostředí GeoGebry tak, aby nabízelo pouze nástroje potřebné pro tyto konstrukce, viz Obr. 3. Použijeme k tomu volbu *Nastavit panel nástrojů* z hlavní nabídky programu.



Obr. 3: Nabídka nástrojů omezená pro eukleidovské konstrukce

2.4 GeoGebra Classroom

Jednoduché eukleidovské konstrukce, například sestavení *osy úsečky*, *kolmice z daného bodu na přímku* nebo *rovnoběžky daným bodem s danou přímkou* je ideální zadávat v prostředí *GeoGebra Classroom* [2]. Můžeme v „přímém přenosu“ sledovat postup řešení jednotlivých žáků a bezprostředně s nimi interagovat. Pro využití tohoto prostředí je třeba vytvořený

materiál uložit na portál geogebra.org. Tím naše péče o soubor ale nekončí. Ještě musíme aktivovat zobrazení panelu nástrojů u appletu, pomocí režimu *Upravit aktivitu – Pokročilé nastavení ...* Když applet vypadá, jak potřebujeme, uložíme ho a stiskneme tlačítko *Vytvořit třídu* v pravém horním rohu okna, v němž je applet zobrazen.

3 Závěr

Ačkoliv je velmi lákavé citovat různé experty na vzdělávání v 21. století, kteří operují s tvrzením, že použití počítače je pro současnou mladou generaci přirozené, viz např. M. Prensky a jeho pojem “digital natives” [6], praxe, stejně jako poznatky kognitivní psychologie [8] ukazují, že abychom mohli ve výuce matematiky těžit z použití počítače, je třeba stále věnovat náležitou pozornost propedeutice.

Literatura

- [1] Eukleides: *Eukleidovy základy (Elementa)*, překlad F. Servít, 1907. Dostupné z: https://commons.wikimedia.org/wiki/File:Eukleides_Servit.pdf
- [2] GeoGebra Team, N. Brůžková: *Nauč se s GeoGebra Třídou*. Oficiální Tutorial. In: geogebra.org, 2021. Dostupné z: <https://www.geogebra.org/m/gvb3mahj>
- [3] V. Havlíčková: *Výuka matematiky na základní škole s podporou digitálních technologií*. Závěrečná práce stud. prog. Studium v oblasti pedagogických věd. Jihočeská univerzita v Českých Budějovicích, České Budějovice, 2022. Dostupné z: <https://wstag.jcu.cz>
- [4] C. Laborde: *Robust and soft constructions: two sides of the use of dynamic geometry environments*. In S.-C. Chu et al. (Eds.), *Proceedings of the 10th Asian Technology Conference in Mathematics (ATCM)* (pp. 22-35). Korea National University of Education, 2005
- [5] Z. Novotný: *Využití programu GeoGebra pro podporu výuky matematiky na základní škole*. Závěrečná práce stud. prog. Učitelství pro základní školy. Jihočeská univerzita v Českých Budějovicích, České Budějovice, 2021. Dostupné z: <https://wstag.jcu.cz>
- [6] M. Prensky: *Digital Natives, Digital Immigrants*. On the Horizon. MCB University Press, Vol. 9 No. 5, October 2001. Dostupné z: www.marcprensky.com
- [7] J. Trgalová: *How to use dynamic geometry in a transformative way*. South Bohemia Mathematical Letters. Volume 29, No. 1, 2021, 77-86. Dostupné z: http://home.pf.jcu.cz/~sbml/wp-content/uploads/2021_Trgalova.pdf
- [8] D. T. Willingham: *Why don't students like school?* Second Edition. Jossey-Bass A Wiley Brand. 2021

Construction of interpolation B-spline curve for technical application

Marta Hlavová, Ivana Linkeová

Faculty of Mechanical Engineering, CTU in Prague

Karlovo nám. 13, 121 35 Prague 2, Czech Republic

email: marta.hlavova@fs.cvut.cz, ivana.linkeova@fs.cvut.cz

Abstract. Interpolating B-spline curve is a piecewise polynomial curve passing through a set of given definition points. In our case, the interpolation curve of the fifth degree is constructed to respect the unit normal vector at each definition point. Definition points and normal vectors are obtained by means of real measurement on a coordinate measuring machine.

Keywords: Interpolation, B-spline curve, NURBS, curve reconstruction

1 Introduction

According to the result requirements, curve reconstruction from a data point set is solved by interpolation or approximation methods [1]. In our case, input data was obtained by tactile measurement on freeform surface and the resulting curve is expected to pass through the measured points. This tactile measurement was performed on coordinate measuring machine (CMM) Zeiss Xenos and the result of this measurement contains not only the coordinates of points on the surface, but also the coordinates of the unit normal vectors of the surface at these points. The normal vector at each measured point defines the normal line and the tangent plane of the surface and gives an important information about the shape of the surface (and the curve on the surface) in the immediate neighbourhood of this point, fig. 1. This contribution is focused on the development of such interpolation curve that respects the given normal vectors as its principal normal vectors at the given points.

The paper is organized as follows. In section 2, the basic properties of clamped uniform B-spline curve are mentioned and the reasons for choosing the fifth degree of this curve are described. An example of such an interpolation curve and its construction is given in section 3. Section 4 summarizes the proposed interpolation method and suggests possible modifications of this procedure.

2 Interpolation B-spline curve

One specific subset of NURBS curves [2] consists of so-called clamped uniform B-spline curves [3], that are non-rational approximation curves given by control points. In this paper, uniform clamped B-spline curve of p -th degree is considered, as they are C^{p-1} continuous and it is possible

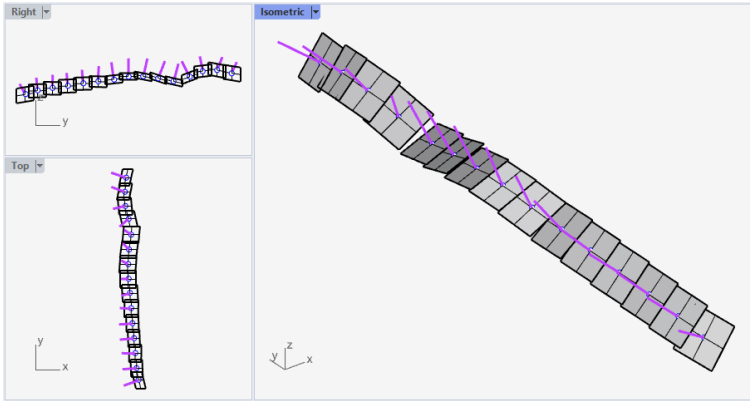


Fig. 1: Visualisation of measured points with normal lines and tangent planes

to decompose them into the Bézier segments [4], fig. 2. Consequently, these curves can be supposed as an interpolation B-spline curves, because they interpolate a set of their Bézier segment endpoints and fulfill the continuity condition. In our case, the points measured by CMM define the endpoints of Bézier segments (hereinafter referred as definition points) and a clamped B-spline curve that preserves the given normal vector at each definition point is constructed by means of decomposition of this interpolation B-spline curve into the simple Bézier segments.

Thus, for clamped uniform B-spline curve of degree p , ($p \geq 3$) given by n control points P_i , $i = 0, \dots, n-1$, ($n \geq p+1$), each Bézier segment k_j , $j = 0, \dots, n-p$ of decomposition is defined by $p+1$ control points V_i^j , $i = 0, \dots, p$. The relative position of each six neighboring control points

$$V_{p-2}^j, V_{p-1}^j, V_p^j, V_0^{j+1}, V_1^{j+1}, V_2^{j+1}$$

of two subsequent segments k^j and k^{j+1} , $j = 0, \dots, n-p-1$ is unambiguously given by C^2 continuity conditions

$$V_0^{j+1} = V_p^j, V_1^{j+1} = V_{p-1}^j + 2\overrightarrow{V_{p-1}^j V_p^j}, V_2^{j+1} = V_{p-2}^j + 4\overrightarrow{V_{p-1}^j V_p^j}.$$

Adding a condition of a given normal vector at point $V_p^j = V_0^{j+1}$ has a strong effect to location of control points V_{p-1}^j and V_1^{j+1} , because they define the tangent vector at this point and therefore they have to lay in tangent plane at endpoint. Hence, the degree p (and number $p+1$ of control points of each Bézier segment) plays a key role in the construction of this kind of interpolation curve.

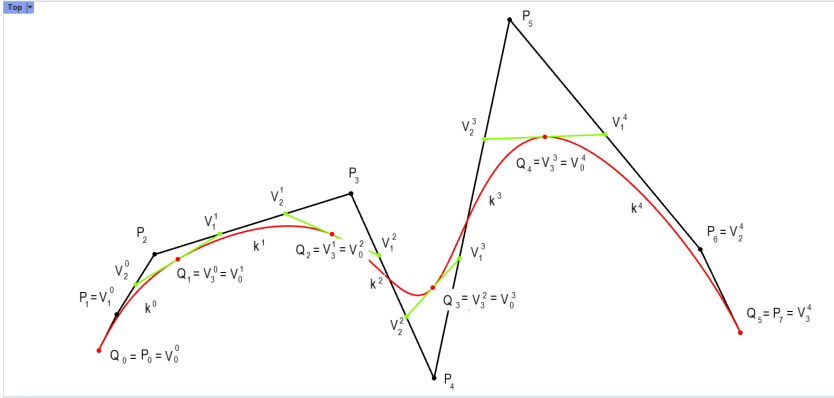


Fig. 2: Decomposition of clamped uniform B-spline cubic curve into Bézier cubic segments

2.1 Degree of interpolation curve

In case $p = 3$ (that is a minimum curve degree to ensure appropriate C^2 continuity), there is impossible to arrange control points of Bézier cubics to respect the given normal vectors, because the location of all control points is given by C^2 condition and is mutually dependent. This fact results not only from the properties of Bézier curves, but can also be derived from the system of equations for individual segments of the interpolation curve. The same result is reached for degree $p = 4$, when C^2 condition combined with additional condition of normal vectors causes an unsuitable connecting of all control points and therefore uncontrollable shape of curve.

Degree $p = 5$ leads to the interpolation B-spline curve composed of C^2 continuously joined Bézier quintic i.e of the fifth degree curves. Six control points for each segment is minimum amount to preserve the given normal vectors and to prevent unwanted dependence of positions of all control points. On the other hand, this amount allows variability of interpolation curve and gives possibilities to modify the shape of the result curve. In the following section, an example of construction of quintic interpolation B-spline curve is described.

3 Quintic Interpolation B-spline curve

To define a quintic interpolation B-spline curve that passes through m , ($m \geq 2$) measured points Q_j , $j = 0, \dots, m - 1$ and satisfies the normal vector condition, the location of the control points V_4^j and V_1^{j+1} of two

neighboring segments k^j and k^{j+1} , $j = 0, \dots, m-2$ is not clearly given. There is only one condition to be preserved: these points have to be placed in tangent plane of surface (at point $Q_j = V_5^{j-1} = V_0^j$, $j = 1, \dots, m-2$).

3.1 Example

In neighboring of inner definition points Q_j , $j = 1, \dots, m-2$, points V_4^j , V_1^{j+1} are arranged on perpendicular projection of line $Q_{j-1}Q_{j+1}$ to this tangent plane and satisfy

$$|V_4^j Q_j| = |Q_j V_1^{j+1}| = \frac{1}{5} \left(\frac{|Q_{j-1}Q_j| + |Q_j Q_{j+1}|}{2} \right).$$

Control points V_3^j and V_2^{j+1} are located on the same line as points V_4^j and V_1^{j+1} in tangent plane at Q_j point,

$$|V_3^j Q_j| = |Q_j V_2^{j+1}| = 2 |V_4^j Q_j| = 2 |Q_j V_1^{j+1}|.$$

In fig. 3, orange tangent plane at inner definition point, light green perpendicular projection of green dotted line connecting two neighboring definition points and red resulting control points of two consequent Bézier segments are shown.

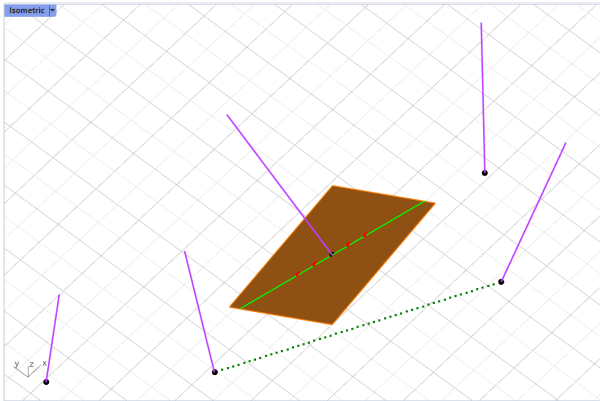


Fig. 3: Control points of interpolation quintic curve segments near the inner definition point

The remaining control points of two outer segments k^0 and k^{m-2} are constructed as follows: Control points V_1^0 and V_2^0 are located on the perpendicular projection of line Q_0Q_1 to the tangent plane at point Q_0 ,

$$|Q_0 V_1^0| = \frac{1}{5} |Q_0 Q_1|, \quad |Q_0 V_2^0| = 2 |Q_0 V_1^0|.$$

Control points V_3^{m-2} and V_4^{m-2} are located on the perpendicular projection of line $Q_{m-2}Q_{m-1}$ to the tangent plane at point Q_{m-1} ,

$$|V_4^{m-2}Q_{m-1}| = \frac{1}{5} |Q_{m-2}Q_{m-1}|, |V_3^{m-2}| = 2 |V_4^{m-2}Q_{m-1}|.$$

In fig. 4, all control points and the resulting interpolation curve are performed.

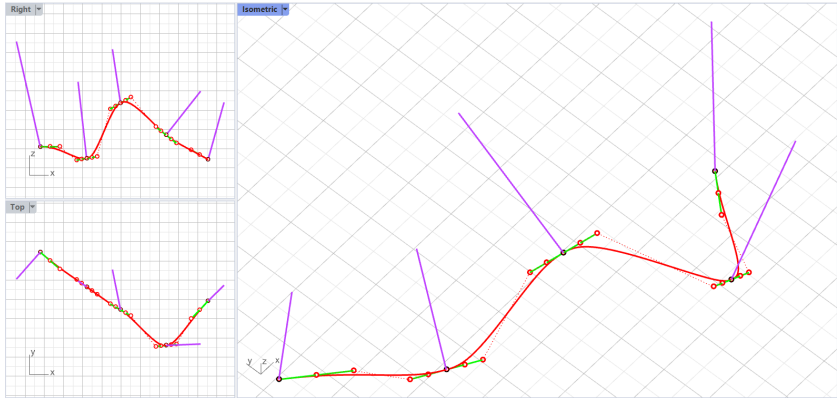


Fig. 4: Example of interpolation B-spline curve (red) of the fifth degree preserving the given normals (purple)

3.2 Shape modification

In a neighborhood of the each inner definition point Q_j , the shape of interpolation curve can be easily modified by a change of location of four control points V_3^j, V_4^j, V_1^{j+1} and V_2^{j+1} . There are an infinite number of ways to place the first pair V_4^j, V_1^{j+1} . Points can be arranged on another line in tangent plane or their distance from definition point $Q_j = V_3^j = V_0^{j+1}$ can be defined differently from the previous model example. Different location of the second pair V_3^j, V_2^{j+1} (not only in tangent plane) allows another possibility of curve shape modification. These changes can be variably applied to any number of definition points and the property of normal vectors will be preserved, fig. 5.

4 Conclusion

The proposed interpolation method using B-spline quintic curve is based only on conditions of C^2 continuous joining of two Bézier curves of the fifth degree. Due to the acceptance of additional condition of normal vectors, this curve can describe reality more accurately than the commonly used

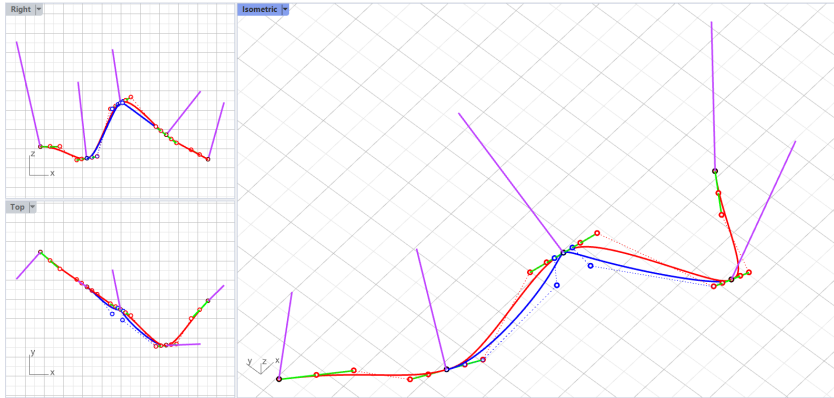


Fig. 5: Shape modification (blue) of interpolation curve (red) by another settings of control points (blue)

interpolation cubic curve because the shape of this curve can be easily modified. By means of extension to surfaces, this procedure of curve reconstruction can be applied to create a precise CAD model of measured surface that respects all irregularities. In metrology, such accurate model of surface can be used as digital twin (calibrated CAD model) of measured freeform surface.

Acknowledgements

This work was supported by the Student Grant Competition of the Czech Technical University in Prague, grant Applications of mathematical-geometric modelling in mechanical engineering SGS21/148/OHK2/3T/12.

References

- [1] D. Salomon: *Computer Graphics and Geometric Modeling*, Springer New York, NY, 1999
- [2] L. Piegl, W. Tiller: *The NURBS Book*, Monographs in Visual Communications. Springer, Berlin, 1997
- [3] G. Farin: *Curves and Surfaces for CAGD: A practical Guide*, The Morgan Kaufmann Series in Computer Graphics, 2002
- [4] M. J. Borden, M. A. Scott, J. A. Evans, T. J. R. Hughes: *Isogeometric finite element data structures based on Bézier extraction of NURBS*, International Journal for Numerical Methods in Engineering 2011, vol. 87, pp. 15-47

Modern technologies in teaching geometry

Michaela Holešová

*Dept. of Structural Mechanics and Applied Mathematics, Faculty of Civil Engineering
University of Žilina, Univerzitná 8215/1, 010 26 Žilina, Slovak Republic*

email: michaela.holesova@uniza.sk

Abstract. Currently, owing to the situation where the use of ICT technologies is necessary, there is a need for materials and methods suitable for such a form of teaching. It is also attractive for students when modern technologies are used in teaching. In the paper, we deal with support means for improving the teaching of geometry and mathematics, not only through additional and extended study materials available through the computer, but also through virtual reality.

Key words: Geometric model, mathematical terminology, corpus, virtual reality

1 Introduction

Geometry should be an essential part of mathematics in education. However, we are observing the opposite trend, geometry is gradually disappearing from mathematics lessons. It's not okay. Geometry is precise and exact science. It is an integral part not only of the scientific and technical world but also of art, sociology, archaeology, biology and even sports. Its applications point to the fact that without it we would often fail to solve simple life situations.

That's why we try to make the teaching of geometry and mathematics more attractive for students by using modern technologies. More and more often, we encounter the fact that if students can use e.g. computer, tablet, virtual reality glasses, or even a mobile phone, so teaching is more interesting and attractive for them. In addition, we should not forget that the correct use of terminology is part of knowledge and it is very important. By creating online dictionaries, suitable corpus and search engine on top of it, it is appropriate to supplement study materials that are also sufficiently accessible to students.

2 Materials and technologies in teaching geometry

New study materials are constantly being created that meet the specific requirements of the present time. More and more people are moving towards the online environment. It is certainly correct to use modern technologies in teaching. Possibilities of additional and extended study materials in the teaching of geometry and mathematics could be divided into the following categories :

- Classic texts – scripts, books, workbooks, etc.
- Electronic texts - digitized educational texts, various online dictionaries, corpuses, etc.

- Real models – paper, wooden, wire, plastic, etc.
- Virtual models - anaglyphs, virtual reality (VR), augmented reality (AR)

We will focus on those we can meet in the online environment. And that with a focus on terminology and the use of virtual reality in teaching.

2.1 Electronic texts

There are many digitized teaching texts, various tasks and topics processed, for example, in the software GeoGebra. However, online terminological dictionaries from geometry or mathematics are absent. Using correct terminology is an inherent part of the mathematical language. Terminological enrichment and expansion of mathematical vocabulary present a permanent process in which some words disappear from the vocabulary, others – new ones – become the part of it.

Within the project KEGA č. 019ŽU-4/2020 The modern approaching and implementation of mathematical terminology for students of technical universities, a database of terms is created with a focus on technical universities. (See [1]). This database will be added to the terminological portal of the Institute of Linguistics of Ľudovíta Štúra of Slovak Academy of Sciences in Bratislava, which is published on the webpage [6], see Fig. 1, Fig. 2. Was made available in 2016 and supported by the Scientific Grant Agency of the Ministry of Education and Culture of the Slovak Republic as part of project no. 2/0114/15. Further development of the portal is ensured by the department of the Slovak National Corpus JÚĽŠ SAV, within the framework of the Agreement on pooling funds for the creation and development of the Slovak National Corpus no. 0323/2017.

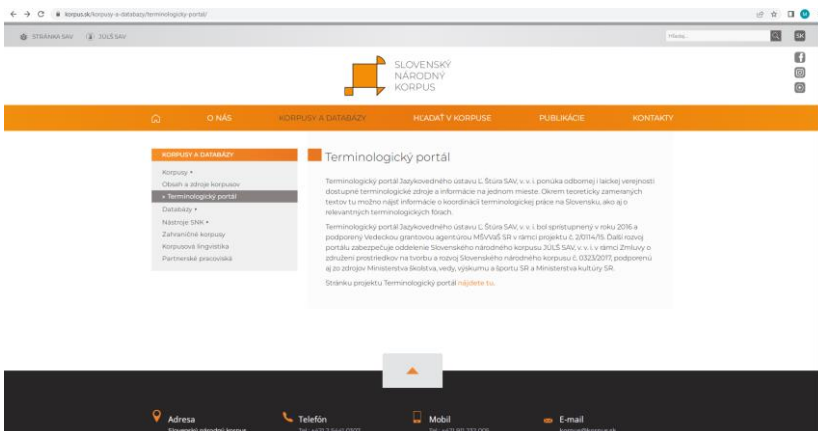


Fig. 1: Terminological portal in [6]

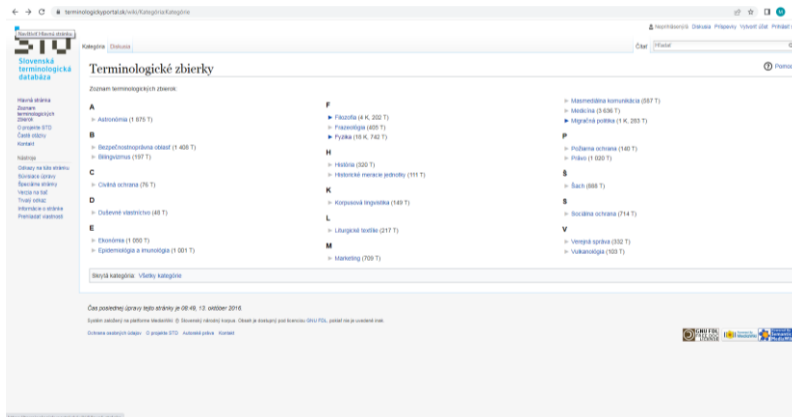


Fig. 2: Terminological collections in [6]

The terms are defined according to relevant sources, the following attributes are given for each term: name of term, area, definition, source of definition, related terms, foreign language equivalent. Synonym and note are optional. See Fig.3. Terms from geometry will be included in the field of mathematics.

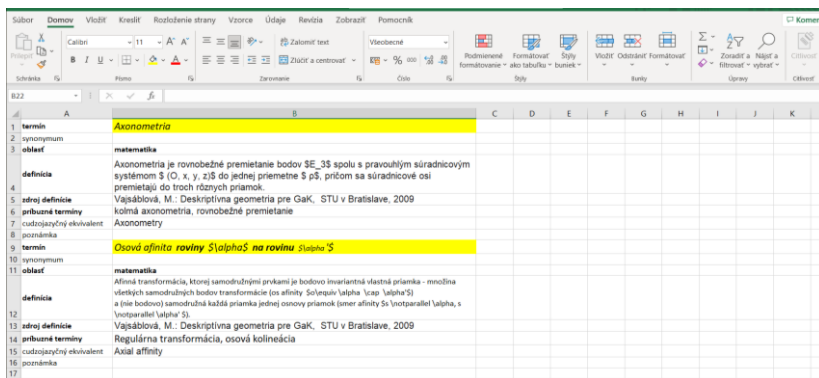


Fig. 3: Terminological database in Excel

2.2 Virtual models

More and more often we come across the fact that it is the virtual world and the models associated with it that are attractive to students. Among the oldest is Anaglyph, which uses the distribution of images for the left and right eye into color components red and green. (See Fig. 4) Subsequently, the 3D model is created with the help of glasses. This method is again very popular and used

in teaching, as we can also see for example in [2]. The GeoGebra software also has an application for creating an anaglyph and this will make it much easier for us to prepare teaching materials.

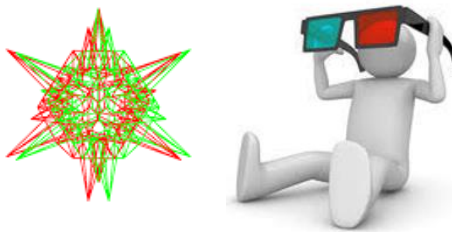


Fig. 4: Anaglyph

The terms virtual reality and augmented reality are quite often confused, even though they are different technologies. Virtual reality (VR) is an environment modeled by means of a computer simulating reality. In Fig. 5 is the model for conditional extremes of the function of two variables created in [5].

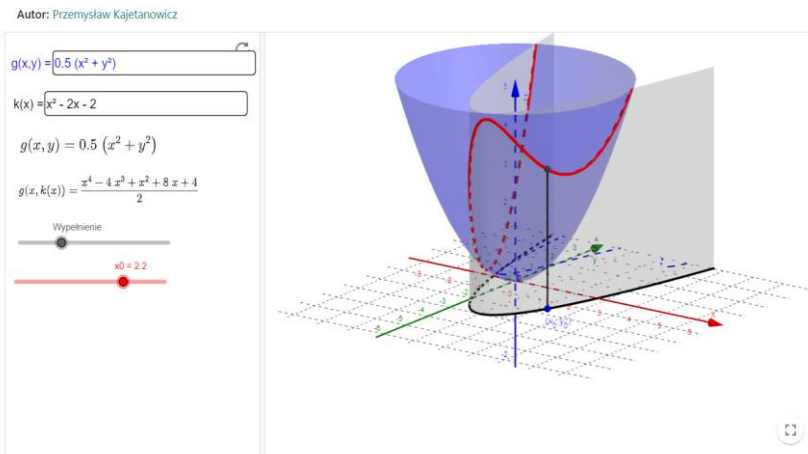


Fig. 5: Conditional extremes of the function of two variables (see [5])

Unlike this technology, augmented reality (AR) leaves a view of the real environment and synthetic 3D graphics are added (see [4]). In Fig. 6 is the model of intersection of two triangles added to the real world. GeoGebra implemented augmented reality in the applications GeoGebra AR and GeoGebra 3D.

Virtual reality enables learners to gain a different perception of the objects increasing their spatial abilities. In the specific case as the mathematics is,

the virtual reality allows to see abstract concepts in a three-dimensional environment which makes them easier to understand, apply.

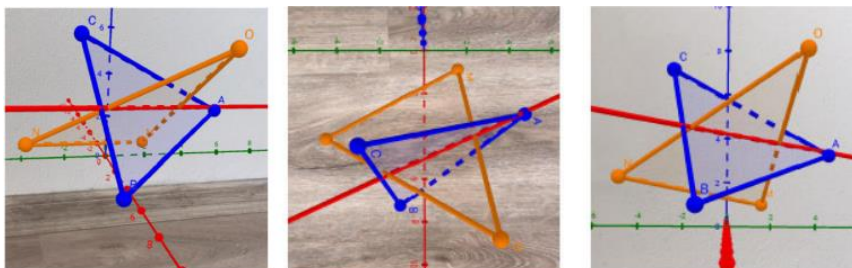


Fig. 6: Mapping of task in augmented reality – a general view, horizontal projection, vertical projection (see [3])

The priority of the international project Mathematical models for teaching three-dimensional geometry using virtual reality (Math3DgeoVR) is the creation 12 teaching modules, each one with a VR application developed for the topic. Cooperating universities are Politechnika Lodzka (the main coordinator), Uniwersytet Slaski – Poland, Universidade de Aveiro – Portugal, Tartu Ulikool – Estonia, University of Žilina – Slovakia.

The project is addressed to students and academics of all fields of engineering faculties. We believe that it will be possible to create teaching materials that will be sufficient for a wide range of students. The developed VR application is aimed at improving students' spatial thinking and correct understanding of geometric issues. The mathematics teaching program will be revised and adapted to the use of a virtual reality application in order to enable, through simulation and visualization, the strengthening and development of spatial imagination in geometry and enable students not only to achieve better study results, but also to better prepare them for practice.

3 Conclusion

The correct use of terminology is conditioned by a correct understanding of concepts. It is important that terms are used correctly even in the online environment, and that is why we believe that the addition of terminology from mathematics and geometry to the Terminology Portal of the Institute of Linguistics of Ludovíta Štúra of Slovak Academy of Sciences will help with this. Considering the overall situation of the society, it is obvious that we will not avoid modern technologies in teaching.

It's amazing to use all the possibilities, for example virtual reality, that technological development allows us. It will certainly be motivating for students and help them to understand some concepts, but we must not forget

that teacher-student interaction should not only be based on the virtual or online world.

Acknowledgements

This paper has been written with the support of Cultural and Educational Grant Agency of Slovak Ministry of Education, project: 019ŽU-4/2020.

The author has been supported of the Project financed under the Erasmus+ Programme, Key Action 2, Strategic Partnerships, project No.: 2021-1-PL01-KA220-HED-000030365.

References

- [1] B. Bačová, E. Leláková: *The modern approach to implementation of Slovak and English mathematical terms into university teaching/learning proces*, EDULEARN22, 14th annual International Conference on Education and New Learning Technologies, Palma de Mallorca, 4th - 6th of July, 2022, ISSN 2340-1117, Barcelona, IATED, 2022, ISBN 978-84-09-42484-9, pp. 2573-2578
- [2] V. Ferdianová: *Using anaglyphs in descriptive geometry*, 15th European Conference on e-Learning ECEL 2016, Proceedings of the 15th European Conference on e-Learning ECEL 2016 Praha, Academic Conferences and Publishing International Limited, ISBN 978-1-911218-17-3, pp. 194-200
- [3] V. Ferdianová, J. Poruba, M. Procházková: *Problem of using augmented reality in selected task in Monge projection*, EDULEARN22 Proceedings of 14th International Conference on Education and New Learning Technologies. 4-6 July, 2022, Palma, Spain, 2022, ISBN 978-84-09-42484-9, pp. 7183-7192
- [4] J. Pelikán: *Augmented reality with HoloLens*, Proceedings of the Slovak-Czech Conference on Geometry and Graphics: 27th symposium on Computer Geometry SCG 2018, 38th conference on geometry and graphics: Blansko, September 10-13, 2018, Slovak Chemistry Library, ISBN 978-80-8208-005-9, pp. 207-214
- [5] <https://www.geogebra.org/m/Zrpf3MCj>
- [6] <https://terminologickyportal.sk/wiki/Kateg%C3%B3ria:Kateg%C3%B3rie>

Examples in multiplicity theory

Pavel Chalmovianský

Department of algebra and geometry

Mlynská dolina, 842 48 Bratislava, Slovakia

email: pavel.chalmoviansky@fmph.uniba.sk

Abstract. We provide several examples playing an important role in the development of the intersection theory for algebraic varieties. The examples demonstrate a computational approach to the multiplicity by computation in Chow ring of a variety as well as importance of the additional approaches such as blowup when the direct computation in the ring needs to be enhanced.

Keywords: intersection theory, Chow ring, blowup

1 Introduction

Intersection is a fundamental construction in mathematics. Algebraic geometry is no exception. Using intersection, one separates objects of certain kind satisfying additional conditions. If the new conditions are independent with the previous ones, we get a proper subset. In algebraic geometry, the conditions are algebraic which means polynomial in some elements.

The intersection theory was formed throughout the whole history of the mathematics mainly as a system of particular approaches in particular situations. Famous calculus published by Hermann Cäsar Hannibal Schubert (1848–1911) was able to compute many complex enumerative tasks in projective spaces. It was still not on strong legs and to find its rigorous foundation was the 15th Hilbert’s problem at the beginning of the 20th century.

In order to achieve the goal, a multiplicity of an algebraic subvariety was required. It was provided by Jean-Pierre Serre (born 1926). Many approaches have been devised inbetween, applied to challenging problems also in other spaces, until Fulton (born 1939)-MacPherson (born 1944) published their approach approximately 40 years ago (see [5]). Several books appeared, dealing with intersection since then such as [4]. We follow some computations from this book.

We demonstrate the theory on several problems.

1. Let C, D be two smooth curves of degree d and genus g in $P^n(\mathbb{C})$. How many common chords do they have?
2. Lines (linear subspaces) on a subvariety in \mathbb{P}^n . Lines on a cubic surface in \mathbb{P}^3 . Lines on the intersection of two quadrics in \mathbb{P}^4 .
3. Steiner’s problem of five conics

2 Problem of common secants

The following problem is easy to understand in geometric as well as computational way. Therefore, it is very convenient to start with.

A *chord of a curve* is a line have at least two points in common with a curve (including limit cases such as tangent lines).

Problem: Let C, D be two smooth curves of degree d and genus g in $P^n(\mathbb{C})$. How many chords do they have in common?

A solution is given for $n = 3$. But in terms of Schubert cells, it can be computed in general.

Let $\mathbb{G}(1, n)$ be the set of all projective lines (1-dimensional subspaces) in n -dimensional projective space over \mathbb{C} . Each line corresponds to a point in $\mathbb{G}(1, n)$. We define $\psi_2(C) \subseteq \mathbb{G}(1, n)$ as a subset of all secants of the curve C . Let $\mathbf{p}, \mathbf{q} \in C$, $\mathbf{p} \neq \mathbf{q}$ and \mathbf{pq} be the line defined by them in $\psi_2(C)$. Consider the mapping $\tau: C \times C \rightarrow \mathbb{G}(1, n)$ defined so outside the diagonal. Take the algebraic closure of the image of the τ (e.g. all tangents of C are added). Clearly, (complex) dimension of the image is 2 – all lines passing through a point can be parameterized by points of the curve C (locally it is given by one parameter) and linearly parameterized by one more parameter.

The problem is now to find the set of elements and its structure in $\psi_2(C) \cap \psi_2(D)$.

The Grassmannian $\mathbb{G}(1, 3)$, formed by all lines in \mathbb{P}^3 , splits into several structural subsets.

Consider a fixed projective flag $V_0 \subset V_1 \subset V_2 \subset V_3$ in $P^3(\mathbb{C})$ and the following subsets of $\mathbb{G}(1, 3)$.

- All lines intersecting a fixed point V_0 denoted $\Sigma_{2,0}$.
- All lines intersecting a fixed point V_0 contained in a plane V_2 denoted $\Sigma_{2,1}$.
- All lines intersecting a fixed point V_0 contained in a line V_1 denoted $\Sigma_{2,2}$.
- All lines intersecting a fixed line V_1 denoted $\Sigma_{1,0}$.
- All lines intersecting a fixed line V_1 contained in a plane V_2 denoted $\Sigma_{1,1}$.
- All lines denoted $\Sigma_{0,0}$.

Since any flag can be rationally trasformed to the fixed flag above, the varieties $\Sigma_{a,b}$ represent classes in the Chow ring of $\mathbb{G}(1, 3)$. For $\Sigma_{a,b}$ its class is denoted $\sigma_{a,b}$. Hence, $\sigma_{a,b} = [\Sigma_{a,b}]$. The codimension of $\Sigma_{a,b}$ is $a + b$ in $\mathbb{G}(1, 3)$, which has dimension 4.

The classes $\sigma_{a,b}$ form a free base of the Chow ring of $\mathbb{G}(1, 3)$ as a \mathbb{Z} -module, i.e. with integer coefficients. The addition in the ring roughly

corresponds to a union of varieties. The multiplication in the ring corresponds to the operation of intersection of varieties.

For the sake of shorter notation $\sigma_a = \sigma_{a,0}$. The table of multiplication in the Chow ring of $\mathbb{G}(1, 3)$ is as follows.

$$\begin{aligned} \sigma_1^2 &= \sigma_{1,1} + \sigma_2, \\ \sigma_1\sigma_{1,1} &= \sigma_1\sigma_2 = \sigma_{2,1}, \\ \sigma_1\sigma_{2,1} &= \sigma_{2,2}, \\ \sigma_{1,1}^2 &= \sigma_2^2 = \sigma_{2,2}, \\ \sigma_{1,1}\sigma_2 &= 0. \end{aligned}$$

Let us come back to the computation of the chord problem. The set $\psi_2(C)$ has codimension 2. Hence, we have

$$[\psi_2(C)] = \alpha\sigma_2 + \beta\sigma_{1,1},$$

due to the codimension of these classes.

Multiplying the equation by $\sigma_{1,1}$ and taking degree, we have

$$\beta = \deg(\sigma_{1,1}[\psi_2(C)]) = \#\{\Sigma_{1,1} \cap \Psi_2(C)\} = \binom{d}{2},$$

since a generic curve of degree d has intersection with generic plane points $\mathbf{p}_1, \dots, \mathbf{p}_d$, they form β chords.

Multiplying the equation by σ_2 and taking degree, we have

$$\alpha = \deg(\sigma_2[\psi_2(C)]) = \#\{\Sigma_2 \cap \Psi_2(C)\} = \binom{d-1}{2} - g,$$

since the number of chords through a fixed point to C can be counted as the number of nodes of the projection $\pi: C \rightarrow P^2(\mathbb{C})$ through the fixed point, which has value α by a well known formula on counting singularities.

Hence, $\#\Psi_2(C)\Psi_2(D) = \deg(\sigma_2 + 3\sigma_{1,1})^2 = 10$ for twisted cubics.

3 Problem of lines on varieties

The set of lines on algebraic varieties is solved using Fano schemes (glued algebraic varieties). Fano scheme $F_k(X)$ contains all the k -dimensional subspaces on X . For lines, $k = 1$.

In order to use it, we find all varieties of certain degree d containing fixed line in \mathbb{P}^n . Let $N = \binom{n+d}{d} - 1$ be the dimension of the Veronese variety parameterizing all varieties of degree d in \mathbb{P}^n . Let

$$\Phi = \{(X, L) \in \mathbb{P}^N \times \mathbb{G}(1, n) : L \subseteq X\}. \tag{1}$$

There are natural projections from Φ to \mathbb{P}^N and $\mathbb{G}(1, n)$. The restriction of defining polynomial of the variety X on a line L is a polynomial of degree d . Over any line, a polynomial of degree d has $d + 1$ coefficients. Hence, the dimension of the set of polynomials of degree d over the line L is $N + 1 - (d + 1) - 1$. The dimension of the $\mathbb{G}(1, n)$ is $2(n - 1)$. Therefore, the dimension of Φ is

$$N + 1 - (d + 1) - 1 + 2(n - 1) = N + 2n - d - 3. \quad (2)$$

And we get that general hypersurface $X \subset \mathbb{P}^n$ of degree d does not contain any line if $2n - d - 3 < 0$.

For $n = 3$ and $d = 3$, we have a finite number of lines since the dimension of Φ given above is 0. The computation of $F_1(X)$ provides the result. The number of lines on a cubic surface is independent of cubic surface since any two are rationally equivalent. To compute the number, it is enough to use the Schubert calculus in a similar way to the previous example and Chern classes of the $\mathbb{G}(1, n)$. In particular on a generic cubic surface X in $P^3(\mathbb{C})$, there are exactly 27 lines.

4 Problem of lines in quadrics intersection

A similar problem is to find all lines in the intersection of quadrics, which is of degree 4 in general.

Problem: Compute the number of lines in the intersection of two generic quadrics in \mathbb{P}^4 .

Using $F_1(X)$ for a generic quadric $X \subset \mathbb{P}^4$ and computing $[F_1(X)]^2$ in $\mathbb{G}(1, 4)$ with a fixed projective flag $V_0 \subset V_1 \subset V_2 \subset V_3 \subset V_4$, $n = 4$ and $d = 2$, we get from the computation of the previous example that

$$\dim F_1(X) = 2 \cdot 4 - 2 - 3 = 3, \dim \mathbb{G}(1, 4) = 6.$$

There are two Schubert cells of codim 3 in $\mathbb{G}(1, 4)$. They are σ_3 (all lines through a fixed point) and $\sigma_{2,1}$ (all lines meeting a fixed line in a fixed hyperplane) with the Chow ring multiplicative relations

$$\sigma_3 \sigma_{2,1} = 0, \sigma_3^2 = \sigma_{2,1}^2 = 1.$$

Hence, $[F_1(X)] = a\sigma_3 + b\sigma_{2,1}$. Using the above relations, this leads to the $a = [F_1(X)]\sigma_3 = 0$ (a generic point is not on a quadric), hence $a = 0$ and $b = [F_1(X)]\sigma_{2,1} = 4$ which is the number of (complex) lines passing through two points $V_1 \cap (X \cap V_3)$. Two lines pass through each such point. Hence $[F_1(X)]^2 = 16$.

5 Problem of five conics

This problem is famous also as the Steiner's problem of five conics. Its solution requires a bit of attention due to obvious singular solutions which should not be counted. They are also called excess of the intersection.

Problem: Given five regular conics in general position in \mathbb{P}^2 . Find all non-singular conics tangent to all of them.

A conic in \mathbb{P}^2 is described as a zero set $Z(F)$ of a quadratic polynomial $F(x, y, z) = ax^2 + bxy^2 + cy^2 + dxz + eyz + fz^2$, uniquely upto a non-zero multiple. Hence, the space of all conics in the projective plane is $\mathcal{Q} = \mathbb{P}^5$.

We start with forming conditions of being tangent to a conic. All conics $Z(F)$ containing a point $\mathbf{p} \in \mathbb{P}^2$ satisfy a linear condition in a, b, c, d, e, f ., hence they form a hyperplane $H_{\mathbf{p}}$ in \mathcal{Q} .

All conics $Z(F)$ tangent to a line $L \subset \mathbb{P}^2$ satisfy a quadratic condition, hence form a quadric H_L in \mathcal{Q} .

All conics $Z(F)$ tangent to a regular quadric $Q \subset \mathbb{P}^2$ satisfy a condition of degree 6, hence form a hypersurface H_Q in \mathcal{Q} .

Jacob Steiner (1796-1863) gave a wrong solution $6^5 = 7776$ to the problem above coming from intersecting $H_{Q_1} \cap \dots \cap H_{Q_5}$ for five conics Q_1, \dots, Q_5 . This number includes also double-line singular conics which are tangent to all conics and in general they should be avoided in the correct answer. How to achieve this?

The double-lines in \mathbb{P}^2 form a Veronese surface V in \mathcal{Q} , which can be seen from the mapping

$$(Ax + By + Cz)^2 \mapsto (A^2 : AB : AC : B^2 : BC : C^2).$$

Using blowup $\text{Bl}_V \mathbb{P}^5$, we extend the space of conics with exceptional divisor (hypersurface) E over the non-reduced conics. Taking the intersection in the extended space provides the correct answer. However, we need to compute in the Chow ring of the extended space $\text{Bl}_V \mathbb{P}^5$.

The Steiner's problem requires the intersection of the strict transforms \tilde{H}_{Q_i} of H_{Q_i} in the blowup. They do not contain all double-lines, just those required by the closure of the strict transforms.

A hyperplane H in \mathcal{Q} blows up to a hypersurface \tilde{H} . Using classes in the Chow rings, $[H]$ maps to $[\tilde{H}]$. A hypersurface of degree d in \mathcal{Q} that does not contain V , maps in blowup to $d[\tilde{H}]$ in the same way. A hypersurface of degree d containing V maps to $d[\tilde{H}] - n[E]$, where n depends on the order of vanishing of the hypersurface along the Veronese surface V representing non-reduced conics.

Now, one has to compute that

$$[\tilde{H}_{\mathbf{p}}] = [\tilde{H}], [\tilde{H}_L] = 2[\tilde{H}] - [E] \text{ and } [\tilde{H}_Q] = 6[\tilde{H}] - 2[E].$$

When computing $[\tilde{H}_Q]^5$, we need to know the result of several subproblems

$$[\tilde{H}_{\mathbf{p}}]^5 = 1, [\tilde{H}_{\mathbf{p}}]^4[\tilde{H}_L] = 2, [\tilde{H}_{\mathbf{p}}]^3[\tilde{H}_L]^2 = 4.$$

And using duality, we get

$$[\tilde{H}_{\mathbf{p}}]^2[\tilde{H}_L]^3 = 4, [\tilde{H}_{\mathbf{p}}]^1[\tilde{H}_L]^4 = 2, [\tilde{H}_L]^5 = 1.$$

Finally, $[\tilde{H}_Q]^5 = (2[\tilde{H}_P] + 2[\tilde{H}_L])^5 = 3264$.

There are technical detail which should be written in several more pages. But I believe that giving the overview of the solution helps to clarify what is going on in the computation.

6 Future work

We are working on multiplicity decomposition and its geometric interpretation [1],[3]. We are looking for known tools and methods. We plan to study more structures in algebraic geometry, especially for low-dimensional objects. We learn more about Chow rings of particular algebraic varieties. Not much is known. We relate the structures with the result of Schenzel and Bođa on local intersection multiplicity [2] and find the geometric interpretation of them as was already partially done in the dissertation thesis of A. Bosáková recently.

Acknowledgement

This work was supported by the grant VEGA 1/0596/21.

References

- [1] A. Bosáková, P. Chalmovianský: *A Note on Local Intersection Multiplicity of Two Plane Curves. Lecture Notes on Data Engineering and Communications Technologies*, 146:175 – 184, 2023
- [2] E. Bođa, P. Schenzel: *Local Bezout estimates and multiplicities of parameter and primary ideals. Journal of Algebra*, 488:42 – 65, 2017
- [3] J. Chalmovianská, P. Chalmovianský: *Computing Local Intersection Multiplicity of Plane Curves via Max-order Basis. GJM*, 7(1):1–9, 2022
- [4] D. Eisenbud, J. Harris: *3264 and all that—a second course in algebraic geometry*. Cambridge University Press, Cambridge, 2016
- [5] W. Fulton: *Intersection theory*, volume 2. Springer-Verlag, Berlin, second edition, 1998

3D Modelling of Geometry Surfaces for the Education of Future Architects

Dana Kolářová, Stanislava Čecháková

*Dept. of load-bearing structures, Fac. of Architecture, Czech Technical University
Thákurova 9, 166 34 Prague 6, Czech Republic
email: kolarova@fa.cvut.cz, cecaksta@fa.cvut.cz*

Abstract. This article is focused on the use of models in architecture, shows the different use of models in the teaching and in the practice of the architect, different processing possibilities and on examples demonstrates the use of modern technologies in the creation of models through 3d printing and interactive computer models in GeoGebra.

Key words: architecture, physical models, digital models, skew arch, relief

1 Introduction

Models play an important role in the education of future architects. They are an integral part of working with space, for both design and construction.

Their importance has been known since ancient times when Marcus Vitruvius Pollio (Roman engineer and architect) mentioned in „the Tenth Book of De architectura” the advantages and disadvantages of both small-scale and full-scale models. [6].

Since the Renaissance period we have been able to observe a noticeable increase in the use of models in architecture and engineering. These models have had different functions, mainly to support and realize the imagination of the new building and were used as 3D drawings, but at the same time their goal was also to educate. There are existing documents concerning important public competitions where competitors had to explain technical solutions with their models. A model of the Rialto Bridge from Venice can be found in the archives of Grunsberg Castle (Germany) which has evidence of a technology transfer.

Even nowadays the role of a model is irreplaceable in engineering design and construction but the processing technologies have changed, we can use laser cutting, 3D printing, CAD modelling. More details about past, current and future use of physical models in engineering design is published in B. Addis book “Physical models” [2].

The major importance of models in the job of an architect is undeniable. We distinguish two approaches in the use of models in the teaching of descriptive geometry: first, we explain spatial relationships (primarily in the chapter surfaces in engineering design); and second, we teach students how to create models for the presentation of their own designs.

2 Models in the Educational Process of Future Architects

The first collection of geometrical educational models was presumably created by Théodore Olivier (1793–1853). He was a former student of Gaspar Monge. He taught descriptive geometry (in France, Sweden) and designed many models to teach and demonstrate descriptive geometry, some of which are movable (string models of ruled surfaces). Collections of his models can be found for example in The Canada Science and Technology Museum (Ottawa) or in The Mandeville Gallery, Union College (New York), and in Europe at the Museum of ISEP (Porto).

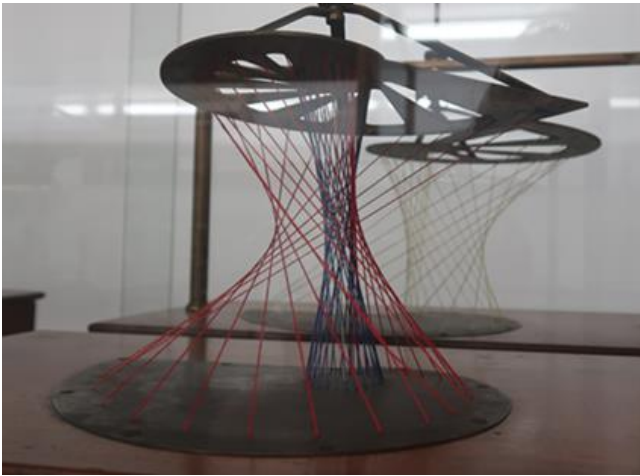


Fig. 1: The Olivier String model in the Museum of ISEP, Porto (photo DK)

Also, at the Faculty of Architecture at CTU in Prague, physical models or pictures are used to support the theoretical lectures of descriptive geometry. Historical models are not preserved at the faculty, so most of physical models we work with have been created in this century.

Another possibility to illustrate spacial solutions is to show our own photos of models from other universities or use materials from DAMM, the Digital Archive of Mathematical Models, which is a free and open research infrastructure offered by the TU in Dresden. It provides access to a growing number of collections worldwide (<https://mathematical-models.org>).

Changes in society, new technologies and new economic conditions bring new challenges. We can create interactive models with GeoGebra software, and can use 3D printing to create new models. The importance of them have not changed.

So, I would like to introduce our models to you: first an interactive model of a warped ruled surface in GeoGebra, secondly a construction of a relief and its 3D print.

2.1 The Skew Arch – GeoGebra Model

GeoGebra software is used at FA CTU Prague for teaching parametrisation of curves and surfaces. A skew arch as a warped ruled surface could be difficult for students, so it is necessary to find the easiest location of the directrix.

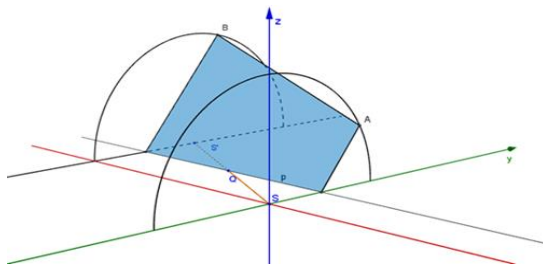


Fig. 2: The Skew Arch - directrix

Using an appropriate choice of location of directrix and points A, B on them we received these coordinates for points:

$$A[0; r\cos(t); r\sin(t)], t \in \langle 0; \pi \rangle$$

B

Consequently, we can find proper equations of the skew arch:

$$pl(t, s) = \left\{ \left[-ls; r\cos(t) - sr \frac{(2\cos(t)-1)^2}{4\cos(t)-5}; r\sin(t) - s2r\sin(t) \frac{2\cos(t)-1}{4\cos(t)-5} \right], \right. \\ \left. t \in \langle 0; \pi \rangle, s \in \langle 0; 1 \rangle \right\}$$

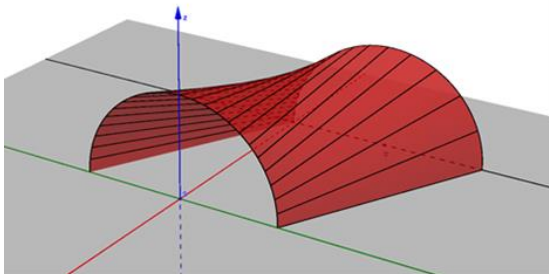


Fig. 3: The Skew Arch - surface

Digital model is available on <https://www.geogebra.org/m/tejcgjtj>.

2.2 Relief – 3D Print Models

During the summer semester of the school year 2021/22 students of the first year had to model a relief using CAD and then 3D print. They could choose their favourite building for it. They were given the freedom of deciding upon their own approach to the construction of relief perspective. We used three main types – affine relief, bas-relief, classical relief.

Thanks to the ability to create the relief in CAD (mostly we use ArchiCAD) and then use 3D printing, the relief can be submitted to the school, a classic solution with using plaster models is now technically impossible to realise as there are such a high number of students.

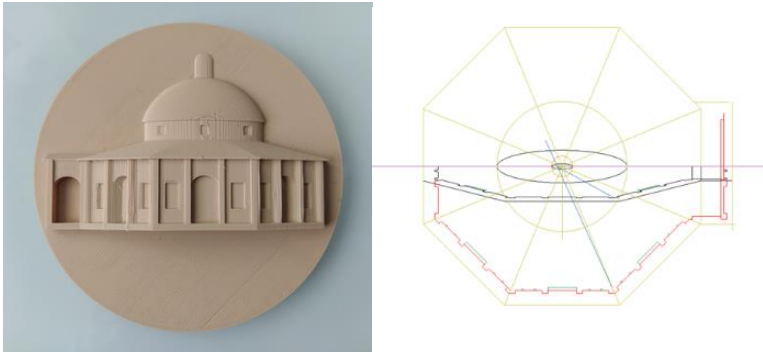


Fig. 4: Affine relief – model of garden house in Kroměříž made by student Táborská

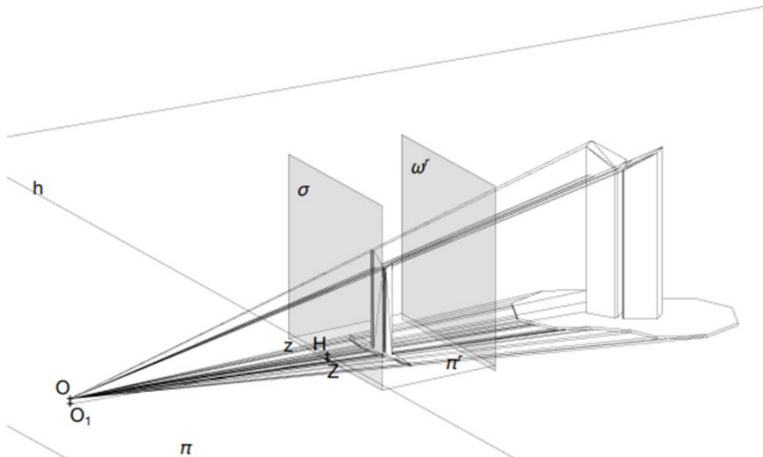


Fig. 5: Relief – CAD model of ventilation towers of Prague metro made by student Votíková

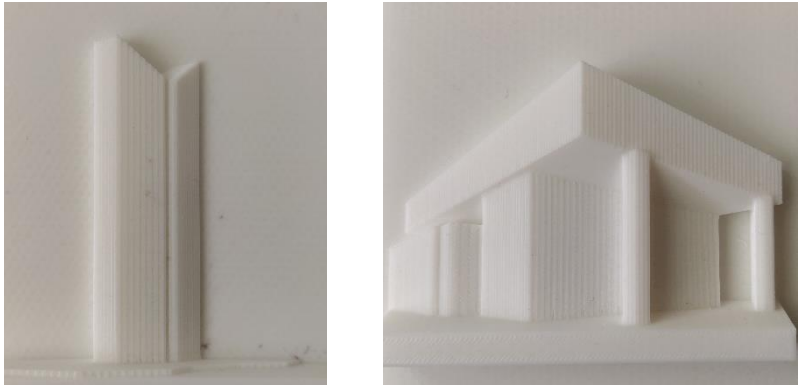


Fig. 6: Relief – 3D print models made by students Votíková and Vu

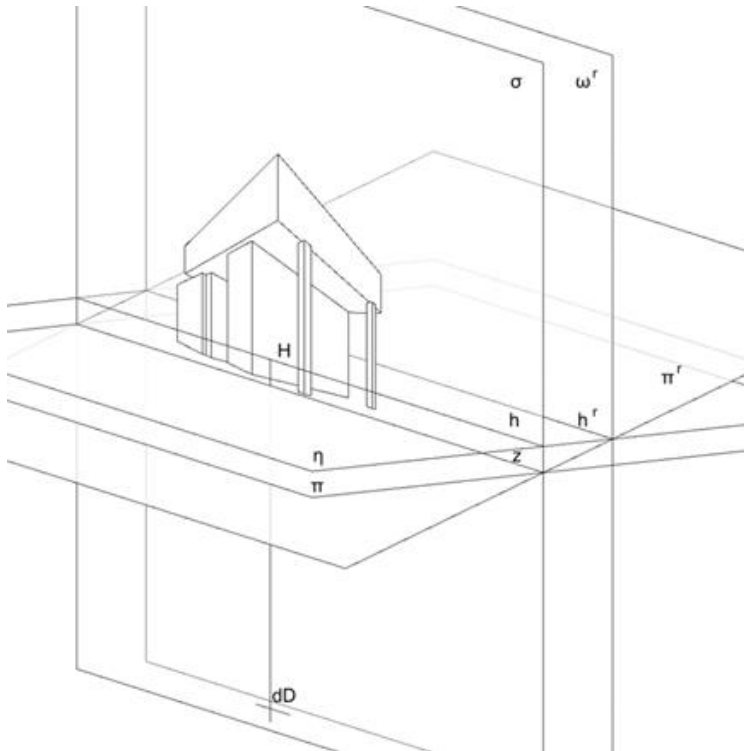


Fig. 7: Relief – CAD model of New building of National Museum Prague made by student Vu

3 Conclusion

Methods of modelling have changed, the meaning for the education of future architects remains. Physical models should be replaced by digital ones. 3D printing and modelling with GeoGebra software could bring new possibilities and great advantage – sharing.

Acknowledgements

This work was supported by the Grant of the Faculty of Architecture of the Czech Technical University in Prague, grant No. 105/1052207E001

References

- [1] B. Addis: *Past, current and future use of physical models in civil engineering design*. ICE-Proceedings-Civil-Engineering-1751-7672. <https://doi.org/http://dx.doi.org/10.1680/jcien.20.00028>
- [2] B. Addis, ed.: *Physical Models: Their historical and current use in civil and building engineering design*. Berlin: Ernst & Sohn, Verlag fur Architektur und technische Wissenschaften GmbH & Co., 2021
- [3] G. Amuroso: *The Reliéf - Perspectives of Bitonti and Borromini: Design and Representation of the Illusory Space*. In *Handbook of Research on Visual Computing and Emerging Geometrical Design Tools*, 420-454. Hershey, PA, USA: IGI Global, 2016
- [4] J. M. Hervé: *Théodore Olivier (1793–1853)*. In *History of Mechanism and Machine Science* 1st ed., 295-318. Dordrecht: Springer Netherlands. https://doi.org/10.1007/978-1-4020-6366-4_13, 2007
- [5] F. Kadeřávek: *Prostorová perspektiva a reliefy*. Praha: NČAV, 1954.
- [6] P. M. Vitruvius: *Deset knih o architektuře*. 3. vyd. Antická knihovna (Arista: Baset): Baset). Praha: Arista, 2001
- [7] J. P. Xavier: *On the Biais Passé: The Olivier String Model and the Representation of Constructive Solutions for the Skew Arch*. In *Handbook of Research on Visual Computing and Emerging Geometrical Design Tools* 1st ed., 337-366. Italy: Politecnico di Milano, 2016

Parametrizace parabolického konoidu a jeho zobrazení v programech GeoGebra a Maple

Parametrization of the parabolic conoid and its display in GeoGebra and Maple programs

Alice Králová

*Ústav matematiky LDF Mendelovy univerzity v Brně
Zemědělská 3, 613 00 Brno, Česká republika
email: alice.kralova@mendelu.cz*

Abstract. In this paper deduction of parametric equations of a parabolic conoid is presented. This allows to create a graphical representation of this surface in the GeoGebra and Maple graphics programs.

Keywords: parabolic conoid, warped surface, parametrization, GeoGebra, Maple.

Klíčová slova: parabolický konoid, zborcená plocha, parametrizace, GeoGebra, Maple.

1 Úvod

Tento příspěvek předkládá návod, jak lze zobrazit plochu technické praxe, konkrétně parabolického konoidu, jejím prostorovým modelem v programech GeoGebra a Maple na základě stanovení její parametrizace. Porovnáme náročnost práce v těchto programech a kvalitu jejich grafických výstupů.

2 Parabolický konoid jako plocha technické praxe

Parabolický konoid patří mezi tzv. *zborcené plochy*, které jsou tvořeny množinou přímek protínajících tři pevně dané řídicí křivky. Jsou-li dvěma řídicími křivkami přímky, jedna vlastní a druhá nevlastní, nazýváme zborcenou plochu *konoidem*. Nevlastní přímka je zadána řídicí rovinou, s níž jsou tvořící přímky konoidu rovnoběžné. Konkrétní zadání řídicích křivek parabolického konoidu je následující

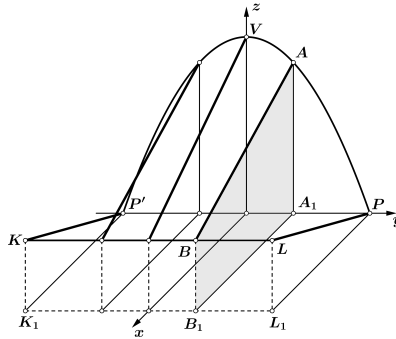
- parabola \mathcal{P} v rovině $\mu = (y, z)$ s osou v ose z a vrcholem $V[0; 0; 10]$ procházející bodem $P[0; 7; 0]$,
- přímka $l = \leftrightarrow KL$ rovnoběžná s osou y , kde $K[12; -7; 4]$ a $L[12; 7; 4]$,
- nevlastní přímka řídicí roviny $\nu = (x, z)$.

Ze zadání plyne rovnice paraboly $\mathcal{P} : z = -\frac{10}{49}y^2 + 10$ a parametrizace úsečky $KL : x = 12, y = k, z = 4$, kde $k \in \langle -7; 7 \rangle$.

Tvořící přímku $p = \leftrightarrow AB$ parabolického konoidu rovnoběžnou s řídicí rovinou ν určíme body $A \in \mathcal{P}$ a $B \in l$. Zobrazíme pouze část plochy konoidu omezené úsekem paraboly \mathcal{P} nad osou y a úsečkou KL , čímž se rozsah na hodnoty na ose y zmenší na interval $\langle -7; 7 \rangle$.

Ze vztahu $M = A + q \cdot \overrightarrow{AB}$ pro obecný bod M úsečky AB plynou parametrické rovnice uvažované části parabolického konoidu \mathcal{K} ve tvaru

$$\mathcal{K} = \left(12q, k, \frac{10}{49} k^2 (q - 1) + 10 - 6q \right), \text{ kde } q \in \langle 0; 1 \rangle, k \in \langle -7; 7 \rangle.$$



Obr. 1: Konstrukce tvořících přímek parabolického konoidu

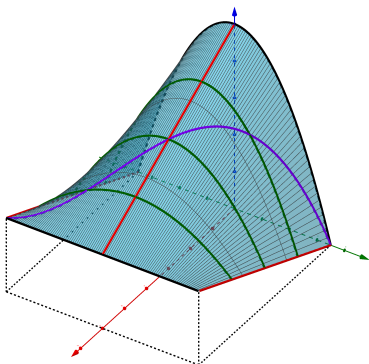
Názorné zachycení tvaru plochy lze získat pomocí řezů vhodně zvolenými rovinami. Roviny rovnoběžné s bokorysnou μ s rovnicí $x = d$, $d \in \langle 0; 12 \rangle$, protínají konoid v parabolách $\mathcal{Q}(y) = (d, y, \frac{5d-60}{294} y^2 + 10 - \frac{d}{2})$, kde $y \in \langle -7; 7 \rangle$. Rovina σ kolmá k půdorysně π procházející body K a P o rovnici $y = 7 - \frac{7}{6}x$ protíná konoid v obecné křivce 3. stupně $\mathcal{C}(q) = (12q, 7 - 14q, 40q^3 - 80q^2 + 44q)$, kde $q \in \langle 0; 1 \rangle$.

2.1 Vizualizace parabolického konoidu v GeoGebře

Vzhledem k tomu, že zadávání příkazů z příkazového řádku v GeoGebře je do značné míry intuitivní, zatímco při práci v Maplu je třeba znát přesnou syntaxi užitých příkazů a striktně ji dodržovat, je užití GeoGebry podstatně jednodušší než užití Maplu. Rovněž grafické výstupy vypadají v GeoGebře lépe než v Maplu verze 11. Na druhé straně při zadávání parametrizace plochy je v GeoGebře třeba, aby oba užití parametry byly omezeny pevnými reálnými hodnotami, protože GeoGebra neakceptuje funkcionální závislost jednoho parametru na druhém. Toto lze považovat za výrazný nedostatek při zobrazování ploch v GeoGebře, který se v Maplu nevyskytuje.

V GeoGebře v nabídce zvolíme Grafický náhled 3D a příkazy zapisujeme do příkazového řádku. Konoid zobrazíme příkazem `Plocha(12q, k, 10/49 k^2(q-1)+10-6q, q, 0, 1, k, -7, 7)`. Vykreslení požadovaných křivek na konoidu provedeme příkazem `Krivka`, například konkrét-

ně příkazem $\text{Krivka}(6, k, -5/49 k^2 + 7, k, -7, 7)$ vykreslíme parabolický řez konoidu v rovině $x = 6$.



Obr. 2: Zobrazení parabolického konoidu v GeoGebře

Názornější představu konoidu lze získat animací, v níž se po konoidu pohybují jeho tvořící úsečky a parabolické řezy. K tomu je třeba zadat dva posuvníky, jež nazveme pos1 s rozsahem od -7 do 7 pro úsečky a pos2 s rozsahem mezi 0 a 1 pro paraboly. Pohyb křivek po konoidu pak generují příkazy $\text{Krivka}(12q, \text{pos1}, 10/49 * \text{pos1}^2 * (q - 1) + 10 - 6q, q, 0, 1)$ a $\text{Krivka}(12 * \text{pos2}, k, 10/49 k^2 * (\text{pos2} - 1) + 10 - 6 * \text{pos2}, k, -7, 7)$.

Abychom dosáhli synchronizace, při níž úsečky i paraboly „proběhnou“ po konoidu za stejně dlouhou dobu, tedy při současném spuštění posuvníků se ukazatelé dostanou z počáteční polohy na konec ve stejném okamžiku, je třeba posuvníky vhodně nastavit. Na obou posuvnících musí být nastavena stejná rychlost animace a musí se shodovat počet vykreslovaných křivek. Budeme-li uvažovat 100 dílčích poloh vykreslovaných křivek, nastavíme na posuvníku pos1 délku kroku na hodnotu $0,14$ a na posuvníku pos2 délku kroku $0,01$.

Případně by bylo možné zajistit souběžný pohyb tvořících úseček a parabolických řezů po konoidu jediným posuvníkem pos . Tomu je třeba přizpůsobit nastavení proměnných q a k . Bude-li hodnota q dána hodnotou posuvníku pos s rozsahem 0 až 1 , musí pozice proměnné k uvnitř intervalu $\langle -7; 7 \rangle$ odpovídat pozici proměnné q v intervalu $(0; 1)$. Z toho plyne vztah $\frac{q-0}{1-0} = \frac{k-(-7)}{7-(-7)} \Rightarrow k = 14q - 7$. Pohyb tvořících úseček po konoidu je dán příkazem

$\text{Krivka}(12q, 14 * \text{pos} - 7, 10/49 * (14 * \text{pos} - 7)^2 * (q - 1) + 10 - 6q, q, 0, 1)$. Pohyb parabolických řezů zajišťuje příkaz uvedený výše, v němž místo pos2 píšeme pos .

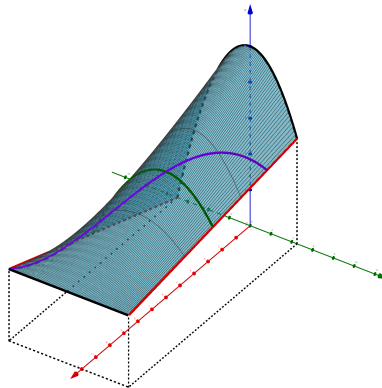
Mohli bychom také vytvořit animaci, která ukazuje vznik paraboly

lického konoidu \mathcal{K} postupným generováním tvořících úseček mezi řídicí parabolou \mathcal{P} a úsečkou KL . Obecný rozdíl vůči předchozímu postupu spočívá v tom, že se posuvník `pos` použije jako mezní hodnota ohraničující rozsah proměnné v rovnici plochy nebo křivky.

Pro animaci vzniku konoidu bude rozsah posuvníku `pos` dán intervalem $\langle -7; 7 \rangle$ a proměnná k se bude pohybovat v „plovoucích“ mezích od -7 po aktuální hodnotu posuvníku. Příkaz má potom tvar `Plocha(12q, k, 10/49 k^2(q-1)+10-6q, q, 0, 1, k, -7, pos)`. Chceme-li na zobrazené části konoidu vykreslit například úsek paraboly v rovině $x = 6$, zadáme příkaz `Krivka(6, k, -5/49 k^2+7, k, -7, pos)`. Pro tvořící úsečku ohraničující vykreslovanou část konoidu použijeme příkaz `Krivka(12q, pos, 10/49* pos^2*(q-1)+10-6q, q, 0, 1)`.

Drobná potíž nastane, pokud bychom při vykreslování křivky $\mathcal{C}(q)$ chtěli použít její výše uvedenou parametrizaci. Hodnotou $q = 0$ je totiž určen bod $P[0; 7; 0]$ a hodnotou $q = 1$ bod $K[12; -7; 4]$. Proto je nejprve třeba upravit parametrizaci tak, aby bod K byl počátečním bodem a bod P byl koncovým bodem vykreslovaného úseku křivky \mathcal{C} .

Protože je $q \in \langle 0; 1 \rangle$, provedeme nahrazení parametru q výrazem $1 - q$. Poté proměnnou q nahradíme proměnnou k pomocí převodního vztahu $q = \frac{k+7}{14}$. Správné vykreslení křivky \mathcal{C} na „rozvíjejícím se“ konoidu zajistí příkaz `Krivka(6-6/7k, k, -5/343k^3-5/49k^2+3/7k+7, k, -7, pos)`.



Obr. 3: Animace vzniku parabolického konoidu v GeoGebře

2.2 Vizualizace parabolického konoidu v Maplu

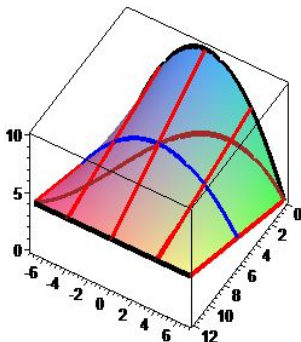
Faktický obsah příkazů užitých pro zobrazení konoidu v Maplu je stejný jako v GeoGebře, rozdílná je syntaxe příkazů.

Základní zobrazení parabolického konoidu \mathcal{K} s několika jeho tvořícími

úsečkami, řídicí parabolou \mathcal{P} , parabolou \mathcal{Q} v rovině $x = 6$ a křivkou \mathcal{C} je dáno posloupností příkazů

```

> with(plots):t1:=thickness=5:bar:=color=red:
> K:=plot3d([12*q,k,10/49*k^2*(q-1)+10-6*q],q=0..1,k=-7..7):
> P:=spacecurve([0,k,-10/49*k^2+10],k=-7..7,t1,color=black):
> l:=spacecurve([12,k,4],k=-7..7,t1,color=black):
> Q:=spacecurve([6,k,-5/49*k^2+7],k=-7..7,t1,color=blue):
> U_1:=spacecurve([12*q,-7,4*q],q=0..1,t1,bar):
> U_2:=spacecurve([12*q,0,10-6*q],q=0..1,t1,bar):
> U_3:=spacecurve([12*q,7,4*q],q=0..1,t1,bar):
> U_4:=spacecurve([12*q,-4,(330-134*q)/49],q=0..1,t1,bar):
> U_5:=spacecurve([12*q,4,(330-134*q)/49],q=0..1,t1,bar):
> C:=spacecurve([12*q,7-14*q,40*q^3-80*q^2+44*q],q=0..1,t1,
color=brown):
> display({K,P,l,Q,U_1,U_2,U_3,U_4,U_5,C},axes=boxed);
    
```



Obr. 4: Zobrazení parabolického konoidu v Maplu

Chceme-li demonstrovat pohyb tvořících úseček a parabolických řezů po konoidu, k uvedenému posloupnosti příkazů přidáme příkazy

```

> A_1:=animate(spacecurve,[12*q,14*pos-7,10/49*(14*pos-7)^2
*(q-1)+10-6*q],q=0..1,t1,color=coral, pos=0..1,frames=50):
> A_2:=animate(spacecurve,[12*pos,k,10/49*k^2*(pos-1)+10
-6*pos],k=-7..7,t1,color=navy, pos=0..1,frames=50):
    
```

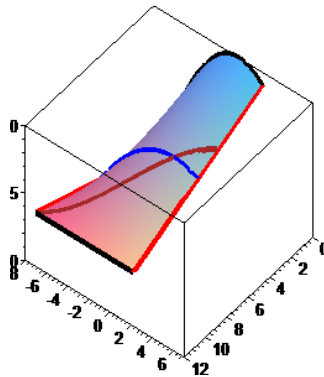
a označení animací A_1 a A_2 připišeme dovnitř příkazu `display`.

Pro vytvoření animace, v níž parabolický konoid \mathcal{K} vzniká postupným generováním svých tvořících úseček mezi řídicí parabolou \mathcal{P} a úsečkou KL , použijeme posloupnost příkazů, v nichž je parametr k shora omezen hodnotou posuvníku pos s rozsahem od -7 do 7 .

```

> K:={ [12*q,k,10/49*k^2*(q-1)+10-6*q] },q=0..1,k=-7..pos,
style=patchnograd:
> t1:=thickness=5:bar:=color=red:
> U:={ [12*q,pos,10/49*pos^2*(q-1)+10-6*q] },q=0..1,t1,bar:
> U_1:=spacecurve([12*q,-7,4*q],q=0..1,t1,bar):
> P:={ [0,k,-10/49*k^2+10] },k=-7..pos,t1,color=black:
> Q:={ [6,k,-5/49*k^2+7] },k=-7..pos,t1,color=blue:
> l:={ [12,k,4] },k=-7..pos,t1,color=black:
> C:={ [6-6*k/7,k,-5*k^3/343-5*k^2/49+3*k/7+7] },k=-7..pos,t1,
color=brown:
> with(plots):
> A_1:=animate(plot3d,[K],pos=-7..7,frames=80):
> A_2:=animate(spacecurve,[U],pos=-7..7,frames=80):
> A_3:=animate(spacecurve,[P],pos=-7..7,frames=80):
> A_4:=animate(spacecurve,[Q],pos=-7..7,frames=80):
> A_5:=animate(spacecurve,[l],pos=-7..7,frames=80):
> A_6:=animate(spacecurve,[C],pos=-7..7,frames=80):
> display({A_1,A_2,A_3,A_4,A_5,A_6,U_1},axes=boxed);

```



Obr. 5: Animace vzniku parabolického konoidu v Maplu

3 Ukázka praktického užití parabolického konoidu

Parabolický konoid je možné využít pro zastřešení vchodového prostoru do budovy. Konoid se dotýká zdi budovy podél úsečky KL a je omezen křivkou \mathcal{A} , která je průsečnicí konoidu s rovinou α procházející úsečkou

PP' a svírající s půdorysnou zvolený úhel. Nastavení úhlu je dáno volbou záporné hodnoty parametru u , jenž ovlivňuje náklon roviny α vůči půdorysně. Prochází-li rovina α body $O[0;0;0]$, $P[0;7;0]$ a bodem W na konoidu \mathcal{K} se souřadnicemi $[12u;0;10-6u]$, má její parametrizace tvar $\alpha(x,y) = (x, y, \frac{5-3u}{6u}x)$, kde $x \in \langle 12u;0 \rangle$, $y \in \langle -7;7 \rangle$.

Výpočtem v programu Maple je možné získat parametrické rovnice křivky \mathcal{A} pro $k \in \langle -7;7 \rangle$ ve tvaru

$$\mathcal{A}(k) = \left(\frac{12u(k^2-49)}{k^2u-49}, k, -\frac{2(3k^2u-5k^2+245-147u)}{k^2u-49} \right).$$

V parametrizaci konoidu \mathcal{K} je potřeba nastavit rozsah proměnné q tak, aby byl konoid omezen křivkou \mathcal{A} . Porovnáním jejich x -ových souřadnic získáme dolní mez parametru q danou výrazem $\frac{u(k^2-49)}{k^2u-49}$.

Pokud jde o rovinu α , vykreslíme její část ve tvaru obdélníku, z něhož je vyjmuta oblast mezi úsekem jeho strany v půdorysně a křivkou \mathcal{A} na konoidu. Jedná se o obdélníky \mathcal{S}_2 a \mathcal{S}_3 s parametrizací $(x, k, \frac{5-3u}{6u}x)$, kde $x \in \langle 12u;0 \rangle$ a parametr k je omezen intervalem $\langle 7;12 \rangle$ nebo $\langle -12;-7 \rangle$. Zbývající částí roviny α je oblast \mathcal{S}_1 se stejnou parametrizací, ale s proměnnou $k \in \langle -7;7 \rangle$ a proměnnou x v mezích od $12u$ po $\frac{12u(k^2-49)}{k^2u-49}$.

Pro lepší představu, jak velká plocha je chráněna před deštěm v situaci, kdy dešťové kapky dopadají kolmo na půdorysnu, vykreslíme její hranici \mathcal{A}_1 . Celou situaci zobrazíme v programu Maplu pomocí těchto příkazů

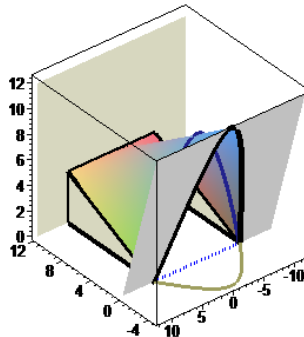
```

> with(plots):t1:=thickness=5:bar:=color=black:om:=color=wheat:
> u:=-0.4:
> K:=plot3d([12*q,k,10/49*k^2*(q-1)+10-6*q],k=-7..7,
q=u*(k^2-49)/(k^2*u-49)..1,style=patchnogrid):
> T_1:=plot3d([12*q,7,z],q=0..1,z=0..4*q,om,style=patchnogrid):
> T_2:=plot3d([12*q,-7,z],q=0..1,z=0..4*q,om,
style=patchnogrid):
> A:=spacecurve([12*u*(k^2-49)/(k^2*u-49),k,
-2*(3*k^2*u-5*k^2+245-147*u)/(k^2*u-49)],k=-7..7,t1,bar):
> P:=spacecurve([0,k,-10/49*k^2+10],k=-7..7,t1,color=navy):
> U_1:=spacecurve([12*q,7,4*q],q=0..1,t1,bar):
> U_2:=spacecurve([12*q,-7,4*q],q=0..1,t1,bar):
> U_3:=spacecurve([12,k,4],k=-7..7,t1,bar):
> U_4:=spacecurve([12,7,z],z=0..4,t1,bar):
> U_5:=spacecurve([12,-7,z],z=0..4,t1,bar):
> U_6:=spacecurve([12*q,7,0],q=0..1,t1,bar):
> U_7:=spacecurve([12*q,-7,0],q=0..1,t1,bar):
> R_1:=plot3d([12,y,z],y=-7..7,z=4..12,om,style=patchnogrid):
    
```

```

> R_2:=plot3d([12,y,z],y=7..12,z=0..12,om,style=patchnogrid):
> R_3:=plot3d([12,y,z],y=-12..-7,z=0..12,om,style=patchnogrid):
> S_1:=plot3d([x,k,(5-3*u)*x/(6*u)],k=-7..7,x=
12*u..12*u*(k^2-49)/(k^2*u-49),style=patchnogrid,color=gray):
> S_2:=plot3d([x,k,(5-3*u)*x/(6*u)],k=7..12,
x=12*u..0,style=patchnogrid,color=gray):
> S_3:=plot3d([x,k,(5-3*u)*x/(6*u)],k=-12..-7,
x=12*u..0,style=patchnogrid,color=gray):
> A_1:=spacecurve([12*u*(k^2-49)/(k^2*u-49),k,0],k=-7..7,
thickness=3,color=khaki):
> P_1:=spacecurve([0,k,0],k=-7..7,thickness=3,color=blue,
linestyle=dot):
> display({T_1,T_2,K,A,P,U_1,U_2,U_3,U_4,U_5,U_6,U_7,R_1,R_2,
R_3,S_1,S_2,S_3,A_1,P_1},axes=boxed);

```



Obr. 6: Zastřešení plochy užitím parabolického konoidu v Maplu

4 Závěr

Na parabolickém konoidu by se daly realizovat další výpočty a provést jejich vizualizace, taktéž by bylo možné vyšetřit vlastnosti parabolického konoidu užitím adekvátní geometrické teorie. Vzhledem k omezenému rozsahu příspěvku zde na toto již nezbyvá místo, v případě zájmu však plný rozsah příspěvku čítající 32 stran mohou poskytnout.

Celkově lze říci, že takovéto zobrazení určité plochy technické praxe může být vhodnou náhradou fyzického modelu této plochy.

Literatura

- [1] F. Machala: *Plochy technické praxe*, Rektorát Univerzity Palackého v Olomouci, Olomouc, 1986
- [2] J. Janyška, A. Sekaninová: *Analytická teorie kuželoseček a kvadrik*, Masarykova univerzita, Brno, 1996
- [3] *Maple 11: User Manual*, Maplesoft, Canada, 2007

CTU freeform standard Pharaoh

Ivana Linkeová, Marta Hlavová

Faculty of Mechanical Engineering, CTU in Prague

Karlovo nám. 13, 121 35 Prague 2, Czech Republic

email: ivana.linkeova@fs.cvut.cz, marta.hlavova@fs.cvut.cz

Abstract. The paper presents a new freeform standard, the CTU freeform standard Pharaoh, with a complex freeform geometry developed and manufactured at the Czech Technical University in Prague. The standard was developed for the purpose of research in the field of applications of mathematical-geometrical modelling, CNC machining and coordinate measurement of engineering components with freeform surfaces.

Keywords: Freeform surface, geometrical accuracy, 3-axis machining, freeform metrology.

1 Introduction

Applications of mathematical-geometric modelling in the design, CNC (Computer Numerically Controlled) machining and inspection of engineering components with freeform surfaces are increasingly important in the scientific approach to solving problems in mechanical engineering practice. In order to be able to develop mathematical-geometrical models with the quality required by a specific technical application of freeform surfaces, CTU (Czech Technical University) freeform standard Pharaoh (hereinafter referred to as Pharaoh) was designed in the Department of Technical Mathematics, manufactured in the Department of Production Machines and Equipment (Faculty of Mechanical Engineering, CTU in Prague) and calibrated in the Czech Metrology Institute, fig. 1.

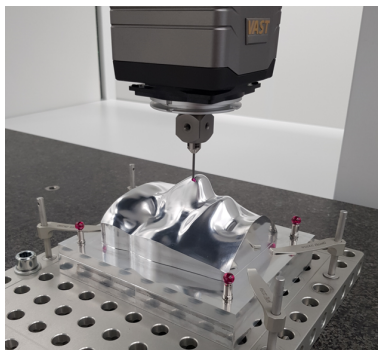


Fig. 1: CTU freeform standard Pharaoh measured on ZEISS XENOS

Freeform surface is represented in all phases (design, machining, inspection) by a CAD (Computer Aided Design) model, from whose geometric properties and quality derives both the accuracy and efficiency of the CNC machining process and the quality of the nominal reference in coordinate measurement. This paper is focused on the design and development of functional freeform surface and CAD model of the standard.

The paper is organised as follows. A development of the freeform surface used as the functional Pharaoh freeform surface is described in section 2. Pharaoh CAD model and calibration is mentioned in section 3. Section 4 concludes the paper.

2 Freeform surface development

The functional freeform surface of the Pharaoh is inspired and derived from the freeform surface of an artificial human head [1] developed and manufactured for the Department of Physics (Faculty of Mechanical Engineering, CTU in Prague). The manufactured human head was used in the simulator (dummy head) intended for research in electroacoustics, i.e. testing electroacoustics systems, measuring the quality of electroacoustic and transducers, measurement of noise protectors, investigating the binaural sound signal, measuring the transfer functions of hearing aids for the hard of hearing, analysis of noise conditions in the working environment, etc. An application of the dummy head in the measurement of monaural and binaural parameters of the Rudolfinum concert halls in Prague is shown in fig. 2 left, [2].

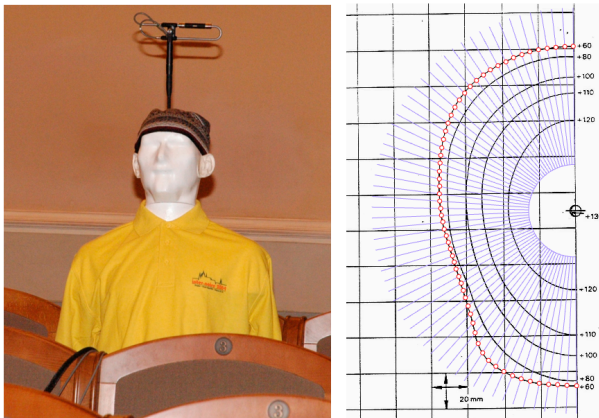


Fig. 2: Dummy head application [2] (left) and digitisation of definition curves (right)

2.1 Dummy head freeform surface

The original shape of the dummy head is based on the definition stated in IEC 959 standard [3] (this standard no longer exists, it was replaced by a newer one), where the shape of the head is given by a system of horizontal section curves drawn in 20 mm square grid. The resulting surface should pass through all the drawn curves in tolerance ± 1 mm. To keep these conditions, interpolation model in a form of Ferguson 12-vector patches connected with C^1 continuity was chosen to represent the dummy head freeform surface. The development of dummy freeform surface was done using Maple system.

Ferguson 12-vector patch $\mathbf{P}(u, v)$ is determined by four definition points $\mathbf{Q}_{i,j}$, $i, j = 0, 1$ and a pair of tangent vectors $\mathbf{Q}_{i,j}^u$, $\mathbf{Q}_{i,j}^v$ at each definition point (the method for estimation of tangent vectors from the point input data is described in [1]) is given by

$$\mathbf{P}_F(u, v) = \mathbf{U} \cdot \mathbf{B}_F \cdot \mathbf{M}_F \cdot \mathbf{B}_F^T \cdot \mathbf{V}^T, \quad (u, v) \in [0, 1]^2, \quad (1)$$

where

$$\mathbf{U} = (u^3 \ u^2 \ u \ 1), \quad \mathbf{V} = (v^3 \ v^2 \ v \ 1),$$

$$\mathbf{B}_F = \begin{pmatrix} 2 & 1 & 1 & -2 \\ 3 & -2 & -1 & 3 \\ 0 & 1 & 0 & 0 \\ 1 & 0 & 0 & 0 \end{pmatrix}, \quad \mathbf{M}_F = \begin{pmatrix} \mathbf{Q}_{0,0} & \mathbf{Q}_{0,0}^v & \mathbf{Q}_{0,1}^v & \mathbf{Q}_{0,1} \\ \mathbf{Q}_{0,0}^u & \mathbf{0} & \mathbf{0} & \mathbf{Q}_{0,1}^u \\ \mathbf{Q}_{1,0}^u & \mathbf{0} & \mathbf{0} & \mathbf{Q}_{1,1}^u \\ \mathbf{Q}_{1,0} & \mathbf{Q}_{1,0}^v & \mathbf{Q}_{1,1}^v & \mathbf{Q}_{1,1} \end{pmatrix}.$$

To obtain definition points from the drawn curves, the curves were manually digitised so that the definition points are given by intersections of the curves with the radial grid with 3° spacing (small enough to meet the required tolerance), fig. 2 right. Thus, the mesh of definition points $\{\mathbf{Q}_{i,j}^{17,119}\}_{i=0,j=0}$, was obtained, fig. 3 left. The resulting C^1 continuous interpolation surface is a composition of all Ferguson patches (1), fig. 3 right.

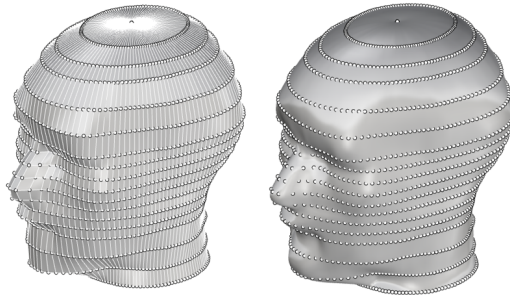


Fig. 3: Definition mesh (left) and C^1 interpolation surface (right)

2.2 Pharaoh freeform surface

During the development of the Pharaoh freeform surface, both new knowledge about the influence of the continuity of CAD model on the efficiency and quality of CNC machining [5], as well as highly demanding problems resulting from advanced freeform metrology tasks were taken into account. Thus, C^3 continuous surface with highly variable curvature was developed. The basis of the Pharaoh freeform surface was represented by the most shaped part selected on the above mentioned dummy head interpolation surface, fig. 4 (a). The original C^1 continuous surface part created by a set of 220 Ferguson 12-vector patches was transformed into C^3 continuous non-uniform biquartic B-spline surface with maximum permissible form deviation ± 0.005 mm. The whole procedure was done using Maple and Rhinoceros systems, form deviations were analysed by Python script [6].

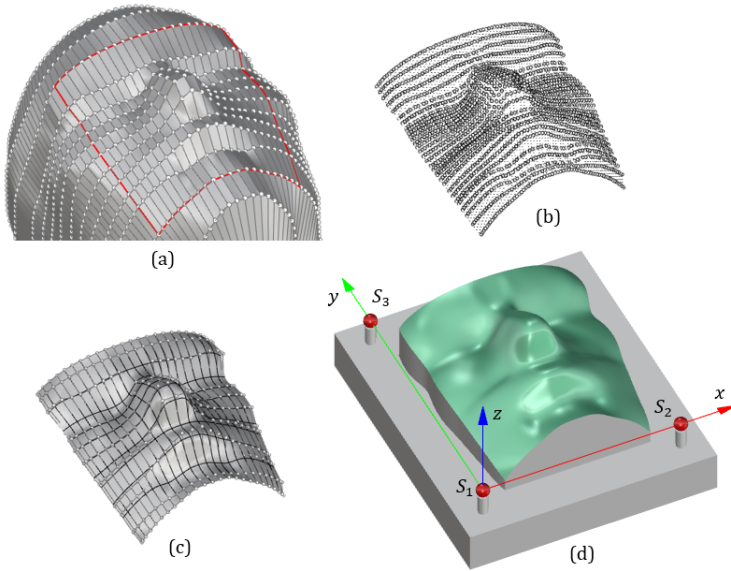


Fig. 4: Pharaoh freeform surface development (a) Part of interpolation surface, (b) Set of bicubic Bézier patches, (c) Uniform bicubic B-spline surface, (d) CAD model with non-uniform biquartic B-spline surface

As Ferguson interpolation model is not implemented in Rhinoceros, each Ferguson patch was transformed into the Bézier bicubic patch [4] first, fig. 4 (b)

$$\mathbf{P}_B(u, v) = \mathbf{U} \cdot \mathbf{B}_B \cdot \mathbf{M}_B \cdot \mathbf{B}_B^T \cdot \mathbf{V}^T, \quad (u, v) \in [0, 1]^2, \quad (2)$$

where

$$\mathbf{B}_B = \begin{pmatrix} -1 & 3 & -3 & 1 \\ 3 & -6 & 3 & 0 \\ -3 & 3 & 0 & 0 \\ 1 & 0 & 0 & 0 \end{pmatrix}, \mathbf{M}_B = \{\mathbf{V}_{i,j}\}_{i=0,j=0}^{3,3}$$

The transformation is given by

$$\begin{aligned} \mathbf{V}_{0,0} &= \mathbf{Q}_{0,0} & \mathbf{V}_{1,0} &= \mathbf{Q}_{0,0} + \frac{1}{3}\mathbf{Q}_{0,0}^u & \mathbf{V}_{0,1} &= \mathbf{Q}_{0,0} + \frac{1}{3}\mathbf{Q}_{0,0}^v \\ \mathbf{V}_{3,0} &= \mathbf{Q}_{1,0} & \mathbf{V}_{2,0} &= \mathbf{Q}_{1,0} - \frac{1}{3}\mathbf{Q}_{1,0}^u & \mathbf{V}_{0,2} &= \mathbf{Q}_{0,1} - \frac{1}{3}\mathbf{Q}_{0,1}^v \\ \mathbf{V}_{0,3} &= \mathbf{Q}_{0,1} & \mathbf{V}_{1,3} &= \mathbf{Q}_{0,1} + \frac{1}{3}\mathbf{Q}_{0,1}^u & \mathbf{V}_{3,1} &= \mathbf{Q}_{1,0} + \frac{1}{3}\mathbf{Q}_{1,0}^u \\ \mathbf{V}_{3,3} &= \mathbf{Q}_{1,1} & \mathbf{V}_{2,3} &= \mathbf{Q}_{1,1} - \frac{1}{3}\mathbf{Q}_{1,1}^u & \mathbf{V}_{3,2} &= \mathbf{Q}_{1,1} - \frac{1}{3}\mathbf{Q}_{1,1}^v \\ & & \mathbf{V}_{1,1} &= \mathbf{Q}_{0,0} + \frac{1}{3}\mathbf{Q}_{0,0}^u + \frac{1}{3}\mathbf{Q}_{0,0}^v \\ & & \mathbf{V}_{1,2} &= \mathbf{Q}_{0,1} + \frac{1}{3}\mathbf{Q}_{0,1}^u - \frac{1}{3}\mathbf{Q}_{0,1}^v \\ & & \mathbf{V}_{2,1} &= \mathbf{Q}_{1,0} - \frac{1}{3}\mathbf{Q}_{1,0}^u + \frac{1}{3}\mathbf{Q}_{1,0}^v \\ & & \mathbf{V}_{2,2} &= \mathbf{Q}_{1,1} - \frac{1}{3}\mathbf{Q}_{1,1}^u - \frac{1}{3}\mathbf{Q}_{1,1}^v \end{aligned}$$

Next, the position of inner four control points $\mathbf{V}_{i,j}$, $i, j = 1, 2$ of each patch were modified so that the conditions for C^2 continuity between two consecutive patches is fulfilled. After that, the set of 220 C^2 continuously connected Bézier patches was composed into C^2 single uniform bicubic B-spline surface, fig. 4 (c) that was finally reconstructed into C^3 non-uniform biquartic B-spline surface, depicted in green in fig. 4 (d).

3 Pharaoh machining and calibration

Pharaoh was machined at the Department of Production Machines and Equipment (RCMT, Faculty of Mechanical Engineering, CTU in Prague) from aluminium by 3-axis milling with ball-end cutter of diameter 6 mm and polished. Calibration of the standard was performed on the National standard of geometrical dimensions of 3D objects ZEISS XENOS [7] in the Unit of Technical Length of the Czech Metrology Institute. The CAD model, fig. 4 (d), was used as the nominal definition in both the machining and calibration.

CAD model of the Pharaoh standard of dimensions (150 × 175 × 90) mm, fig. 4 (d), consists of the prismatic base and freeform surface. Three high quality reference spheres S_1 , S_2 , S_3 – ruby Renishaw probes D8R L16 are screwed into the base to define workpiece Cartesian coordinate system. The origin lies at the centre of sphere S_1 , positive x -axis is given by S_1S_2 and z -axis is perpendicular to the plane given by the centres of all three spheres.

The freeform surface was calibrated with evenly distributed 45078 points with approximate distance 0.5 mm in both u - and v -directions. The normal deviations of all points from the surface were measured and the calibration results were evaluated according to ČSN EN ISO 1101 geometric specification – Surface profile related to the base defined by reference spheres. The coefficient of thermal expansion $\alpha = 23 \cdot 10^{-6} \text{K}^{-1}$ was used to compensate for the reference temperature of 20°C. Laboratory temperature was (20.0 ± 0.1)°C. The calibration results are given in the form of colour map of deviations, fig. 5 left and histogram of deviations fig. 5 right. Surface profile of the Pharaoh freeform surface is (0.1537 ± 0.0016) mm.

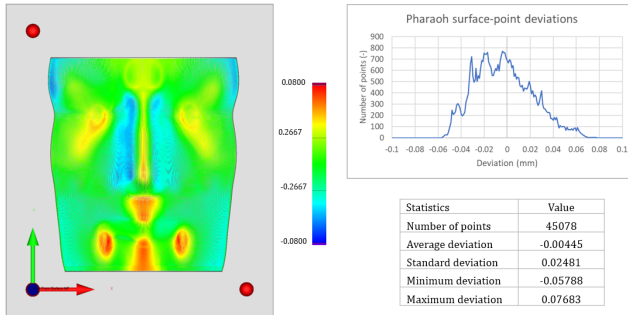


Fig. 5: Colour map of deviations (left) and histogram of deviations (right)

4 Conclusion

The development and calibration results of the CTU freeform standard Pharaoh are described in the paper. The standard will be applied when solving research tasks in freeform mathematical and CAD modelling, in the field of high-precision CNC machining and advanced freeform metrology. Future work will be focused on freeform digital twin development for the purpose of high precise CAD reference for coordinate measurement.

Acknowledgements

This work was supported by the Student Grant Competition of the Czech Technical University in Prague, grant Applications of mathematical-geometric modelling in mechanical engineering SGS21/148/OHK2/3T/12.

References

- [1] I. Linkeová: *Manufacturing an artificial human head*, Journal for Geometry and Graphics, 2003, 7(1), pp. 89–99
- [2] M. Brothánek, V. Jandák, O. Jiříček, P. Švec: *Monaural and binaural parameters of Rudolfinum concert halls in Prague*, Applied Acoustics, vol. 73, No 11, 2012, pp. 1201–1208
- [3] IEC 959: Provisional Head and Torso Simulator for Acoustic Measurements on Air Conduction Hearing Aids, 1990
- [4] L. Piegl, W. Tiller: *The NURBS Book*, Monographs in Visual Communications. Springer, Berlin, 1997
- [5] D. Kučera: *Influence of CAD model geometry on quality and efficiency of machining on CNC machine tools*, CTU in Prague, Faculty of Mechanical Engineering, Master Thesis, 2021
- [6] J. Müller: *Analysis of point-surface deviation*, Proceedings of the 8th Czech — Slovak Conference on Geometry and Graphics, Czech Republic, Olomouc, 2022
- [7] V. Zelený, I. Linkeová, J. Sýkora, P. Skalník: *ZEISS XENOS coordinate measuring machine declared the National standard of geometrical dimensions of 3D objects*, Metrologie, vol. 28, 2019, pp. 4–7

Analýza odchylky bodu od plochy

Analysis of point-surface deviation

Jakub Müller

*České vysoké učení technické v Praze, Fakulta strojní, Ústav technické matematiky
Karlovo nám. 13, 121 35 Praha 2 - Nové Město, Česká republika
email: jakub.muller@fs.cvut.cz*

Abstract. The Rhinoceros program belongs to CAD softwares that allows the user to work with very precise model, especially when focused on its surface. One of the main elements of surface analysis is the "Point Deviation" function used to determine the deviations between two geometries, e.g. points measured on an actually manufactured model from a nominal CAD model. The result is a visualization of the deviations of the measured points from the CAD model. The problem with this visualization is its ambiguity caused by not distinguishing between positive and negative orientation of the deviations and thus a visible distinction between undercutting or addition of material.

The paper presents a script, created in the Python programming language, is to create own custom function capable of calculating the individual deviations of the points of the real model with subsequent determination of their orientations based on the outer-pointing unit normals of the monitored surface. Script provides text and graphic output including visualization on a CAD model and basic statistics.

Keywords: CAD model, point-surface deviation, geometrical analysis

Klíčová slova: CAD model, odchylka bodu od plochy, geometrická analýza

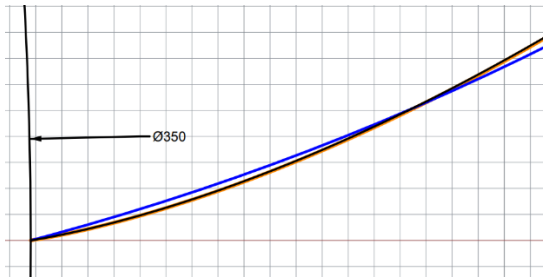
1 Úvod

Computer Aided Design, zkráceně CAD, představuje v dnešní době jeden z nejsnazších a nejefektivnějších způsobů pro tvorbu jak dvou dimenzionálního, tak tří dimenzionálního modelu. Souhrnně se jedná o kategorii softwarů, které na základě matematiky, geometrie a grafiky zprostředkovávají tvorbu modelů z okruhů strojírenství, architektury, elektroniky a řady dalších.

V případě strojírenství představuje CAD model základní prvek pro CNC (Computer Numerical Control) obrábění, kdy je CAD model s pomocí CAM (Computer Aided Manufacturing) softwaru užít pro programování drah nástrojů CNC strojů. Kvalita finálního obrobku je pak ovlivněna mechanickými a tepelnými podmínkami obrábění. Opomíjeným faktorem je přesnost užitého CAD softwaru. Cílem příspěvku je, na základě tohoto problému, zhotovení skriptu schopného porovnání reálného modelu s modelem referenčním pro možnost kvalitní vizualizace nepřesností skutečného modelu.

2 Nepřesnost CAD softwaru

Jedním z hlavních faktorů ovlivňující kvalitu CAD softwaru je jeho přesnost modelování. Každý CAD software disponuje možností nastavení přesnosti. Problém přichází v případě složitějších modelů, které obsahují například transcendentní křivky. Takové modely jsou pak výsledkem aproximace, model se může stát nepřesným a pro užití CNC přímo nevhodným. Na obrázku 1 je černě zobrazena část kruhové evolventy generované odvalováním tečny po kružnici o průměru 350 mm, modrou je zvýrazněna evolventa vytvořená programem Autodesk Inventor, oranžovou je pak zobrazena evolventa tvořená programem PTC Creo 4 Parametric.



Obr. 1: Porovnání evolvent (kresleno v 10 mm čtvercové mřížce)

Uvažujeme-li pak interpolační křivku z pluginu Grasshopper jako referenční, odchylka evolventy programu Creo 4 je 0,032 mm, v případě Inventoru pak 0,480 mm.

2.1 Skript pro zjištění odchylky bodu od plochy

Rhinoceros 7 nabízí pro řešení odchylky bodů od plochy funkci Point Deviation [5]. Nevýhodou této funkce je absence orientace vypočtené odchylky.

Vlastní skript pojmenovaný Oriented Point Deviation vyžaduje zadání mraku pozorovaných bodů a referenční plochy. Na základě geometrie si následně hledá nejbližší body ležící na referenční ploše, které prováže s odpovídajícími body normálou k tečné rovině plochy v daném bodu referenční plochy. Jakmile je takto vytvořena spojnice mezi dvěma body, skript využije vzájemnou polohu jejich krajních bodů společně s orientací normály referenční plochy k vyhodnocení orientace získané spojnice. Výsledkem je tak vytvoření orientované úsečky definující odchylku pro pozorovaný bod.

Jakmile je takto skriptem zpracován každý bod zadaného mraku, začne výpočet statistik na základě délky a orientace každé spojnice. Následuje kompletní výpis statistiky spolu s rozdělením všech spojníc do barevných vrstev závislých na velikosti odchylky, kdy jednotlivé intervaly vrstev jsou dány podle vypočtených statistik.

2.2 Modelování ploch ozubení

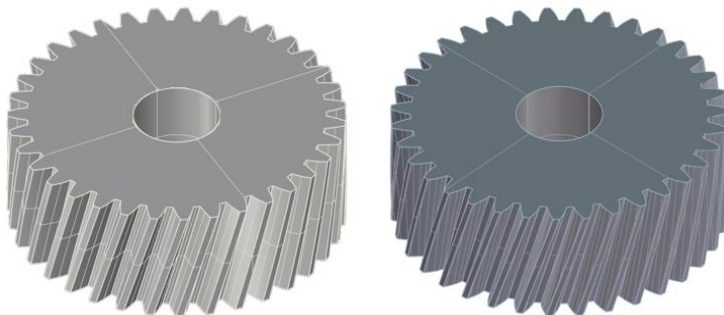
Pro ukázkou byl zvolen příklad modelu ozubeného kola s šikmým evolventním ozubením. Zadané parametry modulu, počtu zubů a úhlu sklonu zubů byly převzaty z [1]. Kolo bylo dále navrhováno v souladu s technickými normami [3] a [4] pro převodová soukolí. Rozměry jsou zaneseny v tabulce 1.

Rozměr	Hodnota	Jednotka
Normální modul m_n	10	mm
Počet zubů z	35	-
Úhel sklonu zubů β	15	°
Průměr roztečné kružnice d	362,355	mm
Průměr základní kružnice d_b	339,242	mm
Průměr hlavové kružnice d_a	388,695	mm
Průměr patní kružnice d_f	343,695	mm
Čelní zubová rozteč p_t	32,525	mm
Čelní šířka zubu s_t	18,651	mm
Čelní šířka zubové mezery e_t	13,874	mm
Tloušťka ozubení b	100	mm

Tabulka 1: Parametry ozubeného kola

K tvorbě modelu byly využity CAD softwary Rhinoceros 7 a Autodesk Inventor. V případě Autodesk Inventoru byla využita vestavěná funkce pro automatické modelování ozubeného soukolí.

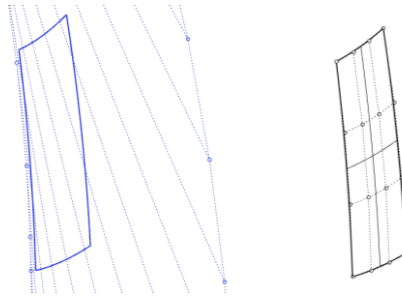
V případě modelu kola v programu Rhinoceros byl využit postup modelování podle [1], kdy se profil zubu skládá ze tří segmentů. Prvním segmentem je válcová plocha hlavy zubu, druhým je válcová plocha paty zubu a třetí segment je plochou tečen šroubovice reprezentující bok zubu. Výsledek obou modelů je na obrázku 2, kde kolo vlevo je model z Autodesk Inventoru, kolo vpravo je model z Rhinoceros 7. Pouhým okem je odchytka tvarů nerozpoznatelná.



Obr. 2: Modely ozubeného kola

2.3 Analýza ploch ozubení

První zkouškou korektnosti geometrie modelu bylo rozvinutí do roviny. Z teorie rozvinutelných ploch [2] vyplývá, že by plocha šikmého evolventního ozubení měla být rozvinutelná do roviny. V případě modelu z Rhinoceros 7 byl model kompletně rozvinutelný viz obr. 3 vlevo, kde je bok zubu zobrazen jako fragment plochy tečen šroubovice. Pro kolo z Autodesk Inventoru se pak stala problematická plocha boku zubu, kterou nebylo možné rozvinout. Po bližší analýze plochy bylo zjištěno, že plocha je substituována zborcenou Bézierovou bikubickou plochou, viz obr. 3 vpravo.



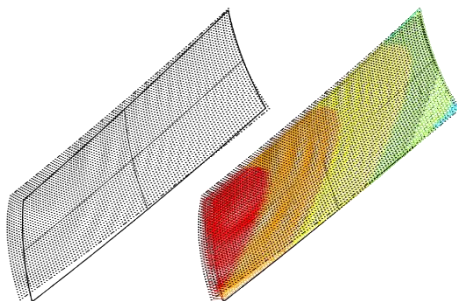
Obr. 3: Plochy boku zubu

Pro další analýzu byl v programu Rhinoceros 7 vytvořen referenční mrak bodů představujících numericky přesné body ležící na ploše tečen šroubovice určené vektorovou rovnicí [2]

$$\mathbf{S}(u, v) = (r(\cos(u) - v \sin(u)), r(\sin(u) + v \cos(u)), p_0(u + v)),$$

kde $u \in [0, 2\pi]$ $v \in [0, 1]$, $r = 181,176$ mm a $p_0 = 676,164$ mm. Výsledný referenční mrak bodů sestával z celkového počtu 4425 bodů.

Měření odchylek ploch od referenčního mraku bylo provedeno s pomocí vytvořeného skriptu Oriented Point Deviation. Při sledování plochy vytvořené Autodesk Inventorem byla zjištěna maximální odchylka 2,596 mm a průměrná odchylka 1,155 mm. Na obrázku 4 je barevné zobrazení odchylky plochy od reference. Na obrázku 5 je pak obrázek výňatku ze skriptem tvořené statistiky, navíc zahrnující směrodatnou odchylku, tvarovou odchylku a další.

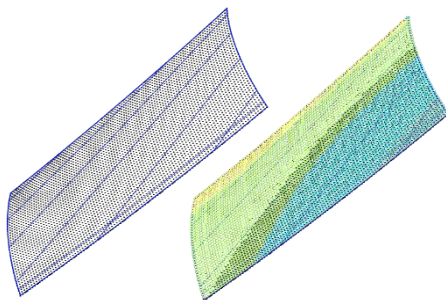


Obr. 4: Odchylka plochy zubu Autodesk Inventoru

```
Statistics  
(Number of points: ', 4425)  
(Average deviation: ', 1.1547539727796912)  
(Standart deviation: ', 0.68010560445531698)  
(Minimal deviation: ', -0.64008019404705263)  
(Maximal deviation: ', 2.5958426165940875)  
(Median: ', 1.1351188776883685)  
(Form Error: ', 3.2359228106411404)
```

Obr. 5: Statistika odchylky plochy zubu Autodesk Inventoru

V případě plochy tvořené s pomocí plochy tečen šroubovice v programu Rhinoceros 7 byla maximální odchylka plochy 0,00274 mm a průměrná odchylka 0,00230 mm. Vizualizace výsledku je na obrázku 6. Na obrázku 7 je pak zobrazena část statistického výstupu skriptu.



Obr. 6: Odchylka plochy zubu Rhinoceros 7

```
Statistics
('Number of points: ', 4425)
('Average deviation: ', 0.002302537119892048)
('Standart deviation: ', 0.002538357719273791)
('Minimal deviation: ', -0.11789899420721772)
('Maximal deviation: ', 0.002737268205777264)
('Median: ', -0.0074749745794068017)
('Form Error: ', 0.12063626241299498)
```

Obr. 7: Statistika odchylky plochy zubu Rhinoceros 7

3 Závěr

Cílem projektu bylo vytvoření vlastní funkce v CAD programu Rhinoceros 7, schopné analýzy odchylky bodu k ploše reálného modelu od jeho nominálního protějšku. Důležitým bodem skriptu je zahrnutí orientace pro odlišení podřezání a přebytku materiálu. Dalším bodem bylo vytvoření vizuálního a statistického výstupu.

Poděkování

Tento článek a výzkum vznikl za podpory projektu Studentské grantové soutěže ČVUT v Praze – Aplikace matematicko-geometrického modelování ve strojírenství SGS21/148/OHK2/3T/12.

Literatura

- [1] J. Müller: *Aplikace rozvinutelných ploch ve strojírenství* [online]. Bakalářská práce. [cit.2022-10-2]. Praha. 2021. Dostupné z: <https://dspace.cvut.cz/handle/10467/97177>
- [2] I. Linkeová, V. Zelený: *Application of ruled surfaces in freeform and gear metrology*. In: Acta Polytechnica. 2021. pp. 99-109
- [3] Norma ČSN 01 4607. *Ozubená kola čelní s evolventním ozubením. Základní profil*. Praha. Úřad pro technickou normalizaci, metrologii a státní zkušebnictví. 1978
- [4] Norma ČSN 03 1014. *Čelní ozubené převody pro převodovky. Základní parametry*. Praha. Úřad pro technickou normalizaci, metrologii a státní zkušebnictví. 1976
- [5] Robert McNeel & Associates, *Manuál Rhinoceros 3D*. 2020. Seattle

Surfaces of technical practice – creating of printed 3D models

Tatiana Rückschlosová

*Department of mathematics and descriptive geometry, Faculty of Civil Engineering,
Slovak University of Technology in Bratislava
Radlinského 11, 810 05 Bratislava, Slovak Republic
email: tatiana.ruckschlosova@stuba.sk*

Abstract. By surfaces of technical practice we mean surfaces (or their parts) whose applications are found in technical industry such as e.g. in construction, engineering, architecture and design. From a geometrical point of view, this includes surfaces of revolution, helical surfaces, or line surfaces. In order to make knowledge and a visual representation of these types of surfaces and their applications even more accessible to students, we supplemented the static and interactive graphic models with a series of printed 3D models. The paper describes the process of their modeling using software and the subsequent processing and issues associated with it in the interest of optimal 3D printing. Printed 3D models serve as one of the visual didactic aids when teaching subjects that focus on geometry or computer graphics.

Keywords: surface of revolution, helical surface, ruled surface, autoCAD, 3D print, printed model

1 Surfaces of technical practice

Students of the Faculty of Civil Engineering and the Faculty of Architecture and Design meet with the projection of technical practice surfaces during Descriptive Geometry course.

They are projected in the Monge's method and in Axonometry. Those are surfaces that are often applied in technical practice and can serve as creative inspiration in the work of future architects or designers. From a geometric point of view, we include surfaces of revolution, helical and line surfaces (especially ruled surfaces) and translational and canal surfaces. These surfaces are very visually processed in electronic study materials, which are available for students and the public on the web: Descriptive geometry II. First part – Surfaces of revolution and helical surfaces, Descriptive geometry II. Second part – Ruled surfaces, translational, sphenoidal and channel surfaces ([2], [3]).

2 Motivation

Practical experience shows that based on how we learn, i.e., we receive and process information, our learning style is formed. Our way of learning is influenced by various motives, the influence of the environment and our psychological traits. According to the theory of learning styles, it is possible to observe three basic learning styles: visual, auditory, and kinesthetic [4].

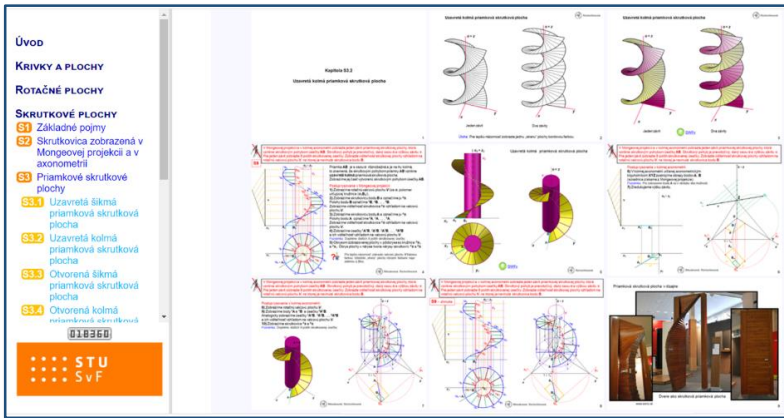


Fig. 1: Sample from study materials Descriptive geometry II.
First part – Surfaces of revolution and helical surfaces

The visual type of student effectively perceives the subject matter in its graphic or pictorial form, i.e., prefers images, graphic symbols, mind maps, color highlighting of text, etc. The auditory type better perceives the spoken word of the teacher during the lecture. He consolidates the subject matter by talking it over to himself or explaining it to his classmates. For the kinesthetic type, it is important to manipulate the subject matter. He has a need to do something, move, touch objects while learning. In doing so, he creates associations between the subject and the subject he is learning.

In practice, these styles are usually mixed to varying degrees for everyone. The above-mentioned learning materials in the form of interactive illustrative presentations, supplemented by the teacher's explanation during a lecture or exercise, are largely suitable for students of the visual-auditory type. For a better understanding of the issue, we decided to supplement the teaching with physical 3D models of some types of surfaces and their applications, to support the kinesthetic component of the learning process. This contribution describes the process of creating a model printed on a 3D printer, from modeling it in software to the issues involved in optimizing its 3D printing.

3 Model creation process

The model creation process could be divided into three phases. The first phase consists of preparing a digital model of the given surface in the software and exporting it to *.stl format. In the second phase, the model is processed in the slicing software (slicer), where appropriate settings are selected regarding subsequent 3D printing. The last stage is the 3D printing itself.

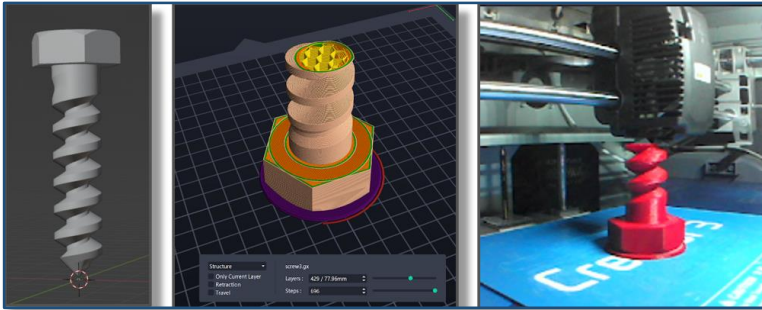


Fig. 2: Three phases of model production: digital model, slicing, 3D print

3.1 Digital 3D model

It is mostly possible to create a digital model in any software designed for modeling 3D objects. In our case, we used AutoCAD and Blender software. Both programs provide a wide range of tools for modeling 3D objects and editing them, although each in a slightly different way.

Before creating the digital model, itself, it is good to clarify in detail how the resulting model should look. Considering the wide range of modeling tools, it is necessary to determine which tool will be appropriate to use when creating the required type of surface. Alternatively, find out how to model the surface if a particular special tool is not available in our software. When we create a model to represent a certain type of surface, we create it as a solid (due to 3D printing capabilities), so it has assigned thickness. Therefore, it is desirable to consider the parameters for the printing itself, such as slope or thickness of the model and choose them appropriately.

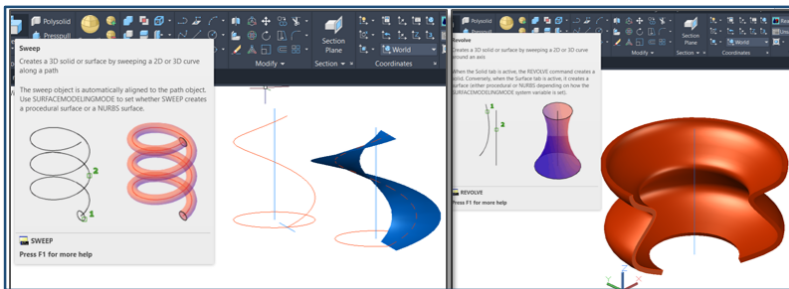


Fig. 3: Example of modeling tools in the 3D environment of AutoCAD

3.2 3D printing tools

We had the opportunity to use the Průša MK3S and FF Creator 3 PRO 3D printers for printing. Those are 3D printers based on the FFF (Fused Filament Fabrication) technology, which work with plastic material in the form of a string (the so-called filament), which after melting is applied in thin layers, creating a spatial model. The filament is placed on a spool in the printer magazine, from which it is gradually released into the print head, where it melts. The FFF technology is one of the cheapest and therefore relatively widespread [5].

Currently, a very wide range of different types of filament plastic materials are available, which differ, e.g., in its firmness, flexibility, different melting temperature, resistance to weather conditions, etc. There are also special filaments that are suitable for contact with food or filaments with a low melting temperature suitable for children. We tried materials such as PLA, ABS, PET-G and ASA. We had the best experience with the PLA, you can find more detailed characteristics of these filaments, for example, here [6].

3.3 3D print preparation

After the creation of the digital model and its export to the *.stl format, the second phase of model processing comes next. In this phase, we load the file into the slicing software, which transforms it into a form that the 3D printer understands (*.gxl). This means that it "cuts" it into layers in which the printer will gradually build the desired model. Printer manufacturers usually offer the relevant slicer compatible with the given type of printer for free download.

In the slicer, we can set various parameters for printing. Depending on the type of material, we choose the temperature of the extruder, the temperature of the bed, the speed of printing or the speed of retraction. Considering the model itself, we set parameters such as shell count, layer height, infill density, supports or raft and brim.

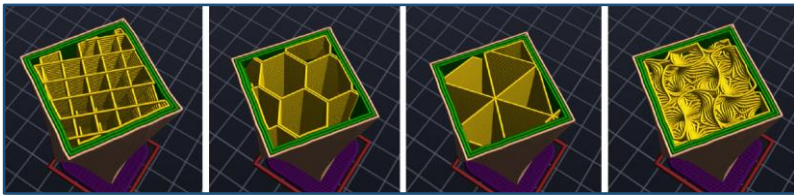


Fig. 4: Types of filling in the FlashPrint slicer at a density of 15%: segmental, hexagonal, triangular, 3D filling

3.4 3D print

The third stage is the process of printing the model itself. The print quality, which can vary widely, depends on the type of 3D printer, the type of filament and the specific setting of individual slicer parameters. During printing, due to various factors, errors may occur, such as incorrect placement of individual layers of filament, which results in incomplete printing, or ugly appearance of the model. The length of printing also depends on the complexity of the model, which lasts from tens of minutes to hours or even days [5].

4 Optimization of printing 3D models

When printing some types of helical surfaces and their application, we discovered that printing a nice model is not entirely easy. The successful printing of the model also depended on the slope of the corresponding helical surface from the pad. The intention was to print the model without the use of supporting structures or use them as little as possible. The 3D printer can print satisfactorily without the use of supports at an angle of inclination of up to 45 degrees.

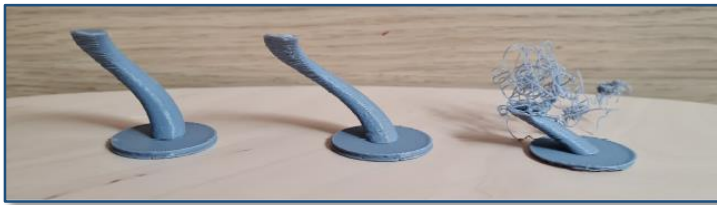


Fig. 5: Models of vinted column with different slopes

Student Daniel Krištof dealt with the task of print optimization in the case of helical surfaces in his bachelor's thesis [1]. He chose a PLA filament as a starting point and test model was used the model with different slope angles (in the shape of curved tower). He monitored print categories such as speed, extruder temperature and filling density in five different combinations. The goal was to determine under what conditions printing of a model with an inclination of 45 degrees or less is still satisfactory.

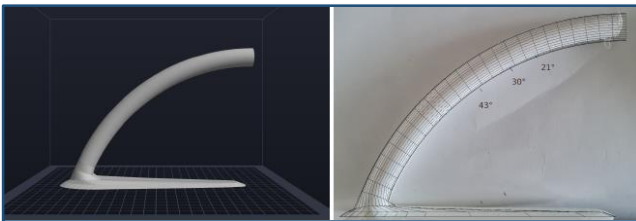


Fig. 6: Test model of different slope angles

The smallest angle (35 degrees) at which the print was evaluated as satisfactory was measured when printing at a third speed (20mm/s). Thus, the printing speed significantly affected the quality of the model. Lowering the temperature of the extruder had a smaller effect on the result, but its advantage was significantly saved time. Therefore, the option to print at a lower temperature (190 degrees of Celsius) and at two-thirds speed (40mm/s) was chosen as the most optimal of the tested combinations.

The overall appearance of the helical surface model as a surface of constant gradient depends on the possible resulting (printable) angle of inclination, depending on the parameters of the helical movement such as the parameter p and the radius r [2].

Another idea to optimize the printing of some line helical surface applications was to divide the model into evenly repeating parts that are easily printed individually and then combined into one complete model. An example is a model of a spiral staircase where the individual segments are connected to each other turned by the appropriate angle.

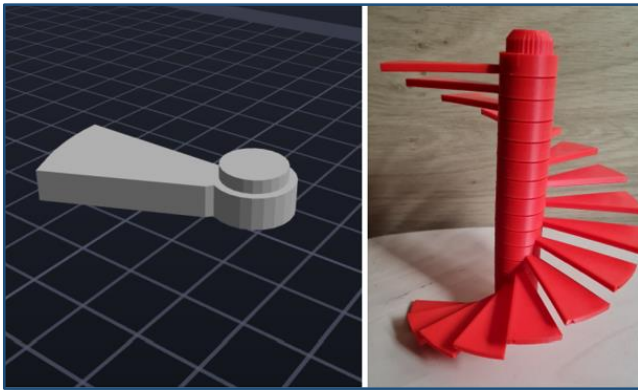


Fig. 7: Segmented model of one pitch of a spiral staircase

5 Conclusion

After familiarizing ourselves with the issue of 3D printing and overcoming various types of problems associated with it, we managed to print a quite varied spectrum of models, which mainly represent helical surfaces or their applications (gallery of pictures 8 – 11). We want to continue with the production of models and supplement the portfolio with other interesting models representing mainly surfaces of revolution and ruled surfaces. We know from experience that students like printed models in vivid colors and it attracts their interest in geometry as such.

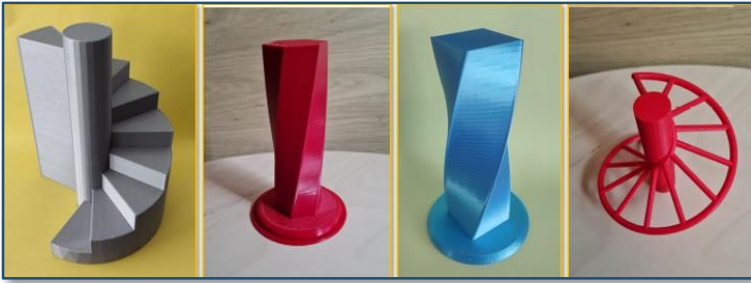


Fig. 8: Models of line helical surfaces and its applications

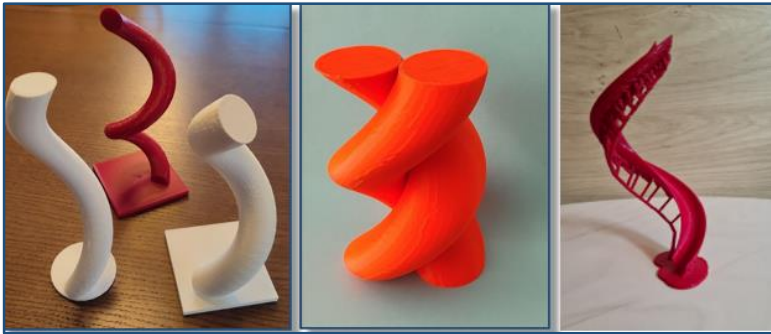


Fig. 9: Models of cyclical helical surfaces and its applications

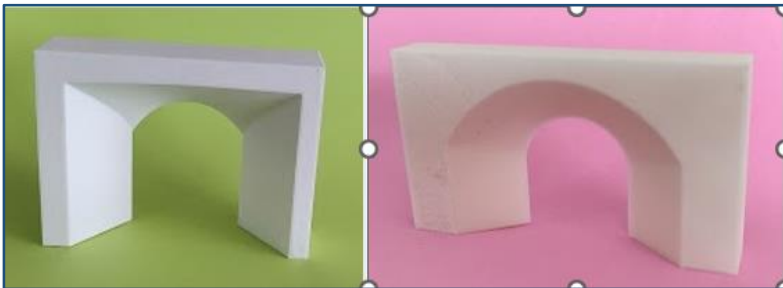


Fig. 10: Models of ruled surfaces – so called Marseille and Montpelliere arcs

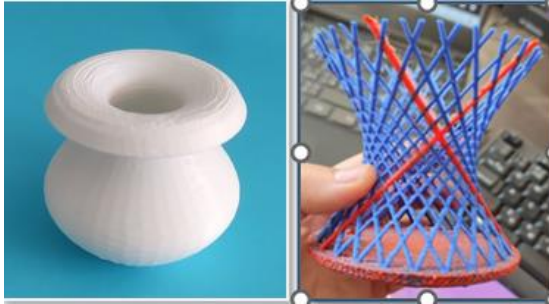


Fig. 11: Models of surfaces of revolution

Acknowledgements

This article was created with the support of grant KEGA 008STU-4/2020

References

- [1] D. Krištof: *Modely aplikácií skrutkových plôch v technickej praxi určené pre 3D tlač*. Bakalárska práca, SvF STU v Bratislave, 2022
- [2] K. Mészárosová, T. Rückschlossová, Z. Tereňová: *Deskriptívna geometria II. Prvá časť – Rotačné a skrutkové plochy*, Vydavateľstvo STU v Bratislave, 2014, ISBN 978-80-227-4275-7
Dostupné na internete: <http://www.math.sk/skriptaDG2/1/>
- [3] K. Mészárosová, T. Rückschlossová, Z. Tereňová: *Deskriptívna geometria II. Druhá časť – Priamkové, translačné, klinové a kanálové plochy*, STU v Bratislave, 2018, ISBN 978-80-227-4767-7.
Dostupné na internete: <http://www.math.sk/skriptaDG2/2/>
- [4] <https://eduworld.sk/cd/eliska-herinkova/3314/vak-ucebne-styly-sposoby-ako-sa-ucime-najlahsie>
- [5] <https://www.tonerpartner.sk/clanky/ako-funguje-stolna-3d-tlaciaren-zakladne-technologie-3d-tlace-25290sk39018/>
- [6] <https://www.tonerpartner.sk/clanky/ako-vybrat-spravne-filamenty-pre-svoju-3d-tlaciaren-26146sk39018/>

Počátky kartografie Od nejstarších památek po středověk

Origins of cartography From ancient relics to the Middle Ages

Jan Šafařík

*Ústav matematiky a deskriptivní geometrie, Stavební fakulta VUT v Brně
Veveří 331/95, 602 00 Brno, Česká republika
email: safarik.j@fce.vutbr.cz*

Abstract. Cartography is a science of maps. People could record their cartographic findings on a map much earlier than in writing. Map and the process of its making has always reflected the time in which it was born portraying the intellectual and technological advancements of each historical period. This paper aims to present the development of cartography from cartographic relics of old time (Egypt, China, and America), the Greek and Roman antique cartography, the medieval ecclesiastic cartography as well as the Arabic cartography with the origins of naval charts.

Keywords: Cartography, cartographic mappings, map, gnomon, portulan chart.

Klíčová slova: Kartografie, kartografická zobrazení, mapa, gnomon, portulánová mapa.

1 Nejstarší kartografické památky

Je prokázáno, že lidstvo dokázalo vyjádřit své geografické znalosti kresbou dříve než písmem. Vznik prvních primitivních geografických náčrtů je kladen do období mladšího paleolitu. Popudem pro jejich vznik byla nejspíš snaha orientovat se v nejbližším okolí, byla to pomůcka pro snazší zapamatování si míst, zpočátku měla především hospodářský význam (lov a sběr potravy), později snad i válečný. Topografický obsah je poměrně bohatý, nicméně jejich přesnost a měřítkové znázornění je velice nepřesné. Nákresy jsou realizovány na různých materiálech – pruty, lastury, kámen, dřevo, kůra, kůže, kosti, skalní stěny.

Není vyloučeno, že jedna z vůbec nejstarších dochovaných prehistorických map pochází z našeho území. Je jí situační pláněk tábořiště lovců mamutů u řeky Dyje (Obr. 1) vyrytý do mamutího klu a nalezený v roce 1962 v Pavlově na jižní Moravě. Jeho stáří se odhaduje na 28 až 24 000 let př. n. l. Další nálezy pocházejí z Mežiríči na Ukrajině, Schaffhausenu ve Švýcarsku, povodí sibiřské řeky Jeniseje a Ladožského jezera. Všechny tyto památky dokumentují nesmírný orientační smysl a cit pro krajinu jejich tvůrců. Svědčí o tom schopnosti tzv. primitivních národů – severoamerických Indiánů, Eskymáků, obyvatel Sibíře...



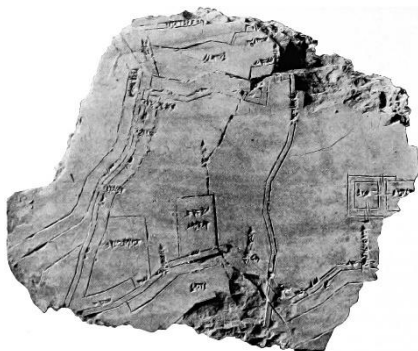
Obr. 1



Obr. 2

2 Počátky kartografie

S objevením institutu „vlastnictví“ nabývá kresba nesoucí informaci charakteru úředního dokumentu. Souběžně s rozvojem podrobných plánů a map malých území se rozvíjí i snaha o pořízení obrazů velkých územních celků a celého světa. Nejstarší starověké památky nalezneme ve středomořském regionu – Mezopotámie, Egypt, a dále pak ve starověké Číně. Objevují se první měřické pomůcky, jako je kružítko, měřický prut, měřický provazec s hůlkou, olovnice.



Obr. 3



Obr. 4

2.1 Mezopotámie

Za nejstarší mapový doklad se považuje *mapa Mezopotámie* vyrytá na hliněné destičce a pocházející z období přibližně 2 400 let př. n. l. Pravděpodobně ze 6. století před Kristem pochází známá *Babylonská mapa světa*, také vyrytá nahliněné destičce (Obr. 2). Mapa zobrazuje známou část světa (Babylon a

Asýrii), řeku Eufrat, kolem mapy je kruhové vyjádření oceánu, z něhož vystupuje sedm cípů (ostrovů?) s nápisy udávajícími vzdálenosti.

Dalším grafickým výtvozem ukazujícím menší územní celky je plán babylonského města Nippur, který je datován ve velmi širokém rozpětí 15. – 8. st. př. n. l. Zachycuje řeku Eufrat s kanály (Obr. 3).

2.2 Egyptská kartografie

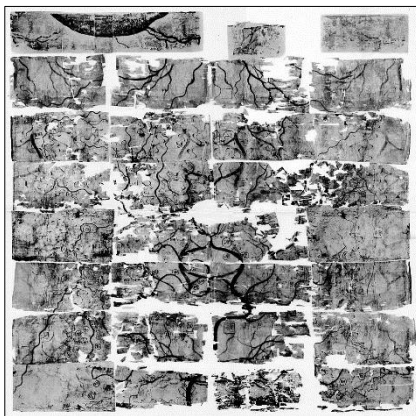
Pravděpodobně již ve 14. století př. n. l. měl starověký Egypt k dispozici podrobné mapování připomínající dnešní katastr. Za Ramesse II. se začalo s podrobným mapováním půdy pro daňové účely, kterého později využili řečtí klasikové jako Eratosthénes. Kartografická díla tohoto období vycházela nejen z rozvinuté praktické geometrie, ale stavěla i na nivelaci (základy pyramid) a na astronomii (orientace pyramid).

Známým dokladem z tohoto období je fragment *Turínského papyru* znázorňující důlní mapu z doby Ramesse IV., cca 1320 př. n. l. (Obr. 4). Z originálů egyptských plánů a map se dochovaly pouze nepatrné fragmenty, neboť mapy byly kresleny na papyru nebo na kůži a časem podléhaly zkáze.

2.3 Čínská kartografie

Kartografické vědomosti starých Číňanů jsou pozoruhodné, neboť již ve 3. století př. n. l. měli topografické mapy. Tyto mapy se však nedochovaly. Z období před 13. stoletím př. n. l. pochází oficiální čínská geografie *Jü-kung*.

V roce 1973 byly u města Čchang-ša v Ma-wang-tuej nalezeny tři mapy nakreslené na hedvábí – vojenská, topografická a plán opevnění sídla prefektury. Předpokládá se, že mapy vznikly v roce 168. př. n. l. Topografická mapa zobrazuje střed provincie Čchu-nan (Obr. 5).



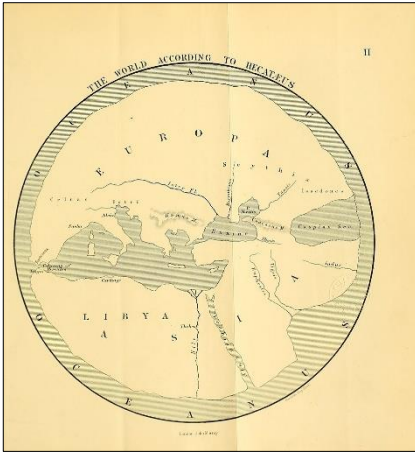
Obr. 5

3 Antická kartografie

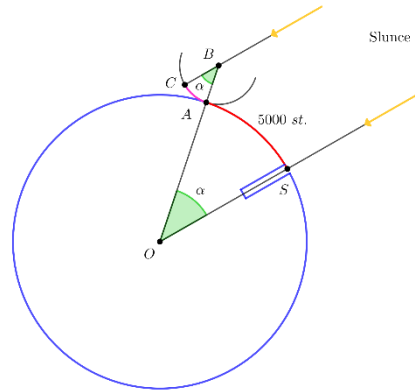
3.1 Řecká kartografie

Moderní kartografie staví na základech položených ve starém Řecku a helénském Egyptě. Řekové jako první považovali zemské těleso za kouli a určili jeho rozměry, používali šedesátinné dělení kruhu na minuty a vteřiny, zavedli

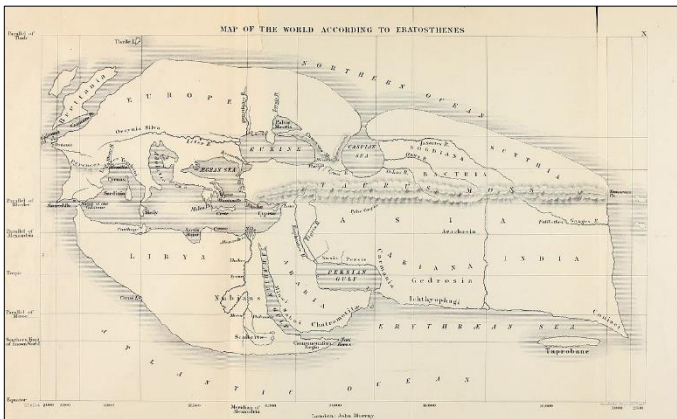
zeměpisné souřadnice, položili základy matematické kartografie, přičemž některá jejich zobrazení se používají dodnes.



Obr. 6



Obr. 7

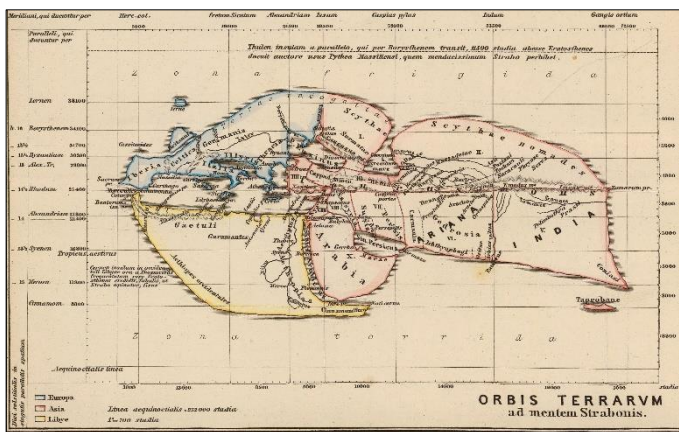


Obr. 8

První starořeckou mapu zemského povrchu vytvořil Anaximandros z Milétu (610 – 465 př. n. l.). Mapa se stejně jako ostatní starořecké mapy nedochovala, lze je však rekonstruovat ze zchovalých literárních pramenů. Hekataion z Milétu (550 – 480 př. n. l.) *Anaximandrovu mapu* opravil, doplnil a opatřil slovním komentářem (Obr. 6). Eratosthénés z Kyrény (276 – 195 př. n.l.) vypočítal obvod Země na základě určení délky meridiánového oblouku mezi městy Alexandria a Syéné (Asuán). Použil k tomu skafé (Obr. 7). Přístroj svým stínem ukázal, že oblouk AC je 50. dílem celé kružnice ($7^{\circ}12'$) a jeho odhad obvodu Země 39 690 km je pozoruhodný. Eratosthénés ve své mapě jako jeden

z prvních vytváří síť rovnoběžek a kolmic na diafragmu. Čáry neměly stejné rozestupy, ale procházely místy určenými astronomickým pozorováním (Obr 8). Prý zobrazovala více území než pozdější Ptolemaiova mapa.

Poseidónios z Apameie (135 – 51 př. n. l.) provedl nové měření Země na základě rozdílu zeměpisných šířek mezi Alexandrií a Rhodem. Jeho obvod Země byl menší než Eratosthénův. Od něj ho později převzal Ptolemaios, což prý ovlivňovalo námořní plavby a možná i působilo na Kolumba, kterému se zdála cesta do Indie západním směrem proveditelná. Kratés z Mallu (2. století př. n. l.) sestrojil první známý glóbus a byla na něm Eratosthénova mapa. Glóbus se nezachoval, ale je známý z opisů antických a arabských učenců. Strabón z Amasie (63 př. n. l. – 23 n. l.) je považován za „otce“ geografie. Na obrázku 9 je rekonstrukce *Strabónovy mapy světa*.



Obr. 9



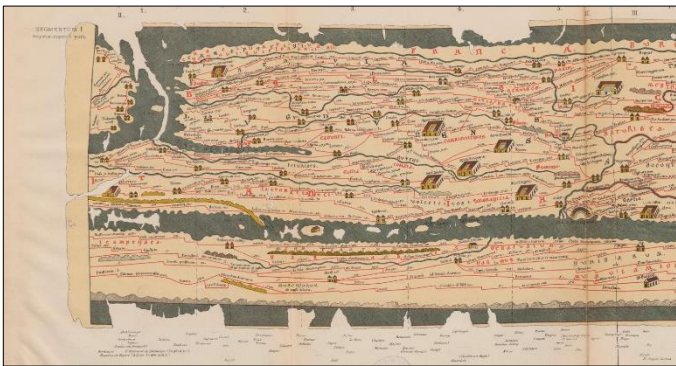
Obr. 10

V oblasti kartografických zobrazení měla velký význam formulace *azimutálních projekcí*. Thales s Milétu (625 – 547 př. n. l.) je autorem *gnómonické projekce*, Apollónios z Pergy (262 – 190 př. n. l.) zavedl *ortografickou projekci* a Hipparchos z Nikaie (190 – 125 př. n. l.) je autorem *stereografické projekce* a jako první používal v astronomii sférickou trigonometrii.

Vrchol řecké kartografie nastal za Klaudia Ptolemaia (100 – 168 n. l.), který je autorem osmidílné *Geografike hységesis*. Dále je autorem kuželového a nepravého válcového přímkového vyrovnávacího kartografického zobrazení. Jeho mapa světa z roku 150 byla zničena v alexandrijské knihovně. Rekonstrukci Ptolemaiovy mapy světa z poloviny 15. století ukazuje obrázek 10.

3.2 Římská kartografie

V Římské říši (*Imperium Romanum*) byla mapa považována za čistě užitkový předmět pro administrativní a vojenské účely. Nepoužívali kartografické metody zobrazování, ale jednalo se spíše o schematické náčrty sloužící jako cestovní itineráře s množstvím dat a údajů. Ukázkou takové pochodové mapy je výřez Agrippovy mapy (*Tabula Peutingeriana*), mapa vznikla ve druhé polovině 13. století na základě kopie Agrippovy mapy ze 4. století (Obr. 11). Marcus Vipsanius Agrippa (63 př. n. l. – 12 n. l.) je také autorem kruhové mapy světa s Itálií ve středu, tato mapa se nedochovala a známe ji jen z pozdějších rekonstrukcí.



Obr. 11

4 Středověká církevní kartografie

Po rozpadu Říše západorímské (476 n. l.) přebírá v Evropě rozhodující ideologický vliv církev. Ta prosazovala Ptolemaiovu geocentrickou soustavu, jeho mapy jsou však nahrazeny úpadkovými mapami, založenými na mýtických představách, zcela bez matematického podkladu. Jsou konstruovány

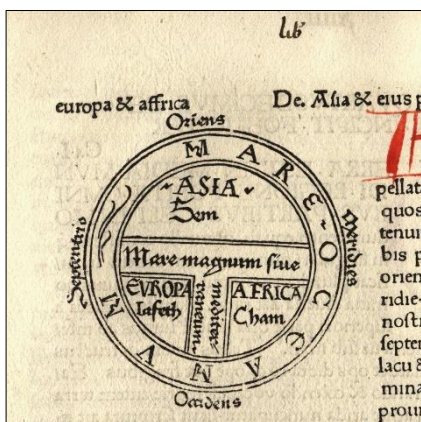
bezprojekční mapy v mnohém navazující na římské a arabské mapy. Neznámá místa jsou do map doplňována podle fantazie.

Kolem roku 535 nebo 547 napsal mnich Kosmas Indikopleustés dvanáctidílnou

publikaci *Christianiké topografía*, ke které přiložil mapu světa. Ta zobrazuje Zemi jako protáhlý čtyřúhelník se čtyřmi zálivy (Středozemní a Černé moře, Arabský a Perský záliv) a čtyřmi řekami (Nil, Ganges, Tigris a Eufrat). Na východní straně mapy je nepřístupná oblast biblického ráje (Obr. 12).



Obr. 12



Obr. 13



Obr. 14

Mapy Země se v období raného středověku často kreslily v podobě kruhu a nazývají se O-T mapy (*Orbis Terrarum*). Jednou z prvních map typu O-T je mapa z první tištěné verze knihy *Etymologiae* od Isidora ze Sevilly. Kniha byla napsána v roce 623 a poprvé vytištěna v roce 1472 v Augsburgu Güntherem Zainerem (Obr. 13). Za nejvýznamnější představitele kruhových map jsou považovány *Ebsdorfská mapa* z roku 1234 a *Herefordská mapa* z roku 1280 (Obr. 14).

5 Kompasové (portulánové) mapy



Obr. 15

Koncem 13. století se s vynálezem kompasu objevují nové typy podrobných námořních map mořského pobřeží, tzv. *kompasové mapy* (Obr. 15). Tyto mapy se zrodily v Itálii, jejich centrem byly Janov, Benátky a Ancona. Mapy nemají zpočátku geografickou síť, ale jen systém kompasových růžic (rumb), jejichž 8, 16, resp. 32 směrových

paprsků pokrývalo mapu a umožňovalo s pomocí kompasu udržovat na moři směr plavby podle zvoleného azimutu – po loxodromě.

Literatura

- [1] J. B. Harley, D. Woodward (eds.): *The history of cartography, Volume 1: Cartography in prehistoric, ancient, and medieval Europe and the Mediterranean*, University of Chicago Press, Chicago, 1987. ISBN 0-226-31633-5
- [2] J. B. Harley, D. Woodward (eds.): *The history of cartography, Volume 2, Book1: Cartography in the Traditional Islamic and South Asian Societies*, University of Chicago Press, Chicago, 1992. ISBN 0-226-31635-1
- [3] J. B. Harley, D. Woodward (eds.): *The history of cartography, Volume 2, Book2: Cartography in the Traditional East and Southeast Asian Societies*, University of Chicago Press, Chicago, 1994. ISBN 0-226-31637-8
- [4] L. Plánka: *Vývoj světové a české kartografie*, Akademické nakladatelství CERM, Brno, 2004. ISBN 80-214-2675-6
- [5] R. Švec: *Kartografické zobrazovací metody*, Státní pedagogické nakladatelství, n. p., Praha, 1956
- [6] M. Vajsáblová: *Matematické základy kartografie*, Slovenská technická univerzita v Bratislave, Bratislava, 2021. ISBN 978-80-227-5114-8
- [7] B. Veverka: *Topografická a matematická kartografie*, Vydavatelství ČVUT, Praha, 1997. ISBN 978-80-227-5114-8

Non-generic curves of given direction

Zbyněk Šír

*Faculty of Mathematics and Physics, Charles University Prague
Sokolovská 83, Praha 186 75, Czech Republic
email: zbynek.sir@mff.cuni.cz*

Abstract. A new method was given recently for constructing rational curves with Pythagorean directions. Existing results focus mostly on the generic cases. We formulate the problem for curves with any given direction and show on the level of examples how non-genericity influences the degree of the constructed curves.

Keywords: tangent indicatrix, rational curve, polynomial curve, Pythagorean hodograph curve, Laurent series

1 Introduction

Polynomial and rational parametric curves are a traditional topic of Computer Aided Geometric Design and frequently appear in geometric modeling or numeric simulations. Following problem was recently studied in the context of curves with Pythagorean hodograph. We provide its formulation independent of the Pythagorean hodograph concept.

Problem 1.1. *Given a rational spatial curve $\mathbf{F}(t)$ determine the vector space of all the spatial rational curves $\mathbf{r}(t)$ having $\mathbf{F}(t)$ for its tangent field, i.e. satisfying*

$$\mathbf{r}'(t) \times \mathbf{F}(t) = 0.$$

This family of curves was first investigated in [1] where the envelope approach to planar rational PH curves was generalized to rational PH space curves. While being rather straightforward and comprehensive, it seems that degree of the denominator polynomial and curve shape are difficult to control. The dual approach was continued in series of papers [3, 4, 5] where the authors solve interpolation problems with with rational spatial PH curves of low class.

In [2, 6] a new and more direct computational approach to Problem 1.1 was developed. It is based on solving of system of linear equations. Despite its complexity an analysis and description of all solutions was given for generic case.

In Section 2 we summarize the principal result of [6] for denominators with single root which is generic. Then we provide one new example for tangent indicatrix of degree 4. In Section 3 we present several new examples for non-generic data. We show how different cases of non-genericity influence one particular kind of solutions. Eventually we conclude the paper.

2 Generic solutions

The case of generic denominators was studied in [6] in great detail and with rigorous proofs. The genericity means that the set of roots of the denominator of \mathbf{r} does not contain any inflection points of \mathbf{F} . For our purposes it is sufficient to consider only denominators with single roots (of possibly higher multiplicity). Then the precise definition of genericity becomes:

Definition 2.1. The data $\mathbf{F}(t)$, β are called *generic* if any three consecutive coefficients \mathbf{f}_{i-1} , \mathbf{f}_i , \mathbf{f}_{i+1} in the Taylor expansion of $\mathbf{F} = \sum_{i=0}^{2a} \mathbf{f}_i(t-\beta)^i$ at β are linearly independent. Otherwise the data are called *non-generic*.

It was shown in that for generic case there exist solutions \mathbf{r} which have minimal possible length of their Laurent expansions at $t = \beta$. Theorem 3.6 of [6] can be equivalently rephrased in the following way:

Theorem 2.2. For generic \mathbf{F} , β there exist precisely following solutions of minimal length which generate the complete space of solutions to Problem 1.1

- One dimensional spaces of solutions of the form

$$\sum_{i=m}^{m+\deg \mathbf{F}} \mathbf{a}_i(t-\beta)^i$$

for any $m < \deg \mathbf{F}$ or $m > 0$. We call these solutions regular.

- One dimensional spaces of solutions of the form

$$\sum_{i=m}^{m+\deg \mathbf{F}+3} \mathbf{a}_i(t-\beta)^i$$

for any $\deg \mathbf{F} \leq m \leq -3$. We call these solutions non-regular.

Let us demonstrate this generic behavior on the following example.

Example 2.3. Let us consider $\beta = 0$ the tangent field with $\deg \mathbf{F} = 4$

$$\mathbf{F} = \begin{pmatrix} -2t^4 + t^3 + t + 1 \\ t^4 + 2t^3 + t^2 + 2t + 1 \\ 3t^4 + 3t^3 + t^2 - t + 1 \end{pmatrix}.$$

The minimal length solutions of Theorem 2.2 have ranges shown in Figure 1. The regular solutions (shown in black) continue regularly toward $\pm\infty$.

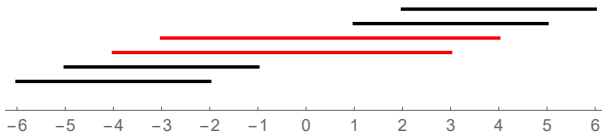


Fig. 1: Ranges of the minimal length solutions for Example 2.3. Regular solutions are potted in black, non-regular in red.

The spaces for each range are one dimensional and we computed their generators explicitly:

$$\begin{pmatrix} -\frac{60}{t^2} + \frac{20}{t^3} + \frac{12}{t^5} + \frac{10}{t^6} \\ \frac{30}{t^2} + \frac{40}{t^3} + \frac{15}{t^4} + \frac{24}{t^5} + \frac{10}{t^6} \\ \frac{90}{t^2} + \frac{60}{t^3} + \frac{15}{t^4} - \frac{12}{t^5} + \frac{10}{t^6} \end{pmatrix},$$

$$\begin{pmatrix} -\frac{120}{t} + \frac{30}{t^2} + \frac{15}{t^4} + \frac{12}{t^5} \\ \frac{60}{t} + \frac{60}{t^2} + \frac{20}{t^3} + \frac{30}{t^4} + \frac{12}{t^5} \\ \frac{180}{t} + \frac{90}{t^2} + \frac{20}{t^3} - \frac{15}{t^4} + \frac{12}{t^5} \end{pmatrix},$$

$$\begin{pmatrix} 8t^3 - 66t^2 + 84t - \frac{36}{t} - \frac{24}{t^2} + \frac{8}{t^3} + \frac{3}{t^4} \\ -4t^3 + 18t^2 + 96t - \frac{72}{t} - \frac{12}{t^2} + \frac{12}{t^3} + \frac{3}{t^4} \\ -12t^3 + 72t^2 + 132t + \frac{120}{t} - \frac{30}{t^2} + \frac{3}{t^4} \end{pmatrix},$$

$$\begin{pmatrix} -12t^4 + 12t^3 - 27t^2 + 84t - \frac{18}{t} - \frac{3}{t^2} + \frac{6}{t^3} \\ 6t^4 + 14t^3 + 18t^2 + 72t - \frac{24}{t} + \frac{6}{t^2} + \frac{6}{t^3} \\ 18t^4 + 18t^3 + 39t^2 - 12t + \frac{48}{t} - \frac{21}{t^2} + \frac{6}{t^3} \end{pmatrix},$$

$$\begin{pmatrix} -24t^5 + 15t^4 + 30t^2 + 60t \\ 12t^5 + 30t^4 + 20t^3 + 60t^2 + 60t \\ 36t^5 + 45t^4 + 20t^3 - 30t^2 + 60t \end{pmatrix},$$

$$\begin{pmatrix} -20t^6 + 12t^5 + 20t^3 + 30t^2 \\ 10t^6 + 24t^5 + 15t^4 + 40t^3 + 30t^2 \\ 30t^6 + 36t^5 + 15t^4 - 20t^3 + 30t^2 \end{pmatrix}.$$

3 Non-generic Laurent cuts

The case of non-generic denominators was not completely analyzed yet. It transpires from the proofs of [6], however, that the regular solutions of Theorem 2.2 will be the same as in the generic case while there can be more non-regular solutions and/or their ranges can be shifted. We will now show this behavior on several examples.

Example 3.1. Let us consider $\beta = 0$ the tangent field with $\deg \mathbf{F} = 4$

$$\mathbf{F} = \begin{pmatrix} t^4 + t^3 + 2t^2 + t + 1 \\ 2t^3 + 3t^2 + 2t + 1 \\ 3t^3 - t + 1 \end{pmatrix}.$$

The vectors $\{\mathbf{F}(0), \mathbf{F}'(0), \mathbf{F}''(0)\}$ are linearly dependent. The minimal length solutions have ranges shown in Figure 2. The regular solutions (shown in black) continue regularly toward $\pm\infty$.

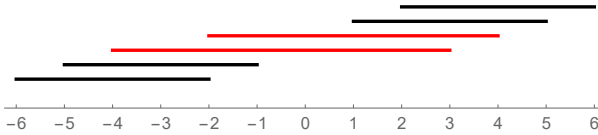


Fig. 2: Ranges of the minimal length solutions for Example 3.1. Regular solutions are potted in black, non-regular in red.

The non-genericity in this case shorten one of the non-regular solutions which now starts at t^{-2} . This is actually a welcome feature which produces a solution with denominator of low degree 2. The spaces for each range are one dimensional and we computed their generators explicitly:

$$\begin{pmatrix} \frac{30}{t^2} + \frac{20}{t^3} + \frac{30}{t^4} + \frac{12}{t^5} + \frac{10}{t^6} \\ \frac{40}{t^3} + \frac{45}{t^4} + \frac{24}{t^5} + \frac{10}{t^6} \\ \frac{60}{t^3} - \frac{12}{t^5} + \frac{10}{t^6} \end{pmatrix},$$

$$\begin{pmatrix} \frac{60}{t} + \frac{30}{t^2} + \frac{40}{t^3} + \frac{15}{t^4} + \frac{12}{t^5} \\ \frac{60}{t^2} + \frac{60}{t^3} + \frac{30}{t^4} + \frac{12}{t^5} \\ \frac{90}{t^2} - \frac{15}{t^4} + \frac{12}{t^5} \end{pmatrix},$$

$$\begin{pmatrix} -18t^3 - 3t^2 - 78t + \frac{66}{t} + \frac{9}{t^2} + \frac{14}{t^3} + \frac{6}{t^4} \\ -54t^2 - 66t + \frac{60}{t} + \frac{30}{t^2} + \frac{22}{t^3} + \frac{6}{t^4} \\ -81t^2 + 144t + \frac{174}{t} - \frac{33}{t^2} - \frac{2}{t^3} + \frac{6}{t^4} \end{pmatrix},$$

$$\begin{pmatrix} 3t^4 + 8t^3 + 12t^2 + 24t + \frac{6}{t^2} \\ 8t^3 + 30t^2 + 36t + \frac{12}{t} + \frac{6}{t^2} \\ 12t^3 + 18t^2 - 48t - \frac{54}{t} + \frac{6}{t^2} \end{pmatrix},$$

$$\begin{pmatrix} 12t^5 + 15t^4 + 40t^3 + 30t^2 + 60t \\ 30t^4 + 60t^3 + 60t^2 + 60t \\ 45t^4 - 30t^2 + 60t \end{pmatrix}.$$

Example 3.2. Let us consider $\beta = 0$ the tangent field with $\deg \mathbf{F} = 4$

$$\mathbf{F} = \begin{pmatrix} t^4 + 2t^3 + t^2 + t + 1 \\ 4t^3 + 2t^2 + 2t + 1 \\ 2t^3 + 3t^2 - t + 1 \end{pmatrix}.$$

The vectors $\{\mathbf{F}'(0), \mathbf{F}''(0), \mathbf{F}'''(0)\}$ are linearly dependent. The minimal length solutions have ranges shown in Figure 3. The regular solutions (shown in black) continue regularly toward $\pm\infty$.

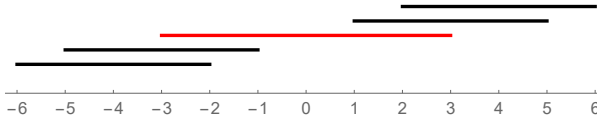


Fig. 3: Ranges of the minimal length solutions for Example 3.2. Regular solutions are potted in black, non-regular in red.

The non-genericity in this case combined the two non-regular solutions into one witch shorter range. The spaces for each range are one dimensional and we computed their generators explicitly:

$$\begin{pmatrix} \frac{30}{t^2} + \frac{40}{t^3} + \frac{15}{t^4} + \frac{12}{t^5} + \frac{10}{t^6} \\ \frac{80}{t^3} + \frac{30}{t^4} + \frac{24}{t^5} + \frac{10}{t^6} \\ \frac{40}{t^3} + \frac{45}{t^4} - \frac{12}{t^5} + \frac{10}{t^6} \end{pmatrix},$$

$$\begin{pmatrix} \frac{60}{t} + \frac{60}{t^2} + \frac{20}{t^3} + \frac{15}{t^4} + \frac{12}{t^5} \\ \frac{120}{t^2} + \frac{40}{t^3} + \frac{30}{t^4} + \frac{12}{t^5} \\ \frac{60}{t^2} + \frac{60}{t^3} - \frac{15}{t^4} + \frac{12}{t^5} \end{pmatrix},$$

$$\begin{pmatrix} 2t^3 + 9t^2 + 12t - \frac{6}{t} + \frac{2}{t^3} \\ 12t^2 + 36t - \frac{6}{t} + \frac{3}{t^2} + \frac{2}{t^3} \\ 6t^2 + 30t + \frac{18}{t} - \frac{6}{t^2} + \frac{2}{t^3} \end{pmatrix},$$

$$\begin{pmatrix} 6t^5 + 15t^4 + 10t^3 + 15t^2 + 30t \\ 30t^4 + 20t^3 + 30t^2 + 30t \\ 15t^4 + 30t^3 - 15t^2 + 30t \end{pmatrix},$$

$$\begin{pmatrix} 10t^6 + 24t^5 + 15t^4 + 20t^3 + 30t^2 \\ 48t^5 + 30t^4 + 40t^3 + 30t^2 \\ 24t^5 + 45t^4 - 20t^3 + 30t^2 \end{pmatrix}.$$

Example 3.3. Let us consider $\beta = 0$ the tangent field with $\deg \mathbf{F} = 4$

$$\mathbf{F} = \begin{pmatrix} t^4 + t^3 + t^2 + t + 1 \\ 2t^4 + t^2 + t + 1 \\ 3t^4 + t^3 + t^2 + t + 1 \end{pmatrix}.$$

In this example the vectors $\{\mathbf{F}(0), \mathbf{F}'(0), \mathbf{F}''(0)\}$ are all multiples of the same vector. The minimal length solutions have ranges shown in Figure 4. The regular solutions (shown in black) continue regularly toward $\pm\infty$.

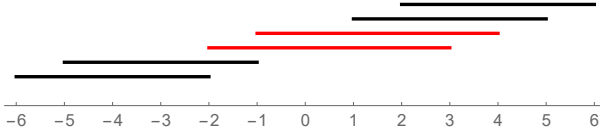


Fig. 4: Ranges of the minimal length solutions for Example 3.3. Regular solutions are potted in black, non-regular in red.

The non-genericity in this case is very strong and shortens both non-regular solutions. This way there exist solutions with linear denominators. The spaces for each range are one dimensional and we computed their generators explicitly:

$$\begin{aligned}
 & \begin{pmatrix} \frac{30}{t^2} + \frac{20}{t^3} + \frac{15}{t^4} + \frac{12}{t^5} + \frac{10}{t^6} \\ \frac{60}{t^2} + \frac{15}{t^4} + \frac{12}{t^5} + \frac{10}{t^6} \\ \frac{90}{t^2} + \frac{20}{t^3} + \frac{15}{t^4} + \frac{12}{t^5} + \frac{10}{t^6} \end{pmatrix}, \\
 & \begin{pmatrix} \frac{60}{t} + \frac{30}{t^2} + \frac{20}{t^3} + \frac{15}{t^4} + \frac{12}{t^5} \\ \frac{120}{t} + \frac{20}{t^3} + \frac{15}{t^4} + \frac{12}{t^5} \\ \frac{180}{t} + \frac{30}{t^2} + \frac{20}{t^3} + \frac{15}{t^4} + \frac{12}{t^5} \end{pmatrix}, \\
 & \begin{pmatrix} 2t^3 + \frac{3}{t^2} \\ 4t^3 - 6t^2 + 6t + \frac{3}{t^2} \\ 6t^3 - 6t^2 + \frac{3}{t^2} \end{pmatrix}, \\
 & \begin{pmatrix} 3t^4 + \frac{12}{t} \\ 6t^4 - 8t^3 + 6t^2 + \frac{12}{t} \\ 9t^4 - 8t^3 + \frac{12}{t} \end{pmatrix}, \\
 & \begin{pmatrix} 12t^5 + 15t^4 + 20t^3 + 30t^2 + 60t \\ 24t^5 + 20t^3 + 30t^2 + 60t \\ 36t^5 + 15t^4 + 20t^3 + 30t^2 + 60t \end{pmatrix}, \\
 & \begin{pmatrix} 10t^6 + 12t^5 + 15t^4 + 20t^3 + 30t^2 \\ 20t^6 + 15t^4 + 20t^3 + 30t^2 \\ 30t^6 + 12t^5 + 15t^4 + 20t^3 + 30t^2 \end{pmatrix}.
 \end{aligned}$$

Example 3.4. Let us consider $\beta = 0$ the tangent field with $\deg \mathbf{F} = 4$

$$\mathbf{F} = \begin{pmatrix} t^4 + t^3 + t^2 + t + 1 \\ t^3 + t^2 + t + 1 \\ t^4 + t^3 + t^2 + t + 1 \end{pmatrix}.$$

In this example the vectors $\{\mathbf{F}(0), \mathbf{F}'(0), \mathbf{F}''(0), \mathbf{F}'''(0)\}$ are all multiples of the same vector. The minimal length solutions have ranges shown in Figure 5. The regular solutions (shown in black) continue regularly toward $\pm\infty$.

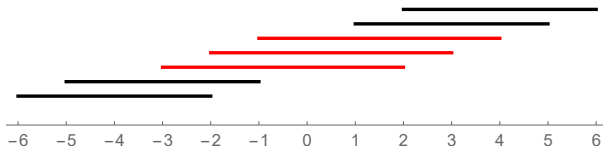


Fig. 5: Ranges of the minimal length solutions for Example 3.4. Regular solutions are potted in black, non-regular in red.

The non-genericity in this case is extremely strong and produces one extra non-regular solutions. The spaces for each range are one dimensional and we computed their generators explicitly:

$$\begin{pmatrix} \frac{30}{t^2} + \frac{20}{t^3} + \frac{15}{t^4} + \frac{12}{t^5} + \frac{10}{t^6} \\ \frac{20}{t^3} + \frac{15}{t^4} + \frac{12}{t^5} + \frac{10}{t^6} \\ \frac{30}{t^2} + \frac{20}{t^3} + \frac{15}{t^4} + \frac{12}{t^5} + \frac{10}{t^6} \end{pmatrix},$$

$$\begin{pmatrix} \frac{60}{t} + \frac{30}{t^2} + \frac{20}{t^3} + \frac{15}{t^4} + \frac{12}{t^5} \\ \frac{30}{t^2} + \frac{20}{t^3} + \frac{15}{t^4} + \frac{12}{t^5} \\ \frac{60}{t} + \frac{30}{t^2} + \frac{20}{t^3} + \frac{15}{t^4} + \frac{12}{t^5} \end{pmatrix},$$

$$\begin{pmatrix} 3t^2 + \frac{2}{t^3} \\ 6t + \frac{2}{t^3} \\ 3t^2 + \frac{2}{t^3} \end{pmatrix}, \begin{pmatrix} 2t^3 + \frac{3}{t^2} \\ 3t^2 + \frac{3}{t^2} \\ 2t^3 + \frac{3}{t^2} \end{pmatrix}, \begin{pmatrix} 3t^4 + \frac{12}{t} \\ 4t^3 + \frac{12}{t} \\ 3t^4 + \frac{12}{t} \end{pmatrix},$$

$$\begin{pmatrix} 12t^5 + 15t^4 + 20t^3 + 30t^2 + 60t \\ 15t^4 + 20t^3 + 30t^2 + 60t \\ 12t^5 + 15t^4 + 20t^3 + 30t^2 + 60t \end{pmatrix},$$

$$\begin{pmatrix} 10t^6 + 12t^5 + 15t^4 + 20t^3 + 30t^2 \\ 12t^5 + 15t^4 + 20t^3 + 30t^2 \\ 10t^6 + 12t^5 + 15t^4 + 20t^3 + 30t^2 \end{pmatrix}.$$

4 Conclusion

We have shown on several examples the structure of the solution space to Problem 1.1 for non-generic data. In the future we plan to systematically elucidate the non-generic data case in general dimension.

Acknowledgements

Zbyněk Šír was supported by the grant 20–11473S of the Czech Science Foundation.

References

- [1] R. T. Farouki, Z. Šír: *Rational Pythagorean-hodograph space curves*. Comput. Aided Geom. Design, 28:75–88, 2011
- [2] B. Kalkan, D. F. Scharler, H.-P. Schröcker, Z. Šír: *Rational Framing Motions and Spatial Rational Pythagorean Hodograph Curves*, accepted to Comput. Aided Geom. Design, 2022
- [3] J. Kozak, M. Krajnc, V. Vitrih: *Dual representation of spatial rational Pythagorean-hodograph curves*. Comput. Aided Geom. Design, 31:43–56, 2014
- [4] J. Kozak, M. Krajnc, V. Vitrih: *G^1 interpolation by rational cubic PH curves in \mathbb{R}^3* . Comput. Aided Geom. Design, 42:7–22, 2016
- [5] M. Krajnc: *Interpolation with spatial rational pythagorean-hodograph curves of class 4*. Comput. Aided Geom. Design, 56:16–34, 2017
- [6] H.-P. Schröcker, Z. Šír: *Partial Fraction Decomposition for Rational Pythagorean Hodograph Curves*, submitted to *Journal of Computational and Applied Mathematics*, preprint arXiv:2210.13177

Geometria pre študijný program Matematicko-počítačové modelovanie na SvF STU v Bratislave

Geometry for study programm Mathematical and Computational Modeling at FCE SUT in Bratislava

Zuzana Tereňová

*Department of Mathematics and Descriptive Geometry, Faculty of Civil Engineering,
Slovak University of Technology in Bratislava
Radlinského 11, 810 05 Bratislava, Slovak Republic
email: zuzana.terenova@stuba.sk*

Abstract. The paper focuses on the course Geometry at the Faculty of Civil Engineering SUT in Bratislava, which is intended for students of the study programm Mathematical and Computational Modeling, and its content is also adapted to this. It combines classical descriptive geometry with the analytical expression of curves and surfaces, which allows students to visualize these curves and surfaces in some mathematical software, e. g. in software Mathematica. Analytical expressions relate to conics and some surfaces of technical practice, namely non-developable ruled surfaces, surfaces of revolution and helical surfaces.

Keywords: Geometry, study programm, mathematical and computational modeling

Kľúčové slová: Geometria, študijný program, matematicko-počítačové modelovanie

1 Študijný program Matematicko-počítačové modelovanie

Všetky študijné programy na Stavebnej fakulte STU v Bratislave majú v prvom semestri štúdia povinný predmet, v ktorom sa študenti oboznámia so základmi deskriptívnej geometrie a s ich aplikáciami v stavebných odboroch. Obsah predmetu sa pre jednotlivé študijné programy líši práve v aplikáciách zobrazovacích metód pri zobrazovaní objektov v konkrétnych oblastiach stavebnej praxe. V tomto článku sa venujeme študijnému programu Matematicko-počítačové modelovanie (MPM).

Absolventi študijného programu MPM získajú vzdelanie v odbore aplikovaná matematika s orientáciou na počítačové modelovanie a analýzu inžinierskych úloh. Počas štúdia sa oboznámia s metódami aplikovanej matematiky (numerické, štatistické, optimalizačné, grafické a vizualizačné metódy). Okrem toho sa naučia pracovať s počítačom (programovacie jazyky, operačné systémy, počítačové siete, licencované softvéry). Získané poznatky aplikujú vo vede a technike a to v rôznych oblastiach, napr. stavebné, elektrotechnické, strojnícke inžinierstvo, bioinžinierstvo, geodézia, informatika, počítačová grafika, spracovanie obrazu, štatistická analýza dát, ako aj v oblasti niektorých

ekonomických a finančných aplikácií. Informácie o študijnom programe MPM a ukážky záverečných prác študentov bakalárskeho a inžinierskeho štúdia sú na stránke [4].

2 Obsah predmetu Geometria

Predmet Geometria, ktorý je zaradený do prvého semestra v bakalárskom štúdiu študijného programu MPM, má stanovený týždenný rozsah výučby na 2 hodiny prednášok a 2 hodiny cvičení. Obsah tohto predmetu tvorí klasická deskriptívna geometria, kde študenti riešia jednotlivé úlohy bez použitia počítača, t. j. rysujú na papier. Okrem toho sú niektoré témy doplnené o analytické vyjadrenia kriviek a plôch, čo umožňuje študentom zobraziť tieto krivky a plochy v nejakom matematickom softvéri. Jednotlivé témy sú podrobnejšie rozpísané v nasledujúcich častiach článku.

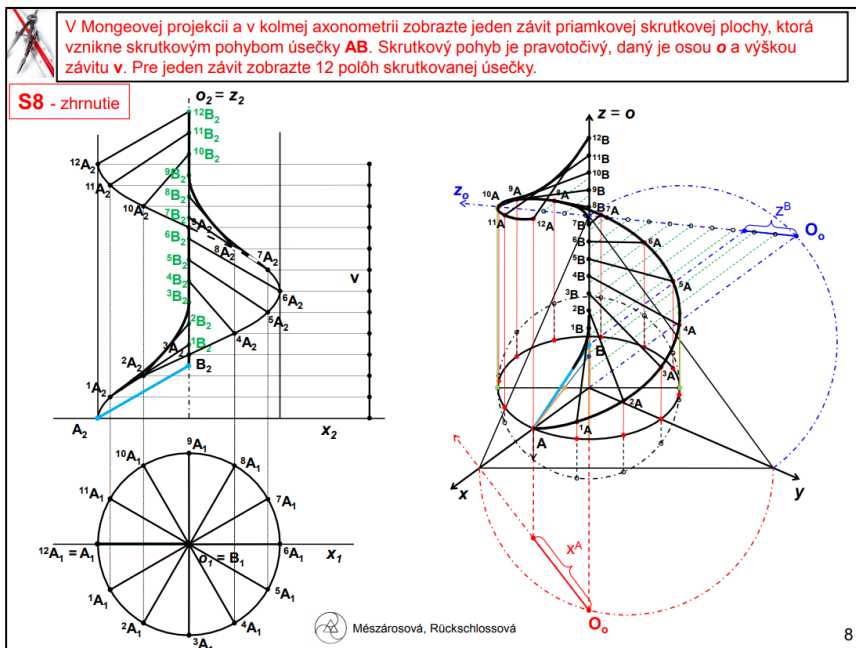
2.1 Deskriptívna geometria

Študenti sa naučia princípy rovnobežného a stredového premietania a tri zobrazovacie metódy (Mongeova projekcia, axonometria, lineárna perspektíva). V jednotlivých zobrazovacích metódach potom zobrazujú objekty. Obsah predmetu tvoria tieto témy:

- Kužeľosečky: definície kužeľosečiek a ich konštrukcie, pričom sa dôraz kladie na konštrukcie elipsy a paraboly.
- Rovnobežné a stredové premietanie: princípy zobrazení a ich vlastností.
- Mongeova projekcia: princíp zobrazenia, zobrazenie jednoduchých telies a ich rezov rovinami rovnobežnými s priemetňami.
- Axonometria: princíp zobrazenia, zobrazenie jednoduchých telies s podstavou v súradnicovej rovine.
- Plochy stavebnej praxe: definície plôch a ich zobrazenie v Mongeovej projekcii a v axonometrii. Sú to
 - priamkové rozvinuteľné a nerozvinuteľné plochy,
 - rotačné plochy,
 - skrutkové plochy,
 - translačné, klinové a kanálové plochy.
- Stredové premietanie a lineárna perspektíva: princíp zobrazenia, zobrazenie telies stopníkovovo-úbežníkovou metódou.
- Čiary: homogénna sústava súradníc, krivosť čiary, interpolácia, aproximácia a spojitosť čiar.

Prednášky aj cvičenia sú spracované vo forme prezentácií programu PowerPoint a študenti ich majú k dispozícii v akademickom informačnom systéme. Okrem toho môžu využívať elektronické skriptá, kde sú spracované rotačné a skrutkové plochy (pozri [1]), priamkové, translačné, klinové a kanálové plochy (pozri [2]) a stredové premietanie a lineárna perspektíva (pozri [3]). Prostredníctvom týchto prezentácií majú študenti dostatočné množstvo riešených

príkladov, čo im umožňuje lepšie pochopiť jednotlivé témy. Na obr. 1 je ukážka jedného príkladu zo skrípt [1], kde je zobrazený jeden závit uzavretej šikmej priamkovej skrútkovej plochy v Mongeovej projekcii a v kolmej axonometrii.

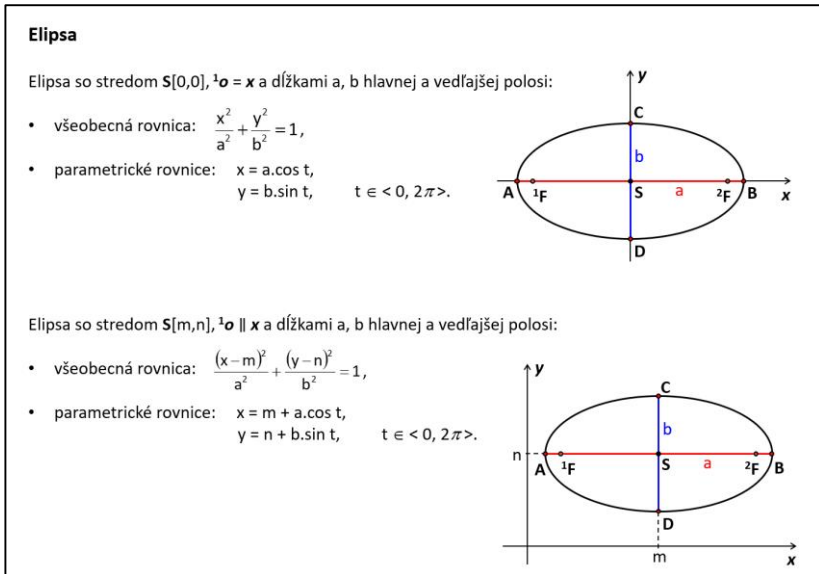


Obr. 1: Uzavretá šikmá priamková skrútková plocha

2.2 Analytické vyjadrenia

Niektoré témy predmetu Geometria sú doplnené o analytické vyjadrenia kriviek a plôch. V rámci tohto predmetu nie je priestor na prácu s nejakým novým softvérom, ale v prvom semestri bakalárskeho štúdia majú študenti študijného programu MPM aj predmet Softvér (Mathematica), kde sa učia pracovať s týmto softvérom. Preto môžu získané analytické vyjadrenia použiť na modelovanie kriviek a plôch práve v softvéri Mathematica.

Pri téme kužeľosečiek sa študenti naučia zistiť typ kužeľosečky z jej všeobecnej rovnice a to pomocou determinantov. Okrem toho sa dozvedia všeobecné a parametrické rovnice kužeľosečiek, ktoré majú osi rovnobežné so súradnicovými osami, obr. 2. Parametrické rovnice týchto kužeľosečiek budú potrebné pri určovaní parametrických rovníc plôch.

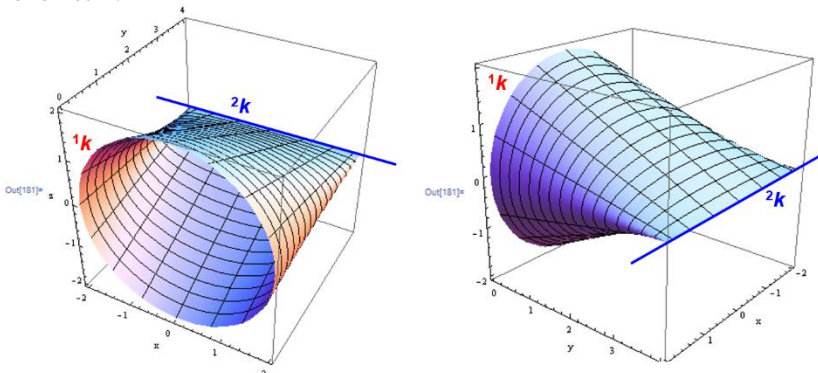


Obr. 2: Analytické vyjadrenie elipsy

Priamkové rozvinuteľné aj nerozvinuteľné plochy vyjadrujeme pomocou parametrických rovníc. Pri nerozvinuteľných plochách uvažujeme s istými obmedzeniami a to kvôli výpočtom rovníc. Pre určujúce krivky týchto plôch platí:

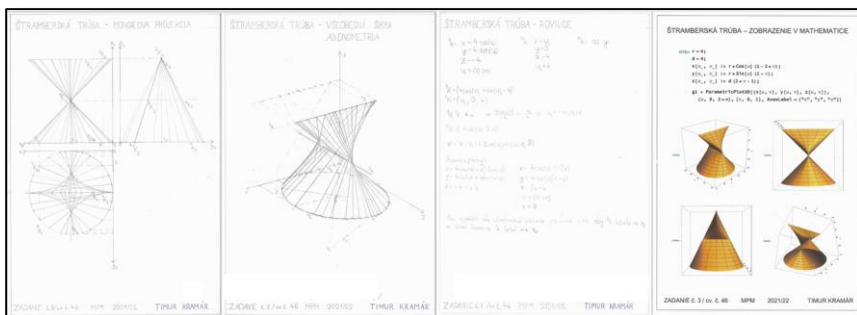
- pri cylindroidoch je riadiaca rovina rovnobežná s niektorou súradnicovou rovinou,
- pri konusoidoch je jedna riadiaca krivka niektorá súradnicová os.

Na obr. 3 je zobrazený kružnicový konoid v softvéri Mathematica. Táto plocha je zobrazená v skriptách [2] a to v Mongeovej projekcii a aj v kolmej axonometrii.



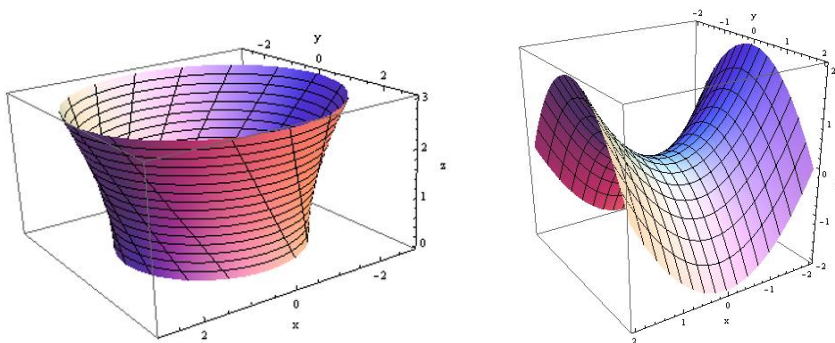
Obr. 3: Kružnicový konoid

Nerozvinuteľné priamkové plochy zobrazujú študenti aj na zadani, ktoré vypracujú doma. Hodnotenie zadania je súčasťou hodnotenia celého predmetu. Študenti zobrazujú jednu plochu v Mongeovej projekcii, v axonometrii, počítajú parametrické rovnice tejto plochy a ako dobrovoľná časť tohto zadania je aj zobrazenie plochy v nejakom matematickom softvéri. Na obr. 4. je jedno takéto vypracované zadanie.



Obr. 4: Štramberská trúba

Parametrické rovnice rotačných, resp. skrutkových plôch, kde os rotácie, resp. os skrutkového pohybu, je súradnicová os z , sa určia jednoducho. Rovnako je to aj s translačnými plochami. Na obr. 5 je v softvéri Mathematica zobrazený jednodielny rotačný hyperboloid a hyperbolický paraboloid ako translačná plocha.



Obr. 5: Jednodielny rotačný hyperboloid a hyperbolický paraboloid

Poslednou témou na predmete Geometria sú čiary. Študenti sa naučia zapisovať vlastné a nevlastné body pomocou homogénnych súradníc, vyjadriť prvú a druhú krivosť čiary a aj geometrický význam týchto krivostí. Okrem toho sa oboznámia s typmi modelovania (interpolácia, aproximácia), s niektorými

kubickými oblúkmi (Fergusonova kubika, Bezierova kubika, Coonsova B-splajn kubika) a so spojitosťou čiar (parametrická a geometrická spojitosť).

3 Záver

Študenti študijného programu Matematicko-počítačové modelovanie získajú v predmete Geometria informácie o princípoch a vlastnostiach rovnobežného a stredového premietania, ktoré neskôr môžu využiť pri svojom ďalšom štúdiu alebo v praxi. Okrem toho sa oboznámia s analytickými vyjadreniami kriviek a plôch, pomocou ktorých ich jednoducho vymodelujú v nejakom vhodnom softvéri.

PodĎakovanie

Tento článok vznikol za podpory grantového projektu KEGA 008STU-4/2020.

Literatúra

- [1] K. Mészárosová, T. Rückschlossová, Z. Tereňová: *Deskriptívna geometria II: Prvá časť – Rotačné a skrutkové plochy*, Slovenská technická univerzita v Bratislave, 2014. ISBN 978-80-227-4275-7. Dostupné online: <http://math.sk/skriptaDG2/1/>
- [2] K. Mészárosová, T. Rückschlossová, Z. Tereňová: *Deskriptívna geometria II: Druhá časť – Priamková, translačné, klinové a kanálové plochy*, Slovenská technická univerzita v Bratislave, 2018. ISBN 978-80-227-4767-7. Dostupné online: <http://math.sk/skriptaDG2/2/>
- [3] K. Mészárosová, Z. Tereňová: *Deskriptívna geometria I: Stredové premietanie a lineárna perspektíva*, Slovenská technická univerzita v Bratislave, 2019. ISBN 978-80-227-4929-9. Dostupné online: <https://www.vydavatelstvo.stuba.sk/online-knihy/deskriptivna-geometria-1>
- [4] <https://www.math.sk/mpm/>

Vedutes and their geometric character

Margita Vajsáblová

*Department of mathematics and descriptive geometry, Faculty of Civil Engineering,
Slovak University of Technology in Bratislava
Radlinského 11, 810 05 Bratislava, Slovak Republic
email: margita.vajsablova@stuba.sk*

Abstract. Vedutes of cities, castles and military fortresses are a frequent part of the historical maps, however, they also form separate works that have an artistic, cartographic, but also geometrical character. From the point of view of archaeological research, vedutes have an important informative character documenting objects of the past times. In the contribution, we will present projection methods used in the vedutes and sample of the analysis of the geometric shape of the Nové Zámky fortress and a comparison with the shape presented on the vedutes by Johann Ledentu.

Keywords: veduta, projection methods, fortress, conformal conic projection

1 Introduction

For us, the vedutes of cities and fortresses have an artistic, but also a historical and documentary value, which makes a significant statement about the events of the given period [4]. A veduta is defined like a highly detailed, usually large-scale painting or, more often, print of a cityscape or some other vista. Vedutes were widespread from the 17th century to the mid-19th century, used e.g. on old maps; veduta painting reached its peak in the 17th and 18th centuries in the Netherlands and Venice.

The creators of vedutes, called vedutists, processed the image of objects on a different geometric level, which significantly affects the value of the statement about the objects of the given time. In the article, we will show the range of projection methods used by vedutists. A frequent phenomenon is that they idealize the geometric regularity of the shapes of parts of cities, castles or fortresses, which we will show using the example of the Nové Zámky fortress. We will also present an analysis of the geometric shape of the Nové Zámky fortress and a comparison with the shape presented on the vedutes by Johann Ledentu.

Vedutes were very often part of historical maps, vedutes of important cities were located on the edges of maps of the world, continents and countries. In the study of their geometric aspects, we worked with vedutes that form a separate work.

2 Geometry and vedutes

In 1686, Anton Ernst Burckhard von Birckenstein (active 1686-1744) published *Erzherzogliche Handgriffe des Zirkels und Linials* in Vienna (three years later in

Augsburg) as a geometry textbook for the eight-year-old Prince Joseph (1678 – 1711), son of the King of Hungary and Bohemia, Archduke of Austria and Emperor of the Holy Roman Empire of the German nation Leopold (1640 – 1705). The book contains 110 vedutes of Hungarian cities, castles, fortresses and mansions, in the upper parts with a structural geometric study, the process of which is described in the introductory part of the book. The vedutes are complemented by figures, often with motifs associated with the Turkish threat and plunder. The author of copper engravings combined with etching (with a uniform size of 163 x 100 mm) is a Dutchman from Utrecht, Justus van der Nypoort (around 1625 – after 1692) [3]. In Fig. 1 (left) is a veduta of the Hungarian city of Hatvan with a construction of a triangle similar to the given triangle and a description of this construction is in Fig. 1 (right).



Fig. 1: Sample from the book *Erzherzogliche Handgriffe des Zirkels und Linial* by Anton Ernst Burckhard von Birckenstein [1]

Vedutists used several projection methods, such as perpendicular projections (horizontal projection, vertical projection), various types of axonometry, central perspective of the object in frontal and non-frontal positions, and also a panorama, which intuitively indicated the properties of a cylindrical perspective.

The veduta, on which the horizontal projection is used, is considered a map city plan, or fortress plan. On the Fig. 7 is veduta of the Nové Zámky fortress created by Johann Ledentu with using **Horizontal orthogonal projection with vertical profiles**.

Vertical orthogonal projection with shading on the vedutes of Fraknó Castle (Burg Forchtenstein) is shown in Fig. 2. This castle is one of the symbols of Burgenland.



Fig. 2: Vertical orthogonal projection on the veduta of Frakno Castle created by Justus van der Nypoort [1]

A demonstration of **Cavalier perspective (axonometry)** is on the veduta on Fig. 3, it is the most beautiful and perhaps the most reliably depicted Trnava, as it looked at the beginning of the 1840s. The author was the young Austrian Josef Jäger (1721–1793). The woodcut was used for the first time only in 1781.



Fig. 3: Cavalier axonometry on the veduta of Trnava created by Josef Jäger [2]

The most used projection method on vedutes was **Central perspective**. An example of **Central perspective of the object in the frontal position** is on the veduta of the Estherházy Castle in Kismarton (Eisenstadt), Fig. 4. Originally built in the Gothic style (1364) by the Kanizsai family, it was rebuilt into a charming Baroque castle in the second half of the 17th century. The castle underwent classicist modifications at the end of the 18th century. Today, two-thirds of all premises are home to the federal government of the state of Burgenland [10]. The veduta of the Estherházy Castle in Kismarton is created by Justus van der Nypoort in a Central perspective of the object in the frontal position, where the Principal point (equal Vanishing point) is to the upper right of the image of the object. It is therefore a **bird's eye perspective**, but it also has an error in the incorrectly projected left garden wall.

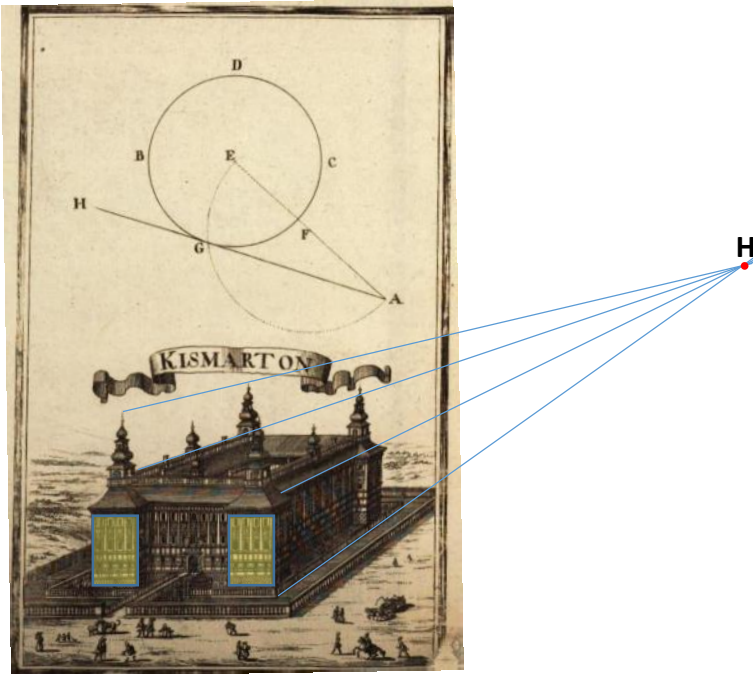


Fig. 4: Central perspective in veduta of Kismarton (Eisenstadt) created by Justus van der Nypoort [1]

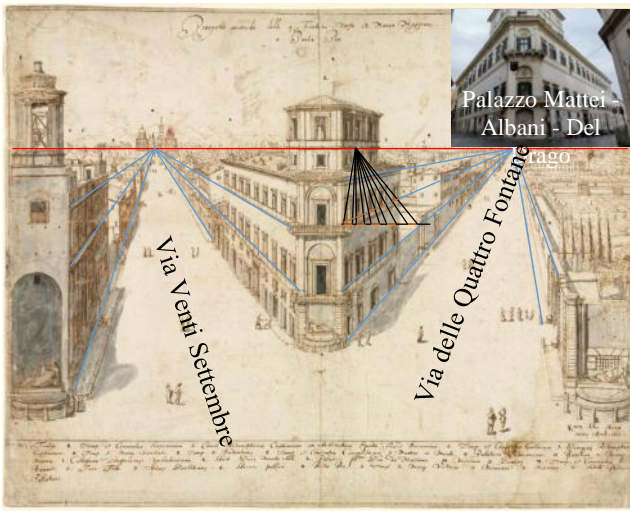


Fig. 5: Central perspective in veduta The Quattro Fontane Looking Toward Santa Maria Maggiore created by Lieven Cruyl [9]

Central perspective of the object in the non-frontal position is applied on the vedutes of Dutch painter **Lieven Cruyl** (1634 – 1720), he is mainly known for his drawings and graphic work depicting cityscapes. The panoramic settings of the drawings and the precise technique are believed to have set a standard for veduta designers and painters after him. He preferred unusual and complex perspectives which reflect the scientific construction of his drawings. In Fig. 5 is his veduta called *The Quattro Fontane Looking Toward Santa Maria Maggiore* with a very precisely used Central perspective of the object in the non-frontal position.

Several vedutes of the 17th and 18th centuries featured the use of a **panorama** with an intuitive application of the geometric properties of the cylindrical perspective. In Fig. 6 is color panorama of the city of Trnava created in 1720. The author of the copper engraving from 1688 is Friedrich Bernhard Werner and the painter Johann Christian Leopold.



Fig. 6: Panorama of Trnava created by F. B. Werner and J. Ch. Leopold [8]

3 Analysis of the fortress Nové Zámky on the vedutes

In 1639 vedutes of the 2nd fortress Nové Zámky (Fig. 7 and 8) were created by Austrian painter, draftsman and engraver Johann Ledentu (1602 – 1654). The ground plan of this fortress was designed according to the model of the so-called „ideal cities“ to meet economic and military needs. It had the form of a regular hexagon with a rectangular street network and a central square. The fortress had 2 gates, Viedenská and Ostrihomská, and 6 bastions: Forgach Bastion (now Calvary); Bohemia Bastion; Ernest Bastion; Ceasarion Bastion; Michael or Fridrich Bastion; Jerome Bastion [7].

Johann Ledentu depicts the fortress of Nové Zámky as a city whose basic shape is a regular hexagon. This precondition was the basis for the creation of both vedutes, in Fig. 8 also see a correctly used Central perspective. As part of the research project, we analyzed the shape of the Nové Zámky fortress, using the following procedure:

- Determining the coordinates of the vertexes of the hexagon of the fortress walls from the map of Nové Zámky in Google Earth (Fig. 9).
- Calculation of geodetic line segment lengths on the ellipsoid GRS 80.
- Calculation of azimuths at the end points of geodetic lines.
- Transformation geodetic lines in the Lambert conformal conic projection with parameters for Slovak Republic (Fig. 10).
- Evaluation of the analysis results.

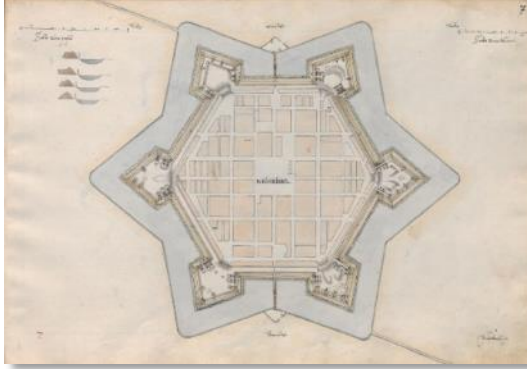


Fig. 7: Ground plan of the Nové Zámky fortress created by Johann Ledentu

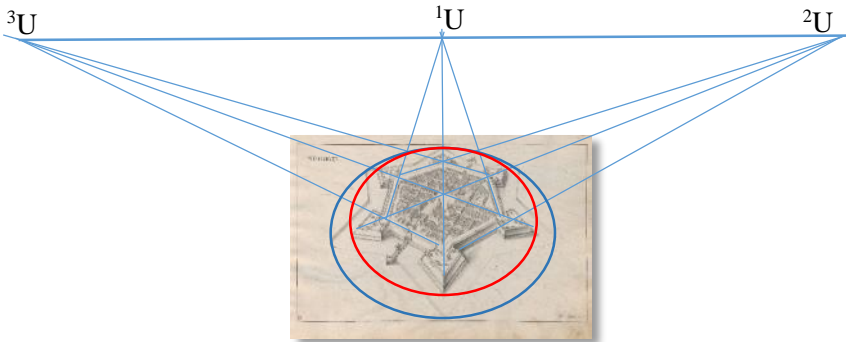


Fig. 8: Central perspective in the veduta of the Nové Zámky fortress created by Johann Ledentu

The Tab.1 shows the results of calculations of the lengths of the geodetic lines of the sides of the hexagon forming the original walls of the fortress and their azimuths. Calculation were realized in software WOLFRAM Mathematica. The results showed that shape of Nové Zámky fortress is **irregular hexagon with one axis of symmetry**, the longest walls have entrance gates and are approximately the same length and the remaining pairs of neighbouring walls are approximately the same length. Transformed hexagon is on the Fig. 10 (left) and displayed in the Google maps is on the Fig. 10 (right).

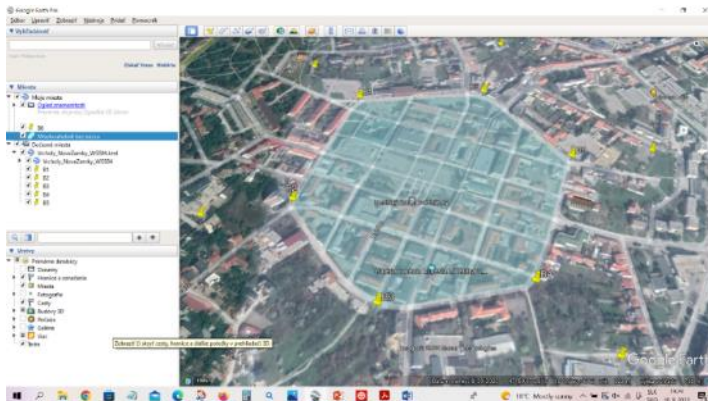


Fig. 9: Determining the coordinates in Google Earth

Bastion name	Latitude	Longitude	Azimuth	Distance [m]
Forgach	47°59'3.21"	18°9'56.35"	19°47'22"	231.6
Bohemia	47°59'10.26"	18°10'0.14"	317°58'13"	222.5
Ernest	47°59'15.76"	18°9'53.21"	266°48'4"	221.7
Caesarion	47°59'14.59"	18°9'43.08"	199°31'2"	232.9
Michael	47°59'7.49"	18°9'39.32"	138°30'53"	213.4
Jerome	47°59'2.32"	18°9'46.15"	82°34'18"	212.9

Tab. 1: Results of analyses

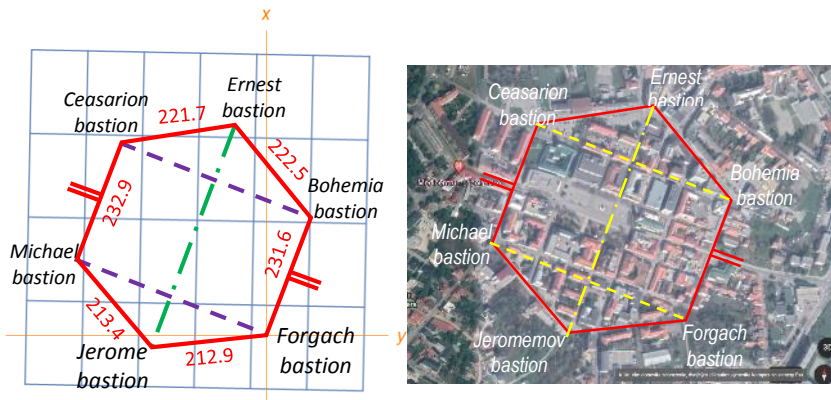


Fig. 10: Walls of the fortress in Lambert conformal conic projection for SR (left) and in the Google maps (right)

4 Conclusion

The paper showed that vedutes form an important part of cultural heritage and speak about the phenomena of the past with varying degrees of reliability. Geometric methods of projection on the vedutes exceed the level of works of art.

The analysis showed that the shape of the Nové Zámky fortress is not as symmetrical as it was supposed to be. Since we analysed only the walls of the fortress, the position of which determined the current shape of Nové Zámky center, it is necessary to investigate the position of other elements of the fortress in cooperation with archaeologists, using other sources such as old maps and surveys.

Acknowledgements

The paper was created with the support of grant projects VEGA 1/0468/20 and KEGA 008STU-4/2020.

References

- [1] A. E. Burckhard von Birckenstein: *Erzherzogliche Handgriffe des Zirkels und Linials*, Verlegung deß Verfassers, Vienna, 1686
- [2] L. Šebák: *Veduty Trnavy (1. časť)*. Kultúra - Blog denníka Sme. Dostupné online: <https://blog.sme.sk/sebak/veda-a-technika/veduty-trnavy-1-cast>
- [3] L. Šebák.: *Veduty miest, hradov, pevností a kaštieľov Karpatskej kotliny*, Kultúra - Blog denníka Sme. Dostupné online: <https://blog.sme.sk/sebak/kultura/veduty-miest-hradov-pevnosti-a-kastielov-karpatskej-kotliny>
- [4] Ľ. Trubíni, T. Lieskovský: *História cisárskej pevnosti Vrábľa*, Fontis, 2019
- [5] *WOLFRAM Mathematica 12.1.1.0*. Copyright 1988-2020 Wolfram Research, Inc.
- [6] *Google Earth*, Verzia 9.174.0.2
- [7] <https://www.novezamky.sk/historia-a-pamiatky-mesta/gs-1603> [cit. 2022-06-13]
- [8] https://www.webumenia.sk/dielo/SVK:GMB.C_6301 [cit. 2022-04-22]
- [9] <https://nationalmuseum-swe.tumblr.com/post/672574878354997248/eighteen-views-of-rome-the-quattro-fontane> [cit. 2022-06-13]
- [10] https://en.wikipedia.org/wiki/Schloss_Esterh%C3%A1zy

Pselical Surfaces

Daniela Velichová

*Institute of Mathematics and Physics, Faculty of Mechanical Engineering,
Slovak University of Technology in Bratislava
Nám. slobody 17, 812 31 Bratislava, Slovak Republic
email: Daniela.velichova@stuba.sk*

Abstract. Pselical surfaces form a specific group of surfaces that can be regarded as generalized two-axial surfaces of revolution, namely surfaces of Euler type. These surfaces can be generated from a basic curve by applying two systems of interlinked central collineations. Armiloid, as one typical representative of this group of surfaces, has been defined synthetically and presented in 1939 by Professor Dr. František Kadeřávek. In this paper we describe the synthetic construction of armiloid, introduce its analytic vector representation and further generalize the group of pselical surfaces. Illustrations of surface form variations are included.

Key words: Pselical surfaces, armiloid, central collineation, generalized surfaces of revolution, modelling surfaces

1 Armiloid and pselical surfaces synthetic definition

Pselical surfaces, and armiloid as one typical representative of this group, were defined and presented in 1939 by Professor Dr. František Kadeřávek (1885 - 1961) in his short paper „Generalisation of surfaces of revolution“ published in the scientific journal *Věstník Královské české společnosti nauk* (1939), třída matematicko-přírodovědná, volume 1939, XVII, [1], see Fig. 1 and Fig. 2.



Fig. 1: The first page of the published paper (digitized version)

Armiloid was defined as surface generated by a composite „movement“ of an arbitrary basic curve (Dr. Kadeřávek used a curve that is the front view of the cast shadow of a straight line on a torus), that is composed from two systems of interlinked central collinear transformations. Axes of these transformations are in two skew and perpendicular lines in the projective space, while centres of one system of the central collineations are located always on the axes of the other system involved. Even more, characteristics of the two related systems are inverse real numbers.

Surfaces generated by described generating principle form the group of pselical surfaces, and they can be generated from an arbitrary basic space curve, circle or ellipse in the simplest form. Illustrations in the article show also special surface forms in specific basic curve position and form. Surface and group names are related to the Latin and Greek words „armilla“ and „ψελιον“ meaning bracelet, based on the shape they resemble.

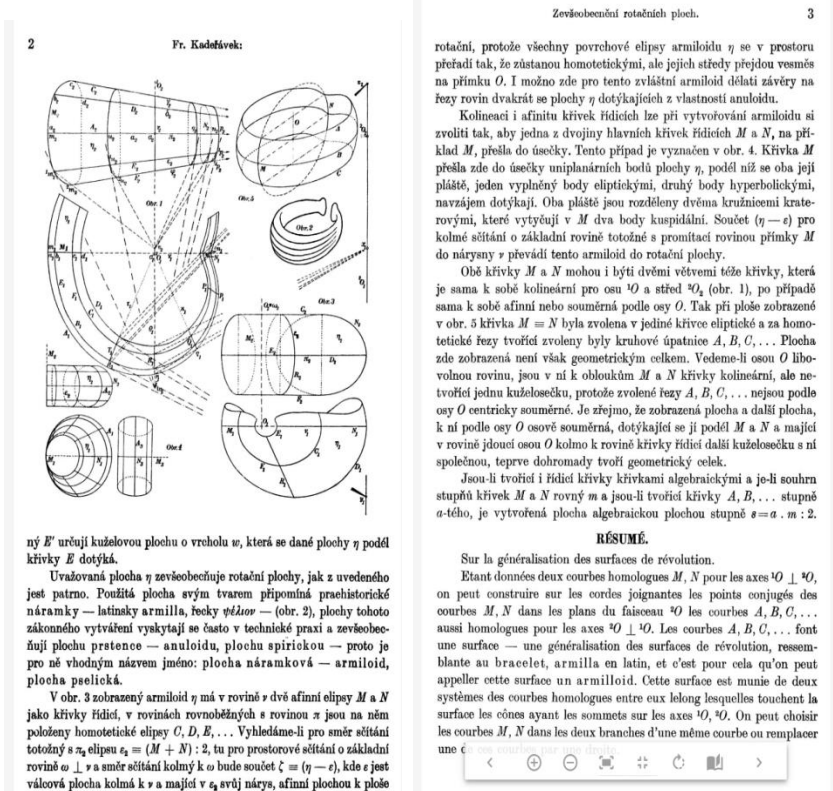
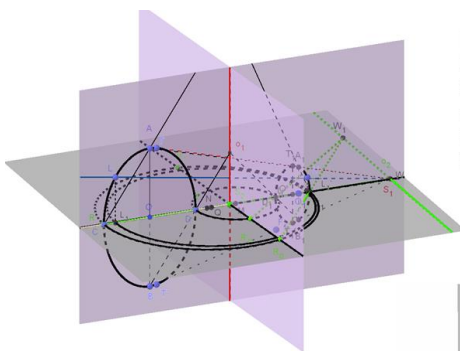


Fig. 2: The second and the third page of the published paper (digitized version)

Synthetic construction of armiloid generated from a basic ellipse had been described in papers [2] and [3], where also vector equation of this particular surface was presented. Animation of this construction could be repeated using GeoGebra program, while using sliders one could easily model the form of the surface based on the parameters representing form of the basic ellipse.

Let the axes of the two collinear systems be two skew lines located in the vertical and in the horizontal plane (frontal and ground image planes in Monge method) and both be perpendicular to the planes pierce line, while centres of the systems are their intersection points with this line, alternately. Basic ellipse in the vertical plane determined by semi-axes and centre on the pierce line be mapped to its collinear image in the vertical plane. Revolving the vertical plane about the axis of this collineation, while its characteristics is changing depending on the angle of rotation, one system of parametric curves on the surface can be generated, see Fig. 3.

Orthographic projections of the basic ellipse and its collinear images onto the horizontal plane generate system of collinear line segments in the other system of central collineations in this plane. Arbitrary chosen curve passing through collinearly dependent points determines the other system of surface parametric curves that are homothetic and collinearly dependent. Generated surface keeps the property of the envelope tangent cone along each curve form this parametric system, which was the reason for the title of Dr. Kadeřávek paper “Generalisation of surfaces of revolution”.



Pencil of planes with axis in line o_1 by revolving the basic vertical plane forming thus pairs of corresponding collinear ellipses to determine the other system of parametric curves on armiloid.

Planes intersect parametric curves of the first system in collinearly corresponding points determining pairs of collinear ellipses with respect to \mathcal{K}^1 (red) and centres moving on o_2 mapped onto horizontal plane to collinear line segments with respect to \mathcal{K}^2 (green).

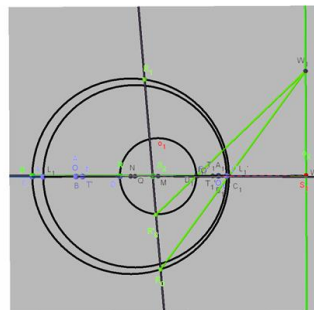


Fig. 3: Example of armiloid parametric curves construction in GeoGebra

2 Analytics representation of pselical surfaces and its generalisation

Consider basic position of the axes of the two collinear systems directly in the coordinate axis z and in the line parallel to the coordinate axis y . Basic ellipse located in the coordinate plane Oxz be determined by semi-axes a (on axis x) and b (on parallel to axis z) and centre with coordinates $O = [m, 0, 0]$. Vector equation of the armiloid is then as follows

$$\mathbf{p}(u, v) = \begin{pmatrix} (m + a \cos 2\pi u)h(v) \cos 2\pi v \\ (m + a \cos 2\pi u)h(v) \sin 2\pi v \\ b k(v) \sin 2\pi u \end{pmatrix}, (u, v) \in [0, 1]^2$$

where $k(v) = \frac{1}{h(v)}$ be functions that represent the two dependently changing characteristics of the two central collineation systems. Values of these functions determine forms of the surfaces, as they influence the form of the basic curve collinear images. Several examples are presented in the Fig. 4.

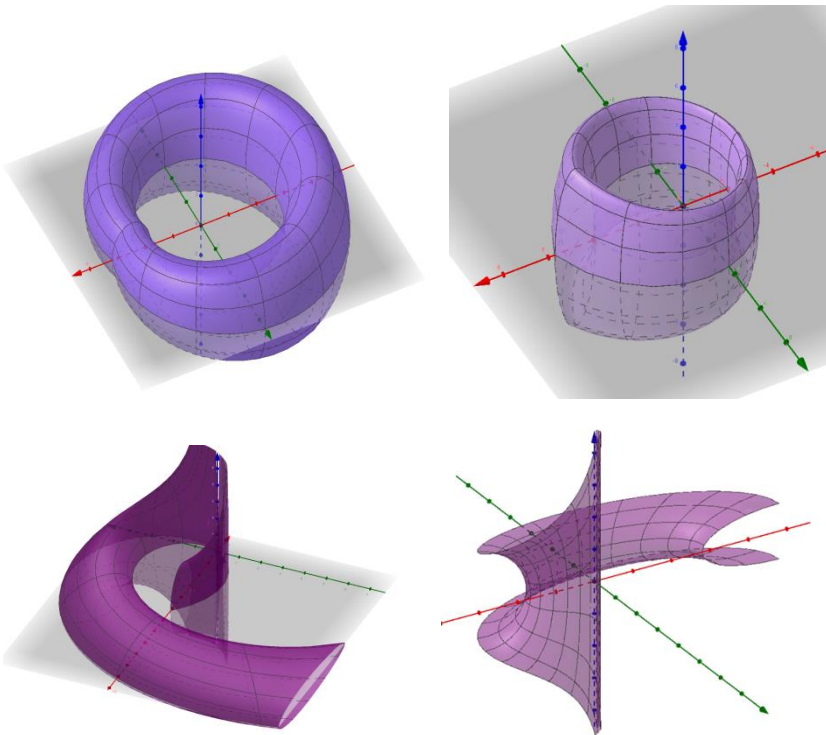


Fig. 4: Example of various forms of pselical surfaces

3 Generalisation of pselical surfaces

Pselical surfaces form a specific group of surfaces that can be regarded as generalised two-axial surfaces of revolution, namely surfaces of Euler type, introduced in papers [4] and [5]. Characteristics functions are constrained by specific limits with respect to their domains and range, as their values influence the form of the generated surfaces. In order to determine a closed surface, functions must be continuous and they have to satisfy the following

$$\forall v \in [0,1]: k(v) = \frac{1}{h(v)}, h(v) \neq 0 \wedge h(0) = h(1)$$

To further generalize this group, we will not consider these constraints and introduce three independent continuous functions defined on the same domain. Then the form of the generalised pselical surfaces parameterisation be

$$\mathbf{p}(u, v) = \begin{pmatrix} (m + a \cos 2\pi u)h(v) \cos 2\pi v \\ (m + a \cos 2\pi u)k(v) \sin 2\pi v \\ b l(v) \sin 2\pi u \end{pmatrix}, (u, v) \in [0,1]^2$$

and many new forms of surfaces can be modelled and investigated.

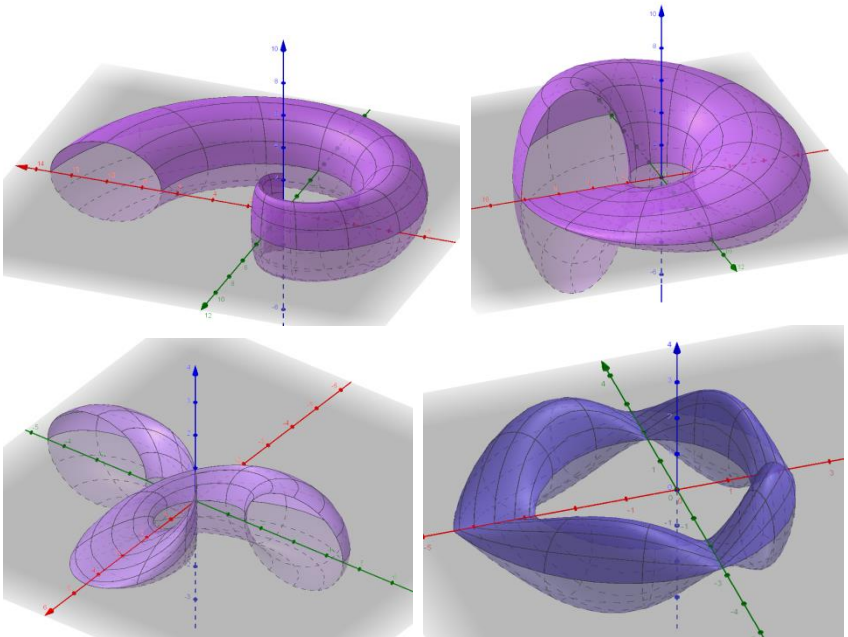


Fig. 5: Example of various forms of generalised pselical surfaces

4 Conclusion

Initial idea of Professor Dr. Kadeřávek to determine a specific group of surfaces by means of their synthetic construction based on 2 related systems of central collineations applied to an arbitrary curve was presented in the paper. Generated group of pselical surfaces with a typical representative “armiloid” was described also analytically, while the main idea of the dependent characteristics of the 2 systems was represented by characteristics functions with special features. Further generalisations were suggested, leading to specific forms of generated surfaces. By means of axial affinities used instead of central collineations, many new forms of surfaces can be generated, as illustrated in Fig. 6.

Thanks to clever old master geometers from the last millennium and their ideas, we can enjoy today, using our sophisticated digital tools, generated wonder shapes they were probably not aware that are possible.

Or maybe they did ...

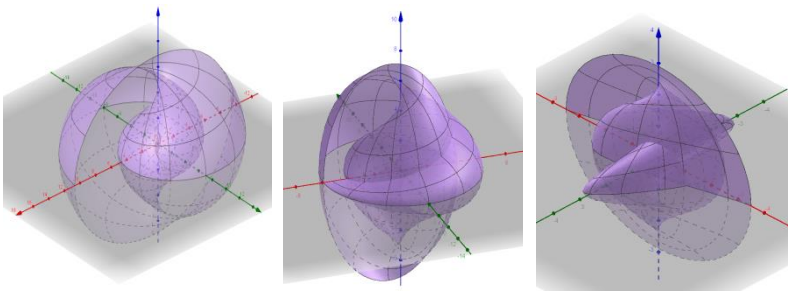


Fig. 6: Examples of interesting forms of generalised pselical surfaces

References

- [1] F. Kadeřávek: *Zovšeobecnění rotačních ploch*. Věstník Královské české společnosti nauk (1939), třída matematicko-přírodovědná, XVII
- [2] D. Velichová: *Armiloid and Other Pselical and Spirical Surfaces*, Proceedings, 26th Conference on Geometry and Computer Graphics, JČU České Budějovice 2006, ČR, ISBN 80-7040-902-9, pp. 289 -294
- [3] D. Velichová: *Pselical Surfaces*, Proceedings, 6th Conference on Applied Mathematics, Aplimat, SjF STU Bratislava 2007, SR, ISBN 978-80-969562-9-6, pp. 273-278
- [4] D. Velichová: *Two-axial surfaces of revolution*, KoG - Scientific and Professional Information Journal of Croatian Society for Constructive Geometry and Computer Graphics, N^o9 (2005), Croatia, pp. 11-20
- [5] D. Velichová: *Generalized surfaces of revolution*, Proceedings of 12th International Conference on Geometry and Graphics ICCGG 2006, Salvador de Bahia, Brasil, CDRom, T33, ISBN 85-86686-39-5

Symmetry – a natural phenomenon causing homo sapiens to become a homo mathematicus

Gunter Weiss

TU Vienna (Austria) & TU Dresden (Germany)

email: weissgunter@gmx.at

Abstract. The term “symmetry” usually translates this Greek-composed word as “equal measure” and interprets it as “Euclidean isometry”. Such a restrictive interpretation is much too narrow, and even it covers a wide field in Geometry and Mathematics it pays to have a broader view on it. Mathematically restricted it mainly deals with the infinite Euclidean plane or n -space and the symmetry groups of infinite or finite objects in such a space. It is global and absolute. In contrast to this, the detection of what is subsumed as “symmetry” acts *locally* on *different abstraction levels* of our natural (and artificial) environment. It means to discover a certain law and structure from a sample of objects in space *and* time. From a few footprints of an animal trail, it is not far to imagine an infinite frieze and apply this insight to ornaments. The detection of structures and similarities requires abstraction abilities. Finally, these abstraction abilities can also be applied to men-created abstractions, e.g. Geometry and Mathematics, but also other fields of science and art. From finding the same abstract structure within different realizations it seems natural to ask for all objects with that structure and to modify that structure to gain a bigger family of related objects. In other words, we deal with and handle “classification problems”. The paper deals with some explicit examples of the above-mentioned topics, focusing on Geometry and esthetical aspects of different symmetry levels.

Key words: Symmetry, reflection, ornament, equidistant set

1 Introduction

Mathematically restricted the term “symmetry” mainly deals with the infinite Euclidean plane or n -space and the symmetry groups of infinite or finite objects in such a space. Symmetry acts *globally* and it is *absolute*. In contrast to this, the detection of what is subsumed as “symmetry” in our environment acts *locally* on *different abstraction levels* of our natural (and artificial) environment. It means to discover a certain law and structure from a sample of objects in space *and* time. From a few footprints of an animal in snow or mud, it is not far to imagine an infinite frieze and apply this insight to ornaments. The detection of structures and similarities requires abstraction abilities. Finally, these abstraction abilities can also be applied to men-created abstractions, e.g. Geometry and Mathematics, but also to other fields of science and art. From finding the same abstract structure within different realizations it seems natural to ask for *all* objects with that structure and to modify that structure to gain and finally to define a bigger family of related objects. In other

words, we deal with and handle “classification problems”. The paper deals with some explicit examples of the above-mentioned topics.

2 “Symmetry”: What is meant by this concept?

We start with comparing the mathematical/geometric standard translation of the concept “symmetry“ as “equal measure“ with the meaning it has at a common, less mathematical viewpoint.

The mathematical point of view speaks of “symmetries” as *congruence relations*, which need a *geometry*, mainly Euclidean, but also a non-Euclidean, affine, projective, Möbius, Laguerre or even more general geometry. In addition, the concept “symmetry group” means the subset of the group of automorphisms of an object, the plane, an n -space, a curve or k - or hyper-surface, and of patterns as e.g. a frieze, rosette, tiling, mosaic. Among symmetries, *reflection* is a special, involutoric case, which can be used to generate geometry, see [1].

The main property of the mathematical concept of “symmetry” is, that it acts globally. Friezes and tilings are imagined as infinite, and the symmetry groups of e.g. Platonic solids act in the whole space!

From a projective geometric viewpoint, reflections are *harmonic axial collineations*, i.e. harmonic homologies with a pair of skew axes, (e.g. point and hyperplane, or, more general, k -space and $(n-1-k)$ -space).

The common general interpretation of the concept “symmetry” seems to comprise many meanings: $\Sigma Y M$ - means “together, common, similar” and it occurs in “symphony, sympathy, symbol, symptom, ...”, but also in “synthesis, synchronous, and syndicate, ...”. The other part, $-M E T P O N$, was/is used for “well-proportioned, harmonic, analog, inner coherence, (same) rhythm, tact, stroke, measure”. We still use “measure” in a wide sense, when “taking measures”, “to pace”, using a “metronome” in music, and speaking of “meter/measure”, “hexameter” etc. of a poem.

By the way, similarly, the standard translation of “Geometry” as “land surveying” should also be questioned. Nile floods provide the planes of the Nile valley with 3 to 5 mm mud, so the bounds of agricultural lands remain visible and land surveying in our sense was not necessary, but of course, it was a need for building temples. When we relate “Geo-“ to “Gaia” (meaning the “world”, the “cosmos”) and “-metry” to its “inner connection and harmony” (see above), we find “Geometry” as a worldview and knowledge cultivated and kept secret by the priestly caste in ancient Egypt. Now the door plate at Platon’s Academy in Athens also makes sense: “No entrance for Geometry-ignoramus!”

We find “symmetry” within all kinds of Art and Science, in dance, music as well as in literature. In a more general sense, it occurs in chemistry, biology, physics, and technics. The characteristic feature of these occurrences is that *“symmetry” is detected via abstraction and acts locally at different levels in natural and artificial structures.*

In the following, we give some examples of such intuitively recognized abstractions of “symmetry”.

3 Intuitively recognized “rough” symmetry

In nature, the traces of animals, a group of dancers, braiding and juggling let us guess abstract frieze and rosette structures, see Fig. 1-3.

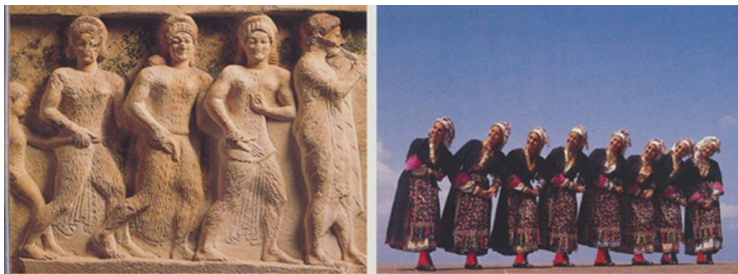


Fig. 1: “Friezes” of dancers



Fig. 2: A trace and braiding are “friezes”.

Fig.3: A meeting as “rosette”,
([3, p.60])

We call animals symmetric in spite of their current state of movement, and we take human faces, hands, body, as well as cattle horn and deer antlers for being “roughly” symmetric. The rhythm of walking, dancing, and breathing represent the idea of frieze-ornaments. Cars and vessels are taken to be symmetric, even so, the steering wheels are not positioned according to the “main” symmetry. Parts of plants, and especially flowers, represent the “idea” of symmetry. Similarly, also the Golden Section can be recognized in nature and art only by approximation as an idea! Pottery, carpet weaving, and basket weaving are further examples, where one can abstract rotational symmetry as well as friezes and wallpaper ornaments. The most natural appearance of symmetry is reflections on quiet water surfaces, see Fig.4.



Fig. 4: Example of a reflection on a quiet water surface.

The key for abstracting (rough) symmetry is the recognition of a generation law of e.g. a frieze from a sample of few elements.

Similarly, also the recognition of a fractal is based only on very few steps of iteration, which already allow guessing its generation law!



Fig. 5: Example of a generalised symmetry based on similarity, showing the idea of a fractal: the romanesco plant.

House facades and architectural details often show “multilevel” (mirror) symmetry, see Fig. 6. From Vitruvius to Palladio, and further from baroque up to now mirror symmetry of buildings plays an important role. Multilevel symmetry suits well to the natural way to look at our environment from different distances: We notice e.g. a forest from abroad, trees being closer, branches and finally leaves, flowers and their inner details. Ornamentation of facades in different cultures follows this scheme, see Fig. 7. Multilevel symmetry suits well to the natural way to look at our environment from different distances: We notice e.g. a forest from abroad, trees being closer, branches and finally leaves, flowers, and their inner details. Ornamentation of facades in different cultures follows this scheme, see Fig. 6-7.



Fig. 6: Examples of multilevel mirror symmetry of facades and its details.
Left: Shaker's house (USA), ([5, p.56]);
right: Shibam houses (Jemen).

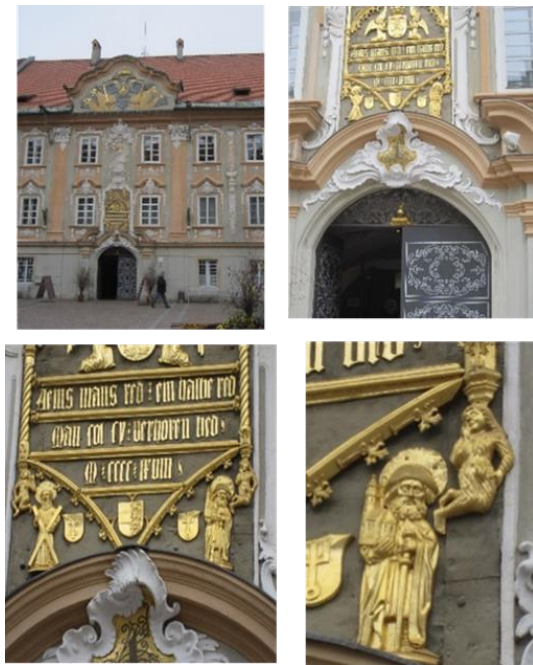


Fig. 7: Example of multilevel mirror symmetry with not symmetric details at the façade of the town hall in St. Veit an der Glan (Austria).

4 Symmetry and its aesthetical and psychological aspects

Temples and churches show symmetry as well in their architecture as in their decoration and ornamentation, independent of cultural background and time. It seems that regularity and symmetry express and symbolize best the perfect harmony of creation, sees Fig. 8, 9.



Fig. 8: Egyptian and Mexican temples, (from [7], and [4, p.143])

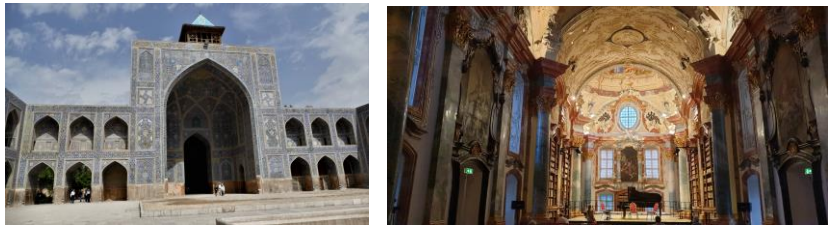


Fig. 9: The Great Mosque at Isphahan (Iran), Monastery Altenburg (Austria)

When the philosophy of the ancient Greeks and their worldview interprets matter as a mixture of Platonic solids, it shows that regularity and symmetry is seen as of divine origin and that it represents the ideal, perfect world. Also J. Kepler's "Harmonices Mundi" is based on this viewpoint. Medieval and baroque monasteries show highly symmetric architecture and decoration at buildings dedicated to worship, while profane buildings often consciously are built with "broken symmetry".

While the above-mentioned facts result from human reasoning about the world, there come also similar facts caused by human psychology of "data processing economy": Symmetry and regularity save data and speed up the interpretation of what we recognize! For example, the sculptured mask Fig. 10 is seen as a face even at skew angle despite of binocular view!



Fig. 10 Granit sculpture “mask”, Oslo (Norway).

The following series of pictures emphasizes the “regularising urge” of human psychology, (Fig. 11).



Fig. 11: “The regularising urge”, ([6, p. 50-51]).

We also notice that architectural and decoration habits up to Worldwar II suit quite well to the natural viewing experience recognizing different details at any distance. Modern architecture neglect that and presents facades belonging rather to fortresses than to civil buildings. For fortresses such decoration-less facades, appearing cool and repellent, this attitude is intended. Modern decoration-less buildings sometimes occur as giant sculptures at far distances, but look boring when being close to them, see Fig. 12.

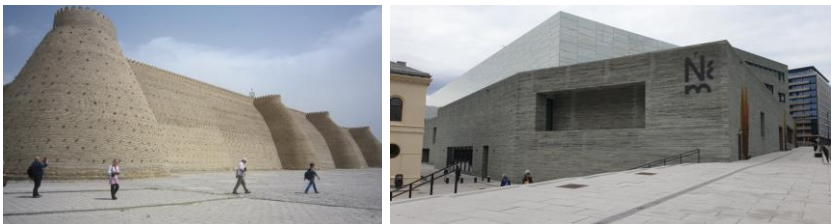


Fig. 12: Medieval city fortification, (Khiva, Uzbekistan) versus modern architecture (National Museum (2021), Oslo, Norway)

5 Symmetry as an abstract elementary mathematical concept

At preschool-, primary and secondary school levels “symmetry” is dealt with as reflection, at first as an abstraction of observations in the pupils’ environment with the purpose to derive properties of congruences. Hereby the first application is the “perpendicular bisector” – a misleading name for the “equidistant set of two points” (rep. of a line segment). In the plane of common view (endowed with a Euclidean structure) this set is just one single line, the axis of a reflection, mapping one point into the other. In a hyperbolic or elliptic plane, this equidistant set consists of a pair of lines, both being axes of a reflection mapping one point into the other. When we enclose the Euclidean plane by an “ideal line”, this line fulfils the equidistant set property, too.

Furthermore, we find that

The equidistant set of linear subspaces of an n -space with Cayley-Klein metric is an object of 2nd degree.

For example, it is well known that, in the Euclidean plane, the equidistant set of a point P and a line l is a parabola. In the hyperbolic plane (Fig. 13 shows the Klein model of a hyperbolic plane with absolute conic ω) this set is a conic again, the construction of which is the hyperbolic version of that of the Euclidean parabola.

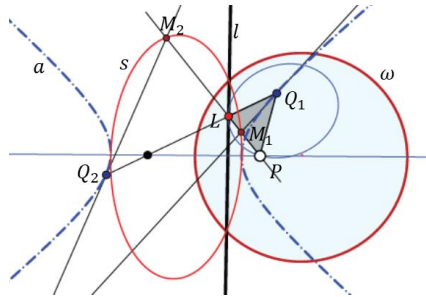


Fig. 13: Equidistant conic of a point P and a line l in a hyperbolic plane.

Just to mention it, in the Euclidean 3-space, the equidistant set of a point P and a plane π is a paraboloid of revolution, the tangent planes of which act as axes of reflection mapping P to a point P' of π and reversely, π to a plane π' through P . The equidistant set of two intersecting lines is a pair of orthogonal planes, each the axis of a reflection. The equidistant set of two skew lines is an ortho-hyperbolic paraboloid, while the equidistant set of a line and a plane is a cone of 2nd degree. Generalizations might concern the metric (e.g. stemming from a normed space), the number of subspaces, and finally, replace the subspaces with submanifolds.

One might ask now, what is the dual to equidistant sets? It would be logical to call it “equiangular sets”, but this concept is already coined for polygons,

where adjacent sides enclose a fixed angle. The concept “isoptic point set” could act as a replacement, even so it is not the proper dualization of equidistant *pointset*, as the correct version should concern *hyperplane sets*. In Fig. 14 we visualize the different approaches:

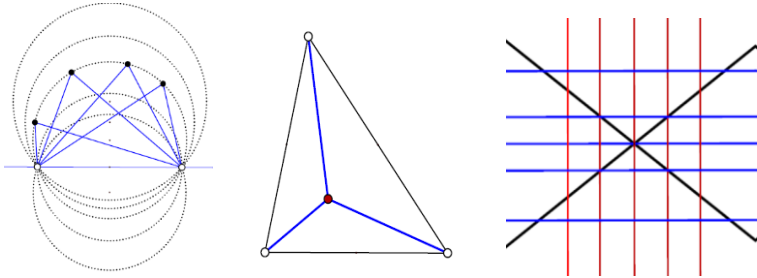


Fig. 14: The isoptic set of two points without prescribed angle does not make sense (left); the isoptic set of three points is their Fermat-Steiner point (middle). The dual of the equidistant set of two points is a pair of two pencils of orthogonal lines intersecting a given pair of lines by the same angle, (right).

In Elementary Geometry, Symmetry resp. reflections are used as a tool for solving extreme value problems. For example, given the points A , B , and a line g , find a point C' on g , such that the distance $AC' + BC'$ gets minimal, (Fig. 15). A similar problem asks for the triangle $P'Q'R'$ inscribed to a given triangle ABC , such that the perimeter of $P'Q'R'$ gets minimal. (The well-known answer is that P' , Q' , and R' are the pedal points of the altitudes of ABC , Fig. 16.)

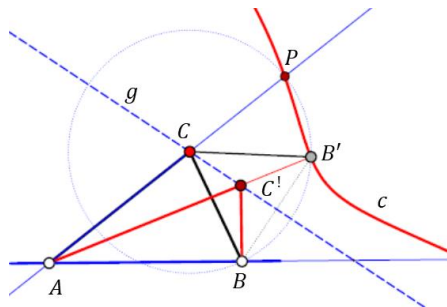


Fig. 15: Point C' on g solves the extreme value problem $\min(AC' + BC')$.

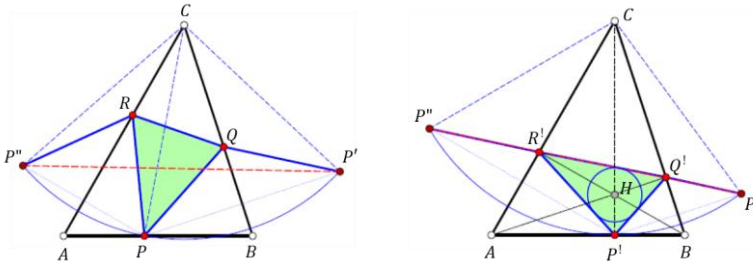


Fig. 16: Of all triangles inscribed to a triangle the altitude pedal point triangle has the shortest perimeter.

As further important mathematical applications of “symmetry”, we mention the well-known “three reflections theorem” and the “Steiner symmetrisation”, the latter solving e.g. “Dido’s extreme value problem”, namely that, of all planar domains with the same perimeter, the circle has the maximal area, (see e.g. [2]). Symmetry is also present in “geometric optics”, in problems of (closed) billiards, and many other topics, which go beyond the scope of this paper.

6 Conclusion

This paper presents some aspects of “symmetry”, and it addresses mainly teachers and aims for their further education. Finally, we might alter F. Nietzsche’s saying that “Life without music is an error” to “Humanity without the idea of symmetry is impossible”.

As the material mostly concerns common knowledge, the list of references can be kept short, and it concerns the few figures, which are not from the author.

References

- [1] F. Bachmann: *Aufbau der Geometrie aus dem Spiegelungsbegriff*. (1973/2012)
- [2] S. Hildebrandt, A. Tromba: *Kugel, Kreis und Seifenblasen. Optimale Formen in Geometrie und Natur*. Birkhauser Verlag Basel 1996
- [3] P. Maréchaux, M. Maréchaux: *Jemen*. DA Verlag Nürnberg 1993
- [4] H. J. Prem, U. Dyckerhoff: *Das alte Mexiko*. Bertelsmann 1986
- [5] J. Sprigg, D. Larkin: *Shaker, Life, Work, and Art*. Ravensburg 1991
- [6] J. R. Wilson: *Wonders of Science*, Life Inc. 1966
- [7] <https://upload.wikimedia.org/commons/f/f9/Hatschepsuttempel.jpg>

Higher-dimensional spaces arising from robot kinematics

Michal Zamboj

*Charles University, Faculty of Education
M. Rettigová 4, Praha 1, Czech Republic
email: michal.zamboj@pedf.cuni.cz*

Abstract. In this paper, we look at some simple robot mechanisms dealing mainly with rotational movement. Our focus lies in visual interpretations of higher-dimensional configuration spaces. Several examples of robot mechanisms will bring us to visualizations of Cartesian products of circles and spheres embedded in the four-dimensional Euclidean space.

Keywords: higher dimension, 3-R robot, spherical joint, torus, 3-sphere

1 Introduction

Various combinations of movements support various geometric interpretations. We examine configurations of two mechanisms: 3-R robot (Figure 1, left) and spherical (or ball) joint mechanism (Figure 1, right). Each configuration will represent a point in a higher-dimensional (configuration) space. When simply stated, the more freedom the movements of the mechanism have, the more dimensional the configuration space is. The main inspiration for this paper was the visual approach presented in [3, Chapter 2]. A profound study of a spherical joint with detailed visualizations is, for example, [1]. Our contribution is in the extension of the visualization of some configuration spaces into the fourth dimension. To visualize four-dimensional objects, we use a double orthogonal projection of a 4-space onto two mutually perpendicular 3-spaces (4-D-DOP) described in [4]. Visualizations and interactive models in this paper are created in *Wolfram Mathematica* and *GeoGebra* software.

2 Visualizing configuration spaces

Lynch and Park [3, p. 12] define *configuration* of a robot as a complete specification of the position of every point of the robot. Next, the n -dimensional space containing all possible configurations of the robot is called the *configuration space*. Each configuration is represented by a point of the configuration space. It is, of course, useful when a point of the configuration space corresponds to some configuration uniquely. For a simple example see Figure 2, in which a 2-R planar robot has two revolving arms, each of them represents a circle (or 1-sphere \mathcal{S}^1) for each position of the second. Thus, the configuration space consists of a torus as a Cartesian product of two circles $\mathcal{S}^1 \times \mathcal{S}^1$.

Similarly, a 3-R robot consists of three revolving arms, so its configuration space might be represented as $\mathcal{S}^1 \times \mathcal{S}^1 \times \mathcal{S}^1$. Such an object is

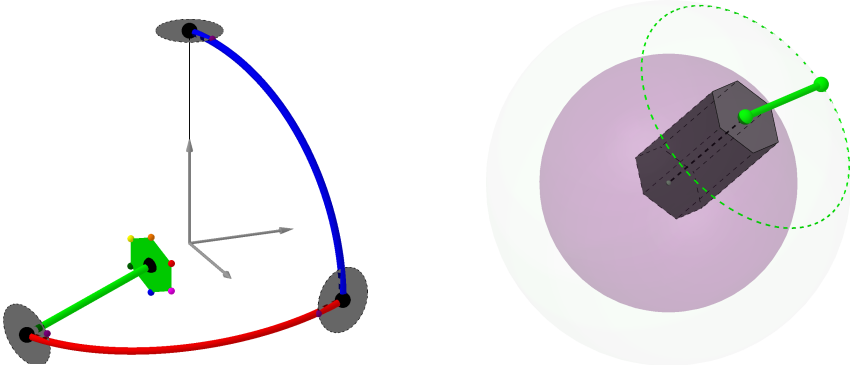


Fig. 1: (left) 3-R robot. Each of the arms can revolute around an axis. Rotations are indicated by circles in joints. (right) Spherical joint with revolving arm. A spherical joint connects the hexagonal prismatic arm of the mechanism to a fixed point, and a revolute joint links the second endpoint to the green arm with the end effector in the figure.



Fig. 2: (left) 2-R planar mechanism. The blue arm revolves about the fixed point, while the red arm is connected with a revolute joint to the second endpoint of the blue arm. (right) The configuration space of the 2-R planar mechanism. The blue and red circles represent the respective rotations of the arms.

a 3-dimensional torus embeddable in the 4-dimensional real space. Furthermore, a spherical joint with a revolving arm consists of a spherical movement composed with a circular movement of the arm. Therefore its configuration space is the Cartesian product of a 2-sphere (\mathcal{S}^2) and a circle (\mathcal{S}^1): $\mathcal{S}^2 \times \mathcal{S}^1$.

2.1 Constructing toroidal hypersurfaces of revolution

To understand the upcoming orthogonal projections from the four-dimensional space, let us first remind images of a 2-sphere and torus of revolution in the Monge's projection (Figure 3). The object is orthogonally projected into two mutually perpendicular planes. Therefore, each point has two conjugated images. For further discussion, it is convenient to observe that rotation (e.g., of the blue generating circle in the figures) creates an affine image in the orthogonal projection.

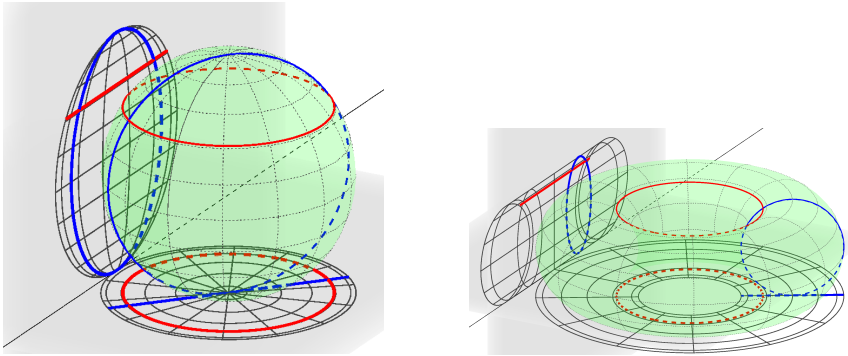


Fig. 3: Principle of Monge's projection. (left) A sphere and its conjugated images, including latitudinal and longitudinal circles. (right) A torus of revolution and its conjugated images, including circles on the surface.

A consecutive construction of the hypersurfaces $\mathcal{S}^2 \times \mathcal{S}^1$, $\mathcal{S}^1 \times \mathcal{S}^1 \times \mathcal{S}^1$ is illustrated in Figure 4. Let us denote T_{dir} a translation in a direction of one of the reference axes (x, y, z, w) and R_{plane} a rotation about one of the reference planes with an argument $\varphi \in \langle 0, 2\pi \rangle$.

$$R_{xy} = \begin{pmatrix} 1 & 0 & 0 & 0 \\ 0 & 1 & 0 & 0 \\ 0 & 0 & \cos(\varphi) & -\sin(\varphi) \\ 0 & 0 & \sin(\varphi) & \cos(\varphi) \end{pmatrix} \quad R_{xz} = \begin{pmatrix} 1 & 0 & 0 & 0 \\ 0 & \cos(\varphi) & 0 & -\sin(\varphi) \\ 0 & 0 & 1 & 0 \\ 0 & \sin(\varphi) & 0 & \cos(\varphi) \end{pmatrix}$$

$$R_{xw} = \begin{pmatrix} 1 & 0 & 0 & 0 \\ 0 & \cos(\varphi) & -\sin(\varphi) & 0 \\ 0 & \sin(\varphi) & \cos(\varphi) & 0 \\ 0 & 0 & 0 & 1 \end{pmatrix} \quad R_{yz} = \begin{pmatrix} \cos(\varphi) & 0 & 0 & -\sin(\varphi) \\ 0 & 1 & 0 & 0 \\ 0 & 0 & 1 & 0 \\ \sin(\varphi) & 0 & 0 & \cos(\varphi) \end{pmatrix}$$

$$R_{yw} = \begin{pmatrix} \cos(\varphi) & 0 & -\sin(\varphi) & 0 \\ 0 & 1 & 0 & 0 \\ \sin(\varphi) & 0 & \cos(\varphi) & 0 \\ 0 & 0 & 0 & 1 \end{pmatrix} \quad R_{zw} = \begin{pmatrix} \cos(\varphi) & -\sin(\varphi) & 0 & 0 \\ \sin(\varphi) & \cos(\varphi) & 0 & 0 \\ 0 & 0 & 1 & 0 \\ 0 & 0 & 0 & 1 \end{pmatrix}$$

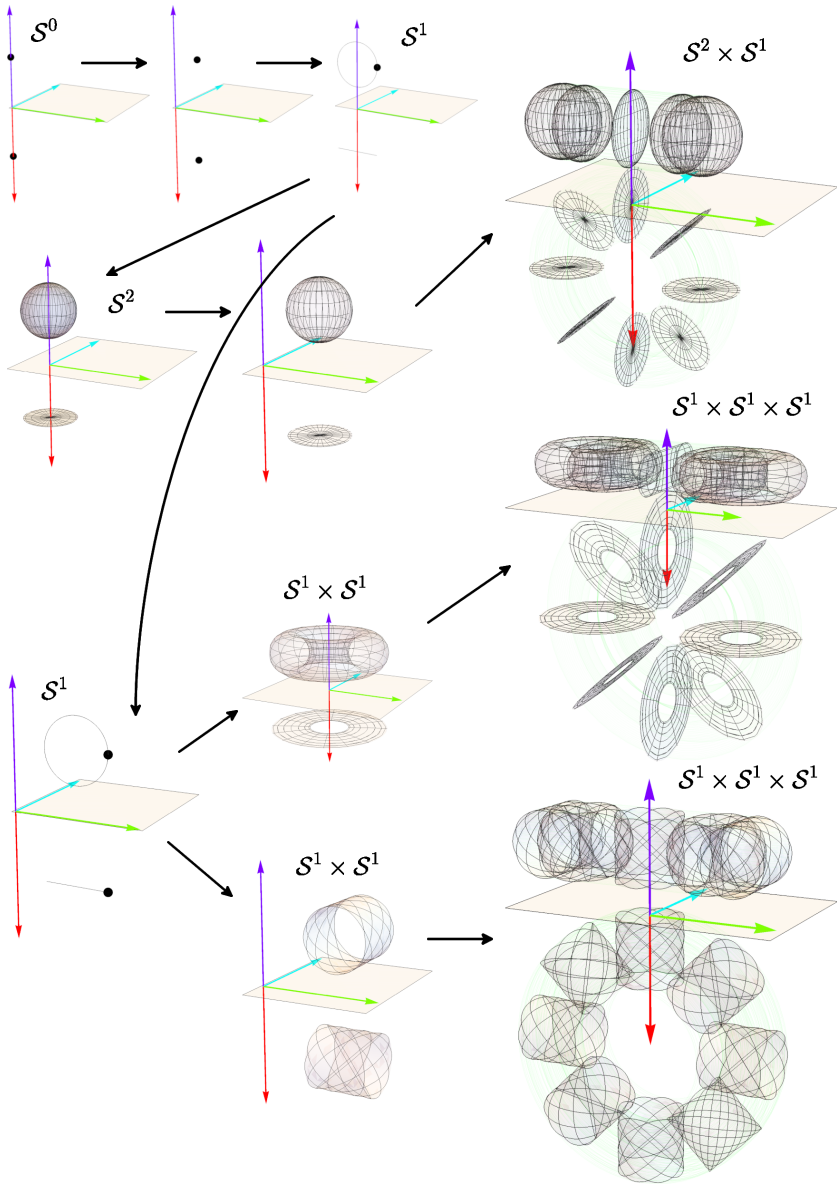


Fig. 4: A diagram with the consecutive construction of the hypersurfaces $\mathcal{S}^2 \times \mathcal{S}^1$ and $\mathcal{S}^1 \times \mathcal{S}^1 \times \mathcal{S}^1$ using rotations and translations, and a construction of $\mathcal{S}^1 \times \mathcal{S}^1 \times \mathcal{S}^1$ from a Clifford torus (bottom illustrations).

The following procedure might be used to construct the surfaces (conjugated images in Figure 4 are translated in z and w directions such that the images do not overlap). Starting with a point (\mathcal{S}^0) at the origin, we use translation T_x (distance r_1) and rotation R_{yw} (angle φ), respectively, to obtain a circle \mathcal{S}^1

$$\begin{pmatrix} r_1 \cos(\varphi) \\ 0 \\ r_1 \sin(\varphi) \\ 0 \end{pmatrix}.$$

For the first case, to construct $\mathcal{S}^2 \times \mathcal{S}^1$, we apply the rotation R_{zw} (angle ψ) to the circle (\mathcal{S}^1) to create a 2-sphere \mathcal{S}^2

$$\begin{pmatrix} r_1 \cos(\varphi) \cos(\psi) \\ r_1 \cos(\varphi) \sin(\psi) \\ r_1 \sin(\varphi) \\ 0 \end{pmatrix}.$$

Using another translation T_x (distance r_2) and rotation R_{yz} (angle θ), we obtain the hypersurface $\mathcal{S}^2 \times \mathcal{S}^1$

$$\begin{pmatrix} (r_2 + r_1 \cos(\varphi) \cos(\psi)) \cos(\theta) \\ r_1 \cos(\varphi) \sin(\psi) \\ r_1 \sin(\varphi) \\ (r_2 + r_1 \cos(\varphi) \cos(\psi)) \sin(\theta) \end{pmatrix}.$$

In the second case, to obtain the hypersurface $\mathcal{S}^1 \times \mathcal{S}^1 \times \mathcal{S}^1$, we return back to the circle \mathcal{S}^1 and apply, for example, translation T_x (distance r_2) and rotation R_{zw} (angle ψ) to obtain a torus $\mathcal{S}^1 \times \mathcal{S}^1$

$$\begin{pmatrix} (r_2 + r_1 \cos(\varphi)) \cos(\psi) \\ (r_2 + r_1 \cos(\varphi)) \sin(\psi) \\ r_1 \sin(\varphi) \\ 0 \end{pmatrix}.$$

Another translation T_x (distance r_3) and rotation R_{yz} (angle θ) of the torus produce the hypersurface $\mathcal{S}^1 \times \mathcal{S}^1 \times \mathcal{S}^1$

$$\begin{pmatrix} (r_3 + (r_2 + r_1 \cos(\varphi)) \cos(\psi)) \cos(\theta) \\ (r_2 + r_1 \cos(\varphi)) \sin(\psi) \\ r_1 \sin(\varphi) \\ (r_3 + (r_2 + r_1 \cos(\varphi)) \cos(\psi)) \sin(\theta) \end{pmatrix}.$$

It should be noted that there are other useful parametrizations of a torus, or toroidal hypersurface in a 4-space. One of the alternatives (see also [2]) is a Clifford flat torus $\mathcal{S}^1 \times \mathcal{S}^1 \in \mathbb{R}^4$ with the following parametrization

$$\begin{pmatrix} \cos(\varphi + \psi) \\ \cos(\varphi - \psi) \\ \sin(\varphi + \psi) \\ \sin(\varphi - \psi) \end{pmatrix}, \text{ for } \varphi, \psi \in \langle 0, 2\pi \rangle.$$

Let us translate it by T_x (distance r_4) and rotate by R_{yz} (angle θ) to obtain $\mathcal{S}^1 \times \mathcal{S}^1 \times \mathcal{S}^1$ as

$$\begin{pmatrix} (r_4 + \cos(\varphi + \psi)) \cos(\theta) - \sin(\varphi - \psi) \sin(\theta) \\ \cos(\varphi - \psi) \\ \sin(\varphi + \psi) \\ \sin(\varphi - \psi) \cos(\theta) + (r_4 + \cos(\varphi + \psi)) \sin(\theta) \end{pmatrix}.$$

2.2 Four-dimensional configuration spaces of a spherical joint and 3-R robot

At last, let us examine the connection between a configuration of a 3-dimensional robot and its representation in the configuration space.

Spherical joint with a revolving arm (Figure 5). For a spherical joint with revolving arm, the configuration space consists of a 2-sphere and its rotation. When fixing the revolving arm, a unique configuration of the spherical joint represents a unique point on the 2-sphere in the 4-space. For simplicity, we can use the same (latitudinal, longitudinal) parameters in spherical coordinates. The rotation of the revolving arm rotates the 2-sphere in the 4-space about the chosen plane. In the figure, the rotation of the 2-sphere produces the affine image in the orthogonal projection.

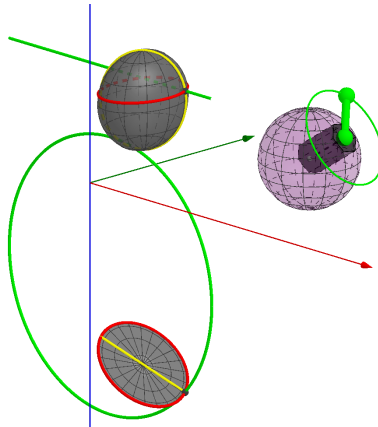


Fig. 5: The spherical joint mechanism and its configuration space in the 4-D-DOP. The upper image corresponds to the projection into the 3-space (x, y, z) , and the lower image into the 3-space (x, y, w) with respect to the parametrization given in the text.

3-R robot (Figure 6). Three revolving arms in 3-R robot create torus surface $\mathcal{S}^1 \times \mathcal{S}^1 \times \mathcal{S}^1$, where each rotation corresponds to one of the circles. In the figure, when we consider the last (green) arm as fixed, the first (blue) and

second (red) arms generate a torus. In the figure, we have used the alternative parametrization of the flat torus from the previous section. The red and blue curves on the torus indicate trajectories of the point in the configurations for the respective rotations. The green curve is the trajectory of the point with respect to the rotation of the green arm for fixed red and blue arms.

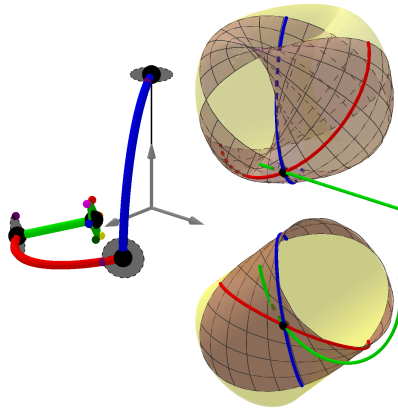


Fig. 6: The 3-robot and images of its configuration space in the 4-D-DOP. All of the rotations are restricted to the intervals $(0, \pi)$. An interactive applet with manipulable elements is on the link: <https://www.geogebra.org/m/xwbc5ve4>.

3 Conclusion

We have presented images of four-dimensional surfaces $\mathcal{S}^2 \times \mathcal{S}^1$ and $\mathcal{S}^1 \times \mathcal{S}^1 \times \mathcal{S}^1$ in the 4-D-DOP visualization method. These surfaces were motivated by representations of the configuration spaces of a spherical joint and 3-R robot mechanisms. Interactive visualizations of configuration spaces in higher dimensional spaces might provide a more comprehensive understanding of the complexity of composing joints or movements. The hypersurfaces shown in this paper are naturally derived from the rotational movement and could be generalized in higher dimensions. However, there are many other further mechanisms with other types of joints, leading to other surfaces. Furthermore, one configuration space may represent configurations of different mechanisms.

References

- [1] K. Abe, K. Tadakuma, R. Tadakuma: *ABENICS: Active Ball Joint Mechanism With Three-DoF Based on Spherical Gear Meshings*, IEEE Transactions on Robotics, 37 (2021), no. 5, pp. 1806-1825
- [2] T. Banchoff: *The Flat Torus in the Three-Sphere*, online: <http://www.geom.uiuc.edu/~banchoff/script/b3d/hypertorus.html>, accessed October 25th, 2022
- [3] K. M. Lynch, F. C. Park: *Modern Robotics*, Cambridge University Press, 2017
- [4] M. Zamboj: *Double Orthogonal Projection of Four-Dimensional Objects onto Two Perpendicular Three-Dimensional Spaces*, Nexus Network Journal, 20 (2018), Issue 1, pp. 267-281

List of Participants

Bartoň	Michael	BCMA Bilbao
Beganová	Juliana	Stavebná fakulta, STU v Bratislave
Bizzarri	Michal	FAV, Západočeská univerzita v Plzni
Brajerčík	Ján	Prešovská univerzita v Prešove
Bulantová	Jana	FAST, Vysoké učení technické v Brně
Cibulka	Jaroslav	Fakulta strojní, ČVUT v Praze
Čečáková	Stanislava	Fakulta architektury, ČVUT v Praze
Ferdiánová	Věra	KMA PF, Ostravská univerzita
Halaš	Radomír	PřF, Univerzita Palackého v Olomouci
Hamajová	Klaudia	FMFI, Univerzita Komenského v Bratislave
Hašek	Roman	KM PF, Jihočeská univerzita v Č. Budějovicích
Hlavová	Marta	Fakulta strojní, ČVUT v Praze
Holešová	Michaela	SvF, Žilinská univerzita v Žiline
Chalmovianský	Pavel	KAG FMFI, Univerzita Komenského v Bratislave
Chodorová	Marie	PřF, Univerzita Palackého v Olomouci
Jukl	Marek	PřF, Univerzita Palackého v Olomouci
Juklová	Lenka	PřF, Univerzita Palackého v Olomouci
Koktavá	Marie	Mendelova univerzita v Brně
Kolářová	Dana	Fakulta architektury, ČVUT v Praze
Kovács	Zoltán	Johannes Kepler University, Linz
Králová	Alice	LDF, Mendelova univerzita v Brně
Lávička	Miroslav	KMA FAV, Západočeská univerzita v Plzni
Linkeová	Ivana	Fakulta strojní, ČVUT v Praze
Mikeš	Josef	PřF, Univerzita Palackého v Olomouci
Molnár	Emil	BUTE, Budapest
Müller	Jakub	Fakulta strojní, ČVUT v Praze
Pech	Pavel	PF, Jihočeská univerzita v Č. Budějovicích
Peška	Patrik	PřF, Univerzita Palackého v Olomouci
Plinta	Martin	Ostravská Univerzita v Ostravě
Rachůnek	Lukáš	PřF, Univerzita Palackého v Olomouci
Richtáriková	Daniela	Strojnícka fakulta, STU v Bratislave
Rückschlossová	Tatiana	Stavebná fakulta, STU v Bratislave
Rýparová	Lenka	PřF, Univerzita Palackého v Olomouci
Sováková	Barbora	Ostravská Univerzita v Ostravě
Szarková	Dagmar	SSGG, Bratislava

Šafařík	Jan	FAST, Vysoké učení technické v Brně
Šír	Zbyněk	MFF, Univerzita Karlova v Praze
Tereňová	Zuzana	Stavebná fakulta, STU v Bratislave
Trnková	Maria	University of California, Davis
Vajsáblová	Margita	Stavebná fakulta, STU v Bratislave
Velich	Iľja	SSGG, Bratislava
Velichová	Daniela	Strojnícka fakulta, STU v Bratislave
Voráčová	Šárka	Fakulta dopravní, ČVUT v Praze
Vršek	Jan	KMA FAV, Západočeská univerzita v Plzni
Weiss	Gunter	Technische Universität Wien
Zamboj	Michal	KMDM PF, Univerzita Karlova v Praha
Zrůstová	Lucie	FAST, Vysoké učení technické v Brně

Proceedings of the
CZECH-SLOVAK CONFERENCE
ON GEOMETRY AND GRAPHICS 2022

Editors:

Miroslav Lávička, Daniela Velichová, Dagmar Szarková

Published by

Vydavateľstvo SCHK

Radlinského 9, 812 37 Bratislava

First Edition

Bratislava 2022

ISBN 978-80-8208-092-9

EAN 9788082080929